CONTROLS ON SOUTHERN OCEAN PHYTOPLANKTON PRODUCTION – A SYSTEMS APPROACH

Ernesto Arturo Molina Balari

Submitted in fulfillment of the requirements for a
Doctor of Philosophy in Quantitative Marine Science

A joint program between the

Commonwealth Science and Industry Research Organization

and the University of Tasmania

March 2012

For my son Pablo

Declaration

This thesis is the result of original research conducted by myself unless stated in the text or acknowledgements. The research was carried out under the supervision of Professor T. W. Trull at the University of Tasmania. All sources of information used have been specifically acknowledged. Individuals who provided data sets have been fully acknowledge.

This thesis may be made available for loan and limited copying in accordance with the *Copyright Act of 1968*

Ernesto Arturo Molina Balari
March 2012

CONTENTS

ABSTRACT

Plankton ecosystems play a significant part in the global cycle of carbon by contributing ~40% of total annual primary productivity. Changes are expected in response to warming, increased ocean stratification, altered supply of iron as a limiting micronutrient, and ecosystem structures. To diagnose these effects, numerical models of plankton ecology have become a key approach. This thesis examines the Nutrient Phytoplankton Zooplankton Detritus (NPZD) ecosystem model of Oschlies & Garcon [1999], and especially the modifications required to simulate phytoplankton biomass in naturally iron-fertilized Southern Ocean waters. This provides perspectives on the sensitivity of Southern Ocean ecosystems to global change.

The NPZD model was used to simulate the phytoplankton bloom that forms in natural iron-fertilized waters of the Kerguelen plateau and adjacent High Nutrient Low Chlorophyll (HNLC) waters. Sensitivity to mixed layer depth and temperature was found to be negligible in comparison to zooplankton grazing, which also strongly modulated the ability of increased iron availability to affect biomass via phytoplankton growth rates. Direct comparison with satellite chlorophyll estimates showed that the base model could not achieve chlorophyll concentrations greater than ~0.6 mg m^{-3}, in comparison to the ~2.7 mg m^{-3} of chlorophyll observed in the Kerguelen bloom. Incorporating an indirect simulation of iron-fertilization provided only a small improvement. An increase in zooplankton grazing (by a factor of 7) was required to achieve the high peak bloom biomass. To match the seasonal cycle and both summer maximum and winter minimum biomass concentrations, it was also necessary to impose seasonal cycles in key photosynthetic parameters (α - initial slope of the photosynthesis/irradiance curve, and μ_{max} - maximal growth rate).

The same model was used to examine the response of plankton ecosystems to temporary iron fertilizations. The model was able to simulate the phase and amplitude patterns of the SOIREE bloom in Antarctic waters, given increases in α and μ_{max} similar to those observed in the field (a factor of 2.5 over 13 days). Simulating a series of SOIREE-like experiments at different times of the seasonal cycle showed that while blooms induced in spring resulted in high surface chlorophyll levels, only blooms induced in summer resulted in both high chlorophyll and high potential carbon export. These findings also emphasized the importance of low overwintering

biomass of phytoplankton and zooplankton to the spring biomass peak. Expanding the simulations to all latitudes of the Southern Ocean revealed distinct variations in the intensity of responses to iron fertilization, and suggested that the optimal time and location for iron fertilization in terms of potential carbon export is early summer in the Subantarctic zone.

Acknowledgements

I would like to thank Professor T.W. Trull for having the stamina to deal with all my frames of mind, and for his superior guidance and undaunted encouragement throughout this endeavor. His deep insight into biogeochemical processes and biological-physical interactions benefited my research greatly. I owe him a great deal of thanks.

I would also like to thank my co-advisors Dr. Andrew Bowie and Dr. Mathieu Mongin. They have been very generous with their time and expertise, and have been a continuous source of encouragement. Thanks for their time, patience, criticisms and insights during my thesis work and during the preparation of this document.

I also want to acknowledge the personal and staff in the University of Tasmania and the ACECRC.

I wish to thank all my friends for all the discussion, inspiration and support. I'm grateful for Anne, Barb and David, Mark, Beca, Michelle, Steve, Rodrigo, Ramon, and Franco.

Last, but certainly not least, I wish to express my sincere thanks to my parents, Nuria and Carlos, for their patient support and continuous love. There is no doubt that my darling son Pablo, who made me realized that there are things much more precious than research work, is the main recipient of my gratitude and endearment.

This research was supported by a scholarship jointly provided by the University of Tasmania and the Antarctic Climate and Ecosystems Cooperative Research Center as part of the Quantitative Marine Science PhD program.

Abbreviations

0d	zero-dimensional
1d	one-dimensional
AAIW	Antarctic Intermediate Water
ACC	Antarctic Circumpolar Current
AASW	Antarctic Surface Waters
AZ	Antarctic Zone
BATS	Bermuda Atlantic Time-series Study
D	Detritus
DCM	Deep Chlorophyll Maximum
dFe	dissolved iron
DIC	Dissolved Inorganic Carbon
DOC	Dissolved Organic Carbon
DVM	Diel Vertical Migration
EP	Export Production
Fe	iron
GCM	General Circulation Model
HNLC	High Nutrient Low Chlorophyll
I	Irradiance
I_{PAR}	Irradiance within the photosynthetically active range
IPFZ	Inter-Polar Frontal Zone
NP	New Production
NPP	Net Primary Production
max	maximum value
min	minimum value
MLD	Mixed Layer Depth
M-M	Michaelis-Menten (function)
N	Nitrogen
NPZD	Nitrogen-Phytoplankton-Zooplankton-Detritus
M	molarity (number of model of a solute in 1L solution)
ODE	Ordinary Differential Equation
OSP	Ocean Station Papa
P	Phytoplankton
PAR	Photosynthetically Active Radiation
P-I	Photosynthesis-Irradiance (curve)
PFZ	The Polar Frontal Zone
PF	Polar Front
POC	particulate organic carbon
PP	Primary Production
Re	Reynolds Number
RuBiscCO	Ribulose-1,5-bisphosphate carboxylase oxygenase
RP	Regenerated Production
SACCF	Southern ACC Front
SAMW	Subantarctic Mode Water

SASW	Subantarctic Surface Waters
SAZ	Subantarctic Zone
SCHL	Surface Chlorophyll
SEEDS	Subarctic pacific iron Experiment for Ecosystem Dynamics Study
SERIES	Subarctic Ecosystem Response to Iron Enrichment Study
SOIREE	Southern Ocean Iron RElease Experiment
STF	Subtropical Front
T	Temperature
t	time
Z	Zooplankton

Unit conversion

Mass and moles

1 mol C = 12.0 g C

1 mol N = 14.0 g N

1 mol Chl *a* = 893.5 g Chl *a*

Standard biological conversions

1 mol N : 6.625 mol C

1 g Chl *a* : 50 g C

1 mol N : 1.59 g Chl *a*

Standard oceanographic measures

1 g C m^{-3} = 12.579 mmol N m^{-3}

1 mg Chl *a* m^{-3} = 0.629 mmol N m^{-3}

1 mmol C m^{-3} = 0.151 mmol N m^{-3}

1mM N m^{-3} = 1mmol N m^{-3}

1 mg at. N m^{-3} = 1 mmol N m^{-3}

CHAPTER ONE

Introduction

1.1 Opening remarks

This thesis is structured into six chapters: two introductory chapters, the first a general introduction, the second an introduction to the specific plankton model used; three chapters of research examining distinct problems; and a final conclusions and discussion chapter. Each research chapter opens with a short introduction to the appropriate subject matter and closes with a full discussion of the results. The final chapter aims to both summarise the thesis and to place the work it contains into context within the field of plankton modelling.

This general introduction is broken into a numbers of different sections. The chapter begins with a background review of the relationship between marine plankton-mediated primary productivity and changes in atmospheric CO_2 content, along with the role of iron in the present ocean. This is followed by a biological and physical introduction to plankton systems, which includes a description of the types of organisms encountered in such systems and modelled in this thesis. The following two sections are an overview of the Southern Ocean circulation, and an introduction to mathematical and ecological modelling. The chapter is then concluded by a brief rationale to outline the importance of plankton ecosystem to global biogeochemical cycles.

All abbreviations used in the text are listed in the preamble preceding this chapter. A table of the model currency units and their standard conversions to other currencies is also included in this section. Throughout almost all the thesis a standard currency is used (mmol N m^{-3}), but at several points where research is compared with other work or measurements, the currencies favoured by such works are used and these conversion measures applied.

1.2 Background

Increasing anthropogenic emissions of the greenhouse gases, such as carbon dioxide (CO_2), methane (CH_4) and nitrous oxide (N_2O), and their role in global warming are currently cause for great concern [*Riebesell et al.*, 2007; *Siegenthaler & Sarmiento*, 1993]. The world's oceans act as a carbon pump by transporting carbon from the surface waters to the ocean depths, through both biological (biological pump) and physico-chemical (solubility pump) processes [*Behrenfeld et al.*, 2006; *Chisholm*, 2000; *Longhurst*, 1991]. The oceans represent the largest carbon reservoirs on Earth, containing ~ 95% of the total circulating carbon within the biosphere, thereby controlling atmospheric CO_2 concentrations [*Siegenthaler & Sarmiento*, 1993]. Globally the oceans cover over 70% of the Earth's surface [*Costanza et al.*, 1997] and act as a primary habitat for photosynthetic organisms, which convert CO_2 into organic matter that may subsequently be used for energy. These photosynthetic microorganisms have long been recognized as the base of the food chain in ocean systems [*Ryther*, 1969]. Marine phytoplankton carry out as much photosynthesis as all the plants on land, contributing to 50% of global primary production [*Carr et al.*, 2006; *Field et al.*, 1998]. This Primary Production (PP) supports almost all marine life.

As in terrestrial plants, the chlorophyll pigment in the phytoplankton absorbs light, which is used as an energy source to fuse water molecules and carbon dioxide into carbohydrates. The major environmental factors that influence phytoplankton growth are light [*Marra*, 1978] and inorganic nutrients [*Dugdale & Wilkerson*, 1991]. When favourable conditions are encountered, phytoplankton can undergo rapid population growth usually referred to as "blooms" [*Riley*, 1942]. However, most of the time phytoplankton growth is either light limited (*e.g.* in winter at high latitudes) or nutrient limited (*e.g.*, in the subtropical gyres). Because light attenuates dramatically with depth, phytoplankton growth is restricted to the euphotic layer. Limiting inorganic nutrients such as nitrogen and phosphorus are constantly removed from the surface waters by the growing phytoplankton. Dissolved inorganic carbon (DIC) is also consumed by phytoplankton. Air-sea transfer of CO_2 at the sea surface keeps it always plentiful in the surface layer, contrary to limiting nutrients. Nevertheless, Sverdrup [1953] stated that in order that a phytoplankton bloom shall

begin it is necessary that in the surface layer the primary production exceeds the organic matter respiration. Assuming that the respiration of organic matter goes on independently of depth (in agreement with the assumption that the organisms are evenly distributed in the mixed layer) and that primary production decreases logarithmically with depth (corresponding to the decrease of light intensity), Sverdrup established that there must exist a *critical depth* such that blooming can occur only if the depth of the mixed layer is less than the critical value. More recently, Platt et al. [1991] pointed out that the Sverdrup critical depth criterion is a necessary, but not sufficient, condition for the initiation of phytoplankton blooms.

Most of phytoplankton are consumed locally by zooplankton, so that the nutrients comprising their biomass are regenerated at the surface and made available for another round of production. The Regenerated Production (RP) is that fraction of PP fuelled by limiting inorganic nutrients remineralised within the euphotic zone [*Eppley & Peterson*, 1979]. The Export Production (EP) is the portion of PP that finds its way to the deep sea through the sinking of dead cells and detritus, through zooplankton diel migrations, and sometimes by downwelling or mixing. Most of the EP is ultimately assimilated by bacteria, which regenerate it into inorganic forms. Globally and at steady state, the bio-mediated downward flux of organic matter is balanced by an upward return flux of inorganic nutrients that fuels New Production (NP). The f-ratio is the fraction of the total primary production that is fuelled by nitrate: (f-ratio = NP/RP+NP) [*Eppley & Peterson*, 1979]. This fraction is significant because it is directly related to the sinking (export) flux out of the surface mixed layer. It is estimated that bacterial respiration equals or exceeds primary production in vast areas of the oligotrophic (unproductive) open ocean [*Del Giorgio et al.*, 1997]. In more productive (eutrophic) ecosystems, primary production typically exceeds respiration allowing the oceans to act as net sinks for atmosphere CO_2 [*Duarte & Agustí* 1998].

Prior to the late 1970s, studies conducted on seawater suffered from the under appreciated possibility of contamination with metals. Even as far back as the 1930s, scientists recognized that factors other than phosphate, nitrate, light, and temperature could regulate phytoplankton growth [*Gran*, 1931]. In fact, it was concluded that iron (Fe) might be one of the factors affecting phytoplankton growth [*Hart*, 1942; *Harvey*, 1937]. Papers of this kind were discounted for decades due to the possibility of Fe

contamination thought to be present in the results. Since trace metals are required in only scarce amounts by marine microorganisms, any mishandling of samples can result in a greater concentration of metal in the collected sample than was present in ambient seawater [*Bruland et al.*, 1979]. Bruland *et al*. [1979] developed intricate cleaning protocols (termed trace metal – clean techniques), which allow scientists to accurately measure trace metals, which are now known to persist at only nanograms per litre (ng L^{-1}) concentrations in seawater. These techniques have allowed for an explosion of research examining the role of trace metals in microbial metabolism, of which the most well studied is Fe.

Iron is the fourth most abundant element in the Earth's crust (around 5.6%) and was present in high concentrations in seawater during the anoxic past of the Earth [*Falkowski*, 1997; *Turner & Hunter*, 2001]. Therefore, and due to its abundance and capacity to transfer electrons, Fe became a key element in many biochemical reactions. With the oxygenation of the atmosphere and oceans approximately 2 billion years ago, Fe was removed from the ocean by precipitation, resulting in the Precambrian "banded iron formations" that have been found in Australia, Asia and North America [*Evans*, 1987]. This removal process led to a shortage of available Fe for organisms in the ocean and Fe became a "hard to get essential element" [*Gran*, 1931; *Martin & Fitzwater*, 1988].

Concurrent with the development of the above ideas, shipboard incubations experiments became critical in understanding the factors that limit primary production in the world's ocean. Martin & Fitzwater [1988] and Martin & Gordon [1988] used these approaches to present evidence that phytoplankton in the open ocean are Fe-limited, which renewed a debate over what actually controls primary production in the sea, as well as how one determines what is a limiting factor [*Banse*, 1990; *Martin et al.*, 1990].

To better understand the relation between phytoplankton-mediated primary productivity and changes in atmospheric CO_2 content, along with the role of iron in the present ocean and why iron is an important element in the ongoing discussion about global warming, one has to understand the theories behind **(i)** the biological pump, **(ii)** High Nutrient Low Chlorophyll (*HNLC*) areas and **(iii)** the iron hypothesis.

(i) The *biological pump* is one of several mechanisms that regulates the greenhouse gas carbon dioxide (CO_2) in the atmosphere and therefore has a role in modulating the climate of the planet. The biological pump (Fig. 1.1) is the sum of a suite of biologically-mediated processes that transfer carbon from the surface of the euphotic zone to the ocean's interior, which in turn affects atmospheric CO_2 concentrations by air-sea gas exchange [*Falkowski et al.*, 1998; *Longhurst*, 1991]. In essence, CO_2 fixed during photosynthesis by autotrophs in the upper ocean is transported to deep waters by sinking organic particulate material (*e.g.*, dead/senescent organisms or faecal pellets) and in the form of dissolved organic carbon (DOC) by physical transport processes such as downwelling. Remineralisation and decomposition processes such as bacterial respiration return the organic carbon to dissolved carbon dioxide, but as these processes are commonly slower than synthesis processes, and because the particulate material is sinking, the biological pump provides net transport of carbon from the surface ocean to deep water [*Raven & Falkowski*, 1999]. The partition of phytogenic carbon between the two major pelagic food webs, namely the "microbial" and the "classical" food webs, control the quantity of carbon flux to depth, and thus the efficiency of the biological pump [*Neuer et al.*, 2002; *Sherr & Sherr*, 1988]. The overall effect of these biological processes is a reduction in the partial pressure of carbon dioxide (CO_2) in surface waters, thereby resulting in the drawdown of atmospheric CO_2, along a concentration gradient from the atmosphere to the surface water [*Metzl et al.*, 1999]. Consequently, this biological sequestration of CO_2 into the deep ocean via sinking of particulate material may prevent CO_2 from reentering the atmosphere for long periods of time of up to centuries. The amount and duration of CO_2 storage in the deep ocean is controlled by the deep ocean circulation and the net flux of carbon deposited and buried in the seafloor sediments [*Sarmiento & Gruber*, 2002].

One essential nutrient for phytoplankton (and therefore the biological pump) is iron. Due to its abundance and capacity to transfer electrons, it is a key element in many biogeochemical processes such as photosynthesis [*Geider & La Roche*, 2004], nitrogenase catalysis, nitrate reductase [*de Baar & La Roche*, 2003; *Timmermans et al.*, 2004], detoxification of reactive oxygen species [*Sunda & Huntsman*, 1995], and nitrogen fixation [*Mills et al.*, 2004]..

Natural sources of iron in the open ocean include atmospheric deposition with dust and rain [*Jickells et al.*, 2005], upwelling and lateral transport [*DiTullio et al.*, 2005; *Lam et al.*, 2006], hydrothermal input [*Tagliabue et al.*, 2010], volcanic eruptions [*Duggen et al.*, 2007] and extra-terrestrial dust [*Johnson*, 2001], with regional variance in the importance of each source. Ice melt also represents a significant contribution to the iron pool via seasonal release [*Lannuzel et al.*, 2007; *Sedwick & DiTullio*, 1997], In coastal and shelf regions, iron from resuspended shelf sediments and upwelling is assumed to be the main source rather than riverine sources [*Elrod et al.*, 2004; *Johnson et al.*, 1999]. Recently, there is also evidence of significant long-range transport of shelf sediments into the open ocean [*Ardelan et al.*, 2010].

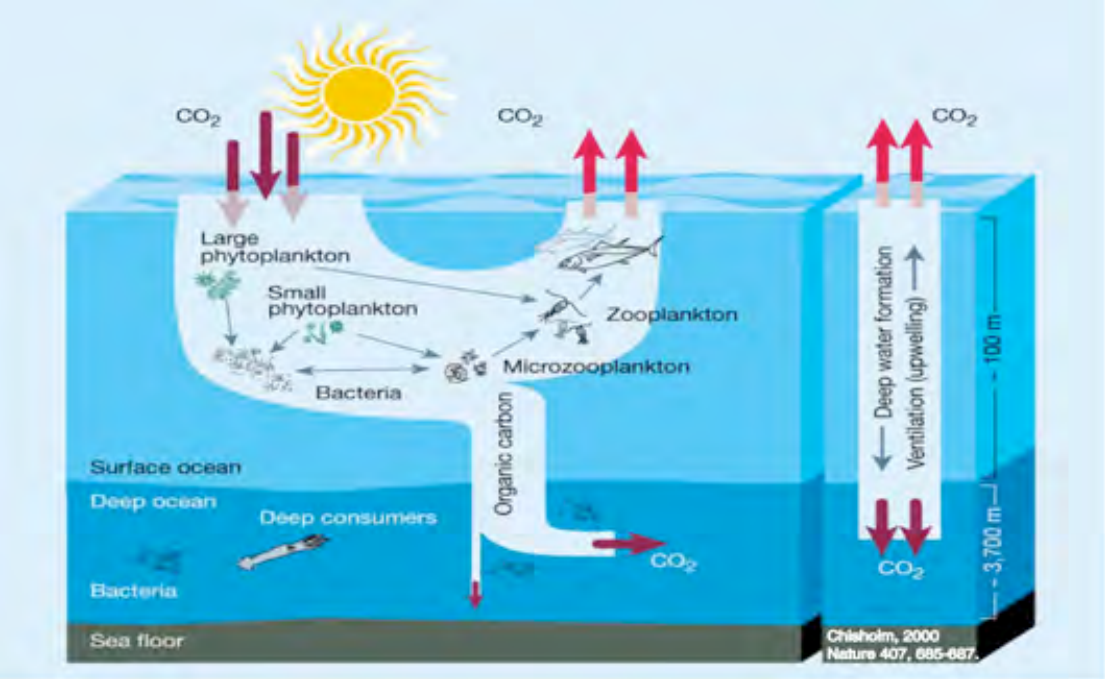

Figure 1.1: A simple schematic representation of the biological pump (left) and physical pump (right) [*Chisholm*, 2000].

(ii) The so called *HNLC* (High Nutrient Low Chlorophyll)-areas are regions of the ocean where the phytoplankton biomass (standing stock) is low in spite of high macro-nutrient availability (nitrate, phosphate, silicic acid) which are apparently not fully utilized by the phytoplankton [*Cullen*, 1991]. The *HNLC* condition has

been observed in the equatorial and north-east Pacific Ocean as well as in the Southern Ocean which comprise 30% of the World Ocean [*de Baar et al.*, 1999]. There are different theories why these areas have low biological productivity. In the Antarctic and subarctic Pacific light limitation is important [*Mitchell et al.*, 1991; *Sunda & Huntsman*, 1997]. In the equatorial Pacific and north of the Polar Front in the Southern Ocean, silicate limitation plays a role [*Dugdale & Wilkerson*, 1998; *Takeda*, 1998]. There may also be other nutrient limitations, for instance other trace metals such as copper [*Coale*, 1991; *Ianni et al.*, 2002] and zinc [*Franck et al.*, 2003]. In oceanic surface waters, the concentration of dissolved iron commonly ranges between 0.02 nM to 1nM. However *HNLC* areas all have extremely low iron concentration (0.02-0.05 nM), reflecting a lack of the natural sources of iron in these regions [*Sedwick et al.*, 2008; *Turner & Hunter*, 2001]. These concentrations are low enough for dissolved Fe (dFe) to be diffusion limiting with respect to growth rates for all but smallest phytoplankton cells (*i.e.* picoplankton: planktonic organisms < 2 μm diameter) [*Sunda & Huntsman*, 1995]. These organisms are more efficient nutrient scavengers under oligotrophic conditions possibly due to their greater surface area-volume ratio and are more effective at assimilating iron [*Sunda & Huntsman*, 1997]. Microzooplankton (grazing organisms ranging from 2 to 20 μm) are responsible for keeping the populations of picoplankton lower by grazing [*Hunt & Hosie*, 2006; *Price et al.*, 1994]. When iron is added to these waters, diatoms are thought to proliferate due to their ability to grow at faster rates than both the organisms that normally graze upon them and the smaller species that compete for nutrients when in limited amounts [*Geider & La Roche*, 2004]. These interactions are difficult to study using shipboard bottle experiments, as they often do not account for grazing activity or vertical export in the water column [*Buma et al.*, 1991].

(iii) First Gran [1931] and then Martin & Fitzwater [1988] developed the *hypothesis of Fe limitation* of the Southern Ocean. Several in-situ iron fertilization experiments were conducted in the three *HNLC* regions [*Boyd et al.*, 2007; *de Baar et al.*, 2005]. The critical role of iron as a limiting nutrient in *HNLC* regions has been repeatedly demonstrated by these experiments and has been established as one of several co-limiting factors in these regions. Similarly,

laboratory analysis of ocean sediment cores suggest that a larger iron supply to the *HNLC* regions in glacial times could have stimulated primary productivity, leading to lower concentrations of atmospheric CO_2 [*Kumar et al.*, 1995; *Petit et al.*, 1999]. More recently, upwelling regions off the west coasts of North and South America have been discovered to be Fe-limited as well [*DiTullio et al.*, 2005; *Eldridge et al.*, 2004].

Geoengineering has boosted the interest in artificial iron enrichment on a large scale as a tool for climate regulation through stimulation of the biological pump [*Aumont & Bopp*, 2006]. However it is uncertain whether extensive artificial iron fertilization is a realistic method to reduce anthropogenic carbon in the atmosphere [*Boyd et al.*, 2007; *Buesseler & Boyd*, 2003; *Chisholm et al.*, 2001]. The ecological consequences and possible unintended climatic feedbacks of such interference in the complex cycle of the global climate through manipulating the marine component are still incalculable and therefore it could be seen as irresponsible [*Trull et al.*, 2008].

1.3 What are plankton?

Essentially, plankton are communities or populations of organisms whose powers of locomotion are insufficient to prevent them form being transported passively by their surrounding medium [*Omori & Ikeda*, 1992].

Although the term is generally confined to microscopic organisms in open water (or pelagic) habitats, it also applies to both organisms of greater size, and to organisms that live in quite different habitats. Macroscopic coelenterates (such as jellyfish) and algae (such as pelagic *Sargassum* sp.) provide examples of larger organisms whose movements are mainly determined by the water currents they find themselves in. The distinction between planktonic species and non-planktonic species is additionally blurred by organisms, such as fish, which shift from the plankton to the *nekton* (organisms whose locomotory abilities are sufficient to allow them to avoid being passively transported) as they grow to adulthood.

In this thesis, however, the plankton under consideration are aquatic and microscopic. More specifically, they are confined to the pelagic environment of the open ocean. This environment has the advantage of being comparatively isolated from the influences of shallower coastal environments.

1.4 Plankton assemblages

The planktonic assemblages of aquatic systems include representatives of every major living group. Although phylogeny and traditional taxonomy are a fundamental source of information about individual plankton species, the intricate mix of species in plankton ecosystems is usually less finely treated in most matters of ecology. Species are in general grouped into classes based on their size, trophic position or coarse phylogenetic/functional group.

1.4.1 Classification by size

One of the principal characteristics used to classify members of the plankton is their size. To some extent this has an historical basis, since plankton groups have often only been discovered and quantified as more and more accurate techniques have become available. Table 1.1 presents an example of size-based classification. Note that while organisms at the top and the bottom of the table are separated by 5 orders of magnitude in length or diameter, in volumetric terms they may be separated by up to 15 orders of magnitude.

In the terrestrial environment, ecological pathways between organisms are often not linked to their size. For instance, photosynthetic organisms such as trees are usually grazed upon by organisms across a wide range of size, from insects through to elephants. In the same way, predatory organisms often feed on sizes of prey above and below their own size. This is partially because gravity dominates terrestrial systems and the medium (air) is relatively non-viscous. Prey to be consumed, or

photoautotrophs to be grazed, consequently remains broadly in one place, allowing the consumer to ingest them at leisure.

Table 1.1: A grouping of planktonic organisms based on size classification. See later text for details about organisms. The latter three groups are often referred to as *net plankton* since they can be accurately quantified by sampling with nets. The former three groups are usually sampled by means of water bottles and sample filtration. After Omori & Ikeda [1992].

Group	Diameter	Major organisms
Ultrananoplankton	< 2 μm	Prokaryotic plankton
Nanoplankton	2 – 20 μm	Small phytoplankton, protistan zooplankton, and fungi
Microplankton	20 - 200 μm	Most phytoplankton and protistan microzooplankton, juvenile metazoan zooplankton
Mesoplankton	200 μm - 2mm	Metazoan zooplankton (*e.g.*, appendicularians, copepods, cladocerans)
Macroplankton	2 – 20 mm	metazoan zooplankton (*e.g.*, pteropods, copepods, euphsiids,)
Megaplankton	> 20 mm	Metazoan zooplankton (*e.g.*, cephalopods, euphasiids, scyphozoans, thaliaceans)

On the other hand, in aquatic ecosystems, the viscosity of the medium makes it much more difficult to move through it, and much easier for organism to find themselves carried passively through it. This is predominantly true for smaller organisms, and this physical phenomenon is often described by a ratio known as the Reynolds number. As a result, often neither prey nor predator are static, and felled prey are unlikely to stay for long at a constant depth even in a still water column. Therefore, predators (grazers) tend to merely consume other organisms of smaller

size, since these organisms can be ingested directly. This situation is exacerbated in pelagic conditions by selective pressures on active consumers to be hydrodynamic so that locomotion (*i.e.*, when chasing prey) through the medium may be more efficient. These pressures tend to prevent the evolution of grasping structures that could otherwise be used to hold prey in one place while they were consumed [*Barnes & Mann*, 1991].

Reynolds numbers (*Re*) are frequently used to quantify the importance of forces due to the viscosity in a given medium. The number is a ratio of the inertial to viscous forces acting on an object. The inertial force here is the force which was required to accelerate the object to the velocity at which it is travelling. The ratio is calculated by dividing the velocity of the object, *u*, times its typical dimension, *d*, by the kinematic viscosity of the medium, *v*:

$$Re = ud/v \tag{1.1}$$

The usual dimension here may be the length or width of an organism around which the fluid flow is occurring. Smaller organisms are more affected than larger ones by the viscosity of the medium, and are therefore more liable to have their movements disrupted by movement of the medium [*Mann & Lazier*, 1996].

Raven [1995] reviewed the dominance of different size and lifestyle classes of photosynthetic organisms in aquatic environments. He concludes that microscopic organisms dominate the pelagic environment through factors such as their better performance at lower irradiances (since they have a higher relative photon absorption than larger plants, and have less non-photosynthetic tissues to “waste” energy on) and their smaller boundary layers (which affect nutrient uptake). Furthermore, since the sea floor in the ocean is normally much deeper than 270 m (the deepest known marine plant life ever recorded; [*Littler et al.*, 1985]), attached macrophytes are excluded from the statement.

In terms of the biological pump, macroplankton produce large, dense faecal pellets, which have a relatively high carbon content and are fast-sinking [*Fortier et al.*, 1994]. For example, salp (tunicate) faecal pellets have a sinking rate of up to 2700 m d^{-1} [*Fortier et al.*, 1994] and a carbon content of up to 37% [*Bruland & Silver*,

1981]. Macroplankton also undergo extensive diel vertical migrations, which further contributes to carbon flux through respiration and egestion at depth [*Longhurst*, 1991]. In contrast, mesoplankton produce relatively small, slow-sinking faecal pellets, with sinking rates of ~ 100 m d^{-1} [*Fortier et al.*, 1994]. In addition, copepods (mesoplankton) demonstrate coprophagy (re-ingestion of faecal pellets) and coprohexy (disintegration of faecal pellets), thereby greatly reducing the amount of faecal material that reaches the ocean bottom [*Lampitt et al.*, 1991; *Noji et al.*, 1991]. Mesoplankton also undergo diel vertical migrations, enhancing in this way their contribution to carbon flux through respiration and egestion at depth.

Microplankton generally contributes little to carbon flux. For example, microzooplankton produce mini-faecal pellets which remain in suspension for extended periods resulting in the majority of the carbon in the pellets being decomposed/recycled by bacteria in the euphotic zone [*Azam et al.*, 1983]. In addition, microheterotrophs generally have high assimilation efficiencies, which result in faecal pellets with a low carbon content. Finally, microplankton do not undertake extensive diel migrations, still further restricting their role in the transport of carbon to depth.

It can be assumed, therefore, that in regions where macrozooplankton represent the most important consumers of phytoplankton, the efficiency of the biological pump will be high [*Fortier et al.*, 1994]. Carbon flux is reduced in regions where mesozooplankton represent the dominant consumers of phytoplankton production, and in a system dominated by microheterotrophs, it would be minimal [*Fahnenstiel et al.*, 1995].

1.4.2 Classification by trophic position

A common way in which planktonic species assemblages have been studied is by grouping the various species present into several groups of broadly analogous functionality. This can simplify both the measurements and analysis of ecosystems. It is also particularly interesting to modellers [e.g. *Jin et al.*, 2006; *Platt et al.*, 2005] since it allows them to represent the systems in question by a relatively small number

of variables. The following sections aim to briefly outline the main characteristics of the two broad ecological groups distinguished in the model in later chapters.

Phytoplankton

Phytoplankton form the foundation of the majority of pelagic marine ecosystems. As photoautotrophs they obtain the energy they use from solar irradiation they absorb using their photosynthetic pigments. This energy is trapped in organic carbon compounds and used by the phytoplankton cells for their different metabolic processes, including cell reproduction. As well as their requirements for irradiance and inorganic carbon (CO_2 or HCO_3^-), phytoplankton cells also make use of a number of inorganic nutrients and trace substances which they normally uptake directly from the surrounding medium. These nutrients are used for various cellular processes including amino acid synthesis (nitrogen nutrients), DNA replication (phosphates), enzyme co-factor (iron, zinc, manganese), cell walls/coverings (silicate, calcium carbonate), carbon fixation (iron, manganese), synthesis of photopigments (iron and others), silica uptake in large diatoms (zinc, cadmium, copper), and others (see GEOTRACES [2006] for a complete review).

Phytoplankton are frequently motile and may use this to position themselves more favourably within the water column with respect to nutrients or irradiance. Alternatively, they may use motility to disrupt the boundary layer of fluid surrounding them to facilitate nutrient uptake. Since the turbulence of mixed layer environment restrains the control of cells over their position within it, this latter role for motility is expected to be the more significant one, at least while the water column is subject to strong mixing.

As in terrestrial ecosystems, photoautotrophs in the ocean also attempt to protect themselves from herbivorous grazers. Ghadouani *et al*. [2004] and Ianora *et al*. [2004] describe chemical interference of zooplankton grazers by their phytoplankton prey. In the former case this occurs through interference with the feeding mechanisms of the grazers, and in the latter case by disruption of the developmental processes of the zooplankton grazer. The formation of complexes or long chains of diatoms cells (*e.g.*,

Chaetoceros sp., *Skeletonema costatum*), as well as the long spines which are characteristic of several diatom and dinoflagellates may at least partially serve the same function [*Van den Hoek et al.*, 1995].

While the statements above are usually true across the species regarded as phytoplankton, there are many major groups of phytoplankton whose differences merit separate discussion. Although the models considered in this thesis do not distinguish these groups, it is not uncommon for models of specific situations to do so, and it may be necessary for any model that aims to be "robust" across the world ocean.

An initial distinction is between photosynthetic eukaryotes and prokaryotes. The former are usually larger and have a cell structure characterised by the possession of a cell nucleus and organelles (themselves formerly symbiotic bacteria – or even other eukaryotes). Prokaryotes are bacteria with relatively simpler cell structure and generally much smaller size. Until recently, prokaryotes in the oceans were believed to be almost exclusively eubacterias ("modern" bacteria). However, a survey of the coastal waters of Antarctica [*DeLong et al.*, 1994] found that up to 34% of the prokaryote biomass was actually made up of archeabacteria, a group of bacteria believed to be of very limited relevance globally. While the full ecological importance of this discovery is yet unclear, it does point out that knowledge of the ocean ecosystem is still very much incomplete.

Although the importance to primary production of the archeabacteria is indeterminate, the eubacteria known as cyanobacteria (Kingdom **Eubacteria**, Division **Cyanophyta**) are of well known significance globally [*Liu et al.*, 1997; *Tortell*, 2000]. In the oceans their importance lies with their fast growth rates and their trophic position as members of the microbial loop [*Azam*, 1998].

One of most important eukaryote groups are diatoms (Kingdom **Eukaryota**, Division **Heterokontophyta**, Class **Bascillariophyceae)**. These algae are distinguished predominantly by their possession of a unique silica cell wall that takes the form of two overlapping frustules, or valves. It is estimated that there are more than 10^4 species in the class [*Smol & Stoermer*, 1999] and that together the marine planktonic diatoms can account for 13 to 26% of annual primary production at the Bermuda Atlantic Time-series [*Brzezinski et al.*, 1998] and for a third of primary

production in the western equatorial Pacific [*Blain et al.*, 1997]. By use of mesocosms experiments, Egge & Aksnes [1985] found that as long as the nutrient silicate remained above certain concentration, diatoms were always able to dominate the phytoplankton assemblage. This would agree with their dominance in spring blooms of certain region when silicate is plentiful. However, silicate (unlike nitrogen nutrients) is not regenerated efficiently by higher trophic levels, and diatoms in general become silicate limited relatively quickly as a consequence and have to wait until mixing deepens enough to re-introduce silicate to the photic zone [*Dugdale et al.*, 1995]. This waiting may occur in deeper waters which are reached by the diatoms either as fast sinking spores [*Van den Hoek et al.*, 1995] or as large aggregates of cells [*Hoffmann et al.*, 2006; *Passow et al.*, 1994]. Deep mixing prior to spring blooms re-introduces both these sunken cells and silicate to the mixed layer.

Another important phytoplankton group are the coccolithophores (Kingdom **Eukaryota**, Division **Prymnesiophyta)**. They are distinguished by their production of organic scales covered in a layer of calcite ($CaCO_3$). These are important in the biogeochemical cycle of carbon, since the production of the scales uses HCO_3^- and therefore increases the concentration of dissolved CO_2. The coccolithophores (of which the species *Emiliana huxleyi* is possibly the most well-known) are also important because of the changes they can induce in the local optical environment [*Balch et al.*, 1996; *Balch et al.*, 2001]. These changes affect both other phytoplankton and the heating of the surface waters of the ocean.

The dinoflagellates (Kingdom **Eukaryota**, Division **Dinophyta)** are an interesting and important group with around 2000 existing species (and a rich fossil record of extinct species). They typically have two flagella and are often distinguished by the complex “armour” which covers them. This is believed to aid in either reducing their sinking rate or deterring grazers, or both. Although they have relatively slower growth rates [*Strom & Morello*, 1998], they can form a major component of the phytoplankton assemblage [*Prezelin et al.*, 2000; *Smith & Asper*, 2001]. Usually their dominance in assemblages occurs in the summer after that of the of the diatoms, and some prefer more stable vertical water column which occurs during these months [*Smol & Stoermer*, 1999]. Additionally they can be a major component of the microzooplankton assemblage [*Blain et al.*, 1997], as facultative or obligate heterotrophs. Raven [2006] reviews the importance of such heterotrophy in

phototrophs. Interestingly, as well as capturing other algae for their photosynthetic capability, dinoflagellates themselves are often found in symbiosis with larger organisms (*e.g.*, corals). They are additionally important because of their role in toxic blooms (known as *red tides* because of their colour), which may affect coastal fisheries [*Rintoul*, 2000; *Strom & Morello*, 1998].

Zooplankton

Similarly to the phytoplankton, the assemblage that makes up zooplankton is also a complex mixture of different species and phylogenetic groups. However, while almost all of the members of the phytoplankton share a common trophic position (*i.e.*, autotrophs), zooplankton species include herbivores, bacterivores, detritivores and carnivores.

Most modelling efforts ignore these subtleties and focus on the grazing of phytoplankton biomass. Because of they smaller size, microzooplankton graze on the smaller fraction of the phytoplankton (*e.g.*, autotrophic bacteria). They also feed on free-living heterotrophic bacteria. In turn, they are consumed by larger, metazoan zooplankton, which may feed on them along with the larger phytoplankton fractions (since their size range overlaps that of eukaryotic phytoplankton). These zooplankton may be adults or juveniles of even larger zooplankton fractions. Some of these juveniles (or larval stages) are only temporary members of the plankton system and later become benthic at adult stages (*e.g.*, bivalves, corals, barnacles, echinoderms). These organisms utilise the plankton as means of dispersal and as a source of food.

An important ecological outcome of zooplankton grazing of phytoplankton is the fate of the biomass consumed. Phytoplankton are often limited by nutrient availability, and if processes don’t replace these nutrients, productivity might cease. As already mentioned, diatoms may become limited because one of their key nutrients, silicate, is not regenerated efficiently. However, other nutrients, including the nitrogen ones considered by the models in this thesis, are regenerated through the zooplankton or their predators, and heterotrophic bacteria. Hutchins & Bruland [1994] have examined the regeneration of trace metal in plankton systems. However, the production of fast sinking faecal pellets by larger organisms, such as the predators of zooplankton, but also the zooplankton themselves, does act to remove biomass from

the mixed layer without giving it sufficient time to be regenerated. As previously indicated, such sinking fluxes of organic material to the deep ocean are of interest. These processes make higher predators, such as larger zooplankton or nekton, an important component of plankton systems.

Microzooplankton are represented by several major protozoan groups. In addition to the dinoflagellates, the ciliates (Kingdom **Eukaryota**, Phylum **Ciliophora**), the tintinnids (subdivision or the ciliates), and the foraminiferans (Kingdom **Eukaryota**, Phylum **Rhizopoda**, Class **Granuloreticulosea**, Order **Foraminifera**) are important groups. The foraminiferans are ameboides characterised by their possession of a shell (organic or calcareous). The ciliates are one of the largest groups of protozoans, and have a relatively high degree or organelle development. Their name derives from the cilia they possess, which are used for locomotion or feeding. They are heterotrophic, like the foraminiferans, but have a much more specialised feeding apparatus (which often includes a cell mouth or *cytostome*). Tintinnids are a widely distributed order of ciliates characterized by the secretion of a shell (or *lorica*) which often contains foreign particles [*Begon et al.*, 1996]. As well as often dominating the ciliate community [*Omori & Ikeda*, 1992], they can be of significant importance in the microzooplankton link to microbial food webs. Juveniles of some of the larger metazoan zooplankton also form part of the microzooplankton (*e.g.*, copepod nauplius larvae).

The meso- and macrozooplankton are represented by many metazoan groups. The most important groups are almost certainly the copepods (Kingdom **Eukaryota**, Phylum **Arthropoda**, Class **Crustacea**, Subclass **Copepoda**). Omori & Takeda [1992] report that in samples of net plankton from most waters, generally 80% or more of the individuals caught are copepods. As a group they include herbivores, omnivores, detritivores and carnivores. Their relatively large size permits much greater mobility and this is often manifested in diel vertical migration, where organisms spend different parts of the day at different depths in the water column. There are several proposed reasons for this migration including predator avoidance, food abundance and metabolism control [*Gonzalez & Smetacek* 1994; *Steinberg et al.*, 2002]. This vertical relocation may have important consequences for sinking particle flux by means of zooplankton egesting consumed material at depth [*Priddle et al.*, 1997].

There are several other important crustacean zooplankton groups, including the euphasiids (*e.g.*, krill) and the cladocerans (*e.g.*, *Daphnia*). These share many of the characteristics of copepods. Other important groups include: cephalopods, pteropods, and heteropods; ctenophores and scyphozoan coelenterates; and the thaliaceans and appendicularians. These latter two groups are considered important because of their production of fast-sinking faecal pellets [*Deibel & Turner*, 1985; *Touratier et al.*, 2003].

An important issue in zooplankton grazing is how specifically the zooplankton graze. At the unicellular level, phagocytosis is one such process used, which requires direct contact between the prey and the predator cells [*Buck et al.*, 1990]. Because of their size and more complex anatomy, multicellular metazoans have numerous different procedures to food acquisition. While some actively hunt (*e.g.*, euphasiids, polychaeta), others rely on passive contact (*e.g.*, coelenterados and ctenophoros; the former use poisoned barbs, the latter adhesive compounds). The appendicularians feed uniquely by using a gelatinous covering that is secreted around their bodies. The thaliaceans feed using a continuously generated mucus net particle-trap. In a related issue, Alcaraz [2002] has suggested that the role of turbulence should be considered in all feeding interactions. As well as directly affecting contact rates between organisms, he proposes that organisms may take advantage of turbulent energy rather than use their own metabolic energy to capture prey.

1.5 Ocean physics

In addition to purely biological interactions, most organisms on the ocean are also greatly influenced by the physics of the medium they inhabit. This influence operates on many different scales, from the forces and factors affecting a single cell to those that control the biological productivity of ocean basins.

1.5.1 Irradiance and ocean heating

The upper ocean is warmed by radiation from the sun. This takes the form of mostly shorter wavelength radiation in the visible and infrared regions of the electromagnetic spectrum. The amount of radiation reaching the top of the Earth's atmosphere varies with both season and latitude given that both of these parameters affect the angle of the incident solar radiation relative to a given position on the Earth (Brock [2009] derived a standard astronomical formulae that can calculate the spatial and temporal patterns of irradiance across the Earth; see Chapter 2). Correcting this radiation flux to account for the effect of the atmosphere is considerably more complicated (Chapter 2 describes the empirical correlation algorithm used in this thesis). Even after entering the Earth's atmosphere, some of the radiation that reaches the surface is lost by reflection at the surface of the ocean (this *albedo* is particularly high when the ocean surface is covered in sea ice and this is especially significant in the Southern Ocean around Antarctica).

Once radiation has penetrated the ocean's surface it is attenuated in the water column as it is absorbed by both the material within the water column, and by water itself. The rate of attenuation varies with the wavelength of the radiation, and for a given wavelength, λ, can be described as follows (*i.e.*, Beer-Lambert Law):

$$I_z = I_0 \, \mathrm{e}^{-K_\mathrm{d}(\lambda)} \tag{1.2}$$

where I_z is the intensity of irradiance at depth *z*, given the intensity of irradiance just below the water's surface, I_0, and the attenuation coefficient for irradiance of wavelength λ, $K_d(\lambda)$ (assuming that $K_d(\lambda)$ is constant down the water column) [*Mann & Lazier*, 1996]. The attenuation coefficient is variable between different wavelengths and varies with the concentration of material within the water column (mainly phytoplankton in oceanic 'blue' waters). For longer wavelength radiation such as infrared, the coefficient can be as high as 20 m^{-1}. The attenuation coefficients of water at shorter wavelengths (*e.g.*, photosynthetic active radiation (PAR)) are considerably smaller (visible red and blue wavelengths have coefficients of around 0.4 and 0.004 m^{-1} respectively). However, even with these low attenuation coefficients, the majority of radiation that enters the water column is absorbed within the first 10 m.

1.5.2 Vertical structure and mixing

One might expect that this pattern of irradiance absorption would lead to a similar thermal vertical structure in the water column, as the energy of the absorbed photons is transformed to thermal energy. However, as measurements of the vertical profile of temperature reveal, processes that mix the water column typically disrupt the pattern of energy dissipation. These processes include stirring by the wind and convection generated by the loss of heat at the surface of the water. This leads to the generation of a so-called *mixed layer* at the surface of the ocean with a relatively homogeneous thermal structure. This layer overlies cooler water, and between the two layers there is a region known as the *thermocline* across which the temperature changes from the relatively higher surface temperatures to the lower deeper ones.

The thermal differences between the mixed layer and the deeper ocean leads directly to differences in the density of the layers. Deeper water is cooler and denser, while mixed layer water is warmer and lighter. A region across which density changes, the so called pycnocline, also separates the layers. This acts to reduce the exchange between the layers. Consequently the layers become relatively isolated, with the isolation increasing with the density difference between the two layers. Since the irradiance used by phytoplankton is mostly confined to the mixed layer (the region in

which irradiance is sufficient to promote net phytoplankton growth is known as the *photic zone*), but the nutrients are replenished from the deep ocean, the reduced interchange between the surface and deep(er) ocean layers has interesting biological consequences (Fig. 1.2).

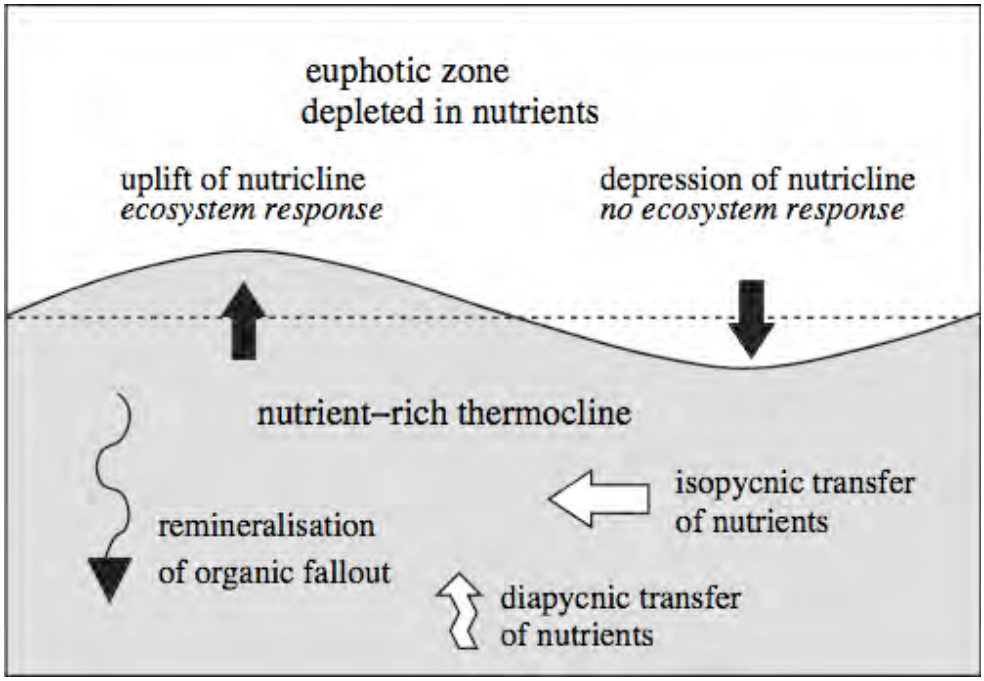

Figure 1.2: Diagrammatic representation of the ecosystem response to an uptlift and depression of the nutricline. When nutrient-rich isopycnals are raised into the euphotic zone, there is biological production. Conversely, when the nutrient-rich isopycnals are pushed into the dark interior, there is no biological response. The nutrient concentrations in the thermocline are maintained by remineralization of organic fallout, diapycnal transfer or lateral influx of nutrients. After Williams & Follows [2003].

The depth of the mixed layer (and thus the extent of the thermocline) varies with wind and solar forcing. The more energy is transferred to the ocean by winds, the greater the turbulence and the deeper the resulting mixed layer. However, the effects of wind mixing can be countered by the increased buoyancy caused by solar heating of the surface waters. Townsend *et al*. [2000] examine the influence of mixing and the stabilization of a shallow mixed layer on the timing of the spring phytoplankton bloom.

The mixing described above takes place mostly as a result of the turbulence introduced into the ocean system by instability mechanisms that affect large-scale water motions. Turbulence itself, despite its appearance as random water movement, is a complex phenomenon produced by the dissipation of kinetic energy to smaller and smaller scales. This process is known as the *energy cascade* [*Hopkins & Fauci*, 2002; *Murray*, 2002]. The kinetic energy is continually transferred to smaller scales until the process creates structures that are small enough that molecular diffusion becomes important and viscous dissipation of energy finally takes place. This restricts eddies to minimum sizes of just a few millimetres. As a consequence, organisms smaller than ~1mm are forced to rely on molecular diffusion to supply them with nutrients, unless they move relative to the water by sinking or swimming [*Mann & Lazier*, 1996].

In addition to turbulent mixing, the mixed layer is also affected by a process known as Langmuir circulation. Above a wind speed of around 3 m s^{-1}, this produces coherent horizontal structures which line up in the same direction as the wind. These structures can be up to 200 m in diameter, and are often identified from the debris accumulation which occurs on the sea surface where two structures converge [*Lotka*, 1925]. As well as providing another mechanism to mix the surface waters, studies have found that in certain regions this structure can cause rapid dispersion of plankton, and in other regions hold them for long periods of time [*Ehn et al.*, 2004; *Volterra*, 1926] (Mann & Lazier [1996] provide a more thorough review of the issue).

1.5.3 Large scale circulation: The Southern Ocean case

The previous section briefly described some of the physical phenomena which affect plankton systems at the small (individual organism) and medium (mixed layer) scale. The model used in this thesis is applied at the medium scale, but is often applied [e.g., *Ehn et al.*, 2008; *Oschlies & Garçon*, 1999; *Solomon*, 2007] at larger scale (*e.g.*, ocean basin). To put such related work in context, this short section outlines some of the physical processes in operation at such scale, focusing on the main area of interest in this thesis: the Southern Ocean.

Representing roughly a third of the world's ocean, the mid- and high-latitude Southern Hemisphere oceans play a significant role in determining the global climate. Covering an expanse of ~ 38 million km^2 of open ocean, it is the largest continuous body of water on Earth and is responsible for linking the Atlantic, Indian, and Pacific Ocean. These waters are the world's largest oceanic sink of CO_2 [*Idso & Singer*, 2009] and wind energy [*Singer*, 2008]. The southern boundary of the Southern Ocean is represented by the Antarctic continent and the northern boundary, although not geographically fixed, coincides with the location of the Subtropical Front (STF) [*Pachauri & Reisinger*, 2007; *Trull et al.*, 2001a].

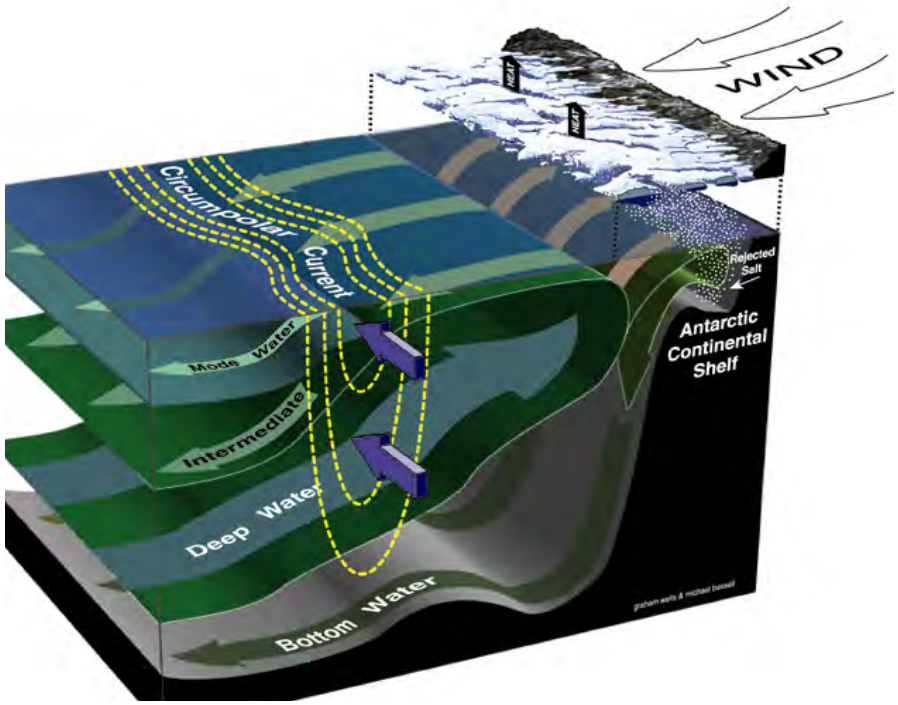

Figure 1.3: A schematic cross-section of the Southern Ocean, illustrating the water mass transformations that connect the layers involved in the Southern Ocean overturning circulation [*Rintoul*, 2000].

In the Southern Ocean, deep water that upwells near the Antarctic spreads poleward and is converted to denser (colder) water over the continental shelf that sinks to become Antarctic Bottom Water. Deep water that upwells further north is made less dense by warming and addition of freshwater (precipitation and sea ice melting water) as it spreads north in to the surface layer of the ocean. The lighter water eventually sinks to form Subantarctic Mode Water (SAMW) and Antarctic Intermediate Water (AAIW) (Fig. 1.3). As the water masses sink from the surface, they carry oxygen and other gases like carbon dioxide with them into the ocean's interior. Southern Ocean water masses 'ventilate' roughly half of the volume of the world ocean and account for about 40% of the total ocean storage of anthropogenic carbon dioxide [*Sabine et al.*, 2004]. Sarmiento *et al.*, [2004] concluded that nutrient-rich Subantarctic Mode Water exported from the Southern Ocean fuels 75% of global ocean primary production. Therefore, changes in Southern Ocean circulation, stratification and sea ice could have global impacts on biological productivity and biogeochemical cycles [*Matear & Hirst*, 1999; *Miller*, 2003].

Two major currents exist within the Southern Ocean, the "East Wind Drift", a narrow current bordering the Antarctic continent, and the "West Wind Drift", commonly referred to as the Antarctic Circumpolar Current (ACC) [*May*, 2001]. The ACC is made up of a series of cores of varying intensities [*Nowlin Jr et al.*, 1977]. The Polar Frontal Zone (PFZ), situated within the ACC, is bounded by two high-speed cores, namely the Subantarctic Front (SAF), to the north, and the Southern ACC Front (SACCF), to the south [*Bees et al.*, 1997; *Orsi et al.*, 1995; *Trull et al.*, 2001a] (Fig. 1.4). These fronts are generally considered to be regions of steep meridional gradients of temperature, salinity and nutrients [*Deacon*, 1982; *Findlay et al.*, 2006] and, therefore, represent important biogeographic boundaries to the distribution of planktonic species (*e.g.*, diatoms dominate in the silica-rich waters in the south, coccolithophores dominate in silica-poor waters north of the Subantarctic Front) [*Freund et al.*, 2006; *Sullivan et al.*, 1993]. It has become accepted terminology to call the region between the Subantarctic and Subtropical Fronts the Subantarctic Zone (SAZ) [*Pollard et al.*, 2002; *Sloyan & Rintoul*, 2001]. There are significant water property changes across the Subtropical Front because the subtropical gyre waters found to the north are much warmer and saltier than waters in the Subantarctic Zone. The position of these fronts varies with time and is strongly affected by the

local bathymetry [*Sokolov & Rintoul*, 2007a]. The boundaries of the PFZ, the SAF and SACCF, demonstrate a high degree of mesoscale variability [*Malthus & Bonar*, 1926], including eddies [*Truscott & Brindley*, 1994] and meanders in both fronts. These mesoscale features result in increased mixing of Subantarctic Surface Waters (SASW) and Antarctic Surface Waters (AASW) within the PFZ, with foreign bodies of water intruding from the north and south as extensions of the SAF and SACCF, respectively [*Perissinotto et al.*, 2000]. An extensive review of the dynamics of the ACC can be found, for example, in [*Miller*, 2003; *Steele & Frost*, 1977].

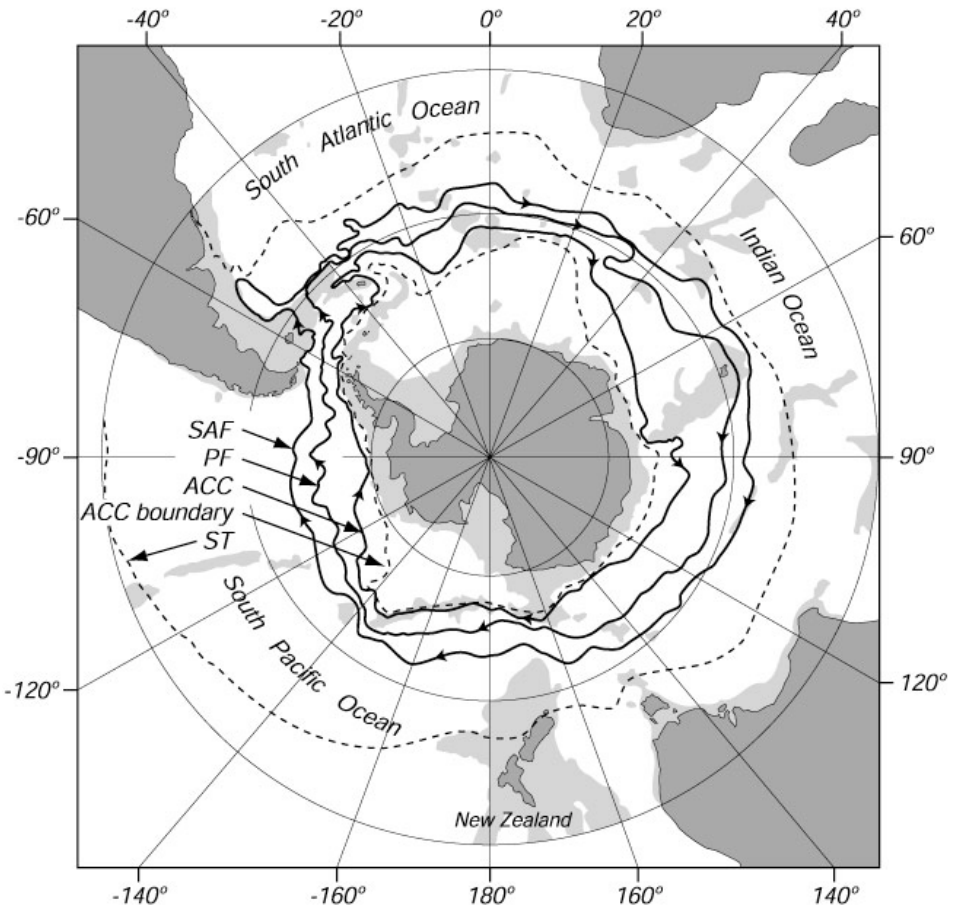

Figure 1.4: Distribution of the Subantarctic and Polar Fronts and associated currents in the Southern Ocean. From Orsi *et al.*, [1995].

The open waters of the PFZ typically exhibit low productivity year-round, with Chl *a* concentrations ranging from 0.12 to 0.42 mg (Chl*a*) m^{-3} [*El-Sayed*, 1988; *Froneman et al.*, 2004] and productivity ranging between 0.1 and 0.3 mg C m^{-2} day^{-1} [*Comiso et al.*, 1993; *Sullivan et al.*, 1993]. Enhanced levels of phytoplankton biomass (>1.5 mg Chl*a* m^{-3}) and productivity (>1 g C m^{-2} day^{-1}) have, however, been documented during austral spring and summer in the vicinity of the major oceanic fronts [*El-Sayed*, 1988; *Laubscher et al.*, 1993; *Moore & Abbott*, 2002] and in the waters surrounding several sub-Antarctic oceanic islands [*Blain et al.*, 2007; *Uitz et al.*, 2009]. Periodic phytoplankton blooms have also been recorded in the open waters of the PFZ [*Parslow et al.*, 2001; *Sokolov & Rintoul*, 2007b]. The factors responsible for an increase in phytoplankton biomass and productivity in these regions include increased water column stability [*Laubscher et al.*, 1993; *Perissinotto & Rae*, 1990], the availability of trace metals [*Baar et al.*, 1995; *Blain et al.*, 2007], macronutrient availability [*El-Sayed et al.*, 1983] and seawater temperature [*Bathmann et al.*, 1997; *Boyd et al.*, 2008].

The temporal variability in the oceanographic conditions in the PFZ is reflected in the zooplankton community. Deacon [1982] suggested that the varying intensities of the SAF and APF may result in an increase in the interchange of Antarctic Surface Water (AASW) and Sub-Antarctic Surface Water (SASW), within the PFZ. Species of either sub-tropical, sub-Antarctic or Antarctic origin may predominate locally within the region [*Carlotti et al.*, 2008; *Hunt & Hosie*, 2006]. The contribution of Antarctic and sub-Antarctic species is determined largely by their position within the PFZ; closer to the APF the zooplankton community is well represented by Antarctic species, while sub-Antarctic species typically dominate in the vicinity of the SAF [*Mayzaud et al.*, 2002; *Pakhomov & Froneman*, 2000].

Previous studies indicate that mesozooplankton, comprising mainly copepods, dominate the zooplankton community in the PFZ in terms of both abundance and biomass [*Hunt & Hosie*, 2006]. Among the larger zooplankton (>2000 μm), chaetognaths, euphausiids and tunicates numerically dominate [*Pakhomov & Froneman*, 2000]. However, the contribution of these larger zooplankton to total zooplankton abundance and biomass is generally <10% [*Carlotti et al.*, 2008; *Pakhomov & Froneman*, 2000].

In terms of spatial variation, enhanced zooplankton abundance and biomass values have been documented in the vicinity of the fronts (the APF and SAF) and in

the waters surrounding the sub-Antarctic islands [*Carlotti et al.*, 2008; *Pakhomov & Froneman*, 2000]. The elevated zooplankton biomass/ abundance values in such regions are presumed to be the result of the high food availability (Chl*a*) generally recorded in these areas [*Blain et al.*, 2007; *Pollard et al.*, 2007].

1.6 Why model?

Although often not stated explicitly, the principle aim of science is to construct models of the world. By incorporating and summarising our knowledge, models are built to capture the essence of particular systems. Ideally, these models allow us to understand what we can observe of the system, and occasionally can be used to predict what the system may do in the future. The former feature of models is particularly useful in directing research agendas and highlighting areas of relative ignorance.

Models may take forms, from simple, qualitative descriptions of a system, through to complex, quantitative forms. In the quantitative sciences, where models are normally verified against measurements of the real world, it is essential for models to be quantitative. Mathematics has thus become a powerful tool, both in formulating models from knowledge about a system, and exploring the constructed model to determine if it has features which make it either testable or unrealistic.

In the case of physics, mathematics has been applied to problems for centuries, and has been remarkably successful in both describing and predicting systems (*e.g.*, Newtonian mechanics, thermodynamics). However, the application of mathematics to biological systems has, historically, been considerably less successful. Systems which biologists study are usually considerably more complex (*e.g.*, because of their heterogeneity) than those studied by physicists, and not obviously amenable to be reduced to a small number of important components. In sub-organism level systems, the objects under study are usually highly complex, being made of thousands of parts (molecular and multi-molecular). In multi-organism systems (such as the planktonic in this thesis) additional complexity enters through variety in the individual

organisms, in their interactions with their physical environment and in their interactions with one another.

Partially because of this, biologists have traditionally studied nature in a mostly qualitative way. For instance, a substantial fraction of ecological research has involved determining detailed food webs to describe the trophic relationships between species in particular ecosystems (see [*Begon et al.*, 1996], for examples). Where numerical approaches have been used, they have been typically statistical or have ignored the dynamics of interacting organisms. Such studies, while useful and providing foundations for other research, are not usually appropriate to the kinds of predictions which ecologists are increasingly asked to make. Forecasting the consequences of many of the impacts of human civilisation on the Earth's ecology requires ecologists to extrapolate to situations outside of their empirical data. This forces ecologist to develop more accurate theoretical models, and necessitates confronting the complexity of biological systems.

Biological modellers are usually forced to deal with this complexity by stripping the system to be modelled down to its bare essentials, making many empirical assumptions about how these essential components interact and then modifying the model to fit with observations made of the real system. There are notable exception to this broad categorization [*Hopkins & Fauci*, 2002; *Murray*, 2002], but these approaches are at present confined to relatively narrow areas of biology.

1.6.1 Historical background

The clergyman Thomas Malthus was one of the first people to frame a biological problem in terms of mathematics. His 1798 work, *An Essay on the Principle of Population*, he described how human population growth is affected by famine, disease and warfare.

During the nineteenth century there were further attempts to apply mathematical techniques to biological problems (including development of statistics, a discipline with firm roots in biology), but it was not really until the twentieth century that major efforts were done.

One of the earliest, and most well-known, ecological models is the predator-prey model of Lotka [1925] and Volterra [1926]. Vito Volterra originally built the model to describe the predator-prey interactions of fish species. Alfred Lotka, who was a biologist and an actuary, independently produced the same model. The model takes the form of a pair of coupled ordinary differential equations (ODEs) with four simple terms representing intra- and inter-specific processes.

$$\frac{dN}{dt} = N(a - bP) \tag{1.3}$$

$$\frac{dP}{dt} = P(cbN - d) \tag{1.4}$$

Prey (N), growth at a constant rate, a, and are consumed by predators (P) at rate b. Predators increase in numbers through consuming prey, where the constant c relates to transfer efficiency (*i.e.*, how much of a prey's biomass/energy can be used by the predator), and they die (*i.e.*, through natural mortality or predation) at a constant rate, d (see Miller [2003] for a more complete description).

As such, the Lotka-Volterra model contains several assumptions which are unrealistic for most natural populations. Amongst these are the assumptions that both the prey growth and predator mortality terms are density independent. Since in most real-life situations, prey population growth is likely to be limited by food availability, and predator mortality is likely to vary with the density of higher predators. Modifying the equations, where prey growth is now density dependent (with K as the maximum possible prey density, or *carrying capacity*), changes the model system so that instead of neutrally-stable cycles, only a stable fixed point exists.

$$\frac{dN}{dt} = N(a(1 - \frac{N}{K}) - bP) \tag{1.5}$$

$$\frac{dP}{dt} = P(cbN - d) \tag{1.6}$$

Despite the simplicity of the Lotka-Volterra model, it is still a popular one amongst modellers. The particular Lotka-Volterra model presented here is not the only one, and the term “Lotka-Volterra” is applied across a wide range of simple predatory-prey or two species models. May [2001], Begon *et al* [1996] and Miller [2003] review the model and some of its variants, and discuss modifications to the basic form, as well as their outcomes (*e.g.*, the construction of the *n* species version of the Lotka-Volterra model).

1.6.2 Mathematical considerations

Again despite its relative simplicity, the Lotka-Volterra model illustrates several major, and often unstated, assumptions of many ecological models. Since some of these bear on the plankton model in this thesis they are discussed below.

- **Discrete versus continuous populations**
  Both predator and prey populations are described by continuous state variables, while in reality biological populations consist of discrete individuals. This discreteness problem is overcome by essentially assuming that the populations of predators and prey are sufficiently large that a continuous variable can adequately describe them.

- **Determinism**
  It is assumed that the system under study can be modelled by deterministic rules. While individual events may occur stochastically, models can assume that large enough numbers of events can be described by deterministic statements based on average behaviour.

- **Homogeneous mixing**

  Populations are assumed to be sufficiently well mixed that they can be adequately represented by a single population at an average density.

- **Averaged rate processes**

  Processes (such as growth, death or decay) are assumed to be adequately described by an average rate. A process, for example, which is known to take an average of 10 days to occur, is commonly modelled as a constant rate of 0.1 d^{-1}. This approach is again strongly tied to the community assumption.

- **Closed system**

  The modelled system is assumed to represent the "entire world". Factors in the real world which effects are believed to be insignificant compared to the effects of the modelled components upon one another are entirely ignored. The model is then a truncation of the real world.

- **Identical inhabitants**

  In addition to assuming that populations can be described by a continuous variable, ecological models usually assume that all individuals in those populations are identical, or at least have no differences of any consequence to the problem under consideration.

In the case of the plankton systems studied in this thesis, good cases can be made for assuming each of these in models. The physical environment, for instance, in which open-ocean plankton systems exist is one in which the surface waters are mixed both by currents within the water itself, and by the action of wind over the surface of the ocean. Wind mixing can be particularly strong, often mixing up to depths of hundreds of meters. Although mixing can create vertical structures, such as Langmuir cells [*Bees et al.*, 1997], which may partition plankton, mixing generally acts to homogenize the surface waters to the top of the seasonal thermocline. As such,

the assumption of plankton as evenly mixed through the surface mixed layer is not unreasonable.

The biological processes considered by most plankton models usually occur over time scales ranging for hours up to days [*Mann & Lazier*, 1996]. While seasonal cycles and certain biological phenomena occur over obviously longer periods, processes relevant to the models used in this thesis (cell division, nutrient uptake, grazing, excretion, decomposition, sinking) occur over relatively short periods of time (minute to hours) and are usually assumed to be adequately represented by exponential rates.

The assumption of identical inhabitants is perhaps the least defensible in the case of the models used in this thesis. The two biological state variables (phytoplankton and Zooplankton) used by Oschlies & Garcon [1999], are intended to cover a trophic spectrum which includes photosynthetic autotrophs, detritivores, grazers, cannibals and predators (and often organisms which indulge in more than one of these lifestyles). The continuous range of size (which encompasses differences in uptake rates, locomotory ability, vulnerability, etc.) and the variety in life history, nutrient requirement, prey preference, and behaviour further complicates attempts to describe plankton systems with a small number of functional groups. However, modellers have found that even simple models, which parameterise only the most important ecological processes (*e.g.*, photosynthesis, nutrient limitation, grazing), can successfully simulate certain key features of plankton dynamics (*e.g.*, spring blooms - [*Fasham et al.*, 1990], autumn blooms [*Findlay et al.*, 2006]; red tides events - [*Truscott & Brindley*, 1994]). Some researchers have found the creation of multiple nutrient, phytoplankton or zooplankton compartments necessary to more accurately capture certain features of data [*Jin et al.*, 2006; *Platt et al.*, 2005], but the success of simpler models suggest that they still have a role to play in plankton and ecosystem modelling.

1.7 Rationale

The work contained within this thesis deals entirely with open-ocean plankton ecosystems. For modelling purposes the surrounding waters of the Kerguelen Plateau are treated as an open ocean system. The effect of coastal margins is not taken into account.

Photosynthesis uses CO_2 as its raw material. Over the past two three decades, the scientific community has become concerned about the level of CO_2 in the atmosphere because of its rise in concentration due to the actions of human civilization (particularly the combustion of carbon-rich fossil fuels and the concurrent clearance of large areas of forested land).

Greenhouse gases influence the thermal balance of the Earth's atmosphere by being transparent to shorter wavelength, visible electromagnetic radiation, but opaque to longer wavelength, infrared radiation. This essentially allows these gases to "trap" thermal energy in the atmosphere, and to warm the surface of the Earth. This effect has been a feature of the atmosphere for billions years, and in the past the concentrations of greenhouse gases have been considerably different to those at present. Past variations in the CO_2 level of the atmosphere have been associated with climate change [*Adams et al.*, 1990; *Falkowski et al.*, 2000] and this, plus the fact that the anthropogenic changes to the atmosphere at present are occurring at rates considerably faster than the natural rates measured from ice-core records [*Monnin et al.*, 2001; *Petit et al.*, 1999], suggests that increasing atmospheric CO_2 is likely to substantially affect both the natural biosphere and human activity.

There are many possible consequences that global warming through an enhanced greenhouse effect may result in changes to sea-level, weather patterns, ocean circulation, species distribution and the geographical range of diseases such as malaria [*Boning et al.*, 2008; *Martens et al.*, 1997; *Poloczanska et al.*, 2007; *Riebesell*, 2004]. For example, in the context of plankton systems, Roemmich & McGowan [1995] report that, concurrent with a 1.5°C rise in surface water temperatures (probably caused by greenhouse warming), zooplankton populations in the California Current have fallen by 80% over a period of 40 years (they suggest that the mechanism is a shallower mixed layer and reduced phytoplankton production). Joos *et al*. [1999] and

Cox *et al*. [2000] draw the attention to several potential pathways of positive feedbacks which may occur as result of global warming (*e.g.* increases in atmospheric water vapour, decreases in reflective snow and ice, methane from wetlands, etc.). Hardin [1985] underlines the potential significance of such positive feedbacks by contrasting the relatively mild climate of the Earth at present with that of its sister planet, Venus, apparently a victim of an over-active greenhouse effect.

Given the potential for climate change to induce large-scale changes in the biosphere, researchers are interested in mechanisms which control or affect the quantity of CO_2 in the atmosphere. For obvious reasons, mechanics which promote "carbon burial" (the removal of CO_2 from the atmosphere to long-term sinks) are of particular interest. A major carbon burial (~80% of the total) route is via the carbonate-silicate cycle, where the weathering of silicate rocks results in the formation of carbonates which are subsequently buried by natural geological processes [*Emerson & Hedges*, 2008]. The remaining carbon burial occurs via biological activity (*i.e.* organic material which is not oxidized and is buried geologically).

In this context, plankton systems are important, since a fraction of their annual production is exported to the deep ocean where it may ultimately be buried [*Adams et al.*, 1990]. Raven [1995] estimates that 0.3% of annual marine production is preserved in deep ocean sediments by this mechanism. While terrestrial production may also bury carbon, the carbon it consumes comes mostly from the atmosphere. Since almost all (95%; Siegenthaler & Sarmiento [1993]) of the global carbon pool exists in the ocean (partially as dissolved CO_2, but mostly as bicarbonate, HCO_3^-), any removal of CO_2 directly from the atmosphere by, for instance, terrestrial primary production, may merely shift the ocean-atmosphere equilibrium and lead to the replacement of the removed atmospheric CO_2 by oceanic CO_2. Consequently, the direct removal of carbon form the oceans by plankton systems is of interest to researchers. Note nonetheless that there is still uncertainty about the potential importance of this carbon sink [*Le Quéré et al.*, 2009].

In relation to a limitation on primary production, and of current interest, is the suggestion by Martin & Fitzwater [1988] that plankton in certain regions of the world ocean are growth-limited by the lack of availability of iron (which is an important micro-nutrient in certain photosynthetic and nutrient reductive enzymes; *Geider &*

LaRoche, 2004). While this suggestion has been vindicated by mesoscale iron enrichment experiments [*Boyd et al.*, 2007], these short-term fertilizations are not able to assess all the ecosystem processes that follow from iron addition, and for this reason it was very useful to explore the role of persistent natural iron inputs in structuring ecosystems and transferring carbon. The Kerguelen Ocean and Plateau compared Study (KEOPS) was designed to examine the area of persistently high phytoplankton biomass that forms over the Kerguelen plateau each year. Shipboard observations in January-February 2005 revealed that the development of the largest phytoplankton bloom in the Subantarctic region [*Sullivan et al.*, 1993] was due to natural iron enrichment [*Blain et al.*, 2007; 2008].

Understanding the mechanisms causing such iron-fuelled blooms, and quantifying their associated primary production (and the fate of this production), is of fundamental importance in assessing global carbon budgets and modelling scenarios of global climate change. Here the aim of this thesis is to combine satellite observations of ocean properties with models of primary production and transport to explore the mechanism by which surface iron fertilization can affect phytoplankton biomass in the Southern Ocean.

For this study, a zero-dimensional biogeochemical model, based on the *NPZD* model developed by Oschlies & Garçon [1999], has been modified. The thesis will focus on the modification of the biogeochemical model to its application in the Southern Ocean surface waters. Since 1999 there has been several iron fertilisation programs [see Boyd *et al.*, 2007 for a comprehensive review] and two natural iron fertilisations studies [*Blain et al.*, 2007; *Pollard et al.*, 2009] in Southern Ocean waters. Data from the first Southern Ocean Iron Release Experiment (SOIREE) and from the first natural iron fertilization study in the Southern Ocean, KEOPS, are used to evaluate the model.

As well as for our understanding of the role of iron in the control of primary production, understanding the mechanisms that drive the plankton dynamics under different iron inputs scenarios are important for climate change studies [*Boyd et al.*, 2008], geoengineering studies [*Lampitt et al.*, 2008], iron biogeochemistry studies [*Bowie et al.*, 2009] and paleo-climate studies of past atmospheric composition [*Watson et al.*, 2000]. Acknowledging that an iron-tracking model would be able to

address additional issues such as iron supply and recycling, emphasis was on the biomass response which does not require and explicit iron model.

In summary given the significance of global warming, and the importance of plankton ecosystems in influencing the global carbon cycle, understanding the physical and biological dynamics which govern plankton communities is a key step towards improving our understanding of the processes which may ultimately weigh heavily on the fate of human civilisation.

This chapter has attempted to lay the foundation for the biology and physics which underlie the model that is applied and modified in this thesis. Additionally, sections have aimed to explain the simplification of this foundation by models.

1.8 References

Adams, J. M., H. Faure, L. Faure-Denard, et al. (1990), Increases in terrestrial carbon storage from the Last Glacial Maximum to the present, *Nature*, *348*(6303), 711-714.

Ardelan, M. V., O. Holm-Hansen, C. D. Hewes, et al. (2010), Natural iron enrichment around the Antarctic Peninsula in the Southern Ocean, *Biogeosciences*, *7*, 11-25.

Aumont, O., and L. Bopp (2006), Globalizing results from ocean in situ iron fertilization studies, *Global Biogeochemical Cycles*, *20*(2), 10.1029.

Azam, F., T. Fenchel, J. Field, et al. (1983), The ecological role of water-column microbes in the sea, *Marine ecology progress series. Oldendorf*, *10*(3), 257-263.

Azam, F. (1998), Microbial control of Oceanic Carbon Flux: The plot thickens, *Science*, *280*, 694-695.

Baar, H. J. W. d., J. T. M. d. Jong, D. C. E. Bakker, et al. (1995), Importance of iron for plankton blooms and carbon dioxide drawdown in the Southern Ocean, *Nature*, *373*, 412-415.

Balch, W. M., K. A. Kilpatrick, P. M. Holligan, et al. (1996), The 1991 coccolithophore bloom in the central north Atlantic: Optical properties and factors affecting their distribution, *Limnology and Oceanography*, *41*, 1669-1683.

Balch, W. M., D. T. Drapeau, and J. J. Fritz (2001), Optical backscattering in the Arabian Sea - Continuous underway measurements of particulate inorganic and organic carbon, *Deep Sea Research I*, *49*(2), 413-431.

Banse, K. (1990), Does Iron Really Limit Phytoplankton Production in the Offshore Sub-Arctic Pacific, *Limnology and Oceanography*, *35*(3), 772-775.

Barnes, R. S. K., and K. H. Mann (1991), *Fundamentals of aquatic ecology*, Blackwell Pub.

Bathmann, U. V., R. Scharek, C. Klaas, et al. (1997), Spring development of phytoplankton biomass and composition in major water masses of the Atlantic sector of the Southern Ocean, *Deep-Sea Research II*, *44*(1-2), 51-67.

Bees, M., I. Mezic, and J. McGlade (1997), Planktonic interactions and chaotic advection in Langmuir circulation, *Mathematics and Computers in Simulation*, *44*(6), 527-544.

Begon, M., J. Harper, and C. Townsend (1996), *Ecology: individuals, populations, and communities*, Wiley-Blackwell.

Behrenfeld, M. J., R. T. O'Malley, D. A. Siegel, et al. (2006), Climate-driven trends in contemporary ocean productivity, *Nature*, *444*(7120), 752-755.

Blain, S., A. Leynaert, P. Tr√©guer, et al. (1997), Biomass, growth rates and limitation of Eqautorial Pacific diatoms, *Deep-Sea Research Part I: Oceanographic Research Papers*, *44*(7), 1255-1275.

Blain, S., B. Quéguiner, L. Armand, et al. (2007), Impacts of natural iron fertilisation on the Southern Ocean, *Nature*, *446*, 1070-1074, doi:1010.1038/nature05700.

Blain, S., B. Queguiner, and T. W. Trull (2008), The natural iron fertilization experiment KEOPS (Kerguelen Ocean and Plateau compared Study): an overview, *Deep Sea Research II*, *55*(5-7), 559-565.

Boning, C. W., A. Dispert, M. Visbeck, et al. (2008), The response of the antarctic circumpolar current to recent climate change, *Nature Geoscience*, *1*(12), 864-869.

Bowie, A. R., D. Lannuzel, T. A. Remenyi, et al. (2009), Biogeochemical iron budgets of the Southern Ocean south of Australia: Decoupling of iron and nutrient cycles in the subantarctic zone by the summertime supply, *Global Biogeochem. Cycles*, *23*.

Boyd, P. W., T. Jickells, C. S. Law, et al. (2007), Mesoscale Iron Enrichment Experiments 1993-2005: Synthesis and Future Directions, *Science*, *315*(5812), 612-617, DOI: 610.1126/science.1131669.

Boyd, P. W., S. C. Doney, R. Strzepek, et al. (2008), Climate-mediated changes to mixed-layer properties in the Southern Ocean: Assessing the phytoplankton response, *Biogeosciences*, *5*(3), 847-864.

Bruland, K., and M. Silver (1981), Sinking rates of fecal pellets from gelatinous zooplankton (salps, pteropods, doliolids), *Marine Biology*, *63*(3), 295-300.

Bruland, K. W., R. P. Franks, G. A. Knauer, et al. (1979), Sampling and analytical methods for the determination of copper, cadmium, zinc and nickel at the nanogram per liter level in seawater, *Analytica Chimica Acta*, *105*(1), 233ñ245.

Brzezinski, M. A., T. A. Villareal, and F. Lipschultz (1998), Silica production and the contribution of diatoms to new and primary production in the central North Pacific, *Marine Ecology Progress Series*, *167*, 89-104.

Buck, K. R., P. A. Bolt, and D. L. Garrison (1990), Phagotrophy and fecal pellet production by an athecate dinoflagellate in Antarctic sea ice, *Marine Ecology Progress Series*, *60*, 75-84.

Buesseler, K. O., and P. W. Boyd (2003), Will ocean fertilization work?, *Science*, *300*, 67-68.

Buma, A. G. J., H. J. W. de Baar, R. F. Nolting, et al. (1991), Metal enrichment experiments in the Weddell-Scotia Seas: Effects of iron and manganese on various plankton communities, *Limnology and Oceanography*, *36*(8), 1865-1878.

Carlotti, F., D. Thibault-Botha, A. Nowaczyk, et al. (2008), Zooplankton community structure, biomass and role in carbon fluxes during the second half of a phytoplankton bloom in the Eastern sector of the Kerguelen shelf (January - February 2005), *Deep Sea Research II*, *55*(5-7), 720-733.

Carr, M. E., M. A. M. Friedrichs, M. Schmeltz, et al. (2006), A comparison of global estimates of marine primary production from ocean color, *Deep-Sea Research Part Ii-Topical Studies in Oceanography*, *53*(5-7), 741-770.

Chisholm, S. W. (2000), Oceanography: Stirring times in the Southern Ocean, *Nature*, *407*, 685-687.

Chisholm, S. W., P. G. Falkowski, and J. J. Cullen (2001), Dis-Crediting Ocean Fertilization, in *Science*, edited, pp. 309-310.

Coale, K. H. (1991), Effects of iron, manganese, copper, and zinc enrichments on productivity and biomass in the subarctic Pacific, *Limnology and Oceanography*, *36*(8), 1851-1864.

Comiso, J. C., C. R. McClain, C. W. Sullivan, et al. (1993), Coastal zone color scanner pigment concentrations in the Southern Ocean and relationships to geophysical surface features, *Journal of Geophysical Research*, *98*, 2419-2451.

Costanza, R., R. D'Arge, R. De Groot, et al. (1997), The value of the world's ecosystem services and natural capital, *Nature*, *387*(6630), 253-260.

Cox, P. M., R. A. Betts, C. D. Jones, et al. (2000), Acceleration of global warming due to carbon-cycle feedbacks in a coupled climate model, *Nature*, *408*, 184-187.

Cullen, J. J. (1991), Hypotheses to Explain High-Nutrient Conditions in the Open Sea, *Limnology and Oceanography*, *36*(8), 1578-1599.

de Baar, H. J. W., J. T. M. de Jong, R. F. Nolting, et al. (1999), Low dissolved Fe and the absence of diatom blooms in remote Pacific waters of the Southern Ocean, *Marine Chemistry*, *66*, 1-34.

de Baar, H. J. W., and J. La Roche (2003), Metals in the oceans: Evolution, biology and global change, *Marine Scientific Frontiers for Europe*, 79ñ105.

de Baar, H. J. W., P. W. Boyd, K. H. Coale, et al. (2005), Synthesis of iron fertilization experiments: from the iron age to the age of enlightenment, *Journal of Geophysical Research. C. Oceans*, *110*, doi:10.1029/2004GC002601.

Deacon, G. E. R. (1982), Physical and biological zonation in the Southern Ocean, *Deep Sea Research*, *29*(1A), 1-15.

Deibel, D., and J. T. Turner (1985), Zooplankton feeding ecology: contents of fecal pellets of the appendicularian *Oikopleura vanhoeffeni*, *Marine Ecology Progress Series*, *27*, 67-78.

Del Giorgio, P. A., J. J. Cole, and A. Cimbleris (1997), Respiration rates in bacteria exceed phytoplankton production in unproductive aquatic systems, *Nature*, *385*(6612), 148-151.

DeLong, E. F., K. Y. Wu, B. B. PrÈzelin, et al. (1994), High abundance of Archaea in Antarctic marine picoplankton, *Nature*, *371*(6499), 695-697.

DiTullio, G. R., M. E. Geesey, J. M. Maucher, et al. (2005), Influence of iron on algal community composition and physiological status in the Peru upwelling system, *Limnol. Oceanogr.*, *50*(6), 1887-1907.

Duarte, C. M., and S. Agustí (1998), The CO_2 balance of unproductive aquatic ecosystems, *Science*, *281*, 234-236.

Dugdale, R. C., and F. P. Wilkerson (1991), Low Specific Nitrate Uptake Rate: A Common Feature of High-Nutrient, Low-Chlorophyll Marine Ecosystems, *Limnology and Oceanography*, *36*(8), 1678-1688.

Dugdale, R. C., F. P. Wilkerson, and H. J. Minas (1995), The role of a silicate pump in driving new production, *Deep-Sea Research I*, *42*(4), 697-719.

Dugdale, R. C., and F. P. Wilkerson (1998), Silicate regulation of new production in the equatorial Pacific upwelling, *Nature*, *391*, 270-273.

Duggen, S., P. Croot, U. Schacht, et al. (2007), Subduction zone volcanic ash can fertilize the surface ocean and stimulate phytoplankton growth: Evidence from biogeochemical experiments and satellite data, *Geophysical Research Letters*, *34*(1).

Ehn, J., M. Granskog, A. Reinart, et al. (2004), Optical properties of melting landfast sea ice and underlying seawater in Santala Bay, Gulf of Finland, *Journal of Geophysical Research-Oceans*, *109*(C9), C09003.

Ehn, J., C. Mundy, and D. Barber (2008), Bio-optical and structural properties inferred from irradiance measurements within the bottommost layers in an Arctic landfast sea ice cover, *J. Geophys. Res*, *113*.

El-Sayed, S. Z., D. C. Biggs, and O. Holm-Hansen (1983), Phytoplankton standing crop, primary productivity, and near-surface nitrogenous nutrient fields in the Ross Sea, Antarctica, *Deep Sea Research*, *30*(8A), 871-886.

El-Sayed, S. Z. (1988), Productivity of the Southern Ocean: a closer look, *Comparative Biochemistry and Physiology Part B: Comparative Biochemistry*, *90*(3), 489-498.

Eldridge, M. L., C. G. Trick, M. B. Alm, et al. (2004), Phytoplankton community response to a manipulation of bioavailable iron in HNLC waters of the subtropical Pacific Ocean, *Aquatic Microbial Ecology*, *35*(1), 79-91.

Elrod, V. A., W. M. Berelson, K. H. Coale, et al. (2004), The flux of iron from continental shelf sediments: A missing source for global budgets, *Geophys. Res. Lett*, *31*, 12.

Emerson, S., and J. Hedges (2008), *Chemical oceanography and the marine carbon cycle*, xi, 453 , [458] of plates pp., Cambridge University Press, Cambridge, UK ; New York.

Eppley, R. W., and B. J. Peterson (1979), Particulate organic matter flux and planktonic new production in the deep ocean, *Nature*, *282*(5740), 677-680.

Evans, A. M. (1987), *An introduction to ore geology*, 2nd ed., 358 pp., Blackwell Scientific Publications, Oxford Oxfordshire.

Evans, G. T., and J. S. Parslow (1985), A model of annual plankton cycles, *Biological Oceanography*, *3*(3), 327-347.

Fahnenstiel, G., M. McCormick, G. Lang, et al. (1995), Taxon-specific growth and loss rates for dominant phytoplankton populations from the northern Gulf of Mexico, *Marine ecology progress series. Oldendorf*, *117*(1), 229-239.

Falkowski, P., R. J. Scholes, E. A. Boyle, et al. (2000), The global carbon cycle: a test of our knowledge of Earth as a system, *Science*, *290*, 291-296.

Falkowski, P. G. (1997), Evolution of the nitrogen cycle and its influence on the biological sequestration of CO_2 in the ocean, *Nature*, *387*, 272-275.

Falkowski, P. G., R. T. Barber, and V. Smetacek (1998), Biogeochemical controls and feedbacks on ocean primary production, *Science*, *281*, 200-206.

Fasham, M. J. R., H. W. Ducklow, and S. M. McKelvie (1990), A nitrogen-based model of plankton dynamics in the oceanic mixed layer, *Journal of Marine Research*, *48*(3), 591-639.

Field, C. B., M. J. Behrenfeld, J. T. Randerson, et al. (1998), Primary production of the biosphere: integrating terrestrial and oceanic components, *Science*, *281*, 237-240.

Findlay, H., A. Yool, M. Nodale, et al. (2006), Modelling of autumn plankton bloom dynamics, *Journal of Plankton Research*, *28*(2), 209.

Fortier, L., J. Le FËvre, and L. Legendre (1994), Export of biogenic carbon to fish and to the deep ocean: the role of large planktonic microphages, *Journal of Plankton Research*, *16*(7), 809.

Franck, V. M., K. W. Bruland, D. A. Hutchins, et al. (2003), Iron and zinc effects on silicic acid and nitrate uptake kinetics in three high-nutrient, low-chlorophyll (HNLC) regions, *Marine Ecology Progress Series*, *252*, 15-33.

Freund, J., S. Mieruch, B. Scholze, et al. (2006), Bloom dynamics in a seasonally forced phytoplankton-zooplankton model: Trigger mechanisms and timing effects, *Ecological Complexity*, *3*(2), 129-139.

Froneman, P., E. Pakhomov, and M. Balarin (2004), Size-fractionated phytoplankton biomass, production and biogenic carbon flux in the eastern Atlantic sector of the Southern Ocean in late austral summer 1997-1998, *Deep Sea Research Part II: Topical Studies in Oceanography*, *51*(22-24), 2715-2729.

Geider, R. J., and J. La Roche (2004), The role of iron in phytoplankton photosynthesis, and the potential for iron-limitation of primary productivity in the sea, *Photosynthesis Research*, *39*(3), 275-301, DOI 210.1007/BF00014588.

GEOTRACES, P. G. (2006), GEOTRACES Science Plan, Scientific Committee on Oceanic Research, Baltimore, Maryland.

Ghadouani, A., B. Pinel-Alloul, K. Plath, et al. (2004), Effects of Microcystis aeruginosa and purified microcystin-LR on the feeding behavior of Daphnia pulicaria, *Limnology and Oceanography*, 666-679.

Gonzalez, H. E., and V. S. Smetacek (1994), The possible role of cyclopoid copepod Oithona in retarding vertical flux of zooplankton faecal material, *Marine Ecology Progress Series*, *113*, 233-246.

Gran, H. H. (1931), On the conditions for the production of plankton in the sea, *Rapp. Proc. Verb. Cons. Int. Explor. Mer*, *75*, 37-46.

Hardin, G. J. (1985), *Filters against folly : how to survive despite economists, ecologists, and the merely eloquent*, x, 240 pp., Viking, New York, N.Y.

Hart, T. J. (1942), Phytoplankton periodicity in Antarctic surface water, *Discovery Reports*, *VIII*, 1-268.

Harvey, H. W. (1937), The supply of iron to diatoms, *Journal of the Marine Biological Association of the United Kingdom*, *22*(1), 205-219.

Hoffmann, L. J., I. Peeken, K. Lochte, et al. (2006), Different reactions of Southern Ocean phytoplankton size classes to iron fertilization, *Limnology and Oceanography*, 1217-1229.

Hopkins, M., and L. Fauci (2002), A computational model of the collective fluid dynamics of motile micro-organisms, *Journal of Fluid Mechanics*, *455*, 149-174.

Hunt, B. P. V., and G. W. Hosie (2006), The seasonal succession of zooplankton in the Southern Ocean south of Australia, part 2: The Sub-Antarctic to Polar Frontal Zones, *Deep Sea Research (Part I, Oceanographic Research Papers)*, *53*, 1203 – 1223.

Hutchins, D. A., and K. W. Bruland (1994), Grazer-mediated regeneration and assimilation off Fe, Zn,and Mn from planktonic prey, *Marine Ecology Progress Series*, *110*, 259-269.

Ianni, C., P. Rivaro, and R. Frache (2002), Distribution of Dissolved and Particulate Iron, Copper and Manganese in the Shelf Waters of the Ross Sea (Antarctica), *Marine Ecology*, *23*, 210-219.

Ianora, A., A. Miralto, S. A. Poulet, et al. (2004), Aldehyde suppression of copepod recruitment in blooms of a ubiquitous planktonic diatom, *Nature*, *429*(6990), 403-407.

Idso, C., and F. Singer (2009), Climate Change Reconsidered, *Report of the Nongovernmental International Panel on Climate Change*.

Jickells, T. D., Z. S. An, K. K. Andersen, et al. (2005), Global iron connections between desert dust, ocean biogeochemistry, and climate, *Science*, *308*(5718), 67.

Jin, X., N. Gruber, J. P. Dunne, et al. (2006), Diagnosing the contribution of phytoplankton functional groups to the production and export of particulate organic carbon, CaCO3, and opal from global nutrient and alkalinity distributions, *Global Biogeochemical Cycles*, *20*(10.1029).

Johnson, K. S., F. P. Chavez, and G. E. Friederich (1999), Continental-shelf sediment as a primary source of iron for coastal phytoplankton, *Nature*, *398*(6729), 697-700.

Johnson, K. S. (2001), Iron supply and demand in the upper ocean: Is extraterrestrial dust a significant source of bioavailable iron?, *Global Biogeochemical Cycles*, *15*(1).

Joos, F., G.-K. Plattner, T. F. Stocker, et al. (1999), Global warming and marine carbon cycle feedbacks on future atmospheric CO_2, *Science*, *284*, 464-467.

Kumar, N., R. F. Anderson, R. A. Mortlock, et al. (1995), Increased biological productivity and export production in the glacial Southern Ocean, *Nature*, *378*, 675-680.

Lam, P. J., J. K. B. Bishop, C. C. Henning, et al. (2006), Wintertime phytoplankton bloomlet in the Subarctic Pacific supported by continental margin iron, *Global Biogeochemical Cycles*, *in press*.

Lampitt, R., E. Achterberg, T. Anderson, et al. (2008), Ocean fertilization: a potential means of geoengineering?, *Philosophical Transactions A*, *366*(1882), 3919.

Lampitt, R. S., T. Noji, and B. V. Bodungen (1991), What happens to zooplankton faecal pellets? Implications for material flux, *Marine Biology*, *104*, 15-23.

Lannuzel, D., V. Schoemann, J. de Jong, et al. (2007), Distribution and biogeochemical behaviour of iron in the East Antarctic sea ice, *Marine Chemistry*, *106*(1-2), 18-32.

Laubscher, R. K., R. Perissinotto, and C. D. McQuaid (1993), Phytoplankton production and biomass at frontal zones in the Atlantic sector of the Southern Ocean, *Polar Biology*, *13*, 471-481.

Le Quéré, C., M. R. Raupach, J. G. Canadell, et al. (2009), Trends in the sources and sinks of carbon dioxide, *Nature Geoscience*, *2*, 831 - 836.

Littler, M. M., D. S. Littler, S. M. Blair, et al. (1985), Deepest known plant life discovered on an uncharted seamount, *Science*, *227*(4682), 57-59.

Liu, H., H. A. Nolla, and L. Campbell (1997), Prochlorococcus growth rate and contribution to primary production in the equatorial and subtropical North Pacific Ocean, *Aquatic Microbial Ecology*, *12*(1), 39-47.

Longhurst, A. R. (1991), Role of the Marine Biosphere in the Global Carbon-Cycle, *Limnology and Oceanography*, *36*(8), 1507-1526.

Lotka, A. (1925), *Elements of physical biology*, Williams & Wilkins company.

Malthus, T., and J. Bonar (1926), *First essay on population 1798*, Macmillan.

Mann, K. H., and J. R. N. Lazier (1996), *Dynamics of marine ecosystems : biological-physical interactions in the oceans*, 2nd ed., 394 pp., Blackwell Science, Boston.

Marra, J. (1978), Effect of short-term variations in light intensity on photosynthesis of a marine phytoplankter: A laboratory simulation study, *Marine Biology*, *46*(3), 191-202.

Martens, W. J. M., T. H. Jetten, and D. A. Focks (1997), Sensitivity of malaria, schistosomiasis and dengue to global warming, *Climatic Change*, *35*(2), 145-156.

Martin, J. H., and S. E. Fitzwater (1988), Iron deficiency limits phytoplankton growth in the north-east pacific subarctic, *Nature*, *331*(6154), 341-343.

Martin, J. H., and R. Michael Gordon (1988), Northeast Pacific iron distributions in relation to phytoplankton productivity, *Deep Sea Research Part A, Oceanographic Research Papers*, *35*(2), 177-196.

Martin, J. H., S. E. Fitzwater, and R. M. Gordon (1990), Iron deficiency limits growth in Antarctic waters, *Global Biogeochemical Cycles*, *4*(5-12).

Matear, R., and A. C. Hirst (1999), Climate change feedback on the future oceanic CO2 uptake, *Tellus*, *51*(3), 722-733.

May, R. (2001), *Stability and complexity in model ecosystems*, Princeton Univ Pr.

Mayzaud, P., V. Tirelli, A. Errhif, et al. (2002), Carbon intake by zooplankton: Importance and role of zooplankton grazing in the Indian sector of the Southern Ocean, *Deep Sea Research II*, *49*(16), 3169-3188.

Metzl, N., B. Tilbrook, and A. Poisson (1999), The annual fCO_2 cycle and the air-sea CO_2 flux in the sub-Antarctic ocean, *Tellus*, *51B*, 849-861.

Miller, C. B. (2003), *Biological oceanography*, 1 v. pp., Blackwell Pub., Oxford.

Mills, M. M., C. Ridame, M. Davey, et al. (2004), Iron and phosphorus co-limit nitrogen fixation in the eastern tropical North Atlantic, *Nature*, *429*(6989), 292-294.

Mitchell, B. G., E. A. Brody, O. Holm-Hansen, et al. (1991), Light Limitation of Phytoplankton Biomass and Macronutrient Utilization in the Southern Ocean, *Limnology and Oceanography*, *36*(8), 1662-1677.

Monnin, E., A. Indermuhle, A. Dallenbach, et al. (2001), Atmospheric CO2 concentrations over the last glacial termination, *Science*, *291*(5501), 112-114.

Moore, J. K., and M. R. Abbott (2002), Surface chlorophyll concentrations in relation to the Antarctic Polar Front: seasonal and spatial patterns from satellite observations, *Journal of Marine Systems*, *37*, 69-86.

Murray, J. (2002), *Mathematical Biology: an introduction*, Springer Verlag.

Neuer, S., R. Davenport, T. Freudenthal, et al. (2002), Differences in the biological carbon pump at three subtropical ocean sites, *Geophysical Reasearch Letters*, *29*(18).

Noji, T. T., K. W. Estep, F. MacIntyre, et al. (1991), Image analysis of faecal material grazed upon by three species of copepods: evidence for coprorhexy, coprophagy, and coprochaly, *Journal of the Marine Biological Association of the United Kingdom*, *71*, 46-480.

Nowlin Jr, W. D., T. Whitworth Iii, and R. D. Pillsbury (1977), Structure and transport of the Antarctic Circumpolar Current at Drake Passage from short-term measurements, *J. Phys. Oceanogr*, *7*(11), 788ñ802.

Omori, M., and T. Ikeda (1992), *Methods in Marine Zooplankton Ecology*, 332 pp., Krieger Publishing Company, Malabar, U.S.A.

Orsi, A. H., T. I. Whitworth, and W. D. J. Nowlin (1995), On the meridional extent and fronts of the Antarctic Circumpolar Current, *Deep-Sea Research*, *42*(5), 641-673.

Oschlies, A., and V. Garçon (1999), An eddy-permitting coupled physical-biological model of the North Atlantic. 1. Sensitivity to advection numerics and mixed layer physics, *Global Biogeochemical Cycles*, *13*(1), 135-160.

Pachauri, R., and A. Reisinger (2007), Climate change 2007: synthesis report. Contribution of working groups I, *II and III to the Fourth Assessment Report of the Intergovernmental Panel on Climate Change, IPCC, Genf*.

Pakhomov, E. A., and P. W. Froneman (2000), Composition and spatial variability of macroplankton and micronekton within the Antarctic Polar Frontal Zone of the Indian Ocean during austral autumn 1997, *Polar Biology*, *23*(6), 410-419.

Parslow, J., P. Boyd, S. R. Rintoul, et al. (2001), A persistent sub-surface chlorophyll maximum in the Polar Frontal Zone south of Australia: seasonal progression and implications for phytoplankton-light-nutrient interactions, *Journal of Geophysical Research. C. Oceans*, *106*, 31543-31557.

Passow, U., A. L. Alldredge, and B. E. & Logan (1994), The role of particulate carbohydrate exudates in the flocculation of diatom blooms., *Deep-Sea Research I*, *41*, 335-357.

Perissinotto, R., and D. Rae (1990), Occurrence of anticyclonic eddies on the Prince Edward Plateau (Southern Ocean): effects on phytoplankton biomass and production, *Deep Sea Research Part A. Oceanographic Research Papers*, *37*(5), 777-793.

Perissinotto, R., L. Gurney, and E. A. Pakhomov (2000), Contribution of heterotrophic material to diet and energy budget of Antarctic krill, *Euphausia superba*, *Marine Biology*, *136*, 129-135.

Petit, J. R., J. Jouzel, D. Raynaud, et al. (1999), Climate and atmospheric history of the past 420,000 years from the Vostok ice core, Antarctica, *Nature*, *399*(6735), 429-436.

Platt, T., D. F. Bird, and S. Sathyendranath (1991), Critical depth and marine primary production, *Proceedings of the Royal Society of London. Series B: Biological Sciences*, *246*(1317), 205.

Platt, T., R. B. Rivkin, and S. Sathyendranath (2005), Ecosystem dynamics based on plankton functional types for global ocean biogeochemistry models, *Global Change Biology*, *11*, 2016-2040.

Pollard, R., R. Sanders, M. Lucas, et al. (2007), The Crozet Natural Iron Bloom and Export Experiment (CROZEX), *Deep-Sea Research II, Volume 54, Issue 18-20, p. , 54*(18-20), 1905-1914.

Pollard, R., I. Salter, R. Sanders, et al. (2009), Southern Ocean deep-water carbon export enhanced by natural iron fertilization, *Nature*, *457*(7229), 577-580.

Pollard, R. T., M. I. Lucas, and J. F. Read (2002), Physical controls on biogeochemical zonation in the Southern Ocean, *Deep Sea Research II*, *49*(16), 3289-3305.

Poloczanska, E. S., R. C. Babcock, A. Butler, et al. (2007), Climate change and Australian marine life, in *Oceanography and Marine Biology, Vol 45*, edited, pp. 407-478, Crc Press-Taylor & Francis Group, Boca Raton.

Prezelin, B. B., E. E. Hofmann, C. Mengelt, et al. (2000), The linkage between Upper Circumpolar Deep Water (UCDW) and phytoplankton assemblages on the west Antarctic Peninsula continental shelf, *Journal of Marine Research*, *58*, 165-202.

Price, N. M., B. A. Ahner, and F. M. M. Morel (1994), The equatorial Pacific Ocean: Grazer-controlled phytoplankton populations in an iron-limited ecosystem, *Limnology and Oceanography*, *39*(3), 520-534.

Priddle, J., M. J. Whitehouse, A. Atkinson, et al. (1997), Diurnal changes in near-surface ammonium concentration - interplay between zooplankton and phytoplankton, *Journal of Plankton Research*, *19*(9), 1305-1330.

Raven, J. A. (1995), Scaling the Seas, *Plant Cell and Environment*, *18*(10), 1090-1100.

Raven, J. A., and P. G. Falkowski (1999), Oceanic sinks for atmospheric CO2, *Plant, Cell & Environment*, *22*(6), 741-755.

Riebesell, U. (2004), Effects of CO2 Enrichment on Marine Phytoplankton, *Journal of Oceanography*, *60*, 719-729.

Riebesell, U., K. G. Schulz, R. G. J. Bellerby, et al. (2007), Enhanced biological carbon consumption in a high CO2 ocean, *Nature*, *450*(7169), 545-548.

Riley, G. A. (1942), The relationship of vertical turbulence and spring diatom flowerings, *J. mar. Res*, *5*(1), 67-82.

Rintoul, S. (2000), Southern Ocean currents and climate, *Papers and proceedings of the Royal Society of Tasmania*, *133*, 41-50.

Roemmich, D., and J. McGowan (1995), Climatic Warming and the Decline of Zooplankton in the California Current, *Science*, *267*(5202), 1324-1326.

Ryther, J. H. (1969), Photosynthesis and fish production in the sea, *Science*, *166*(3901), 72-76.

Sabine, C. L., R. A. Feely, N. Gruber, et al. (2004), The oceanic sink for anthropogenic CO_2, *Science*, *305*, 367-371.

Sarmiento, J. L., and N. Gruber (2002), Sinks for anthropogenic carbon, *Physics Today*, *55*(8), 30-36.

Sarmiento, J. L., N. Gruber, M. A. Brzezinski, et al. (2004), High-latitude controls of thermocline nutrients and low latitude biological productivity, *Nature*, *427*, 56-60.

Sedwick, P. N., and G. R. DiTullio (1997), Regulation of algal blooms in Antarctic Shelf waters by the release of iron from melting sea ice, *Geophysical Research Letters*, *24*, 2515-2518.

Sedwick, P. N., A. R. Bowie, and T. W. Trull (2008), Dissolved iron in the Australian sector of the Southern Ocean (CLIVAR SR3 section): Meridional and seasonal trends, *Deep-Sea Research Part I: Oceanographic Research Papers*, *55*(8), 911-925.

Sherr, E., and B. Sherr (1988), Role of microbes in pelagic food webs: a revised concept, *Limnology and Oceanography*, 1225-1227.

Siegenthaler, U., and J. Sarmiento (1993), Atmospheric carbon dioxide and the ocean, *Nature*, *365*(119-125).

Singer, S. (2008), *Nature, not human activity, rules the climate: summary for policy makers of the report of the Nongovernmental International Panel on Climate Change*, The Heartland Institute.

Sloyan, B. M., and S. R. Rintoul (2001), The Southern Ocean limb of the global deep overturning circulation, *Journal of Physical Oceanography*, *31*(1), 143-173.

Smith, W. O. J., and V. L. Asper (2001), The influence of phytoplankton assemblage composition on biogeochemical characteristics and cycles in the southern Ross Sea, Antarctica, *Deep-Sea Research I*, *48*, 137-161.

Smol, J. P., and E. F. Stoermer (1999), *The diatoms : applications for the environmental and earth sciences*, xii, 469 pp., Cambridge University Press, Cambridge, UK ; New York, NY.

Sokolov, S., and S. R. Rintoul (2007a), Multiple jets of the Antarctic Circumpolar Current south of Australia, *Journal of Physical Oceanography*, *37*, 1394-1412, doi:1310.1175/JPO3111.1391.

Sokolov, S., and S. R. Rintoul (2007b), On the relationship between fronts of the Antarctic Circumpolar Current and surface chlorophyll concentrations in the Southern Ocean, *J. Geophys. Res. – Oceans*, *112*(C07030), doi: 10.1029/2006JC004072.

Solomon, S. (2007), *Climate Change 2007: the physical science basis: contribution of Working Group I to the Fourth Assessment Report of the Intergovernmental Panel on Climate Change*, Cambridge Univ Pr.

Steele, J., and B. Frost (1977), The structure of plankton communities, *Philosophical Transactions of the Royal Society of London. Series B, Biological Sciences*, *280*(976), 485-534.

Steinberg, D. K., S. A. Goldthwait, and D. A. Hansell (2002), Zooplankton vertical migration and the active transport of dissolved organic and inorganic nitrogen in the Sargasso Sea, *Deep-Sea Research I*, *49*(8), 1445-1461.

Strom, S. L., and T. A. Morello (1998), Comparative growth rates and yields of ciliates and heterotrophic dinoflagellates, *Journal of Plankton Research*, *20*(3), 571.

Sullivan, C. W., K. R. Arrigo, C. R. McClain, et al. (1993), Distributions of phytoplankton blooms in the Southern Ocean, *Science*, *262*(5141), 1832-1837.

Sunda, W. G., and S. A. Huntsman (1995), Iron uptake and growth limitation in oceanic and coastal phytoplankton, *Marine Chemistry*, *50*(1-4), 189-206.

Sunda, W. G., and S. A. Huntsman (1997), Interrelated influence of iron, light and cell size on marine phytoplankton growth, *Nature*, *390*, 389-392.

Sverdrup, H. (1953), On conditions for the vernal blooming of phytoplankton, *Journal du Conseil*, *18*(3), 287.

Tagliabue, A., L. Bopp, J. C. Dutay, et al. (2010), Hydrothermal contribution to the oceanic dissolved iron inventory, *Nature Geoscience*, *3*, 252-256.

Takeda, S. (1998), Influence of iron availability on nutrient consumption ratio of diatoms in oceanic waters, *Nature*, *393*, 774-777.

Timmermans, K. R., W. Stolte, and H. J. W. de Baar (2004), Iron-mediated effects on nitrate reductase in marine phytoplankton, *Marine Biology*, *121*(2), 389-396, 310.1007/BF00346749.

Tortell, P. D. (2000), Evolutionary and ecological perspectives on carbon acquisition in phytoplankton, *Limnology and Oceanography*, *45*(3), 744-750.

Touratier, F., F. Carlotti, and G. Gorsky (2003), Individual growth model for the appendicularian

Oikopleura dioica, *Marine Ecology Progress Series*, *248*, 141-163.

Trull, T. W., S. R. Rintoul, M. Hadfield, et al. (2001a), Circulation and seasonal evolution of Polar waters south of Australia: Implications for iron fertilisation of the Southern Ocean, *Deep Sea Research (Part II, Topical Studies in Oceanography)*, *48*(11/12), 2439-2466.

Trull, T. W., A. R. Bowie, J. Jabour, et al. (2008), Position Analysis: Ocean Fertilisation - Science and Policy Issues, 20 pp, Antarctic Climate & Ecosystems Cooperative Research Centre (ACECRC), Hobart, Tasmania.

Truscott, J., and J. Brindley (1994), Equilibria, stability and excitability in a general class of plankton population models, *Philosophical Transactions: Physical Sciences and Engineering*, *347*(1685), 703-718.

Turner, D. R., and K. A. Hunter (2001), *The biogeochemistry of iron in seawater*, 396 pp., Wiley, Chichester, Sussex.

Uitz, J., H. Claustre, F. B. Griffiths, et al. (2009), A phytoplankton class-specific primary production model applied to the Kerguelen Islands region (Southern Ocean), *Deep-Sea Research Part I: Oceanographic Research Papers*, *56*, 541-560.

Van den Hoek, C., D. G. Mann, and H. M. Jahns (1995), *Algae: an introduction to phycology*, Cambridge University Press.

Volterra, V. (1926), Fluctuations in the abundance of a species considered mathematically, *Nature*, *118*(2972), 558-560.

Watson, A. J., D. C. E. Bakker, A. J. Ridgwell, et al. (2000), Effect of iron supply on Southern Ocean CO2 uptake and implications for glacial for atmospheric CO_2, *Nature*, *407*, 730-733.

Williams, R., and M. Follows (2003), Physical transport of nutrients and the maintenance of biological production, in *Ocean Biogeochemistry: The Role of the Ocean Carbon Cycle in Global Change*, edited by M. J. R. Fasham, p. 297, Springer, New York.

CHAPTER TWO

Model description

2.1 Introduction

Following the pioneering development of ecosystem models used to trace the flow of material between various components in an ecosystem [*Evans & Parslow*, 1985; *Fasham et al.*, 1990; *Frost*, 1987; *Steele & Frost*, 1977], several marine plankton models with different complexity have been developed. For the Southern Ocean, one-dimensional plankton models like SWAMCO [*Lancelot et al.*, 1991], the KERFIX simulation of Pondaven *et al.* [1998; 2000], the AESOPS modelling program [*Fennel et al.*, 2003a; b], or the real-time forecasting during the CROZEX experiment [*Popova et al.*, 2007], have been used to investigate ecosystem dynamics in the context of research cruises or station time series. The physical environment in these models has been reduced to the variability of the mixed layer depth.

On the other hand, coupled ocean-ecosystem models with simple parameterizations of biogeochemical fluxes between four and five compartments have been developed for global [*Doney et al.*, 2009; *Le Quéré et al.*, 2005; *Moore et al.*, 2002a; 2002b; *Tagliabue et al.*, 2009a] and regional applications [*Chai et al.*, 2007; *Fennel et al.*, 2003a; *Findlay et al.*, 2006; *Ji et al.*, 2008; *Machu et al.*, 2005; *Oschlies*, 2001; *Tagliabue & Arrigo*, 2003].

The Oschlies & Garçon [1999] (hereafter OG99) model of the marine ecosystem is one of several which aim to describe the seasonal dynamics of the open-ocean planktonic ecosystem [*Aumont et al.*, 2003; *Evans & Parslow*, 1985; *Fasham et al.*, 1990; *Frost*, 1993]. Although originally proposed in [*Oschlies & Garçon*, 1998], several refinements have subsequently been made, leading to the choice of OG99 as the reference model upon which the research detailed in this thesis is based.

Two versions of the simple nitrogen-based *NPZD* pelagic model are used in this study. The original version of the model is identical to the one described by OG99, and the optimised model is that described by Schartau & Oschlies [2003a] (hereafter SO03a). It's differences with respect to the original version are the optimised parameter values, the inclusion of a temperature dependence of all remineralisation rates, a quadratic phytoplankton mortality and a linear loss from phytoplankton back to the dissolved inorganic nitrogen (DIN) pool (*i.e.* exudation rate).

While the models are complex enough to cover many aspects of the nonlinear ecosystem dynamics, they are simple and efficient to investigate the general principles of biological-physical processes and to predict potential outcomes based on idealized scenarios. These models are built on certain assumptions (see Chapter 1), so they are useful to explore the driving mechanism under specific conditions.

The models track the biogeochemical cycle of nitrogen. Following the nitrogen-based ecosystem model developed by Fasham *et al.* [1990], nitrogen is distributed among the compartments phytoplankton, zooplankton, nitrogen-containing detritus, and the nutrient nitrate. The focus is on the phytoplankton production and subsequent consumption by zooplankton. There is not explicit modelization of bacterial pools or processes, instead this is simply described by a remineralisation rate that returns nitrogen to the nitrate pool. This approach is appropriate for the focus on seasonal production responses to iron, and particularly so for the Southern Ocean where nitrate is not depleted and thus the details of nitrogen regeneration are not significant. For work in other oceans or with other emphasis, for example nitrogen regeneration [*Bopp et al.*, 2001], or dimethylsulphide (DMS) production by bacteria [*Bonner-Knowles et al.*, 2005], more explicit modelling of the bacterial loop is required [*Aumont et al.*, 2002; *Gabric et al.*, 1993].

The OG99 model has been used in a series of model studies performed in the North Atlantic [*Garcon et al.*, 2001; *Oschlies et al.*, 2000; *Oschlies*, 2001] and in global applications [*Pasquero et al.*, 2005; *Schmittner et al.*, 2008]. For their simulations they relied on parameter values similar to those published by Sarmiento *et al.* [1993] and Fasham *et al.* [1993], which were adopted from published laboratory experiments or approximated from rates derived from *in situ* measurements.

The SO03a version of the model is the result of an attempt to identify a single set of parameter values that improves the performance of the preliminary *NPZD*-model version (*i.e.*, OG99) at three different locations where time-series data were available (*i.e.*, BATS site, NABE site, and OWS-INDIA). By assimilating observations, Schartau & Oschlies [2003a; 2003b] provided optimal parameter estimates for the *NPZD*-model which could subsequently be used in a basin-scale simulation.

Although the OG99 model has several failings, some of which have been addressed in subsequent papers [*Oschlies*, 2002; *Oschlies & Schartau*, 2005], it has several features which recommend it:

(i) It is a relatively detailed model of the ecosystem, incorporating the most important biotic compartments plus abiotic and detritus compartments;

(ii) It takes account of two of the more significant aspects of the ocean, vertical mixing and solar irradiance (mesoscale features that have been the focus of research in biogeochemical modelling for the last ten years);

(iii) Despite having four compartments and around twenty parameters (many of them have not been evaluated in the field or by experimental work, and some of which cannot reasonably be estimated at all), it is simpler than some of the more detailed ecosystem models [*Aumont & Bopp*, 2006; *Fennel et al.*, 2003a; *Fujii et al.*, 2005; *Lancelot et al.*, 2000; *Mongin et al.*, 2006]

In this chapter, the OG99 and the SO03 models are introduced. Each of the model's four equations and their derivations are detailed. The models are also compared to each other. This comparison is important because the paucity of data and the lack of any mechanistic theories underlying the ecological interactions under study, often makes the choice of model appear more a case of personal preference than objective merit. The chapter is then concluded by a Southern Ocean application (*i.e.*, *HNLC*-reference simulation) that uses data from the Kerguelen Ocean and Plateau compared Study (KEOPS), and from the French Kerguelen Point Fix Station (KERFIX), both located in the Indian sector of the Southern Ocean.

2.2 Model equations

The models consist of four coupled interacting components, describing changes in the concentrations of nutrients (*N*), phytoplankton (*P*), zooplankton (*Z*) and detritus (*D*). All components of the model are in units of mmol N m^{-3}. Both are formulated as a bi-layer system with an upper, well-mixed layer (down to the seasonal thermocline) containing *N*, *P*, *Z* and *D*, and a lower layer containing no *P*, *Z* or *D* but an excess of nutrients, N_0 [*Evans & Parslow*, 1985]. Therefore the only input to the ocean surface system is expressed by $w^+ N_0\ MLD^{-1}$ which represents nutrients entering from below the mixed layer.

The OG99 model describes the open-ocean plankton ecosystem with four coupled ordinary differential equations (ODEs). These describe the time-evolution of mixed layer concentration of *N*, *P*, *Z* and *D*. The mixed layer has a depth of *MLD*.

$$\frac{dN}{dt} = rem\ D + \varepsilon_Z\ Z\ - \mu(MLD, t, N)\ \ P - \frac{(N_0 - N)w^+(t)}{MLD}$$

$$= \textit{remineralisation + Z excretion – loss P growth - entrainment from the deep ocean}$$

$$\frac{dP}{dt} = \mu(MLD, t, N)\ P - G(P)\ Z - \varepsilon_P\ P - \frac{w^+(t)P}{MLD}$$

$$= \textit{growth – grazing loss – natural mortality – mixing and dilution}$$

$$\frac{dZ}{dt} = \gamma_z\, G(P)\ Z - zmort\ Z^2 - \varepsilon_Z\ Z - \frac{w^+(t)Z}{MLD}$$

$$= \textit{grazed P – mortality – excretion – mixing and dilution}$$

$$\frac{dD}{dt} = (1 - \gamma_z)\ G(P)\ Z + \varepsilon_P\ P + zmort\ Z^2 - rem\ D - \left(\frac{w_S + w^+(t)D}{MLD}\right)$$

$$= \textit{lost grazed P + P mortality + Z mortality – remineralisation}$$

$$\textit{– sinking, mixing and dilution}$$

For the optimised model, the respective terms are

$$\frac{dN}{dt} = rem(T)\, D + \varepsilon_Z(T)\, Z + \varepsilon_P(T)\, P - \mu(MLD, t, N)\ P - \frac{(N_0 - N)w^+(t)}{MLD}$$

$$= \textit{remineralisation + Z excretion + P exudation – loss P growth - entrainment from the deep ocean}$$

$$\frac{dP}{dt} = \mu(MLD, t, N)\, P - G(P)\, Z - \varepsilon_P(T)\, P - pmort\ P^2 - \frac{w^+(t)P}{MLD}$$

$$= \textit{growth – grazing loss – exudation - natural mortality – mixing and dilution}$$

$$\frac{dZ}{dt} = \gamma_z\, G(P)\, Z - zmort\, Z^2 - \varepsilon_Z(T)\, Z - \frac{w^+(t)Z}{MLD}$$

$$= \textit{grazed P – mortality – excretion – mixing and dilution}$$

$$\frac{dD}{dt} = (1 - \gamma_z)\, G(P)\, Z + pmort\, P^2 + zmort\, Z^2 - rem(T)\, D - \left(\frac{w_S + w^+(t)D}{MLD}\right)$$

$$= \textit{lost grazed P + P mortality + Z mortality – remineralisation – sinking, mixing and dilution}$$

The coupling between the equations takes the form of flows of the model currency, nitrogen, between the compartments (currency is expressed here in volumetric terms, mmol N m^{-3}). These flows represent biological and physical processes such as grazing, nutrient uptake and mixing. Table 2.1 lists the definitions and descriptions of the ecological processes not defined explicitly in the equations given previously. Table 2.2 lists all of the model parameters, their definitions and units, and their baseline values form OG99 and SO03a.

Surface chlorophyll-*a* is not a prognostic variable but is diagnosed from the model. Following Hurtt & Armstrong [1996], a chlorophyll-to-nitrogen ratio is used to convert modelled phytoplankton in nitrogen units to phytoplankton observed in chlorophyll *a* units by

$$\text{Chl } a = 1.59\, P \qquad (2.1)$$

where Chl *a* is in mg Chl/m^3, and 1.59 is calculated from 0.02 g Chl *a* (g C^{-1}) for open ocean phytoplankton [*Fasham et al.*, 1990] and the Redfield ratio C:N = 106:16 [*Redfield et al.*, 1963]. It is know that the elemental composition of phytoplankton is variable, and respond to light levels and to the availability of macronutrients [*Geider*

& La Roche, 2002], however in the Southern Ocean where nitrate is not depleted these changes in the elemental composition of phytoplankton are thought to be due to shifts in the species composition [*Hoffmann et al.*, 2006].

The mixed layer is assumed to be sufficiently well mixed that the model components can be represented by a constant, homogeneous concentration throughout it (*i.e.*, that the physical mixing processes occur at rates which are fast when compared to the growth rates of the biological components of the models). Consequently, vertical space is represented only implicitly in the phytoplankton light-limited growth term and in the loss of material through mixing with the deep ocean. The horizontal space is entirely ignored here.

In addition to the interactions between the equations, all the compartments are forced by one, two or three of the forcing functions: the seasonal cycles of mixed-layer depth (MLD), solar irradiance (SRA) and sea surface temperature (SST).

Figure 2.1 illustrates the basic structure of the full ecosystem model. Various ecological and chemical pathways link the four compartments. Since there is sinking flux of detritus (out of the model domain) and the model is conservative (*i.e.*, nitrogen can only enter or leave the modelled mixed layer via nutrient supply or sinking), the model requires a physical supply of new nitrate (*i.e.*, entrainment; see section 2.3.2), or it will eventually exhaust nitrogen.

Table 2.1: Model functions, their definitions and a description of the ecological processes concerned. The temperature dependence in the parameters marked with an asterisk is exclusive of the SO03a model configuration.

Function	Ecological process	Definition
μ	Phytoplankton growth	$\min\{\mu_I(t, MLD, P), \mu_N(N)\}$
$\mu_I(t, MLD, P)$	Light-limited phytoplankton growth	$\frac{1}{MLD}\int_0^{MLD} F(I_0(t)e^{-(kw+kcP)z})dz$
$F(I)$	Photosynthesis-irradiance curve	$\frac{\mu_{\max}\alpha I}{\sqrt{(\mu_{\max}^2+\alpha^2 I^2)}}$
$\mu_{\max}(T)$	Maximum phytoplankton growth rate	ab^{cT}
$\mu_N(N)$	Nitrate limitation	$\mu_{\max}(\frac{N}{K_N+N})$
$G(P)$	Zooplankton grazing on phytoplankton	$\frac{g\ pc\ P^2}{g+pc\ P^2}$
$\varepsilon_P(T)$	Phytoplankton specific mortality rate*	$0.04\times b^{cT}$
$\varepsilon_Z(T)$	Excretion*	$0.01\times b^{cT}$
$rem(T)$	Remineralisation rate*	$0.048\times b^{cT}$

The following sections describe the four equation and the three forcing functions used in the models.

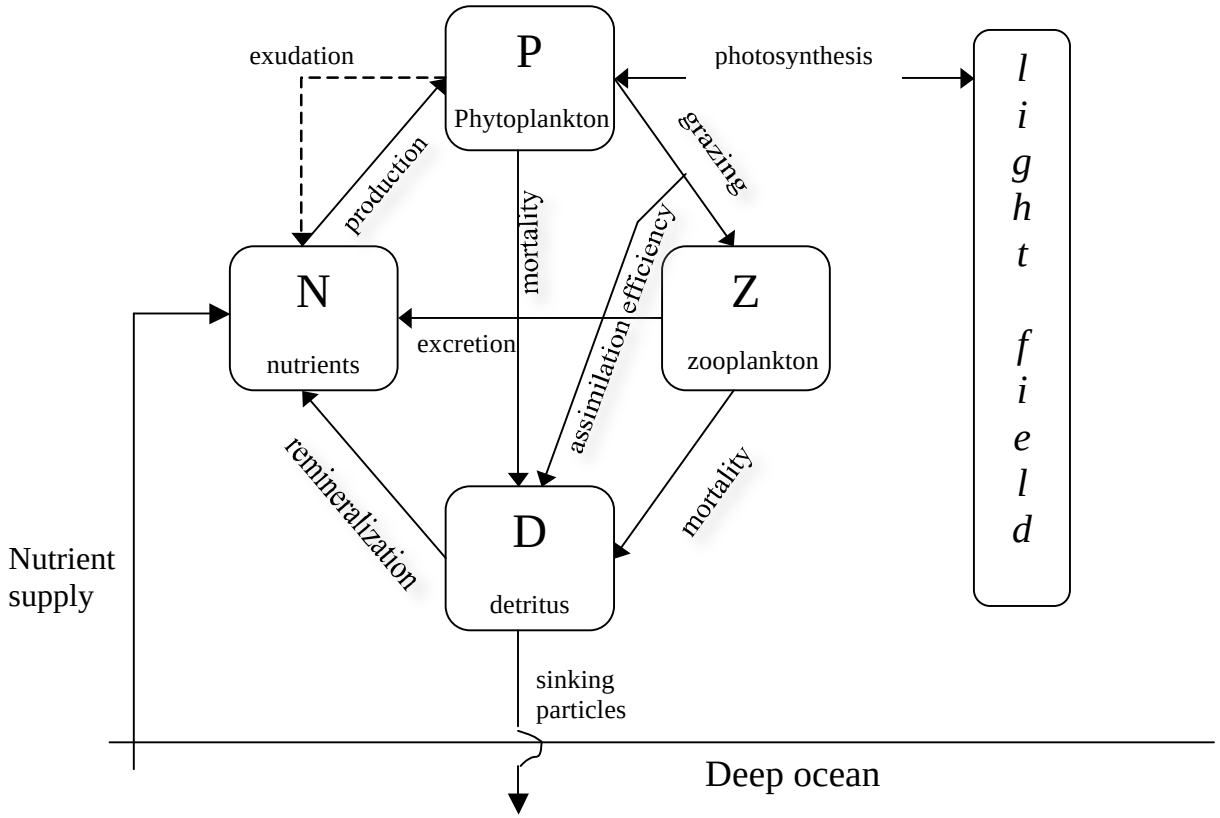

Figure 2.1: Diagrammatic representation of the lower trophic level food web models (OG99 and SO03a). The four compartments (state variables) including nitrate (*N*), phytoplankton (*P*), zooplankton (*Z*) and detritical organic nitrogen (*D*), and all pathways have been shown. Arrows represent the direction of mass flux. The inclusion of a phytoplankton exudation flux (dashed line) back to the nitrate pool represents the schematic difference between the two ecosystem model configurations.

Table 2.2: The model parameters and their values as used in OG99 and SO03a.

Parameter	*Symbol*	*Original OG99*	*Optimized SO03a*	*Units*
		Phytoplankton (P) Coefficients		
Initial slope of P-I curve	α	0.025	0.256	$d^{-1}/(W\ m^{-2})$
Ratio of PAR to total Irradiance	PAR	0.43	0.43	*non-dimensional*
Attenuation coefficient of seawater	k_w	0.04	0.04	m^{-1}
Light attenuation by phytoplankton	k_c	0.03	0.047	$m^{-1}\ (mmol\ N\ m^{-3})^{-1}$
Maximum growth rate parameters	μ_{max}	ab^{cT}	ab^{cT}	
	a	0.6	0.27	(d^{-1})
	b	1.066	1.066	*non-dimensional*
	c	1.0	1.0	$(°C)^{-1}$
Nitrate uptake half-saturation constant	K_N	0.5	0.7	$(mmol\ N\ m^{-3})$
Quadratic mortality rate	*pmort*	---	0.025	$(mmol\ N\ m^{-3})^{-1} d^{-1}$
Specific mortality rate	ε_P	0.03	0.04 x b^{cT}	(d^{-1})
		Zooplankton (Z) Coefficients		
Assimilation efficiency	γ_z	0.75	0.925	*non-dimensional*
Maximum grazing rate	g	2.0	1.575	(d^{-1})
Prey capture rate	*pc*	1.0	1.6	$(mmol\ N\ m^{-3})^{-2}\ d^{-1}$
Quadratic mortality rate	*zmort*	0.20	0.34	$(mmol\ N\ m^{-3})^{-1}\ d^{-1}$
Excretion rate	ε_Z	0.03	0.01 x b^{cT}	(d^{-1})
		Detrital (D) Coefficients		
Remineralisation rate	*rem*	0.050	0.048 x b^{cT}	(d^{-1})
Sinking rate	w_S	5.0	18.0	$m\ d^{-1}$
		Mixed layer (ML) Coefficients		
Subthermocline nitrate Concentration	N_0	30	30	$(mmol\ N\ m^{-3})$

2.2.1 Phytoplankton

The local change of the phytoplankton biomass in the standard model is controlled by growth, grazing by zooplankton, and physiological or non-grazing mortality. The optimised model adds a quadratic mortality term and a remineralisation parameter (*i.e.* exudation rate) that is temperature dependent. Terminology and definitions are summarised in tables 2.1 and 2.2.

$$\frac{dP}{dt} = \mu(MLD, t, N)\, P - \mathrm{G}(P)\, Z - \varepsilon_P\, P - \frac{w^+(t)P}{MLD} \tag{2.2}$$

$$\frac{dP}{dt} = \mu(MLD, t, N)\, P - \mathrm{G}(P)\, Z - \varepsilon_P(T)\, P - pmort\ P^2 - \frac{w^+(t)P}{MLD} \tag{2.3}$$

where,

$$\mu(t, MLD, P, N) = \min\ \{\ \mu_I\ (t, MLD, P),\ \mu_N\ (N)\ \} \tag{2.4}$$

Phytoplankton growth, μ, is limited by both irradiance I, and nutrient availability. It is described by the smaller of the maximum possible growth in the given depth-integrated irradiance field, μ_I, and the limitation imposed by the ambient nutrient concentration, μ_N.

$$\mu_I\ (t, MLD, P) = 2\frac{1}{MLD}\int_0^{\tau}\ \int_0^{MLD} F(I_0(t)e^{-(kw+kcP)z})dzdt \tag{2.5}$$

where,

$$F(I) = \frac{\mu_{\max}\alpha I}{\sqrt{(\mu_{\max}^2 + \alpha^2 I^2)}} \tag{2.6}$$

Maximum possible irradiance-limited growth, μ_I, is calculated by integrating surface irradiance both down through the water column (dz) to the top of the

thermocline, and through the day (*dt*; where τ takes the value half of the day length). I_0 (*t*) is the quantity of irradiance just below the surface of the ocean.

Depth-integration attenuates the irradiance exponentially due to absorption by the photosynthetic pigments of the phytoplankton, k_c, and by the sea water itself, k_w, Although ignored in this model, particulate material present in the sea water (including particulate organic material) plays a significant role in the submarine absorption of radiation [*Garver et al.,* 1994]. Both k_w and k_c were assigned average values inside the ranges measured in the field. Note that irradiance is not spectrally resolved here, and is essentially treated as if it consists only of photons which are attenuated at some average rate down the water column (*i.e.*, k_w is assigned a value of 0.04 m^{-1} which falls between the comparable values of 0.4 and 0.004 m^{-1} for red and blue light respectively). Since vertical space is not represented explicitly in these models, the mixed layer is assumed to be sufficiently homogeneous for the phytoplankton (as well as the other model compartments) to have a uniform vertical distribution.

Given the water irradiance, a standard empirical function, *F(I),* is used to describe the phytoplankton photosynthesis-irradiance (P-I) relationship. This function is based on the monotonic saturating function of Smith [1936], recommended by Jassby & Platt [1976], and uses the maximum phytoplankton growth rate, μ_{max}, and the initial slope of the P-I curve, α, together with irradiance to calculate growth. Figure 2.2 illustrates this relationship of maximum phytoplankton growth to irradiance for temperate waters. For high values of *I*, *F* asymptotically approaches μ_{max}, and photoinhibition is not modelled.

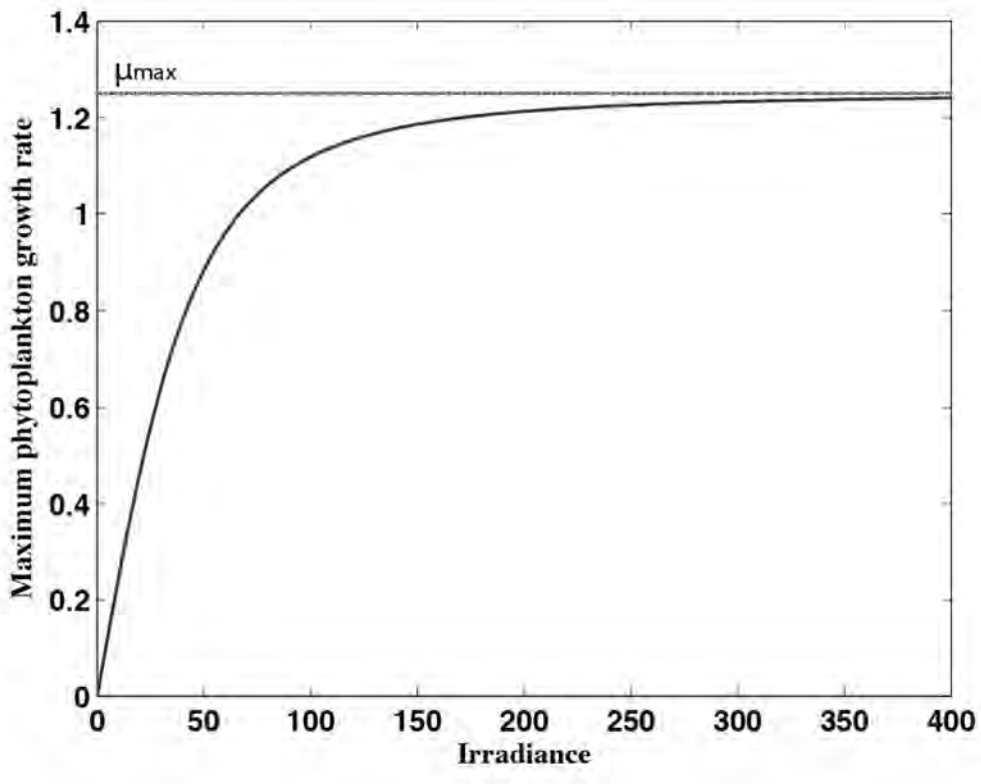

Figure 2.2: The photosynthesis-irradiance (or P-I) curve used in this model. The shape of the curve is controlled here by two parameters; μ_{max}, the maximum phytoplankton growth rate, and α, the initial slope of the curve. Irradiance in W m^{-2}, growth rate in d^{-1}.

Drawing on a large number of studies, Eppley [1972] derived the following empirical relationship between maximum phytoplankton growth and temperature,

$$\mu_{max} = 0.6\ (1.066)^{cT} \qquad (2.7)$$

where T is the temperature in degrees Celsius, a is a reference rate (Table 2.2) and b is a constant determined by measurements, typically of order 1.01-1.2, with 1.066 a useful mean determined by Eppley. This equation has been used in several model developments [*e.g.*, *Aumont & Bopp*, 2006; *Fasham*, 1993; *Sarmiento et al.*, 1993] to determine average values of μ_{max} across the year.

Figure 2.3 illustrates the temperature dependence of four terms used here. The maximum phytoplankton growth (μ_{max}) represented in both models (*i.e.*, OG99 and

SO03a), and the remineralisation parameters (*i.e.*, ε_P, ε_Z and *rem*) which are only a function of temperature in the optimised SO03a model.

$$\mu_{\max}(T) = a \cdot b^{cT}, \qquad \varepsilon_p(T) = \varepsilon_p \cdot b^{cT}$$
$$\varepsilon_Z(T) = \varepsilon_Z \cdot b^{cT}, \qquad rem = rem \cdot b^{cT} \tag{2.8}$$

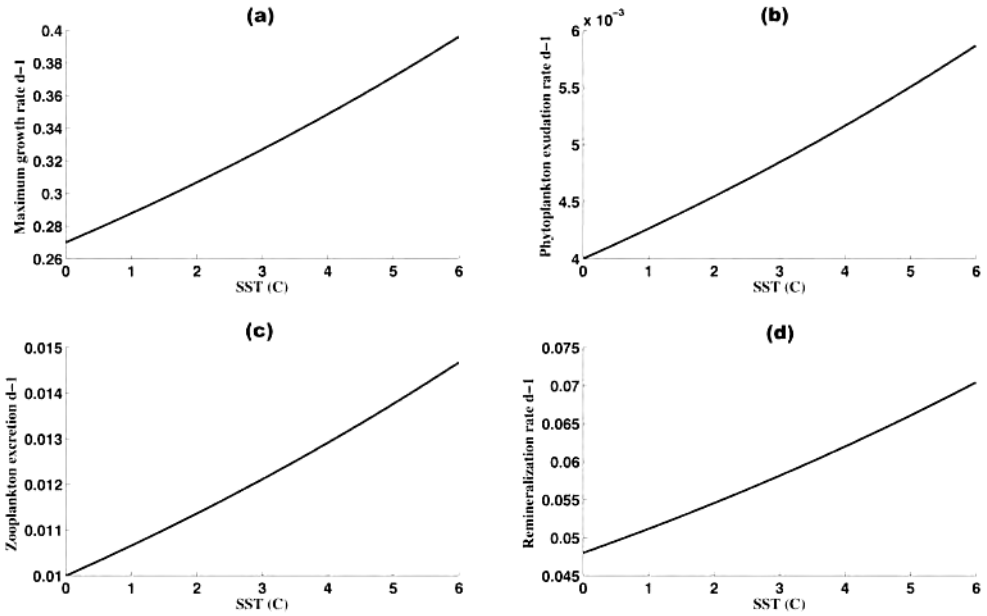

Figure 2.3: Temperature effects on **a**: maximum growth rate ($\mu_{\max}$); **b**: phytoplankton exudation (ε_P); **c**: zooplankton excretion (ε_Z) and d: detrital remineralisation rates (*rem*). The standard version of the model, OG99, only incorporates the temperature dependence function in $\mu_{\max}$.

Light-limited growth is integrated analytically, both down the water column and through the day, using a formulation derived by Evans & Parslow [1985]. This formulation assumes that irradiance, $I_0(t)$, forms a triangular shape, rising linearly from 0 at dawn to a maximum at noon and then declining to 0 at dusk. It also assumes that, through a given day, the phytoplankton population remains constant. In practice,

variation of I_0 (t) with time of day is calculated from latitude, and day number using the standard trigonometric/astronomical formulae [*Brock*, 1981].

To show the relations of the light-dependent growth rate functional form with surface irradiance, temperature, mixed layer depth, together with an arbitrary range of values for alpha (α), a series of simulations were carried out (Figs. 2.4 and 2.5).

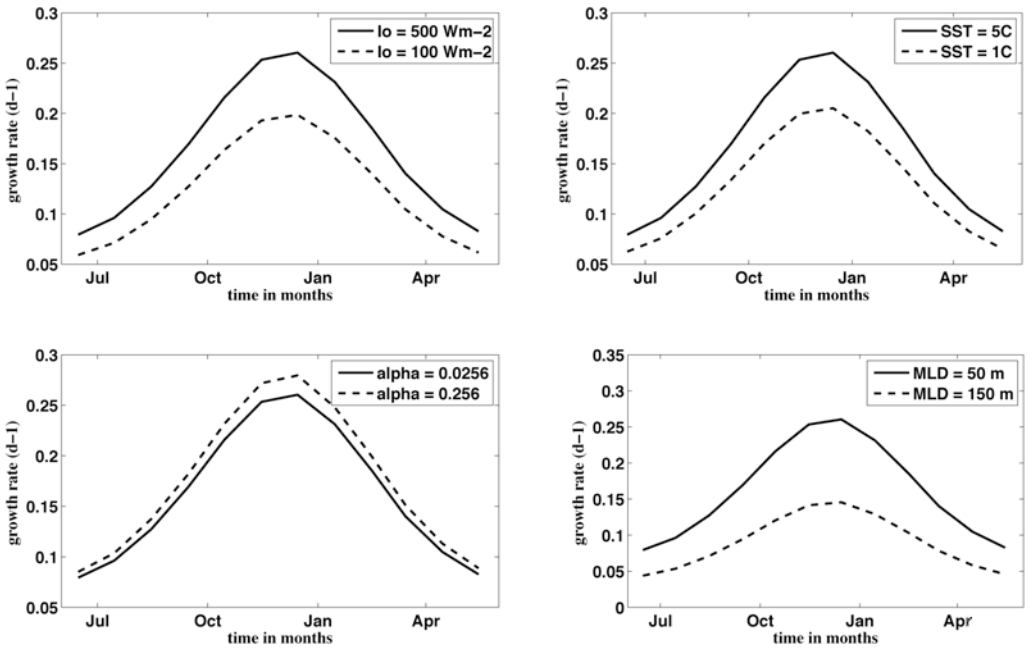

Figure 2.4: Light-limited phytoplankton growth rate function (μ_I) with a set of two arbitrary values of surface irradiance (I_0), sea surface temperature (SST), mixed layer depth (*MLD*) and alpha (α).

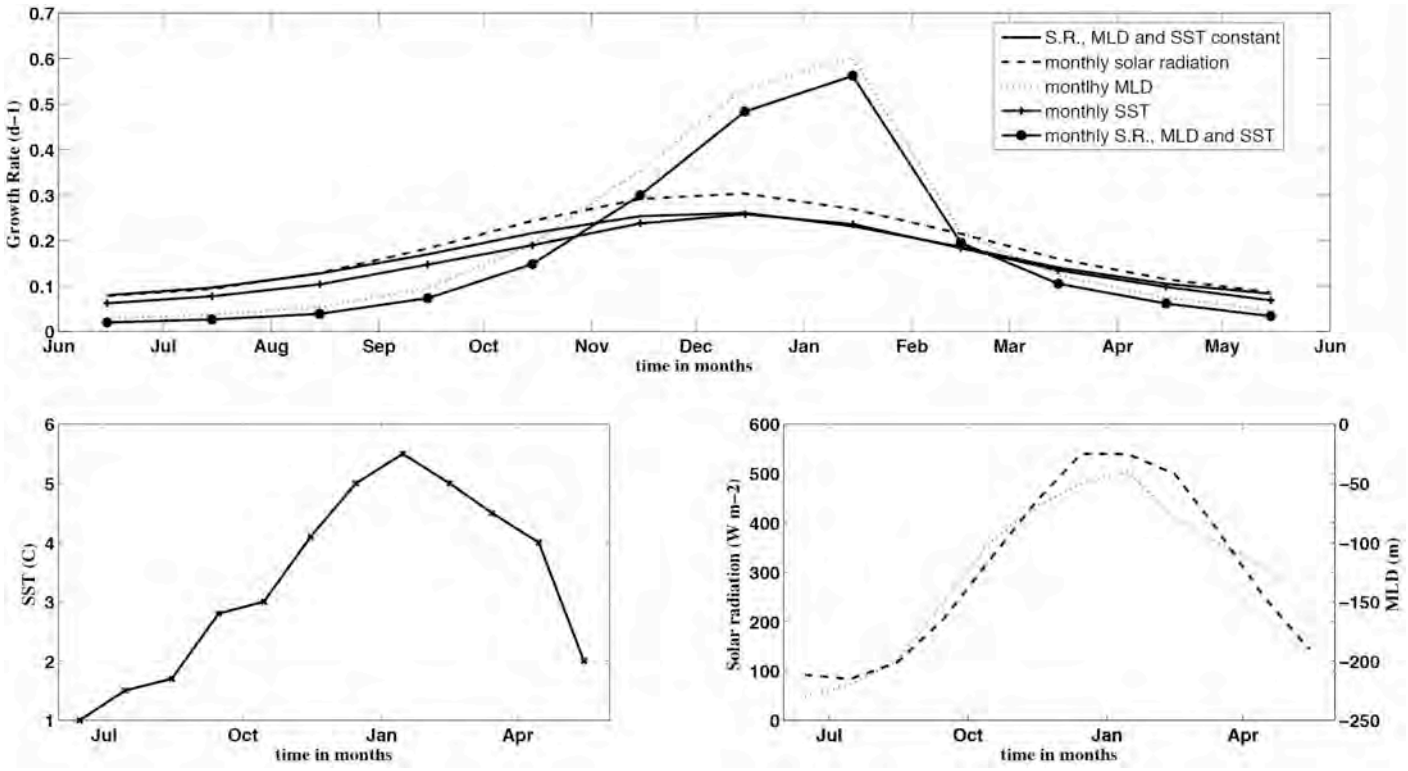

Figure 2.5: Top panel -Light-limited phytoplankton growth rate function (μ_I) calculated with seasonal (monthly) forcing values of solar radiation (S.R), sea surface temperature (SST) and mixed layer depth (*MLD*); **Bottom panels** –SST (solid line), *MLD* (dotted line) and S.R (dashed line) values used to calculate μ_I.

Nitrogenous nutrients are represented in these models only by nitrate (NO_3^-). The Michaelis-Menten functional form (also known as Monod) is adopted for uptake kinetics. This form is hyperbolic and requires a half-saturation term (K_N for nitrate) which specifies the concentration of nutrient at which uptake is half the maximum rate. Figure 2.6 illustrates a standard Michaelis-Menten curve.

$$\mu_N(N) = \mu_{\max}\left(\frac{N}{K_N + N}\right) \tag{2.9}$$

In this equation K_N is the half saturation constant for phytoplankton uptake on nitrate (N). Although a value of 0.5 mmol N m^{-3} was chosen for K_N, which is representative of experimental observations [*Boyd*, 2002; *Falkowski & Stone*, 1975]. the effect of different values for K_N is here tested.

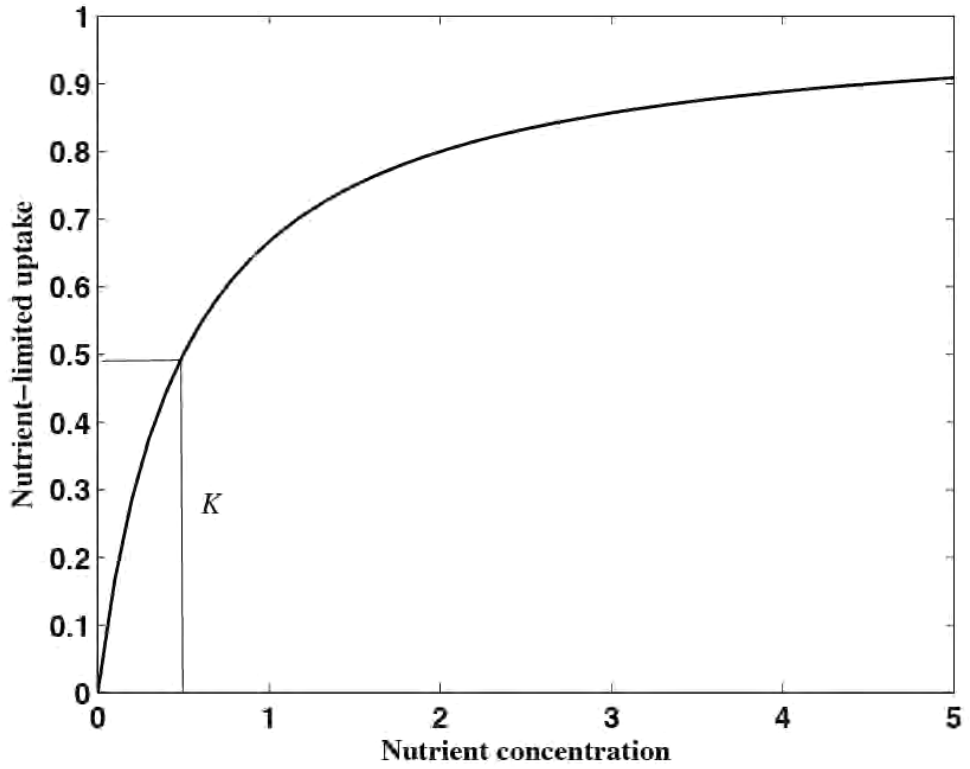

Figure 2.6: The Michaelis-Menten curve for uptake of a nutrient with a half-saturation constant, *K*, of 0.5 mmol N m^{-3} (blue). The black lines mark uptake of half the maximum rate at the specified value of *K*. Concentration in mmol N m^{-3}.

Figure 2.7 shows that using a smaller K_N = 0.1 mmol N m^{-3} [*Denman & Peña*, 1999] or a higher K_N value of 1mmol N m^{-3} [*Lancelot et al.*, 2000] has little effect (less than 5% of variation in the uptake in the Southern Ocean region) on the nutrient uptake factor.

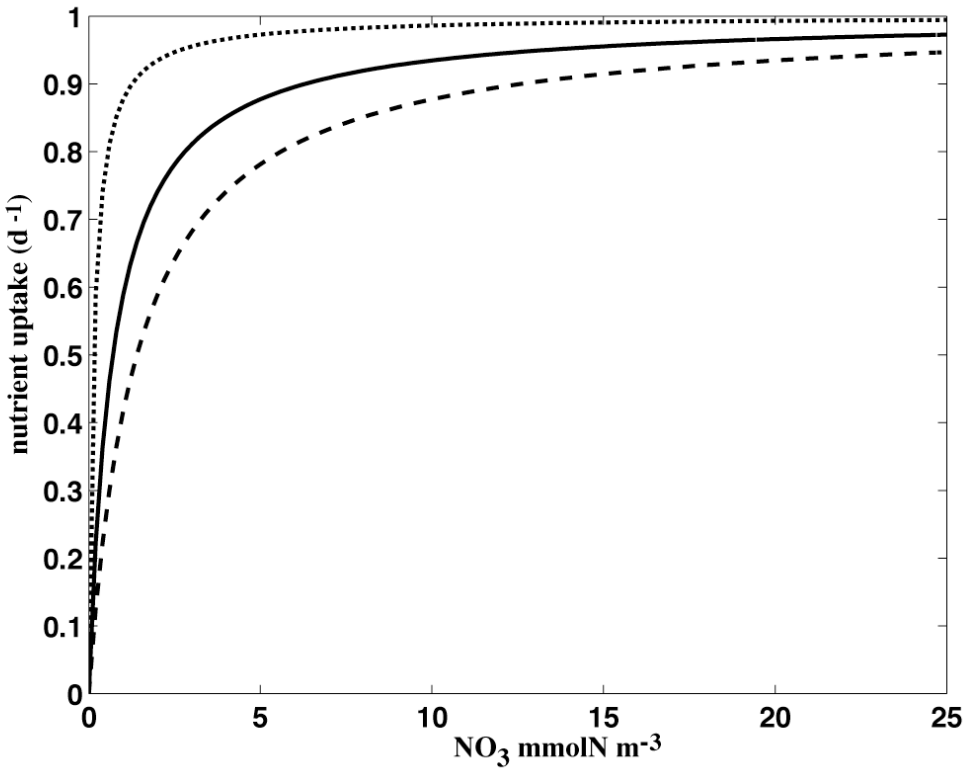

Figure 2.7: Nutrient (nitrate) uptake as a function of external nutrient concentration with three half-saturation constants for nitrate. K_N = 0.1 mmol N m^{-3} (dotted line), K_N = 1 mmol N m^{-3} (dashed line) and K_N = 0.5 mmol N m^{-3} (solid line). Nutrient uptake rate remains virtually unchanged at ambient nutrient concentration in the Southern Ocean (> 20 mmol N m^{-3}).

Phytoplankton mortality is defined as physiological death and subsequent lysis of phytoplanktonic cells. The phytoplankton natural mortality term is really a hybrid of several loss processes. These include viral infections, cell death due to an imbalance in respiration and photosynthesis and general cell death by senescence. It is difficult to determine this parameter from field measurements or laboratory experiments because it varies with time and space as well as the physiological condition.

Phytoplankton exudes a fraction of their net primary production as dissolved organic material. The amount varies in space and time and by species, and estimates of the percentage of primary production exuded range up to 70% [*Moloney & Field*, 1991]. However, despite the potential significance of exudation, the reasons for it are not entirely clear. Several suggestions have been made including exudation as a means to regulate cell osmotic potential, to ensure the correct stoichiometric ratios of

different elements without “switching off” the photosynthetic apparatus, and to establish a local bacterial community [*Thingstad et al.*, 2005].

In the standard model (OG99) used here, and many other models [*Findlay et al.*, 2006; *Gruber et al.*, 2006; *Hense et al.*, 2003; *Stock et al.*, 2008], phytoplankton mortality is parameterized using a linear function with a mortality rate, ε_P, with the resulting organic matter being allocated to the detrital pool, *D*.

In contrast, in the optimized model (SO03*a*) phytoplankton mortality is parameterized using a quadratic form [*e.g., Aumont & Bopp*, 2006; *Tagliabue et al.*, 2009b], and the parameter ε_P represents dissolved organic nitrogen (DON) that is exuded from the phytoplankton cells back the nitrate pool, *N*. It is included in the SO03*a* model as a function of temperature (see Table 2.1). Since estimates of natural phytoplankton mortality are exceedingly rare, the values of the parameters ε_P and *pmort* were here used to parameterise algal biomass stocks.

As described in the later section on the mixing dynamics, the final term controls phytoplankton losses due to dilution by entrainment of formerly subthermocline waters when the mixed layer deepens. Because it is assumed that there are no phytoplankton in the lower layer, changes in mixed layer depth affect phytoplankton biomass only when the mixed layer deepens ($w(t) > 0$), when water from below the mixed layer is mixed with surface waters, producing a dilution of phytoplankton within the upper mixed layer. As the mixed layer shallows, no new water is mixed into the surface; therefore phytoplankton concentrations do not change.

2.2.2 Zooplankton

The terms in these equations encompass, respectively, grazing on phytoplankton, predation losses, excretion losses and a dilution term.

$$\frac{dZ}{dt} = \gamma_z G(P)\, Z - zmort\, Z^2 - \varepsilon_Z\, Z - \frac{w^+(t)Z}{MLD} \qquad (2.10)$$

$$\frac{dZ}{dt} = \gamma_z G(P)\, Z - zmort\, Z^2 - \varepsilon_Z(T)\, Z - \frac{w^+(t)Z}{MLD} \qquad (2.11)$$

As stated previously, in the optimised model (SO03a) the excretion ($\varepsilon_Z(T)\, Z$) is temperature-dependent and in the standard model the excretion ($\varepsilon_Z\, Z$) is not.

Natural mortality is parameterized as a quadratic function of zooplankton biomass. Steele & Henderson [1992] have shown that the mathematical form of this term, which is also known as the "closure term" because it closes the model at the top trophic level, can have a large influence on the dynamics and they favoured a quadratic functional form. Fasham [1995] and Edwards & Brindle [1999] provided further support for the quadratic form, and here it is used in both models.

The zooplankton quadratic mortality term represents increasing populations of predators as zooplankton populations increase and is supposed to be more stable (*i.e.*, not inducing oscillatory behaviour in the model) than a linear or near-linear term. In other words, as the main interest is on the factors controlling the building up of phytoplankton blooms, carnivores are not modelled explicitly; their effect are simulated in the quadratic mortality of herbivores.

The form of system closure has attracted considerable attention in the last ten years [*Denman*, 2003; *Edwards & Yool*, 2000; *Franks*, 2002; *Platt et al.*, 2005], but observationally and experimentally the best choice of term is, at this time, unclear.

The grazing rate on phytoplankton $G(P)$ is defined by a Holling type III function [*Fasham*, 1995] as,

$$G = \frac{g\ pc\ P^2}{g + pc\ P^2} \qquad (2.12)$$

where, g is the maximum grazing rate and pc is a parameter that relates the rate of capture of prey items to prey density (*i.e.*, prey capture rate). Figure 2.8 shows how the relationship between total grazing and the concentration of the food item (*i.e.*, phytoplankton) is affected by both g and pc constant values. The quadratic form of this grazing function at low values of P provides a threshold for grazing, considered to be a source of model stability [*Denman & Peña*, 1999].

Zooplankton are inefficient in assimilating the grazed phytoplankton, therefore only a fraction, γ_z, of the total grazing is assumed to lead to zooplankton growth. This is essentially the same formulation used by Fasham *et al*. [1990], but simplified due to the occurrence of only one food type, *i.e.* phytoplankton. The unassimilated fraction, (1 - γ_z), assumed to consist of a combination of faecal pellets and uningested phytoplankton parts, is allocated to the detrital pool.

Finally, zooplankton concentrations are also affected by changes in mixed layer depth, in the same way as phytoplankton. In these models it is assumed that the zooplankton remain in the vicinity of their food source (the phytoplankton) and do not undergo migration. However, in the real world, herbivorous zooplankton have the ability to propel themselves through the water and often have a diurnal cycle depending upon the species [*Fasham et al.*, 1999; *Miller*, 2003].

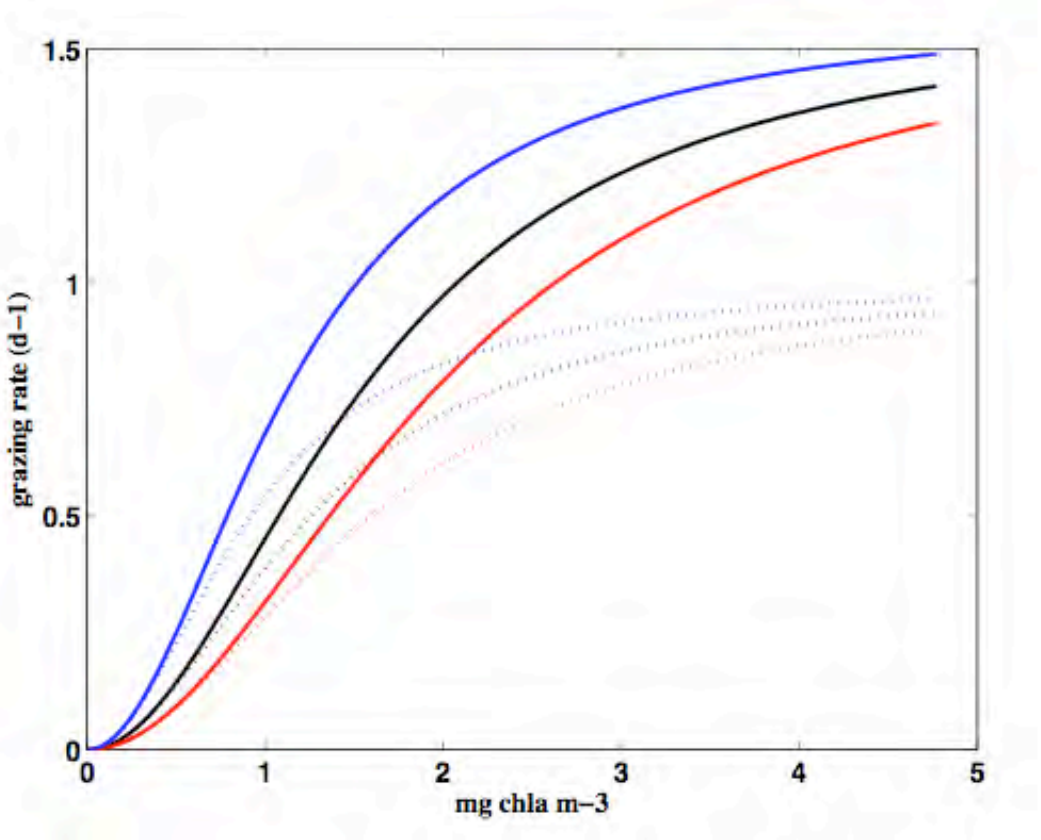

Figure 2.8: Relationship between grazing and phytoplankton concentration (mg Chla m^{-3}) with different values assigned to the parameters *g* and *pc*. The default's values, listed in Table 2.2, give the black line. Red and blue lines are for *pc* = 1.0 and 3.0 (mmol $m^{-3})^{-2}$ day^{-1} respectively, and dotted lines show same relationships but with *g* = 1 d^{-1}.

2.2.3 Nitrate

The terms in these equations encompass, respectively, gains due to remineralisation, excretion, entrainment, and exudation (only for the SO03a model version), and losses due to uptake by phytoplankton, and mixing.

$$\frac{dN}{dt} = rem\ D + \varepsilon_Z\ Z\ - \mu\,(MLD, t, N)\ \ P - \frac{(N_0 - N)w^+(t)}{MLD} \qquad (2.13)$$

$$\frac{dN}{dt} = rem(T)\ D + \varepsilon_Z(T)\ Z + \varepsilon_P(T)\ P - \mu\,(MLD, t, N)\ \ P - \frac{(N_0 - N)w^+(t)}{MLD} \qquad (2.14)$$

Nitrate is assumed in the model to be at non-zero concentrations below the thermocline. All the other model state variables are assumed to return to nitrate through chemical and biological degradation.

Assuming that the upper layer is always perfectly mixed, the dilution process due to the mixed layer deepening is balanced by nutrient addition from the inactive lower layer containing nutrients (N_0) but not plankton. In practice, the rate at which this process will decrease or increase upper layer nutrient concentrations is given by w^+MLD^{-1} ($N_0 - N$) (see section 2.2.6). The actual value of deep nitrate is strongly related to latitude [*Rintoul & Trull*, 2001; *Strass & Woods*, 1991], and for the reference simulations N_0 is set to a value of 30 mmol N m^{-3} [*Lourey & Trull* 2001; *Lucas et al.*, 2007; *Parslow et al.*, 2001].

Although in this work, the subthermocline concentration, N_0, has been assumed to be constant with time and mixed-layer depth, other authors [*e.g.*, *Fasham*, 1995; *Frost*, 1993], have considered more realistic formulations. For instance, Steel & Henderson [1993] assumed N_0 to be constant above certain fixed depth but take the form of a linear increasing function of depth below this depth.

2.2.4 Detritus

The detritus pool *D* represents sinking, suspended and dissolved organic nitrogen (PON and DON) created by phyto- and zooplankton. The terms in these equations encompass, respectively, inputs from the inefficiency of zooplankton grazing on phytoplankton, inputs of dead phytoplankton and zooplankton cells, and losses through breakdown to soluble compounds and sinking/mixing/dilution.

$$\frac{dD}{dt} = (1 - \gamma_z)\, G(P)\, Z + \varepsilon_P\, P + zmort\, Z^2 - rem\, D - \left(\frac{w_S + w^+(t)D}{MLD}\right) \qquad (2.15)$$

$$\frac{dD}{dt} = (1 - \gamma_z)\, G(P)\, Z + pmort\, P^2 + zmort\, Z^2 - rem(T)\, D - \left(\frac{w_S + w^+(t)D}{MLD}\right) \qquad (2.16)$$

The majority of these terms have been defined in previous equations and the reader is directed back to earlier sections for their derivation and biological meaning.

All the dead material from phytoplankton and zooplankton, as well as the zooplankton feeding inefficiency ("sloppy feeding" or digestive inefficiencies) material from grazing processes, drop into the detrital pool.

In the OG99 reference model, detritus breaks down to the *N* pool at a constant rate, *rem*. The advantage of this simplification is that it allows the regeneration process to be parameterized into a single linear function. In the SO03a model, the remineralisation term is parameterized as a function of temperature (Eq. 2.8).

The linear form of this rate used in the OG99 model is less objectionable since detritus is not subject to the density dependent effects (*e.g.*, viral infection, predation) which afflict the previous three compartments. The rate was chosen within the range of observations [*Fennel et al.*, 2003a; *Li & Peng*, 2002; *Oschlies & Garçon*, 1999].

In the ocean the nature of the inputs to the detrital compartment mean that it consists of relatively large particles of material (*e.g.*, faecal pellets, aggregated cells). These particles (as a single pool in this model) are assumed to sink out of the mixed

layer, and the final sinking/mixing/dilution loss term is modified to incorporate a sinking velocity, w_S (Eqs. 2.15-2.16).

Choosing a value for this process is complicated by differently-sized particles sinking at different velocities, and by the difficulty in separating living particles from detrital ones when measurements are made. Using a regression of particles flux against particle density data (*i.e.*, how much sinks out versus how much there is in the water column), Fasham [1993] estimated a sinking velocity of 4 m d^{-1}. This estimated was used by Oschlies & Garcon [1999] to suggest an appropriate magnitude for the parameter, and then a value of 5.0 m d^{-1} was chosen on the basis of model performance.

A series of values, ranging from 1 to 10 m d^{-1}, have been reported for the Southern Ocean [*Fennel et al.*, 2003a; *Hense et al.*, 2000; *Mongin et al.*, 2006] and recently, Popova *et al* [2007] informed a detrital sinking velocity of 4 m d^{-1} for the Subantarctic Zone.

As indicated in Chapter 1, sinking fluxes out of the mixed layer are of interest biogeochemically since some of the material lost in this way is ultimately buried geologically.

2.3 Forcing functions

In addition to the dynamical behaviour of the model, OG99 uses three forcing functions to drive the system. Both represent physical processes which are, it is assumed, unaffected by the biological dynamics of the upper mixed layer.

Lovelock [2000] suggests a mechanism by which marine phytoplankton may influence cloud seeding patterns (and thus the sea irradiance) through the release of dimethyl sulphide (DMS) [see also *Liss et al.*, 1993]. Sathyendranath *et al*. [1991] and Kahru *et al.* [1993] discuss how the absorption of solar radiation by phytoplankton pigments can influence sea surface temperatures (and thus the water column stability to mixing). However, processes such as these are ignored here. All models in this thesis use the forcing functions as described below.

2.3.1 Solar irradiance

With the following astronomical formulae [*Brock*, 1981], we calculate the length of a day and the photosynthetically active radiation (*PAR*) entering the ocean any given time and latitude.

Declination of the Earth, δ

$$\delta = -0.406\cos(2\pi T) \tag{2.17}$$

daylength 2τ

$$2\tau = \frac{\arccos(-\tan(\delta)\tan(\phi))}{\pi} \tag{2.18}$$

where T is in years and ϕ is the latitude (in radians). Assuming a triangular temporal evolution of solar radiation (starting with 0 Wm^{-2} at sunrise and peaking at midday), total radiation at noon, I_{noon}, is chosen such that the input of solar radiation integrated over 24 hours equals the average daily solar shortwave radiation (*SRA*)

$$I_{noon} = \frac{SRA}{\tau} \tag{2.19}$$

and, irradiance reaching the surface at noon is then further corrected to only account for the ratio of *PAR* to total radiation

$$I_{PAR} = I_{noon} \times PAR \tag{2.20}$$

We therefore have a simplified light profile, $I(z, t)$, which goes into the equation 2.12 to be then analytically integrated over time (t) and depth (z)

$$I(z,t) = I_{PAR}(t)\exp\left(-(k_w + k_p P)z\right) \quad (2.21)$$

Figure 2.9d illustrates the annual cycle of daily average incident short-wave radiation (*SRA*) used to calculate the mixed-layer light field and to determine the growth rate of phytoplankton. Seasonal variations in surface radiation are based on the 1-D model reported by Mongin *et al*. [2006] for the KERFIX site in the Indian sector of the Southern Ocean.

2.3.2 Mixed layer depth

Unlike the solar forcing detailed above, the dynamics of the mixed layer are modeled entirely empirically. Figure 2.9a shows the seasonal cycle of mixed-layer for the locations of the Kerguelen Ocean and Plateau compared Study (KEOPS). As no biogeochemical model has been specifically developed so far for the Kerguelen plateau, the mixed layer depth are taken from a turbulent kinetic energy one-dimensional (80 vertical levels) model calibrated at the nearby HNLC KERFIX time series site [*Mongin et al.*, 2006]. This mixed layer depth represents the mean obtained using 6-hourly (ECMWF) wind and radiation forcing for the 1989-1995 period in the 1-D model.

Daily values of mixed layer depth are then used to specify the rate of change (Fig. 2.9c), $w(t)$, in the depth.

$$\frac{dMLD}{dt} = w(t) \quad (2.22)$$

Changes in the mixed layer depth affect the model asymmetrically [*Evans & Parslow*, 1985]. A deepening of the mixed layer ($w > 0$) will mix water from below with surface water, producing a dilution of phytoplankton, zooplankton, and detritus and a mixing of surface and deep nutrients. Whereas when the mixed layer shallows ($w < 0$) no new water is introduced into the mixed layer and the concentrations of

nitrate, phytoplankton and zooplankton remain constant in the mixed layer. This asymmetry is included in the model by defining:

$$w^{+}(t) = \max\,(w(t), 0) \tag{2.23}$$

For example, when the mixed layer is shallowing, $w(t)$ is negative and $w^{+}(t)$ is zero. By substituting this into the phytoplankton equation, the concentration of phytoplankton remains constant since detrainment, whilst reducing total phytoplankton biomass in the mixed layer, does not alter its concentration. By contrast, in the case of a deepening mixed layer, $w^{+}(t) = w(t)$, and the concentration of phytoplankton falls. Here, subthermocline water (which is assumed to contain no phytoplankton cells) is introduced into the mixed layer, increasing the volume of the mixed layer and consequently reducing phytoplankton concentration, although not reducing their total biomass.

2.3.3 Temperature

Mean monthly values of Sea Surface Temperature (SST) were obtained from the Physical Oceanography Distributed Active Archive Center (PO.DAAC) at the NASA Jet Propulsion Laboratory, Pasadena, CA. http://podaac.jpl.nasa.gov. These data was linearly interpolated to generate values of surface temperature on intermediate days, and Figure 2.9b shows the resulting seasonal cycle of SST in the vicinity of the Kerguelen plateau in the Subantarctic zone of the Southern Ocean.

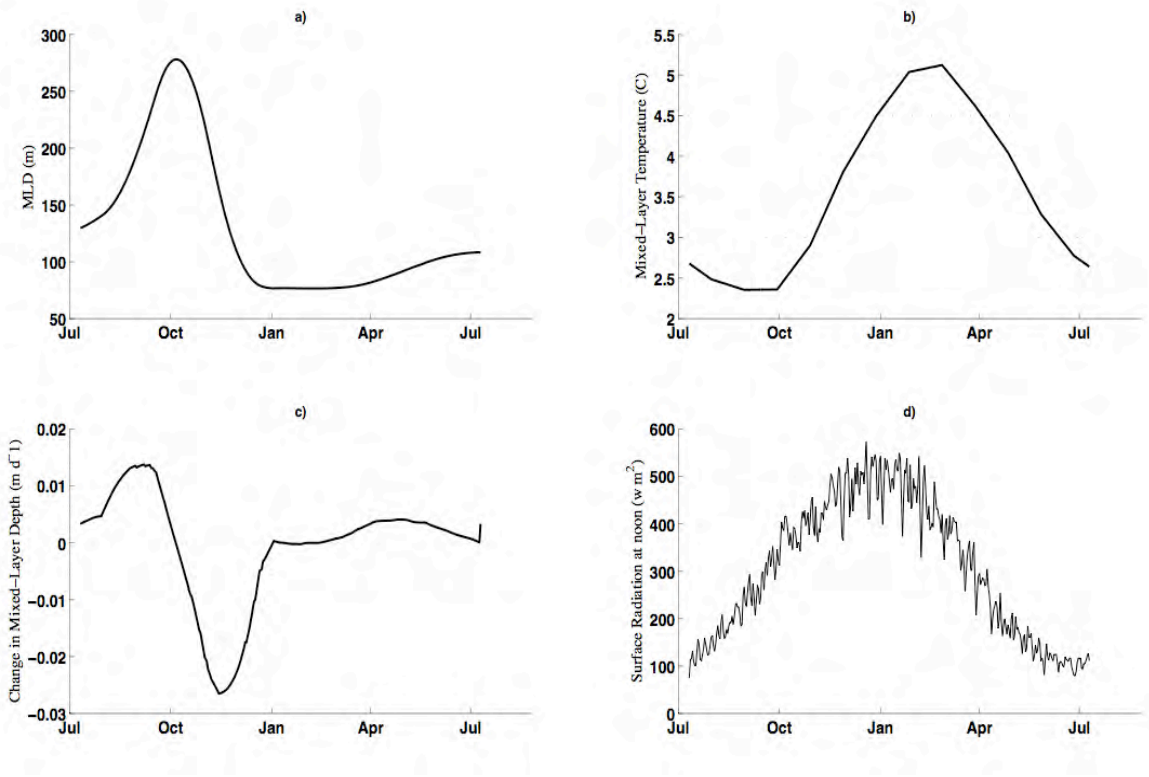

Figure 2.9: Forcing functions of the ecosystem model for the Southern Ocean HNLC-reference simulation. Seasonal variations for **a)** depth of the mixed layer (m), **b)** temperature of the mixed layer (°C), **c)** the rate of the change of the mixed layer depth (m d^{-1}), and **d)** daily average incident short-wave radiation (W m^{-2}).

2.4 The reference simulation

The temporal variation of the state variables was calculated by integrating the set of differential equations of the models (Table 2.2, Eqs. (2.2-2.3), (2.10-2.11), (2.13-2.14), (2.15-2.16)) using an explicit fourth-order Runge-Kutta time-stepping algorithm. The use of the adaptive time step algorithm was chosen to speed integration and maintain accuracy. The simulations were run for three years, with the last year of data being used in the analysis.

Initial values of chemical and biological state variables were 29 mmol N m^{-3}, 0.1 mmol N m^{-3}, 0.01 mmol N m^{-3}, and 0.01 mmol N m^{-3}, for nitrate, phytoplankton,

zooplankton and detritus, respectively. These initial concentrations were inferred from observed climatologies [*Conkright et al.*, 2002; *Mitchell et al.*, 1991] for nitrate and phytoplankton, and set to arbitrary low values for zooplankton and detritus.

The simulations begin on July 11, near the annual winter minimum in phytoplankton biomass and productivity at the KEOPS *HNLC*-reference site (-51° 38' S - 77° 58' E). In these first simulations the sinking rate of detritus D was set to 0 (*i.e.*, a closed system with no losses from the model domain). Model results, using the parameter values shown in Table 2.2, for the surface mixed layer are presented in Figure 2.10.

Typically by the second year, both models achieved a steady state annual cycle which was not sensitive to the initial conditions. The steady state solution is taken here to mean stability in all state variables on the longest time scale of variability in environmental forcing (i.e. one year), allowing for variability in any or all model state variables on shorter time scales. The standard (OG99) and optimized (SO03a) simulations feature a seasonal cycle of plankton (Fig. 2.10) with concentrations in agreement with observations (*i.e. HNLC* condition) [*Moore & Abbott*, 2000; 2002; *Sokolov & Rintoul*, 2007b]. In October, when the solar radiation increases and the mixed layer retreats, phytoplankton growth begins.

Using the standard and optimized models, phytoplankton biomass reaches its maximum in early November with concentrations of 0.6 mg Chl*a* m^{-3} and in December with concentrations of 0.9 mg Chl*a* m^{-3}, respectively (Fig. 2.10b).

Zooplankton (Fig. 2.10c) starts to develop in November shortly after the onset of phytoplankton growth and reaches its maximum in January with maximum concentrations of 0.4 mmol N m^{-3} (*i.e.* 31 mg C m^{-3}) and 0.8 mmol N m^{-3} (*i.e.* 63 mg C m^{-3}), for the standard and optimized simulations respectively.

Nitrate is not depleted at anytime (Fig. 2.10a), and simulated nitrate concentrations are in the rate of observations during the KEOPS campaign (at the *HNLC* sites) with concentrations > 21 mmol m^{-3} in summer [*Mongin et al.*, 2008; *Trull et al.*, 2008]. The absence of a strong decrease in nitrate concentration in summer is a prominent feature of the ecosystem near the Antarctic Polar Front and has been repeatedly observed [*Trull et al.*, 2001a; *Van Oijen et al.*, 2004] and is also a

distinctive feature of model studies in the Southern Ocean [*Mongin et al.*, 2006; *Pondaven et al.*, 1998].

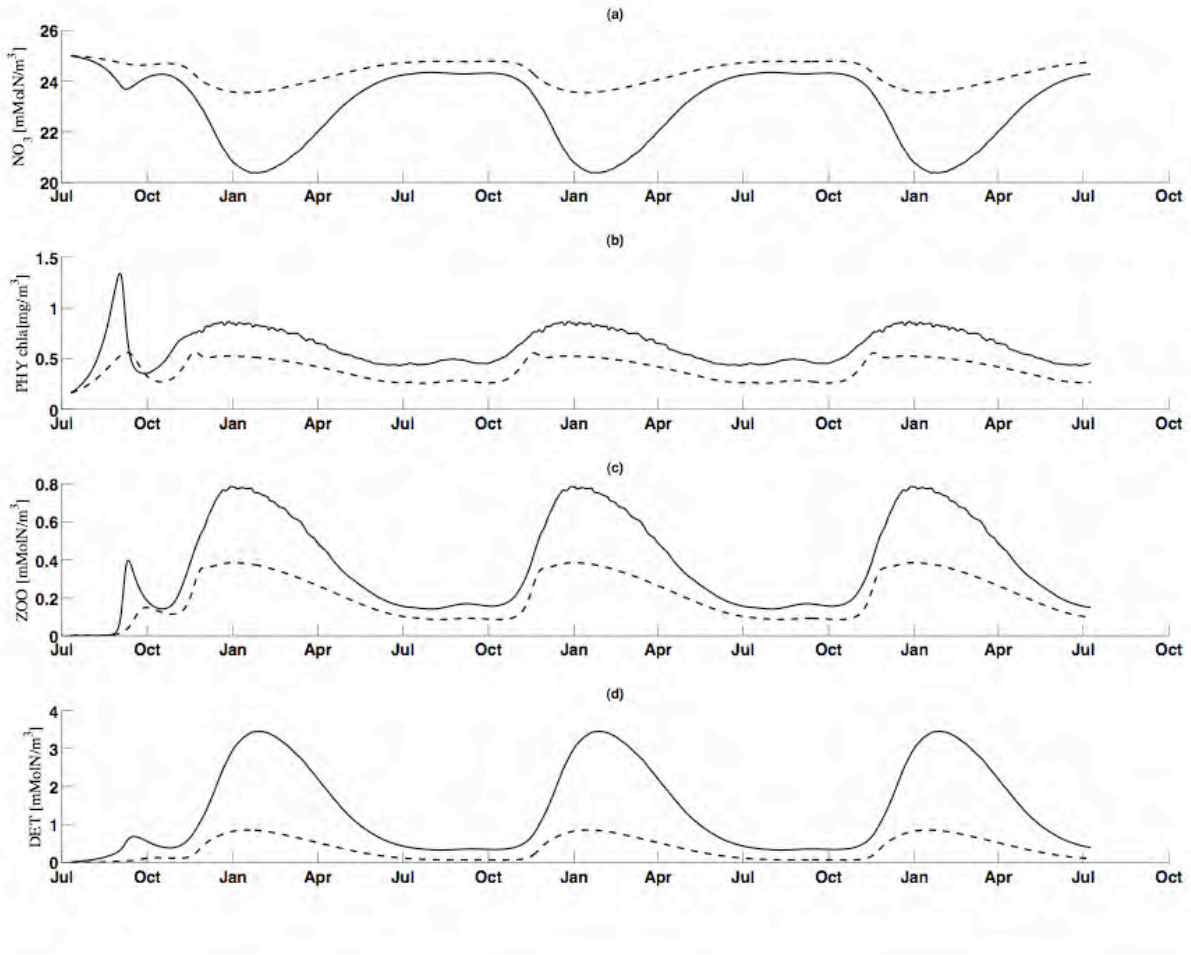

Figure 2.10: Standard model OG99 (dashed line) and optimized model SO03a (solid line) simulated concentrations of (a) nitrate, (b) phytoplankton, (c) zooplankton and (d) detritus for the Southern Ocean reference experiment.

When compared to each other, the temporal variability of phytoplankton concentrations is reduced in the standard (OG99) model version. The amplitude of the seasonal cycle shows a reduction compared to the optimized (SO03a) version. Phytoplankton biomass is always smaller than 0.5 mg Chl*a* m^{-3} which is half the maximum reached in the SO03a run. Moreover, the spring bloom simulated by the OG99 model peaks earlier by more than a month compared to the SO03a run.

The smaller amplitude of the seasonal cycle simulated by the OG99 model results mainly from two changes in the ecosystem model. Firstly, the initial slope of P-I

curve (α) is increased by a factor of 10 in the SO03a configuration (Table 2.2). Secondly, the zooplankton quadratic mortality rate is higher in the optimized model by a factor of 1.7. The reduced half saturation constant for nitrate uptake in the OG99, and the presence of a rapid recycling of nitrogen from phytoplankton back to the DIN compartment produces a considerably slower drawdown of nutrients during spring and summer.

In the optimized version of the *NPZD*-model (SO03a) the maximum growth rate of phytoplankton, as well as the phytoplankton specific mortality, the remineralisation rate and the zooplankton excretion rate, depend on the ambient temperature (Eq. 2.8). Calibrated for the typical temperatures at the three different North-Atlantic sites used in the optimisation process (*i.e.* BATS, NABE and OWS-INDIA), the resulting rates within the temperature range of the Polar Front in the Southern Ocean are extremely low.

The optimal parameters that are a compromise among all three locations can differ from values being optimal for another location. This is not a great surprise, but it clarified how the parameter estimates need to be interpreted. Nevertheless, one has to accept that ecosystem models always remain simplified representations of the real environment. It will, therefore, hardly be possible to give reliable approximations of biogeochemical fluxes without investigating the model's parameter space as well.

In this study, the baseline ecosystem modelling will be done with the standard OG99 model, and the results will be used to consider whether important parameters, such as those entering phytoplankton growth rate parameterizations or the mortality terms, could be changed to better account for the different ecosystem conditions found on and around the naturally iron-fertilized Kerguelen Plateau in the Southern Ocean.

2.5 Summary

This chapter has aimed primarily to introduce and describe the reference model, the OG99, and the optimized version of it, the SO03a model. Since the OG99 model is only one of many which are used in studies of plankton ecosystems, the chapter has also compared one to another, to draw attention to the differences in both the structures of these models, and the choices of functional responses used in them. This variety reflects some ignorance about the nature of the pathways, but also the simplification of models so that they remain analytically tractable and sometimes more accurate. The chapter is then concluded by a simulation of the *HNLC* surface waters south-east of the Kerguelen plateau in the Subantarctic zone.

2.6 References

Aumont, O., S. Belviso, and P. Monfray (2002), Dimethylsulfoniopropionate (DMSP) and dimethylsulfide (DMS) sea surface distributions simulated from a global three-dimensional ocean carbon cycle model, *J. Geophys. Res*, *107*(C4), 1-21.

Aumont, O., E. Maier-Reimer, S. Blain, et al. (2003), An ecosystem model of the global ocean including Fe, Si, P colimitations, *Global Biogeochemical Cycles*, *17*(2), 1060.

Aumont, O., and L. Bopp (2006), Globalizing results from ocean in situ iron fertilization studies, *Global Biogeochemical Cycles*, *20*(2), 10.1029.

Bonner-Knowles, D., G. Jones, and A. Gabric (2005), Dimethylsulphide production in the Southern Ocean using a nitrogen-based flow network model and field measurements from ACE-1, *Journal of Atmospheric & Ocean Science*, *10*(2), 95-122.

Bopp, L., P. Monfray, O. Aumont, et al. (2001), Potential impact of climate change on marine export production, *Global Biogeochemical Cycles*, *15*, 81-99.

Boyd, P. W. (2002), Environmental factors controlling phytoplankton processes in the Southern Ocean, *Journal of Phycology*, *38*(5), 844-861.

Brock, T. (1981), Calculating solar radiation for ecological studies, *Ecological Modelling*, *14*(1-2), 1-19.

Chai, F., M. S. Jiang, Y. Chao, et al. (2007), Modeling responses of diatom productivity and biogenic silica export to iron enrichment in the equatorial Pacific Ocean, *Global Biogeochemical Cycles*, *21*(3).

Conkright, M. E., R. A. Locarnini, H. E. Garcia, et al. (2002), World Ocean Atlas 2001: Objective Analyses, *Data Statistics, and Figures, CD-ROM*

Documentation, National Oceanographic Data Center, Silver Spring, MD, 1ñ17.

Denman, K. (2003), Modelling planktonic ecosystems: parameterizing complexity, *Progress in Oceanography*, *57*(3-4), 429-452.

Denman, K. L., and M. A. Peña (1999), A coupled 1-D biological/physical model of the northeast subarctic Pacific Ocean with iron limitation, *Deep-Sea Research Part II: Topical Studies in Oceanography*, *46*(11-12), 2877-2908.

Doney, S. C., I. Lima, J. K. Moore, et al. (2009), Skill metrics for confronting global upper ocean ecosystem-biogeochemistry models against field and remote sensing data, *Journal of Marine Systems*, *76*(1-2), 95-112.

Edwards, A. M., and J. Brindley (1999), Zooplankton mortality and the dynamical behaviour of plankton population models, *Bulletin of Mathematical Biology*, *61*(2), 303-339.

Edwards, A. M., and A. Yool (2000), The role of higher predation in plankton population models, *Journal of Plankton Research*, *22*(6), 1085-1112.

Eppley, R. W. (1972), Temperature and phytoplankton growth in the sea, *Fisheries Bulletin*, *70*, 1063-1085.

Evans, G. T., and J. S. Parslow (1985), A model of annual plankton cycles, *Biological Oceanography*, *3*(3), 327-347.

Falkowski, P., and D. Stone (1975), Nitrate uptake in marine phytoplankton: energy sources and the interaction with carbon fixation, *Marine Biology*, *32*(1), 77-84.

Fasham, M. (1995), Variations in the seasonal cycle of biological production in subarctic oceans: A model sensitivity analysis, *Deep Sea Research Part I: Oceanographic Research Papers*, *42*(7), 1111-1149.

Fasham, M. J. R., H. W. Ducklow, and S. M. McKelvie (1990), A nitrogen-based model of plankton dynamics in the oceanic mixed layer, *Journal of Marine Research*, *48*(3), 591-639.

Fasham, M. J. R. (1993), Modelling the marine biota, in *The global Carbon Cycle*, edited by M. Heimann, pp. 457-504, Springer Verlag, Berlin.

Fasham, M. J. R., P. W. Boyd, and G. Savidge (1999), Modeling the relative contributions of autotrophs and heterotrophs to carbon flow at a Lagrangian JGOFS station in the Northeast Atlantic: The importance of DOC, *Limnology and Oceanography*, *44*(1), 80-94.

Fennel, K., M. R. Abbott, Y. H. Spitz, et al. (2003a), Modeling controls of phytoplankton production in the southwest Pacific sector of the Southern Ocean, *Deep-Sea Research Part II: Topical Studies in Oceanography*, *50*(3-4), 769-798.

Fennel, K., M. R. Abbott, Y. H. Spitz, et al. (2003b), Impacts of iron control on phytoplankton production in the modern and glacial Southern Ocean, *Deep-Sea Research Part II: Topical Studies in Oceanography*, *50*(3-4), 833-851.

Findlay, H., A. Yool, M. Nodale, et al. (2006), Modelling of autumn plankton bloom dynamics, *Journal of Plankton Research*, *28*(2), 209.

Franks, P. J. S. (2002), NPZ models of plankton dynamics: Their construction, coupling to physics, and application, *Journal of Oceanography*, *58*(2), 379-387.

Frost, B. (1987), Grazing control of phytoplankton stock in the open subarctic Pacific Ocean: A model assessing the role of mesozooplankton, particularly the large calanoid copepods Neocalanus spp, *Marine ecology progress series. Oldendorf*, *39*(1), 49-68.

Frost, B. W. (1993), A modelling study of processes regulating plankton standing stock and production in the open subarctic Pacific Ocean, *Progress in Oceanography*, *32*(1-4), 17-56.

Fujii, M., N. Yoshie, Y. Yamanaka, et al. (2005), Simulated biogeochemical responses to iron enrichments in three high nutrient, low chlorophyll (HNLC) regions, *Progress in Oceanography*, *64*(2-4), 307-324.

Gabric, A., N. Murray, L. Stone, et al. (1993), Modelling the production of dimethylsulfide during a phytoplankton bloom, *Journal of geophysical research*, *98*(C12), 22805-22822,22816.

Garcon, V., A. Oschlies, S. Doney, et al. (2001), The role of mesoscale variability on plankton dynamics in the North Atlantic, *Deep Sea Research Part II: Topical Studies in Oceanography*, *48*(10), 2199-2226.

Garver, S., D. Siegel, and B. Mitchell (1994), Variability in near-surface particulate absorption spectra: what can a satellite ocean color imager see?, *Limnology and Oceanography*, *39*(6), 1349-1367.

Geider, R. J., and J. La Roche (2002), Redfield revisited: variability of C:N:P in marine microalgae and its biochemical basis, *European Journal of Phycology*, *37*(1), 1-17.

Gruber, N., H. Frenzel, S. C. Doney, et al. (2006), Eddy-resolving simulation of plankton ecosystem dynamics in the California Current System, *Deep-Sea Research Part I: Oceanographic Research Papers*, *53*(9), 1483-1516.

Hense, I., U. V. Bathmann, and R. Timmermann (2000), Plankton dynamics in frontal systems of the Southern Ocean, *Journal of Marine Systems*, *27*(1-3), 235-252.

Hense, I., R. Timmermann, A. Beckmann, et al. (2003), Regional and interannual variability of ecosystem dynamics in the Southern Ocean, *Ocean Dynamics*, *53*(1), 1-10.

Hoffmann, L. J., I. Peeken, K. Lochte, et al. (2006), Different reactions of Southern Ocean phytoplankton size classes to iron fertilization, *Limnology and Oceanography*, 1217-1229.

Hurtt, G. C., and R. A. Armstrong (1996), A pelagic ecosystem model calibrated with BATS data, *Deep-Sea Research Part II: Topical Studies in Oceanography*, *43*(2-3), 653-683.

Jassby, A., and T. Platt (1976), Mathematical formulation of the relationship between photosynthesis and light for phytoplankton, *Limnology and Oceanography*, *21*(4), 540-547.

Ji, R., C. Davis, C. Chen, et al. (2008), Influence of local and external processes on the annual nitrogen cycle and primary productivity on Georges Bank: A 3-D biological-physical modeling study, *Journal of Marine Systems*, *73*(1-2), 31-47.

Kahru, M., J. Lepp‰nen, and O. Rud (1993), Cyanobacterial blooms cause heating of the sea surface, *MARINE ECOLOGY-PROGRESS SERIES*, *101*, 1-1.

Lancelot, C., C. Veth, and S. Mathot (1991), Modelling ice-edge phytoplankton bloom in the Scotia-Weddell sea sector of the Southern Ocean during spring 1988, *Journal of Marine Systems*, *2*, 333-346.

Lancelot, C., E. Hannon, S. Becquevort, et al. (2000), Modeling phytoplankton blooms and carbon export production in the Southern Ocean: dominant controls by light and iron in the Atlantic sector in Austral spring 1992, *Deep Sea Research-Part I-Oceanographic Research Papers*, *47*(9), 1621-1662.

Le Quéré, C., S. P. Harrison, P. I. Colin, et al. (2005), Ecosystem dynamics based on plankton functional types for global ocean biogeochemistry models, *Glob Change Biol*, *11*, 2016ñ2040.

Li, Y.-H., and T.-H. Peng (2002), Latitudinal change of remineralization ratios in the oceans and its implication for nutrient cycles, *Global Biogeochemical Cycles*, *16*(4), doi:10.1029/2001GB001828.

Liss, P., G. Malin, and S. Turner (1993), Production of DMS by marine phytoplankton, Springer.

Lourey, M. J., and T. W. Trull (2001), Seasonal nutrient depletion and carbon export in the Subantarctic and Polar Frontal Zones of the Southern Ocean south of Australia, *Journal of Geophysical Research. C. Oceans*, *106*(C12), 31463-31488.

Lovelock, J. (2000), *The ages of Gaia: a biography of our living earth*, Oxford University Press.

Lucas, M., S. Seeyave, R. Sanders, et al. (2007), Nitrogen uptake responses to a naturally Fe-fertilised phytoplankton bloom during the 2004/2005 CROZEX study, *Deep Sea Research Part II: Topical Studies in Oceanography*, *54*(18-20), 2138-2173.

Machu, E., A. Biastoch, A. Oschlies, et al. (2005), Phytoplankton distribution in the Agulhas system from a coupled physical-biological model, *Deep Sea Research Part I: Oceanographic Research Papers*, *52*(7), 1300-1318.

Miller, C. B. (2003), *Biological oceanography*, 1 v. pp., Blackwell Pub., Oxford.

Mitchell, B. G., E. A. Brody, O. Holm-Hansen, et al. (1991), Light Limitation of Phytoplankton Biomass and Macronutrient Utilization in the Southern Ocean, *Limnology and Oceanography*, *36*(8), 1662-1677.

Moloney, C., and J. Field (1991), The size-based dynamics of plankton food webs. I. A simulation model of carbon and nitrogen flows, *Journal of Plankton Research*, *13*(5), 1003.

Mongin, M., D. M. Nelson, P. Pondaven, et al. (2006), Simulation of upper-ocean biogeochemistry with a flexible-composition phytoplankton model: C, N and Si cycling and Fe limitation in the Southern Ocean, *Deep-Sea Research II*, *53*(5-7), 601-619.

Mongin, M., E. Molina, and T. W. Trull (2008), Seasonality and scale of the Kerguelen plateau phytoplankton bloom: A remote sensing and modeling analysis of the influence of natural iron fertilization in the Southern Ocean, *Deep Sea Research Part II: Topical Studies in Oceanography*, *55*(5-7), 880-892.

Moore, J., and M. Abbott (2000), Phytoplankton chlorophyll distributions and primary production in the Southern Ocean, *Journal of Geophysical Research*, *105*(C12), 28709-28722.

Moore, J. K., and M. R. Abbott (2002), Surface chlorophyll concentrations in relation to the Antarctic Polar Front: seasonal and spatial patterns from satellite observations, *Journal of Marine Systems*, *37*, 69-86.

Moore, J. K., S. C. Doney, J. A. Kleypas, et al. (2002a), An intermediate complexity marine ecosystem model for the global domain, *Deep-Sea Research II*, *49*, 403-462.

Moore, J. K., S. C. Doney, D. M. Glover, et al. (2002b), Iron cycling and nutrient-limitation patterns in surface waters of the World Ocean, *Deep-Sea Research II*, *49*, 463–507.

Oschlies, A., and V. Garçon (1998), Eddy-induced enhancement of primary production in a model of the North Atlantic Ocean, *Nature*, *394*(6690), 266-269.

Oschlies, A., and V. Garçon (1999), An eddy-permitting coupled physical-biological model of the North Atlantic. 1. Sensitivity to advection numerics and mixed layer physics, *Global Biogeochemical Cycles*, *13*(1), 135-160.

Oschlies, A., W. Koeve, and V. Garcon (2000), An eddy-permitting coupled physical-biological model of the North Atlantic 2. Ecosystem dynamics and comparison with satellite and JGOFS local studies data, *Global Biogeochemical Cycles*, *14*(1), 499-523.

Oschlies, A. (2001), NAO-induced long-term changes in nutrient supply to the surface waters of the North Atlantic, *Geophysical Research Letters*, *28*(9), 1751-1754.

Oschlies, A. (2002), Can eddies make ocean deserts bloom, *Global Biogeochemical Cycles*, *16*(4), 1106.

Oschlies, A., and M. Schartau (2005), Basin-scale performance of a locally optimized marine ecosystem model, *Journal of Marine Research*, *63*(2), 335-358.

Parslow, J., P. Boyd, S. R. Rintoul, et al. (2001), A persistent sub-surface chlorophyll maximum in the Polar Frontal Zone south of Australia: seasonal progression and implications for phytoplankton-light-nutrient interactions, *Journal of Geophysical Research. C. Oceans*, *106*, 31543-31557.

Pasquero, C., A. Bracco, and A. Provenzale (2005), Impact of the spatiotemporal variability of the nutrient flux on primary productivity in the ocean, *J. Geophys. Res*, *110*.

Platt, T., R. B. Rivkin, and S. Sathyendranath (2005), Ecosystem dynamics based on plankton functional types for global ocean biogeochemistry models, *Global Change Biology*, *11*, 2016-2040.

Pondaven, P., C. Fravalo, D. Ruiz-Pino, et al. (1998), Modelling the silica pump in the Permanently Open Ocean Zone of the Southern Ocean, *Journal of Marine Systems*, *17*(1-4), 587-619.

Pondaven, P., D. Ruiz-Pino, C. Fravalo, et al. (2000), Interannual variability of Si and N cycles at the time-series station KERFIX between 1990 and 1995 - A 1-D modelling study, *Deep-Sea Research I*, *47*(2), 223-257.

Popova, E. E., R. T. Pollard, M. I. Lucas, et al. (2007), Real-time forecasting of ecosystem dynamics during the CROZEX experiment and the roles of light, iron, silicate, and circulation, *Deep Sea Research Part II: Topical Studies in Oceanography*, *54*(18-20), 1966-1988.

Redfield, A. C., B. H. Ketchum, and F. H. Richards (1963), The influence of organisms on the composition of seawater, in *The Sea*, edited by M. N. Hill, pp. 26-77, Inter-Science, New York.

Rintoul, S. R., and T. W. Trull (2001), Seasonal evolution of the mixed layer in the Subantarctic Zone south of Australia, *Journal of Geophysical Research. C. Oceans*, *106*(C12), 31447-31462.

Sarmiento, J., R. Slater, M. Fasham, et al. (1993), A seasonal three-dimensional ecosystem model of nitrogen cycling in the North Atlantic euphotic zone, *Global Biogeochemical Cycles*, *7*, 417-417.

Sathyendranath, S., A. Gouveia, S. Shetye, et al. (1991), Biological control of surface temperature in the Arabian Sea.

Schartau, M., and A. Oschlies (2003a), Simultaneous data-based optimization of a 1D-ecosystem model at three locations in the North Atlantic: Part I-Method and parameter estimates, *Journal of Marine Research*, *61*(6), 765-793.

Schartau, M., and A. Oschlies (2003b), Simultaneous data-based optimization of a 1D-ecosystem model at three locations in the North Atlantic: Part II-Standing stocks and nitrogen fluxes, *Journal of Marine Research*, *61*(6), 794-820.

Schmittner, A., A. Oschlies, H. D. Matthews, et al. (2008), Future changes in climate, ocean circulation, ecosystems, and biogeochemical cycling simulated for a business-as-usual CO2 emission scenario until year 4000 AD, *Global Biogeochemical Cycles*, *22*.

Smith, E. (1936), Photosynthesis in relation to light and carbon dioxide, *Proceedings of the National Academy of Sciences of the United States of America*, *22*(8), 504.

Sokolov, S., and S. R. Rintoul (2007b), On the relationship between fronts of the Antarctic Circumpolar Current and surface chlorophyll concentrations in the Southern Ocean, *J. Geophys. Res. – Oceans*, *112*(C07030), doi: 10.1029/2006JC004072.

Steele, J., and B. Frost (1977), The structure of plankton communities, *Philosophical Transactions of the Royal Society of London. Series B, Biological Sciences*, *280*(976), 485-534.

Steele, J. H., and E. W. Henderson (1992), The role of predation in plankton models, *Journal of Plankton Research*, *14*(1), 157-172.

Steele, J. H., and E. W. Henderson (1993), The significance of interannual variability, *Towards a model of ocean biogeochemical processes*, 237ñ260.

Stock, C. A., T. M. Powell, and S. A. Levin (2008), Bottom-up and top-down forcing in a simple size-structured plankton dynamics model, *Journal of Marine Systems*, *74*(1-2), 134-152.

Strass, V., and J. Woods (1991), New production in the summer revealed by the meridional slope of the deep chlorophyll maximum, *Deep Sea Research Part A. Oceanographic Research Papers*, *38*(1), 35-56.

Tagliabue, A., and K. R. Arrigo (2003), Anomalously low zooplankton abundance in the Ross Sea: An alternative explanation, *Limnology and Oceanography*, *48*(2), 686-699.

Tagliabue, A., L. Bopp, and O. Aumont (2009a), Evaluating the importance of atmospheric and sedimentary iron sources to Southern Ocean biogeochemistry, *Geophysical Research Letters*, *36*(13), L13601.

Tagliabue, A., L. Bopp, O. Aumont, et al. (2009b), Influence of light and temperature on the marine iron cycle: From theoretical to global modeling, *Global Biogeochemical Cycles*, *23*(2).

Thingstad, T., L. ÿvreÂs, J. Egge, et al. (2005), Use of non-limiting substrates to increase size; a generic strategy to simultaneously optimize uptake and minimize predation in pelagic osmotrophs?, *Ecology Letters*, *8*(7), 675-682.

Trull, T. W., S. R. Rintoul, M. Hadfield, et al. (2001a), Circulation and seasonal evolution of Polar waters south of Australia: Implications for iron fertilisation of the Southern Ocean, *Deep Sea Research (Part II, Topical Studies in Oceanography)*, *48*(11/12), 2439-2466.

Trull, T. W., D. Davies, and K. Casciotti (2008), Insights into nutrient assimilation and export in naturally iron-fertilized waters of the Southern Ocean from nitrogen, carbon and oxygen isotopes, *Deep Sea Research Part II: Topical Studies in Oceanography*, *55*(5-7), 820-840.

Van Oijen, T., M. Van Leeuwe, E. Granum, et al. (2004), Light rather than iron controls photosynthate production and allocation in Southern Ocean phytoplankton populations during austral autumn, *Journal of Plankton Research*, *26*(8), 885.

CHAPTER THREE

Model sensitivity

3.1 Introduction

In chapter 2, the models (*i.e.*, OG99 and SO03a) were described. While the aim was to introduce both models to the reader, it was also noted that several of the parameters caused significant differences between the models' reference simulations of the Subantarctic HNLC-plankton system. It was therefore determined that the original non-optimized model, the OG99, would be used as the standard model in the next sections of this thesis. In this chapter, the model sensitivity to the parameter space (i.e. the range of values of parameters) and to the main forcing functions was investigated.

Because the principal aim of this thesis was to combine observations of ocean properties with a biogeochemical model to explore the mechanism by which surface iron fertilization can affect phytoplankton biomass in the Southern Ocean, two contrasted environments: **(i)** the natural iron-fertilized waters of the Kerguelen Plateau, and **(ii)** the nearby HNLC offshore waters, were chosen as a representative example of a surface water iron-enrichment experiment.

Since 1930, explanations for environmental control of algal stocks have been the subject of much speculation [*Boyd et al.*, 2001; *Cullen*, 1991; *Hart*, 1934; *Martin*, 1990a] A number of candidate mechanisms for environmental control have been advanced, including temperature, irradiance, silicic acid, inhibition of nitrate uptake by ammonium, iron, grazing pressure, and several combinations of simultaneous limitation of algal processes [*Boyd*, 2002; *Morel et al.*, 1991].

With a simple NPZD-model a number of explanations for the elevated phytoplankton biomass over the Kerguelen plateau were investigated, these can be reduced to four main hypotheses.

Hypothesis 1: Differences in the mixed layer depth

Hypothesis 2: Differences in the algal growth rates

Hypothesis 3: Differences in the zooplankton grazing rates

Hypothesis 4: Differences in zooplankton mortality rates

The approach adopted was to develop a base-line simulation that resulted in a good representation of the annual biological cycle at an offshore site of the Kerguelen plateau, representative of the HNLC conditions. The sensitivity of the model results to the various parameters that pertain to each hypothesis was then studied to see which of the hypotheses were necessary to reproduce the observed on-Plateau persistent annual cycle and whether any of them could be considered a sufficient explanation.

3.2 Standard Simulation

The ecosystem model parameters used by Oschlies & Garçon [1998; 1999] were determined for the North Atlantic domain. It is not surprising then that the application to other regions may require some parameter adjustments. Parameters were modified somewhat so that the simulations provided a better match to the surface chlorophyll (SCHL) observations at the HNLC reference site (off-Plateau site from now on). The original OG99 parameter-set resulted in a HNLC bloom that was slightly bigger than the observed bloom at the off-Plateau site (Fig. 3.1). Two parameters were tuned to better simulate the observations. The prey capture rate, *pc*, was increased from 1.0 to 1.5 (mmol m^{-3})$^{-2}$ day^{-1}, and the zooplankton excretion rate (zooplankton losses going to Nitrate) was also lowered from 0.03 to 0.01 day^{-1}. Thus, the preliminary set of parameters values (Table 2.2) was taken from OG99, and from manual fitting of the model results with observed biomass.

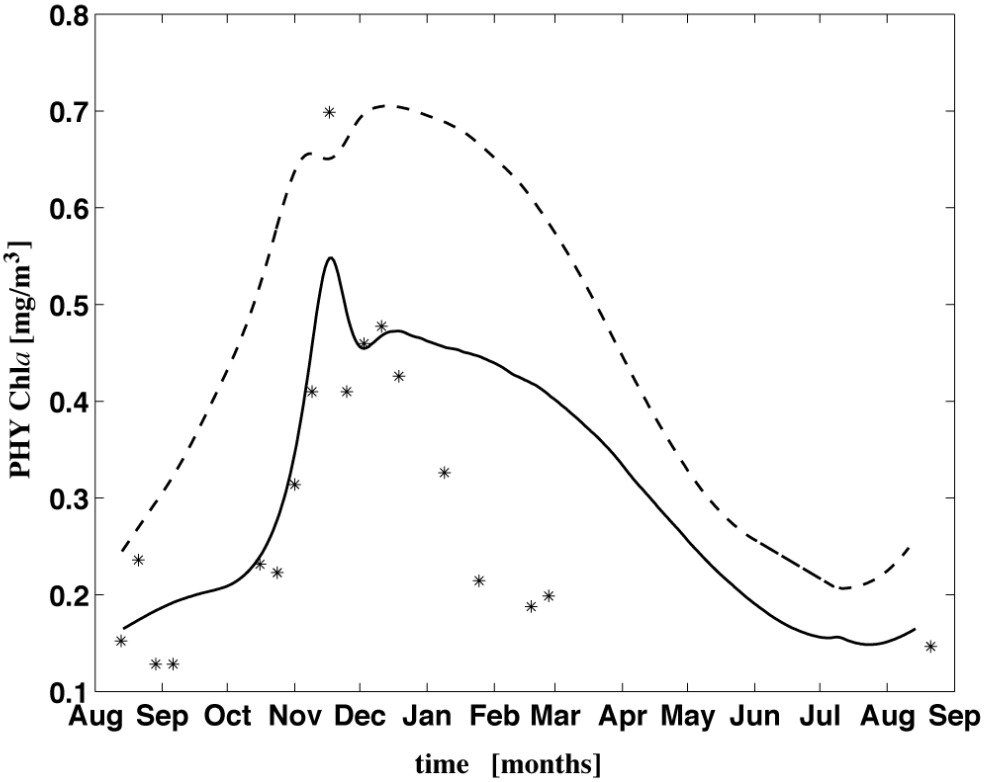

Figure 3.1: The seasonal cycle at the off-Plateau site using the ecosystem model with the 'original' parameter set (Table 2.2) are illustrated by the dashed line, and the solid line illustrates the simulated SCHL with our preliminary set of parameters values (Table 4.2). SCHL satellite observations at the off-Plateau site are denoted with asterisks.

With the set of parameters that resulted in a reasonable representation of the SCHL annual cycle at the off-Plateau site, we determined the standard run that was used as the basis for a series of parameter sensitivity analysis.

Because they cannot be regarded as global constants, the assignment of values to the biological parameters is especially challenging in new model applications. In such exercises it obviously helps to have some knowledge of the sensitivity of the model to the parameters values.

3.3 Parameter Sensitivity Analysis

A parameter sensitivity analysis of a model of an annual cycle presents problems of data presentation. It is of course possible to show the simulated annual cycle of the state variables for various parameter values. However, taking into account the number of parameters to be studied this approach would quickly lead to an unmanageable numbers of figures. It was therefore decided to define a set of statistics that could be used to summarize the essential features of the modeled cycles for comparisons with observations. As the aim is to investigate the parameters controlling the magnitude of the spring bloom and the nitrate cycle, the statistic P_{max}, a mean of phytoplankton concentration over the bloom period (02 October – 20 April), was an evident preference.

The first approach to this problem was to test the sensitivity of each parameter in turn by running the model to steady state with the parameter altered first to a higher and then to a lower value [*Fasham et al.*, 1990]. The choice of upper and lower values was based, where possible, on knowledge of the likely range of the parameter in question [*Bowie et al.*, 1985; *Hansen et al.*, 1997]. When such information was not available the low and high values were chosen to be half and twice the standard value respectively (see Table 3.1 for choice of values). For each parameter the model was run to steady state and the statistic P_{max} of the output calculated. The sensitivity was quantified by calculating a normalized sensitivity *S(p)*, defined as,

$$S(p) = \frac{((E(p) - E_S)E_S^{-1}}{((p - p_S)p_S^{-1})} \tag{3.1}$$

where E_s is the value of a given statistic for the standard case with parameter value p_s, and $E(p)$ is the value for the case when parameter is given the value p. This index measures the fractional change in the statistic for a fractional change in the parameter [*Fasham*, 1995; *Franks et al.*, 1986]. Values of S for P_{max} were calculated, and the results (Table 3.1) give an estimate of how much P_{max} will be altered by a different value of each parameter.

Table 3.1 Normalized parameter sensitivity, *S(p)*, of the mean phytoplankton concentration during the bloom period (P_{max}).

Parameter	Symbol	Standard Value	Parameter range		Normalized sensitivity P_{max}	
Initial slope of P-I curve	α	0.025	0.02	0.05	0.23	0.08
Attenuation coefficient of seawater	k_w	0.04	0.03	0.05	-0.25	-0.37
Maximum growth rate coefficient	a	0.6	0.27	2.0	0.45	0.08
Light attenuation by phytoplankton	k_P	0.03	0.02	0.1	0.05	0.01
Phytoplankton mortality rate	ε_P	0.03	0.015	0.1	-0.03	-0.11
Half saturation constant for N uptake	K_N	0.5	0.0005	3.86	0.0	0.0
Maximum grazing rate	g	2.0	0.5	4.0	-0.21	-0.02
Prey capture rate	pc	1.5	0.75	3.0	-1.07	-0.35
Z Quadratic mortality rate	$zmort$	0.2	0.02	2.0	0.48	0.13
Zooplankton excretion rate	ε_Z	0.01	0.0078	0.15	0.06	0.04

A first point to note was that *S* (*p*) values could be divided into two classes. There are those that do not have a large effect on the value of P_{max}, such as light attenuation coefficient due to phytoplankton, half saturation constant for nitrate uptake, zooplankton excretion rate, and phytoplankton mortality rate. Then there are the parameters that have a large effect, such as the initial slope of the P-I curve (α), the maximum phytoplankton growth rate coefficient (*a*), the light absorption of seawater (k_w), the prey capture coefficient of the grazing model (*pc*), the maximum grazing rate (*g*), and the zooplankton mortality rate (*zmort*).

A second point of interest arising from this study was that the value of S (p) (i.e. normalized sensitivity) for a decreased value of a parameter was dissimilar in magnitude to that for an increased value, with the exception of the zooplankton quadratic mortality rate and the attenuation coefficient of seawater; this could suggest that the standard run of the model is strongly constrained by the zooplankton mortality term (*i.e.*, the so called *closure term*), which is not unexpected since previous modeling efforts [*Edwards & Brindley*, 1999; *Franks*, 2002; *Steele & Henderson*, 1992] showed that the choices (of the form of the closure term) can determine the overall patterns in all variables [*Fasham*, 1993; *Gruber et al.*, 2006]. The sensitivity analysis also showed that k_w was one of the more critical parameters and so in cases where good data are available it would be worth using a more accurate parameterization of light absorption.

It is important to mention that these results only apply to the particular run of the model that was used as the standard case, and they cannot reveal any critical effects that might be due to interactions between sets of parameters. However, they do at least give an initial idea of where research might be directed to improve the predictive power of the model.

Since a complete exploration of the parameter space has not been done so far and varying all the parameters independently throughout their viable ranges is practically impossible, attention was mainly focused on parameters that were or outlined by the preliminary sensitivity analysis (Table 3.1) or were considered to have a bearing on the four hypotheses proposed in the Introduction.

Sensitivity to changes in mixed layer depth (Hypothesis 1)

As discussed earlier, the main forcing functions in the model were the annual cycles of mixed layer depth and solar radiation. Daily mixed layer depths for the Kerguelen Plateau area were obtained from a one-dimensional model calibrated at the nearby HNLC KERFIX site [*Mongin et al.*, 2006]. The resulting seasonal cycle is plotted in Figure 2.8, together with surface solar-radiation and mixed-layer temperature.

Hypothesis 1 proposed that the presence of a bloom at the fertilization zone above the plateau was attributable to a shallow mixed layer in the wake of the Kerguelen archipelago. Although there is not a seasonal cycle of observations, the reported weak circulation in the bloom region [*Park et al.*, 2008a; 2008b; *Roquet et al.*, 2009] that could create an area with a long residence time might substantiate this assumption. The simulations carried out with the *NPZD*-model (Fig. 3.2) have shown that this cannot be a sufficient condition, because even with a shallow mixed layer a bloom cannot be obtained if the values of the other parameters remain unchanged.

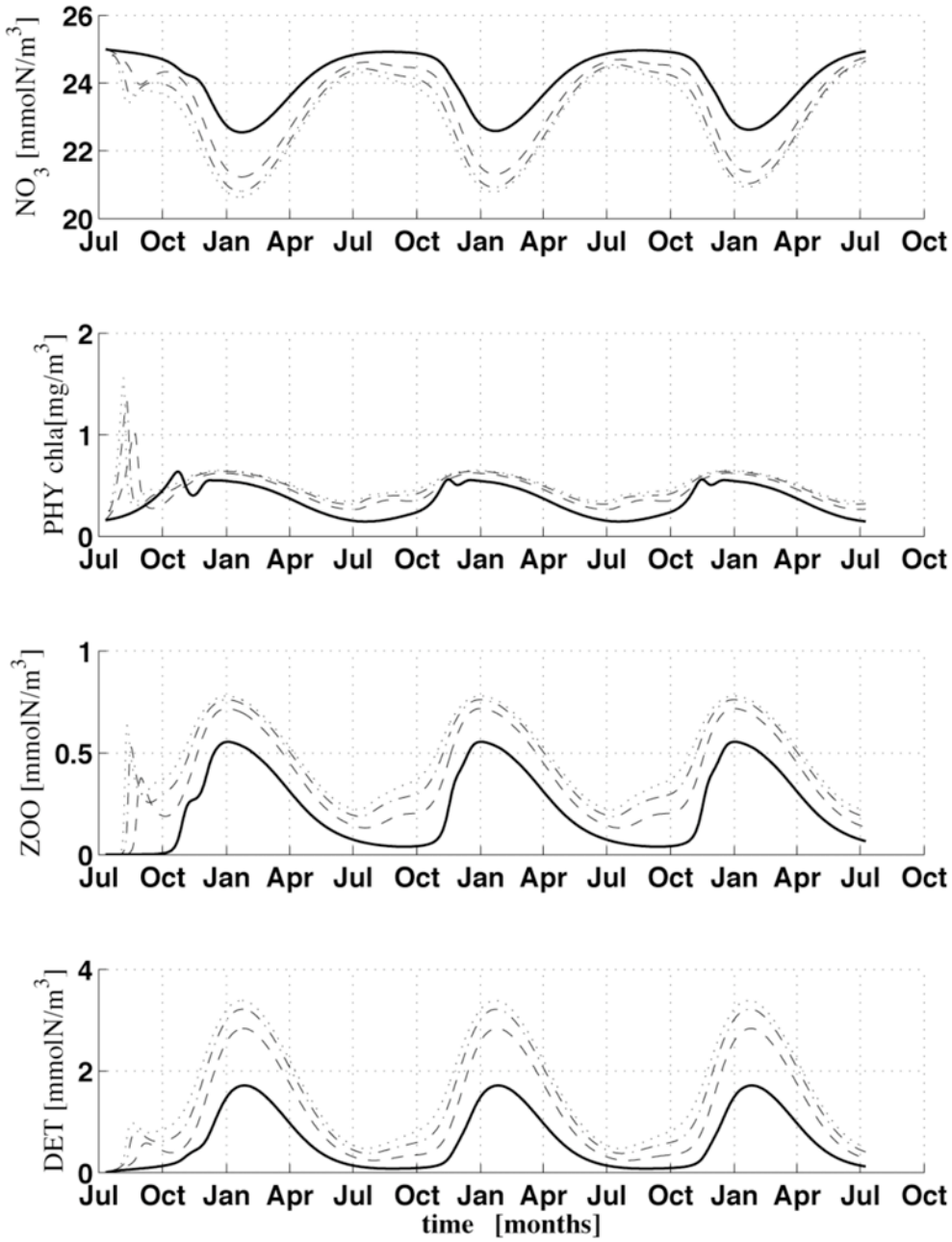

Figure 3.2: Simulated concentrations of nitrate (top), phytoplankton (middle) and zooplankton (bottom) in the standard simulation (solid) and in simulations with a mixed layer two (dashed), three (dashed-dotted) and four (dotted) times shallower respectively.

Sensitivity to variations in the algal growth rates (Hypothesis 2)

For fixed environmental conditions, the phytoplankton growth rate is determined by the parameters a, α, b, c, K_N, and ε_P. This section will concentrate on the first two parameters. For the first analysis the parameter a was varied independently over the range 0.6-3.0 day^{-1}. The resulting simulated seasonal cycles of nitrate, phytoplankton, zooplankton, and detritus are shown in Figure 3.3. The seasonal evolution of algal biomass shows that the magnitude of the chlorophyll maxima varied only slightly with the induced changes in the parameter a. For values of $a \geq 0.6$ day $^{-1}$ and $a \leq 3.0$ day^{-1}, the chlorophyll maxima only varies between 0.56–0.71 mgChl$a$ m^{-3}. This insensitivity of the algal biomass to a (maximum growth rate parameter) could happen because the presence or the absence of the spring bloom depends on the magnitude of the growth rate of phytoplankton in winter which, because of the low light levels at this time of the year, is relatively insensitive to the value of a. Another explanation for such insensitivity lies on the previous sensitivity analysis (Table 3.1), where the results suggest that the standard model is strongly controlled by zooplankton biomass and hence could prevent the spring bloom to take place. The increase in zooplankton biomass with increasing a (Fig. 3.3), also supports this argument.

When exploring the model sensitivity to variations in α, the model response was similar to the results obtained when varying the maximum growth rate parameter, a. Changes in α over the range 0.025-0.5 day^{-1}/(W m^{-2}) resulted in slightly higher values of algal biomass, ranging between 0.56 and 0.69 day^{-1}/(W m^{-2}) respectively (Fig. 3.4). This result is not unexpected because it is the zooplankton biomass in the winter that is a critical factor in determining the grazing pressure on the spring phytoplankton, and as shown in Figure 3.4 the zooplankton winter biomass is relatively high and capable to graze fast enough to prevent a bloom.

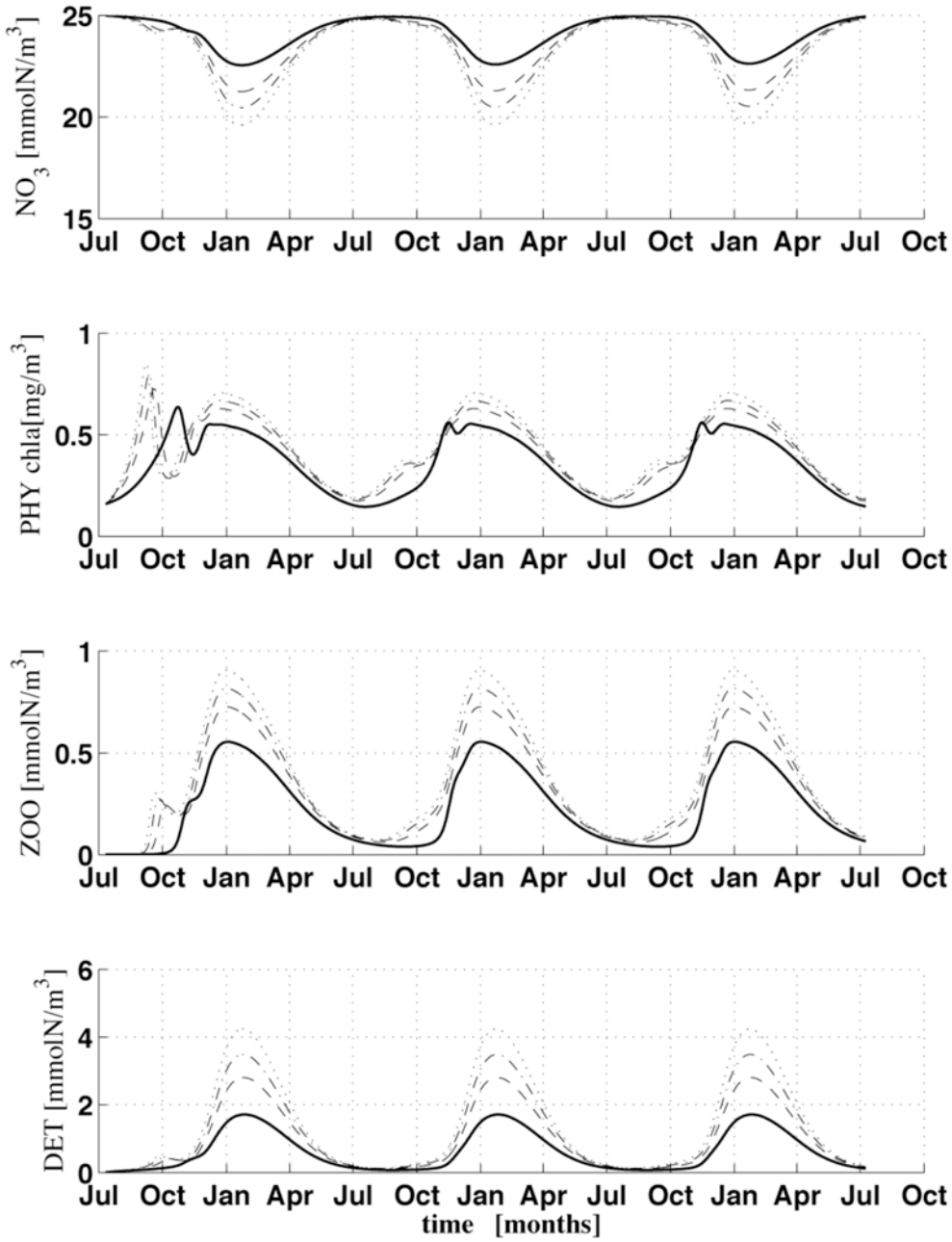

Figure 3.3: Simulated concentrations of nitrate (top), phytoplankton (second from the top), zooplankton (second from the bottom) and detritus (bottom), in the standard simulation (solid line) and in simulations with a maximum growth rate parameter *a* of 1.2 day^{-1} (dashed line), 1.8 day^{-1} (dashed-dotted line), and 3.0 day^{-1} (dotted line) respectively.

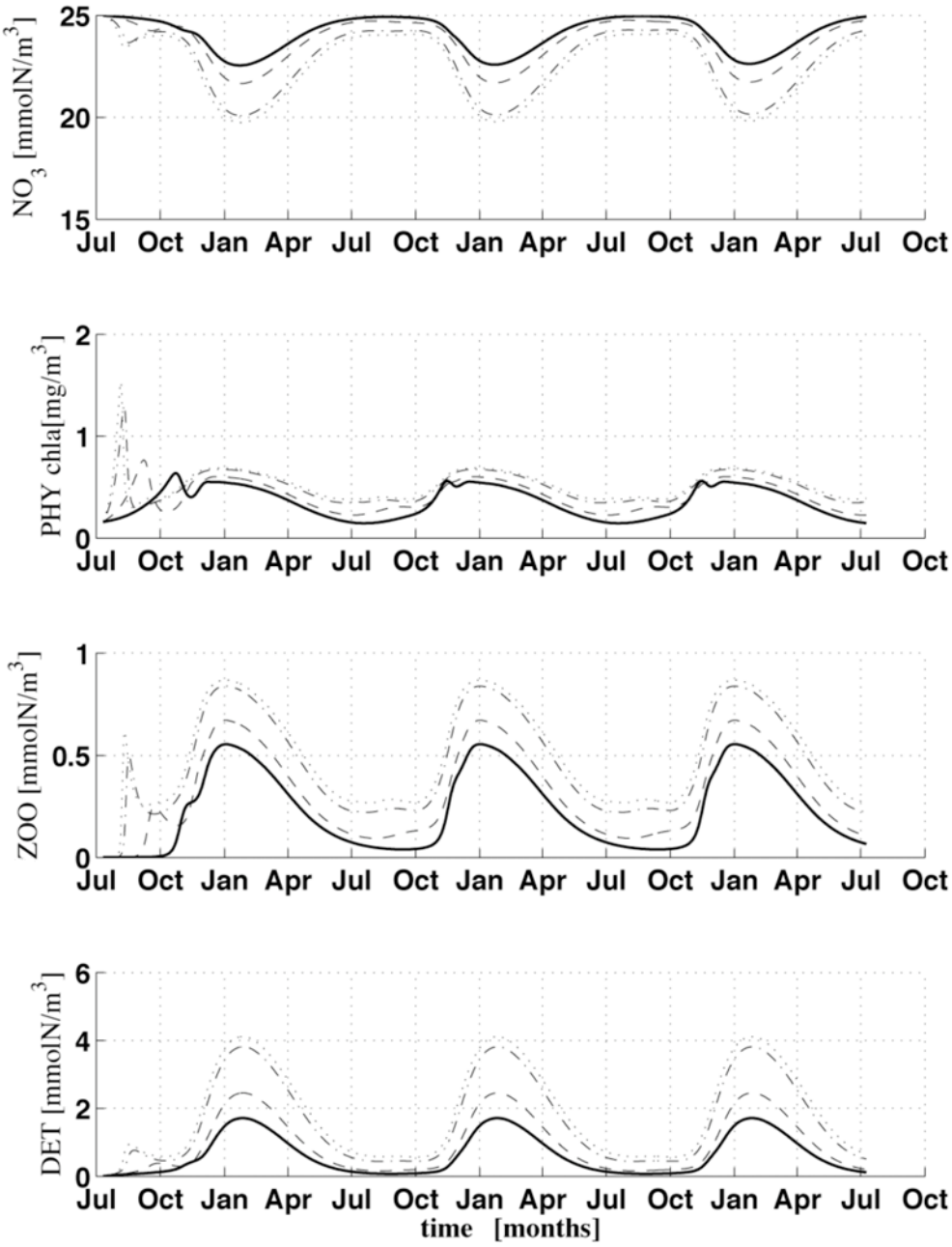

Figure 3.4: Simulated concentrations of nitrate (top), phytoplankton (second from the top), zooplankton (second from the bottom) and detritus (bottom), in the standard simulation (solid line) and in simulations with α of 0.05 (dashed line), 0.25 (dashed-dotted line), and 0.5 $day^{-1}/(W\ m^{-2})$ (dotted line) respectively.

Sensitivity to variations in the zooplankton grazing rates (Hypothesis 3)

The effect of herbivore grazing was studied by varying independently the parameters *g* and *pc*. The values of *P*, *Z*, and *D* (Fig. 3.5-3.6) are, in general, negatively correlated with *g* and *pc*. However, the simulated seasonal cycle of SCHL showed that a small spring bloom (SCHL approximately equal to 1 mg m^{-3}) occurs only if either $g \leq 0.35$ or $pc \leq 1.0$ (mmol N $m^{-3})^{-2}$ day^{-1}. Obviously, if the maximum potential grazing pressure (determined by *g*) of the herbivores is too low then, as the phytoplankton growth rate increases in the spring, the herbivores will be unable to graze fast enough to prevent a bloom. The model's sensitivity to *pc* is because, at low phytoplankton concentrations, zooplankton grazing will be mainly controlled by this parameter (Eq. 2.16) [*Franks et al.*, 1986].

These results demonstrate that in order to obtain a better simulation of the iron-fuelled phytoplankton bloom observed over the plateau, the herbivore grazing parameters need to be more typical of microzooplankton than mesozooplankton (*i.e.*, large zooplankton have high ingestion rates) [*Hansen et al.*, 1997]. So observed large size of zooplankton in the bloom area [*Carlotti et al.*, 2008] argues against reduced grazing performance on phytoplankton, unless these zooplankton were predominantly carnivorous [*Irigoien et al.*, 2005], which is unknown. Moreover, as has been previously shown (Fig. 3.5-3.6), the presence of an herbivore population with a low grazing rate does not itself guarantee that an intense phytoplankton spring bloom will occur.

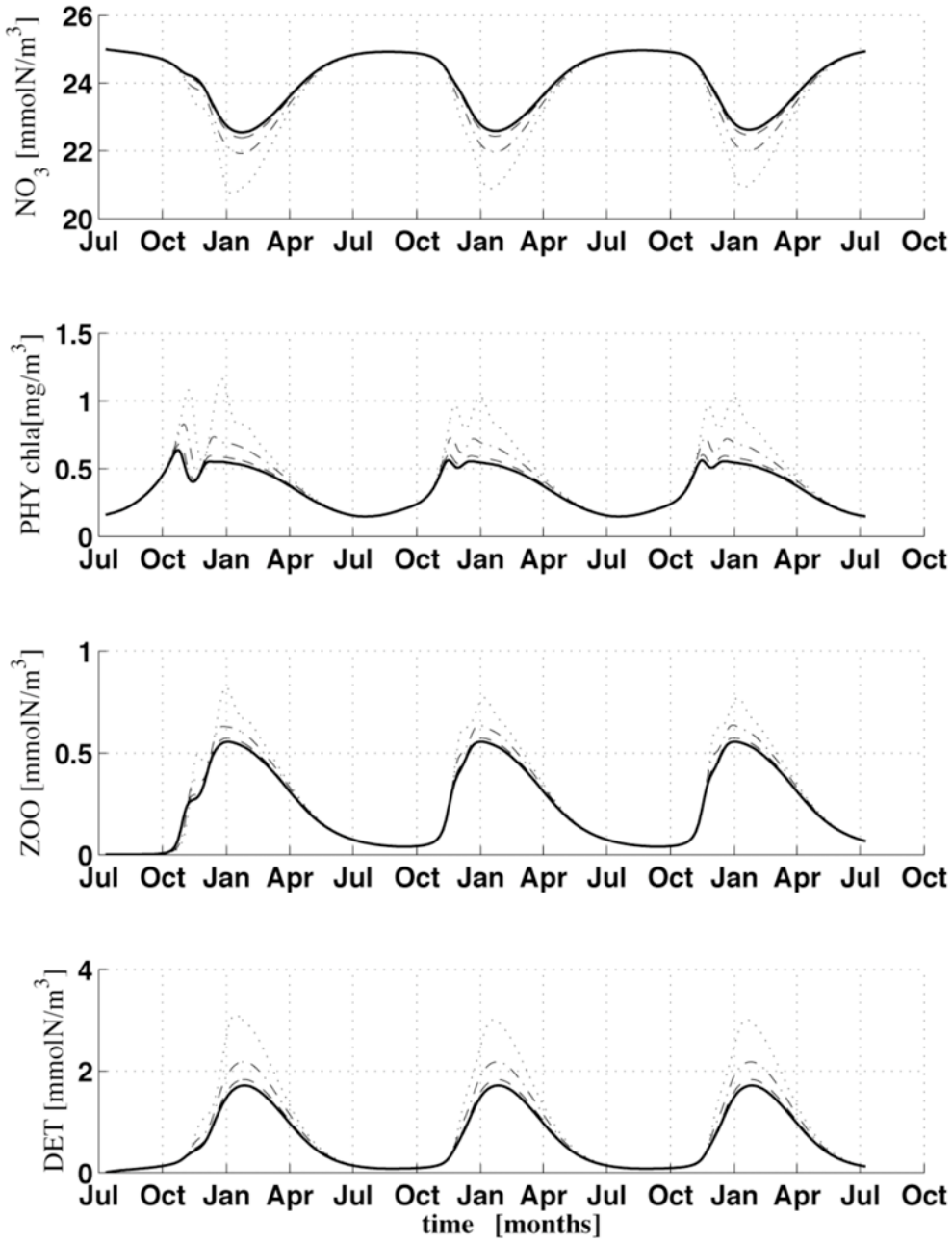

Figure 3.5: Simulated concentrations of nitrate (top), phytoplankton (second from the top), zooplankton (second from the bottom) and detritus (bottom), in the standard simulation (solid line) and in simulations with a maximum potential grazing rate *g* of 1.0 (dashed line), 0.5 (dashed-dotted line), and 0.35 day^{-1} (dotted line) respectively.

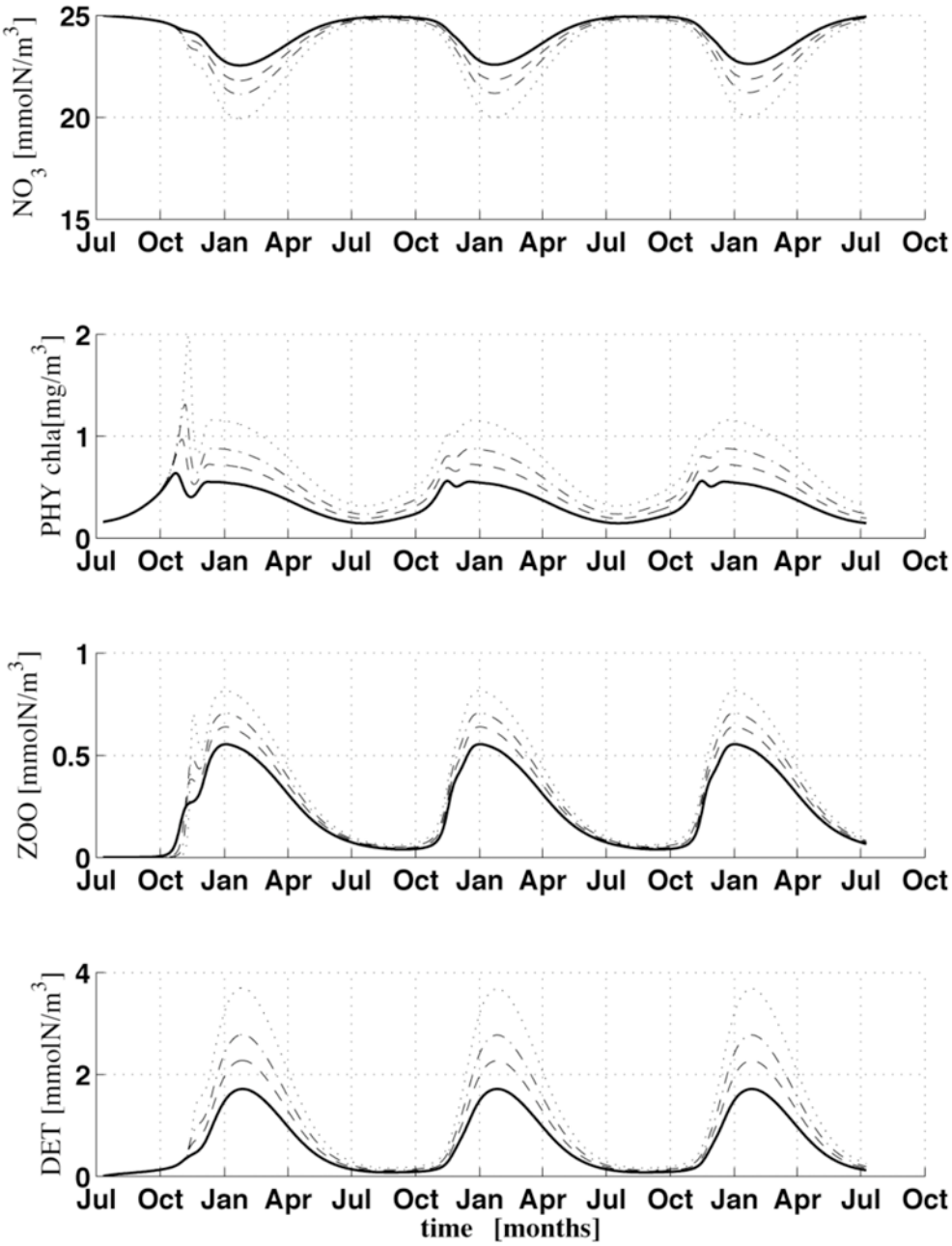

Figure 3.6: Simulated concentrations of nitrate (top), phytoplankton (second from the top), zooplankton (second from the bottom) and detritus (bottom), in the standard simulation (solid line) and in simulations with an herbivore grazing parameter *pc* of 1.0 (dashed line), 0.75 (dashed-dotted line), and 0.5 (mmol N m^{-3})$^{-2}$ day^{-1} (dotted) respectively.

Sensitivity to variations in the zooplankton mortality rate (Hypothesis 4)

Because the highest trophic level of the food web that is explicitly modeled is that comprising zooplankton, the rate of zooplankton mortality due to consumption by higher predators is represented by a quadratic function, which assumes that higher predators have a biomass proportional to their prey [*Edwards & Yool*, 2000; *Franks*, 2002]. Therefore, the effect on the seasonal cycles of varying the degree of zooplankton mortality can be investigated by varying the constant of the quadratic function, the parameter *zmort*. A set of simulations was performed in which *zmort* was varied between 0.2-2 (mmol N m^{-3})$^{-1}$ day^{-1}. As *zmort* increased over this range *Z* is reduced by a half, *N* decreases by ca. 20%, and *P* increases by ca. 166%. The results (Fig. 3.7) showed that, as would be expected, algal biomass increased as the zooplankton mortality is increased (*i.e.*, more predation). This apparently simple feature of the model can cause the seasonal cycle to switch from a situation in which *N* was high and *P* low to a situation in which the reverse was true, showing that the value of the closure parameter *zmort* can drastically effect the phytoplankton and nitrate cycles as previously reported [*Edwards & Brindley*, 1999; *Freund et al.*, 2006; *Frost*, 1993; *Steele & Henderson*, 1992; *Tsuda et al.*, 2007].

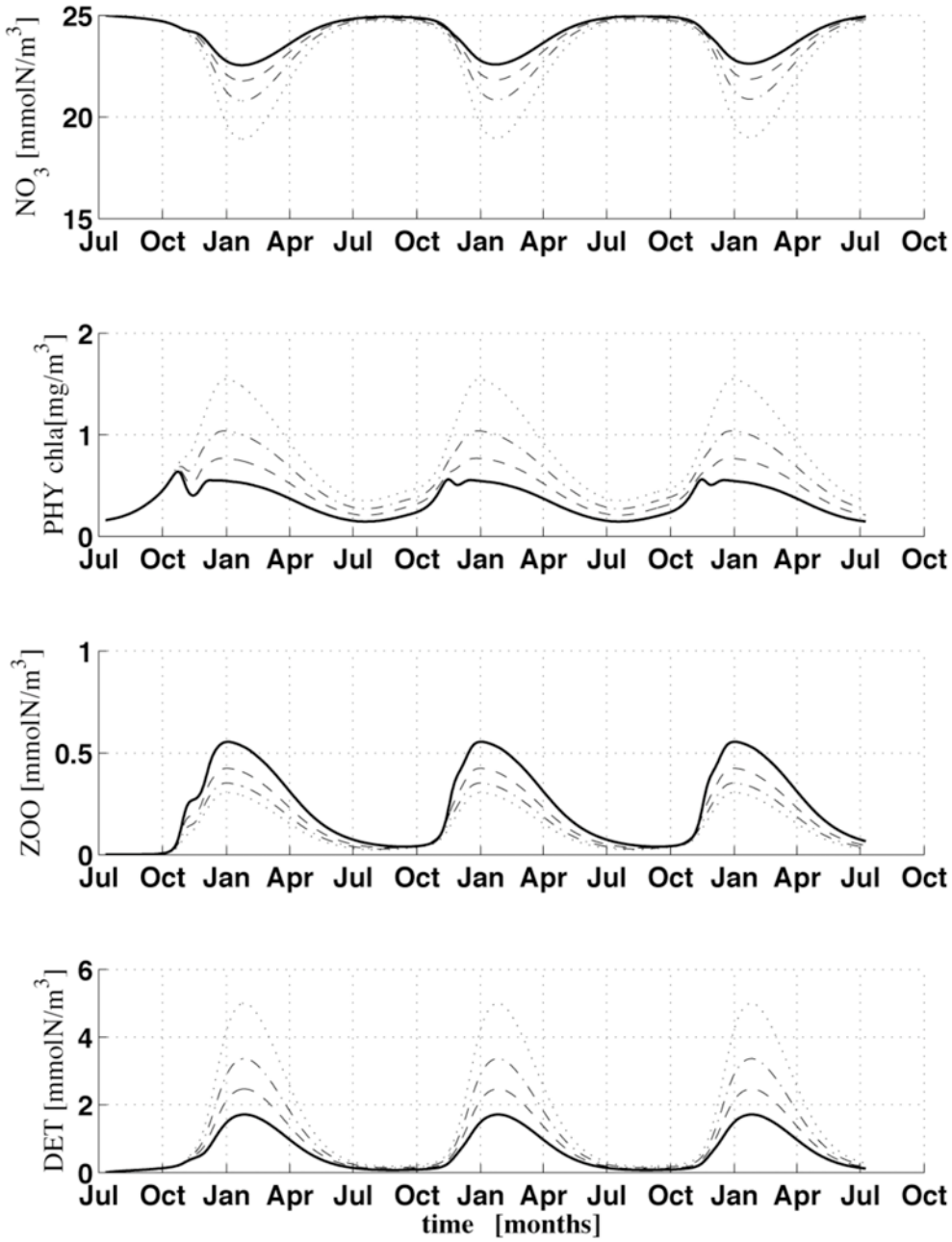

Figure 3.7: Simulated concentrations of nitrate (top), phytoplankton (second from the top), zooplankton (second from the bottom) and detritus (bottom), in the standard simulation (solid line) and in simulations with a zooplankton mortality rate *zmort* of 0.5 (dashed line), 1.0 (dashed-dotted line), and 2.0 (mmol N m^{-3})$^{-1}$ day^{-1} (dotted line) respectively.

3.4 Discussion and Conclusions

Various hypotheses that have been proposed to explain the absence (or presence) of a spring bloom in the wake of the Kerguelen Plateau in the Indian sector of the Southern Ocean were evaluated by means of a sensitivity analysis of a seasonal mixed layer ecosystem model. It is suggested that in some sense the sensitivity of the model to its parameters is a reflection of the sensitivity of the plankton ecosystem to those processes parameterized [*Franks et al.*, 1986], however it is also important to keep in mind that the following conclusions are specific to this model and how it is set up. The less sensitive the model, the larger the degree of inaccuracy that may be tolerated in the choice of parameters.

Two essential features of the plankton dynamics in the off-Plateau waters of the Southern Ocean (HNLC) are accounted for by the standard simulation of this model. First, the relatively low phytoplankton stock, which is strongly influenced by both the modeled feeding behavior of the grazer and the predation mortality imposed on the grazer (Figs. 3.5-3.7). Second, the year-round high NO_3 concentration which depends not only on the rate of utilization of NO_3 by the phytoplankton, but on the rate of vertical mixing and the nitrogen recycling efficiency of the pelagic food web. Observations suggest that the critical difference between reference stations for the off-Plateau site (HNLC) and for the on-Plateau site (central plateau bloom) lies in the presence or absence of a spring phytoplankton bloom and therefore the following discussion concentrates on the factors affecting the maximum phytoplankton concentration.

The parameter sensitivity analysis (Table 3.1) gave preliminary information on the set of parameters that might control the magnitude and duration of the simulated phytoplankton spring bloom in the standard run. The effects of independently varying these parameters (α, *g*, *pc*, *a*, *zmort*), and those induced by changes in the *MLD*, informed about the general dynamics of the model and the underlying causal features of a spring bloom.

The following conclusions can be drawn from this model sensitivity study:

1) It was found that the base-line simulation was insensitive to the mixed layer depth being decreased (Fig. 3.2). These results give no support to *Hypothesis 1*, namely that it is the difference in the *MLD* between the off- and on-Plateau sites that is the key factor giving rise to the differences in the observed seasonal biological cycle.

2) Seasonal cycle plots (Figs. 3.3-3.4) showed that the model was equally insensitive to changes in both phytoplankton growth rate parameters, a and α, which disproves *Hypothesis 2* if the rest of the parameters remain unchanged.

3) By reducing zooplankton grazing rates, the increase of phytoplankton (*i.e.*, diatoms) biomass was significantly higher (Figs. 3.5-3.6). However, the presence of zooplankton with a low maximum grazing rate or prey capture rate is not a sufficient condition for the presence of an intense spring bloom.

4) The sensitivity analysis showed that increasing the zooplankton mortality, by reducing the biomass of the herbivores, allows a spring bloom to occur (Fig. 3.7). These results support *Hypothesis 4*, but in order for this hypothesis to explain the on- versus off-Plateau differences it would have to be shown that such parameters were significantly different in the two locations.

Clearly, the adopted and subjectively tuned model works sufficiently well to engage in a detailed analysis of the simulated Kerguelen plateau phytoplankton bloom. In particular, there is merit in proceeding with an analysis focusing on the contrasting seasonal cycles found on and around the Kerguelen plateau.

3.5 References

Bowie, G. L., W. B. Mills, D. B. Porcella, et al. (1985), Rates, constants, and kinetics formulations in surface water quality modeling, *Env. Res. Lab., USEPA, EPA/600/3-85/040. Athens, GA*.

Boyd, P. W., A. C. Crossley, G. R. DiTullio, et al. (2001), Control of phytoplankton growth by iron supply and irradiance in the subantarctic Southern Ocean: Experimental results from the SAZ Project, *Journal of Geophysical Research*, *106*(C12), 31573-31584.

Boyd, P. W. (2002), Environmental factors controlling phytoplankton processes in the Southern Ocean, *Journal of Phycology*, *38*(5), 844-861.

Carlotti, F., D. Thibault-Botha, A. Nowaczyk, et al. (2008), Zooplankton community structure, biomass and role in carbon fluxes during the second half of a phytoplankton bloom in the Eastern sector of the Kerguelen shelf (January - February 2005), *Deep Sea Research II*, *55*(5-7), 720-733.

Cullen, J. J. (1991), Hypotheses to Explain High-Nutrient Conditions in the Open Sea, *Limnology and Oceanography*, *36*(8), 1578-1599.

Edwards, A. M., and J. Brindley (1999), Zooplankton mortality and the dynamical behaviour of plankton population models, *Bulletin of Mathematical Biology*, *61*(2), 303-339.

Edwards, A. M., and A. Yool (2000), The role of higher predation in plankton population models, *Journal of Plankton Research*, *22*(6), 1085-1112.

Fasham, M. (1995), Variations in the seasonal cycle of biological production in subarctic oceans: A model sensitivity analysis, *Deep Sea Research Part I: Oceanographic Research Papers*, *42*(7), 1111-1149.

Fasham, M. J. R., H. W. Ducklow, and S. M. McKelvie (1990), A nitrogen-based model of plankton dynamics in the oceanic mixed layer, *Journal of Marine Research*, *48*(3), 591-639.

Fasham, M. J. R. (1993), Modelling the marine biota, in *The global Carbon Cycle*, edited by M. Heimann, pp. 457-504, Springer Verlag, Berlin.

Franks, P. J. S., J. S. Wroblewski, and G. R. Flierl (1986), Behavior of a simple plankton model with food-level acclimation by herbivores, *Marine Biology*, *91*(1), 121-129.

Franks, P. J. S. (2002), NPZ models of plankton dynamics: Their construction, coupling to physics, and application, *Journal of Oceanography*, *58*(2), 379-387.

Freund, J., S. Mieruch, B. Scholze, et al. (2006), Bloom dynamics in a seasonally forced phytoplankton-zooplankton model: Trigger mechanisms and timing effects, *Ecological Complexity*, *3*(2), 129-139.

Frost, B. W. (1993), A modelling study of processes regulating plankton standing stock and production in the open subarctic Pacific Ocean, *Progress in Oceanography*, *32*(1-4), 17-56.

Gruber, N., H. Frenzel, S. C. Doney, et al. (2006), Eddy-resolving simulation of plankton ecosystem dynamics in the California Current System, *Deep-Sea Research Part I: Oceanographic Research Papers*, *53*(9), 1483-1516.

Hansen, P. J., P. K. Bj¯rnsen, and B. W. Hansen (1997), Zooplankton grazing and growth: Scaling within the 2-2,000-?m body size range, *Limnology and Oceanography*, *42*(4), 687-704.

Hart, T. J. (1934), *On the phytoplankton of the south-west Atlantic and the Bellingshausen Sea, 1929-31*, University Press.

Irigoien, X., K. J. Flynn, and R. P. Harris (2005), Phytoplankton blooms: a'loophole'in microzooplankton grazing impact?, *Journal of Plankton Research*, *27*(4), 313.

Martin, J. H. (1990a), Glacial-interglacial CO_2 change: The iron hypothesis, *Paleoceanography*, *5*, 1-13.

Mongin, M., D. M. Nelson, P. Pondaven, et al. (2006), Simulation of upper-ocean biogeochemistry with a flexible-composition phytoplankton model: C, N and Si cycling and Fe limitation in the Southern Ocean, *Deep-Sea Research II*, *53*(5-7), 601-619.

Morel, F. M. M., J. G. Reuter, and N. M. Price (1991), Iron nutrition of phytoplankton and its possible importance in the ecology of ocean regions with high nutrient and low biomass, *Oceanography*, *4*, 56-61.

Oschlies, A., and V. Garçon (1998), Eddy-induced enhancement of primary production in a model of the North Atlantic Ocean, *Nature*, *394*(6690), 266-269.

Oschlies, A., and V. Garçon (1999), An eddy-permitting coupled physical-biological model of the North Atlantic. 1. Sensitivity to advection numerics and mixed layer physics, *Global Biogeochemical Cycles*, *13*(1), 135-160.

Park, Y.-H., J.-L. Fuda, I. Durand, et al. (2008a), Internal tides and vertical mixing over the Kerguelen Plateau, *Deep Sea Research II*, *55*(5-7), 582-593.

Park, Y.-H., F. Roquet, J.-L. Fuda, et al. (2008b), Large-scale circulation over and around the Northern Kerguelen Plateau, *Deep Sea Research II*, *55*(5-7), 566-581.

Roquet, F., Y. H. Park, C. Guinet, et al. (2009), Observations of the Fawn Trough Current over the Kerguelen Plateau from instrumented elephant seals, *Journal of Marine Systems*, *78*(3), 377-393.

Steele, J. H., and E. W. Henderson (1992), The role of predation in plankton models, *Journal of Plankton Research*, *14*(1), 157-172.

Tsuda, A., S. Takeda, H. Saito, et al. (2007), Evidence for the grazing hypothesis: Grazing reduces phytoplankton responses of the HNLC ecosystem to iron enrichment in the western subarctic pacific (SEEDS II), *Journal of Oceanography*, *63*(6), 983-994.

CHAPTER FOUR

Combined remote sensing – modelling investigation of the Kerguelen bloom

4.1 Introduction

In the world ocean, the latitudes between 40^{o} and 60^{o} are a major sink of atmospheric CO_2 [*Takahashi et al.*, 2002]. The Southern Ocean frontal zones with their elevated phytoplankton biomass and productivity [*Moore & Abbott*, 2000; *Sokolov & Rintoul*, 2007b], and especially the Subantarctic Zone (SAZ) [*Lourey & Trull* 2001], have been of special interest for the studies of the global carbon cycle [*Le Quéré et al.*, 2007; *Metzl et al.*, 1999]. Subantarctic surface waters contain high levels of nitrate and phosphate, low silicate and relatively modest levels of chlorophyll, in most regions (a condition known as HNLC for High-Nitrate, Low-Chlorophyll) [*Cullen*, 1991; *Rintoul & Trull*, 2001]. The availability of light, iron and silicic acid [*Boyd et al.*, 2001; *Franck et al.*, 2000; *Martin et al.*, 1990b; *Mitchell et al.*, 1991], and grazing pressure [*Frost*, 1991; *Mayzaud et al.*, 2002; *Pitchford & Brindley*, 1999] are now understood to be the major controls on phytoplankton production in the Subantarctic.

Several studies have shown that marine pelagic primary productivity in the Subantarctic is very unevenly distributed and that phytoplankton blooms are primarily localized around remote islands, near some fronts of the ACC, over large topographic features, and downstream of continental masses [*Blain et al.*, 2001; *Sokolov & Rintoul*, 2007b; *Sullivan et al.*, 1993]. Remotely sensed measurements of ocean color have also revealed the complex temporal variability of surface chlorophyll (SCHL) [*Moore & Abbott*, 2002; *Sokolov*, 2008], showing that phytoplankton populations in subantarctic waters undergo strong seasonal cycles, with prominent phytoplankton pigments accumulations or ‘blooms’ occurring particularly in the spring but also to a lesser extent in the autumn [*Comiso et al.*, 1993; *Trull et al.*, 2001a].

The low lights levels dominating during early spring followed by iron limitation after the onset of water column stratification are suggested as the main factors affecting the seasonal cycle of phytoplankton growth [*Boyd et al.*, 1999; *Fennel et al.*, 2003]. Nevertheless, during austral summer, when phytoplankton is light saturated [*Figueiras et al.*, 1999], diatom growth may become silicon limited, particularly in Subantarctic waters [*Brzezinski et al.*, 2001; *Franck et al.*, 2000; *Leblanc et al.*, 2005].

Co-limitation by iron and light is also observed in the SAZ, such that under low light levels the phytoplankton cellular demand for iron increases [*Boyd*, 2002; *Sunda & Huntsman*, 1997]. However, the relative importance of physical, chemical and biological factors in controlling phytoplankton bloom events in the SAZ may vary with location and time [*Lancelot et al.*, 2000], and the simultaneous limitation by multiple factors is not fully understood. For instance, it is well recognized that grazing is but one factor controlling the biomass and productivity of phytoplankton in nutrient-rich areas of the open sea [*Cullen*, 1995; *Morel et al.*, 1991; *Tsuda et al.*, 2007], and the SAZ is not the exception [*Hall et al.*, 2004; *Mayzaud et al.*, 2002]

In recent years the iron-limitation hypothesis in HNLC regions [*Martin*, 1990a; *Martin et al.*, 1990b] has been demonstrated for Southern Ocean waters in several mesoscale iron-fertilization experiments where iron additions both in the Atlantic sector [EisenEx, *Bakker et al.*, 2005; Eifex, *Strass et al.*, 2005] and in the Pacific sector [SOIREE, *Boyd et al.*, 2000; SOFeX, *Coale et al.*, 2004] promoted chlorophyll *a* increase and nitrate decrease [see review by *Boyd et al.*, 2007]. Although these deliberate iron enrichments have determined the impact of adding iron on the planktonic ecosystem, short-term and small-scale fertilizations are not able to take into account all the ecosystem processes that follow from increased iron availability. In this context, it is very useful to study the effects of natural iron enrichments on the marine pelagic food web and carbon cycling.

During January-February 2005 the Kerguelen Ocean and Plateau compared Study (KEOPS) showed that the phytoplankton bloom in the Kerguelen Plateau region was due to a natural iron enrichment [*Blain et al.*, 2007]. The bloom was observed over the area between the two islands, and then spreads eastwards apparently under the influence of the Antarctic Circumpolar Current (ACC) [*Mongin et al.*, 2008] (Fig. 4.2).

At the same time the project found that in 2004-05 the bloom began in early November, attained a maximum of phytoplankton biomass (~ 3 mg chlorophyll *a* per litre) in December, and collapsed in late February [*Blain et al.*, 2008a]. Measurements showed that sub-surface waters contain elevated concentrations of iron [*Blain et al.*, 2008b], and that intense internal tides may deliver this iron to the surface [*Park et al.*, 2008b] to fuel the observed high phytoplankton production and associated consumption of carbon dioxide.

Identifying the major processes that control the phytoplankton bloom development in the Kerguelen plateau region, and developing conceptual models of the sensitivity of these processes to climate variability and change, will inform us about the role of the biological pump in the Southern Ocean in regulating atmospheric carbon dioxide. In order to explore these mechanisms, a comprehensive description of the Kerguelen plateau bathymetry, SCHL distributions, and surface circulation is here combined with the lower trophic level ecosystem model described in previous sections. The model is used to investigate the seasonal cycle of the bloom and to test whether it is capable of capturing the recurrent phytoplankton blooms over a seasonal time scale in that particular region.

In other words, taking into consideration the results from Chapter 3, we here focus on determining a combination of model parameters that could account for the main differences, in regulating primary productivity, between the HNLC and the iron-rich waters.

4.2 Hydrographic setting

The Kerguelen plateau is a large area of relatively shallow sea-floor in the Indian sector of the Southern Ocean that extends for more than 2300km southeast from the Kerguelen Islands (49°S, 70°E) [*Frey et al.*, 2000] (Fig. 4.1). It's full extent reaches as far south as the Princess Elizabeth Trough near 63°S, but our interest is focused on the portion of the plateau north of the Fawn Trough, between and to the east of the Kerguelen and Heard Islands (Fig. 4.1). From here on we refer to this region as "the plateau".

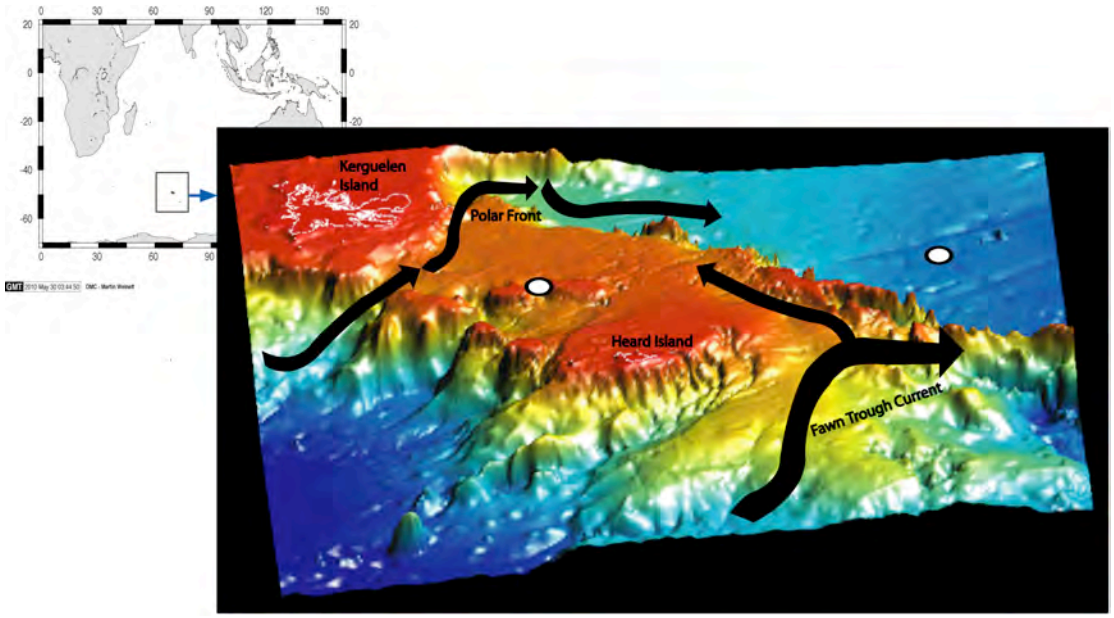

Figure 4.1: Three-dimensional bathymetric map of the Heard Island region. Data was produced by Geoscience Australia and supplied by the Australian Antarctic Data Centre. Approximate location of the on- and off-Plateau study sites are also illustrated with white circles.

High-energy internal tidal waves that interact with the bathymetry enhance the vertical eddy diffusivity above the plateau, and hence the supply of subsurface iron and other nutrients [*Park et al.*, 2008a]. This supply from below appears to be the main source of iron to fuel the recurrent and persistent phytoplankton bloom during austral summer, with negligible aeolian iron dust fluxes from the Kerguelen desert [*Blain et al.*, 2008b]. Despite the high primary production and standing stock of chlorophyll *a* in the Kerguelen bloom, surface water nitrate depletion was insufficient to limit phytoplankton production, although near complete depletion of silicic acid did occur [*Mosseri et al.*, 2008]. Similar decoupling of the Si and N cycles was observed during experimental iron fertilisation experiments [*Boyd et al.*, 2007], and also resembles the general much larger depletion of silicic acid than nitrate in surface waters from south to north across the Southern Ocean [*Ellwood et al.*, 2008; *Trull et al.*, 2001a].

Most of the area of study (49°S-53.5°S 69°E-78°E) is shallower than 1000m. In addition to Kerguelen and Heard Islands, there are three bathymetric features that

seem relevant to the spatial distribution of SCHL: i) the relatively deep (~650m) trough that runs east-west across the plateau just south of Kerguelen Island, ii) the main area of relatively shallow bathymetry (~500m) which is round in shape and includes five shallower seamounts, and iii) the relatively shallow (300-500m deep) southeastern extension of the plateau (including the William Ridge) which is delimited by a northwest-southeast trough of deeper (~600 m) waters (Fig. 4.1). For simplicity, we refer to these features hereafter as i) the Polar Front trough, ii) the main plateau, and iii) the southeastern trough and ridge.

The Kerguelen plateau acts as a barrier and forces the large-scale flow of the Antarctic Circumpolar Current (ACC) to divide. Approximately 2/3 of the transport goes north of Kerguelen Island [*Park et al.*, 2008b] and exhibits strong meandering and eddy activity [*Pollard et al.*, 2002; *Sokolov & Rintoul*, 2007b]. The remaining flow passes through the Fawn Trough where it divides the northern and southern portions of the plateau (Fig. 4.1). Further east, the flow through the Fawn Trough turns back north and west along contours of bathymetry east of the Williams Ridge before turning to flow eastward again. The division of the ACC leads to relatively sluggish circulation across the plateau [*Park et al.*, 2008b]. Some waters enter our study region from south of Heard Island along contours of bathymetry and flow north and back west across the plateau; others enter from the west, north of Heard Island, flow northward and exit to the east in the branch of the Polar Front [*Roquet et al.*, 2009] (Fig. 4.1). Based on CTD and ADCP observations made during the KEOPS cruise, surface velocity is weak (2-8 cm s^{-1}). More detailed discussion of the circulation is presented in Park *et al.* [2008a; 2008b].

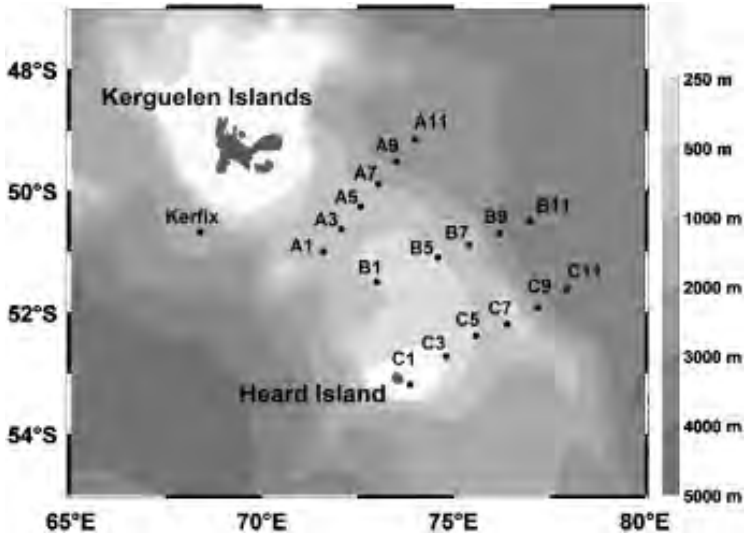

Figure 4.2: Geographic location of the sampling stations and bathymetry of KEOPS study area. From Uitz *et al.*[2009].

From 19 January to 13 February 2005 the KEOPS cruise carried out an oceanographic survey onboard the R/V Marion Dufresne. Three transects (labeled A, B and C) composed of 11 stations each were visited as well as the time-series site KERFIX (Fig. 4.2). Station A03 (50.38°S/72.05°E) located above the Kerguelen Plateau in the core of the bloom was here defined as the reference station for the central plateau bloom ("on-Plateau", hereafter), and station C11 (51.31°S/77.58°E) was defined as the reference station for the HNLC conditions ("off-Plateau", hereafter).

4.2.1 Observations

Silicate was strongly depleted (<5 µM) and possibly limiting to diatom growth at all Stations along Transect A, and at Stations B01 to B03. These sites corresponded to the highest chlorophyll concentrations in the microplankton fraction. For Transect C, silicate concentrations were always higher than 10µM in surface. The maximum value, ~23µM, was measured at C11. Nitrate concentrations remained high (>20 µM) on all three transects and phosphate concentrations were always >1µM. For the Transect A, nitrate showed an increasing gradient from A01 from A11 with values ranging between 21 and 28µM. For Transect C, values were always higher than for

Transect A with >27 µM in surface waters for all stations. The vertical distribution of silicic acid and nitrate concentrations for both reference stations (*i.e.*, on-Plateau and off-Plateau) are presented in Figure 4.3. Ammonium concentrations in the upper layer (0-100m) were low, around 0.5 to 1 µM. A maximum value (up to 2 µM) was observed at stations A1-A3-A5 at around 120m, corresponding to the maximum of chlorophyll, indicating an intensive regeneration area.

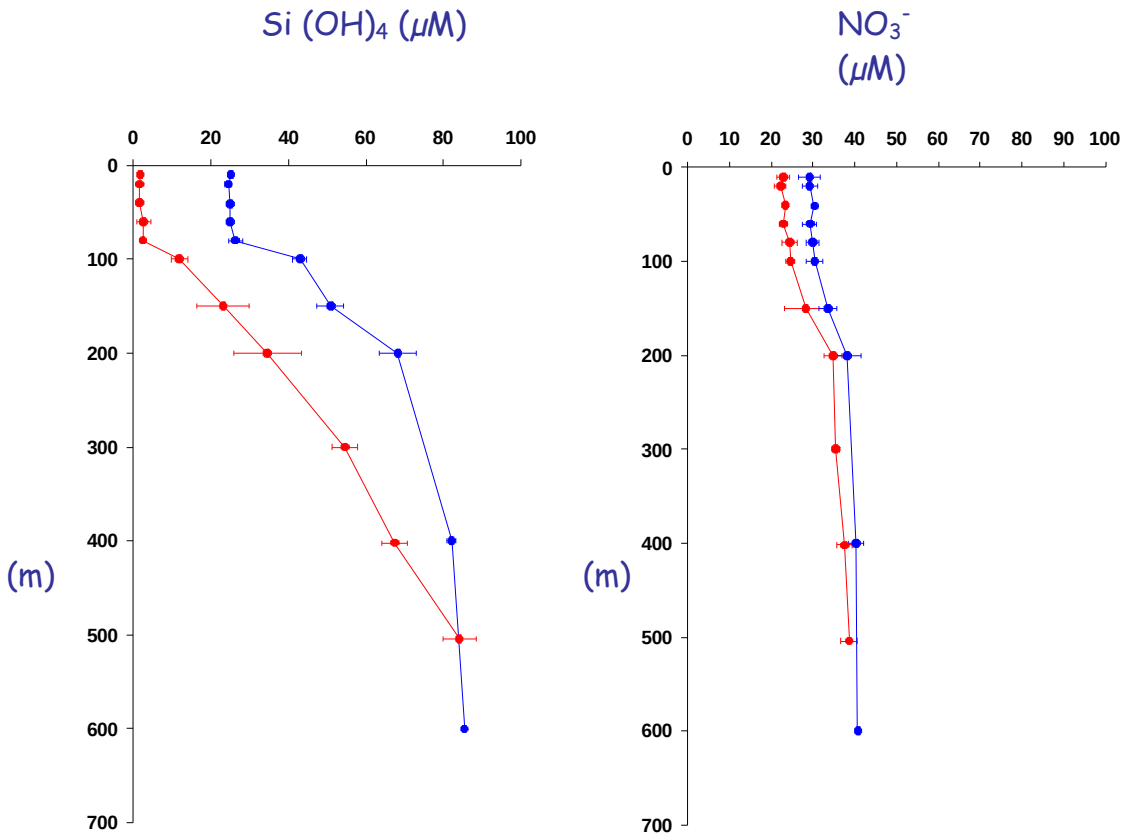

Figure 4.3: On-Plateau (A03; in red) and off-Plateau (C11; in blue) vertical distribution of silicic acid and nitrate (µM). From Mosseri *et al.* [2008], Trull *et al.* [2008a], and Blain *et al.* [2008b] in the Deep-Sea Research KEOPS special issue.

Surface concentrations of dissolved iron (dFe) inside and outside the plateau were low (0.09 nM), but typical of surface waters of the open Southern Ocean. However, below 125 m, dFe over the plateau increased with depth reaching a maximum of ~

0.35 nM (mean) at 500 m, in contrast to outside of the plateau where dFe concentrations were ~ 0.18 nM (mean) at 600m (Fig. 4.4).

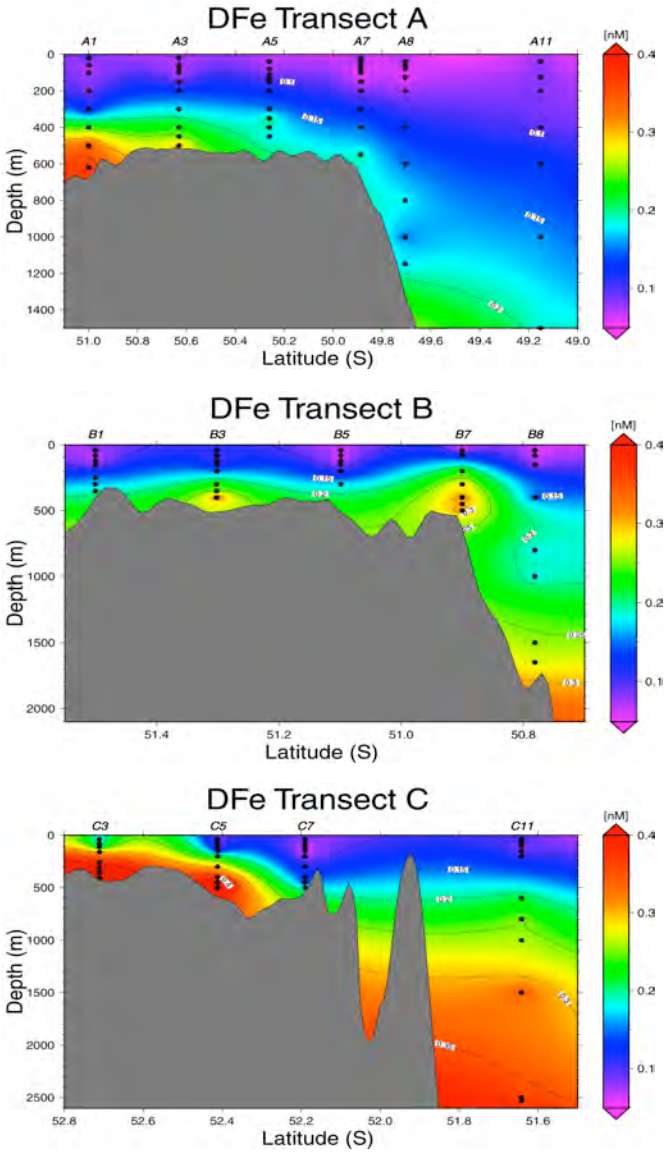

Figure 4.4: Dissolved iron distributions for Transects A, B and C. Concentrations in between stations at each transect are based in spatial extrapolation and do not represent real measurements. Published by Blain *et al*. [2008b] in Deep-Sea Research KEOPS special issue.

Extremely high chlorophyll standing stocks, amongst the highest reported from Polar waters in the Southern Ocean, were found at stations A01 to A05 and B01 to B05. These concentrations greatly decreased towards the east of the transects. The

highest chlorophyll-*a* concentrations of the cruise (~ 4 mg·m^{-3}) were measured along the B transect [*Uitz et al.*, 2009]. The C transect showed lower chlorophyll concentrations (less than 0.5 mg·m^{-3}). The vertical distribution of chlorophyll *a* at the reference stations (A03 and C11) along with B01 and KERFIX stations are shown in figure 4.6. In surface waters, chlorophyll was evenly distributed with depth at almost all stations. Thin subsurface peaks in chlorophyll at stations A03 (Fig. 4.5) and A05 (data not shown) could be indicative of a sinking phytoplankton bloom [*Mosseri et al.*, 2008]. When looking at the integrated values, A03 shows the highest value with around 200 mg·m^{2} and a decreasing pattern to A11 (Fig. 4.6). There was little difference in column chlorophyll in waters > 1000m deep in the KEOPS region, but these totals were significantly higher than in Polar waters in the Antares study region west of Kerguelen during the same months [*Blain et al.*, 2002]. Column integrated chlorophylls in shallow water (<1000m) on the plateau were much higher than in deep water, and higher on transect A compared to transect C (Fig. 4.7).

Table 4.1: Comparison of column-integrated production (mg C m^{-2}) and chlorophyll (mg Chl*a* m^{-2}) during KEOPS. From Uitz *et al*. [2009].

Parameter	Transect A	Transect B	Transect C
Column chlorophyll off the plateau	**25-25**	**23 -23**	**21**
Column chlorophyll on the plateau	**29 - 50**	**30 - 82**	**19 - 28**
Column production off the plateau	**860 - 1360**	**225 - 400**	**156**
Column production on the plateau	**815 - 2247**	**600 -2650**	**245 - 625**

On the plateau, primary production (PP) along transects A (A01-A05) and B (B01-B05) were extremely high (> 1.7 grams carbon m^{-2} d^{-1}), and considerably higher than along transect C where PP was less than 0.4 gr C m^{-2} d^{-1}, except at C01. Deep-water sites on transect B (B09 and B11) and the KERFIX site (south of the Kerguelen island to the west of the plateau) also showed low daily PP values. The remaining stations (A06-A11, B07, C01) are a mixture of deep-water and Plateau sites and daily production results in this region (> 0.4 and <1.7 g C m^{-2} d^{-1}). Primary production in this last group of stations was higher than in other Polar waters (about 2 times greater), and may indicate the same enrichment processes that were involved in the high production region were acting here, but the time frame had shifted i.e., the bloom may be in decline at these stations. Integrated PP and chlorophyll for each transect are presented in Table 4.1.

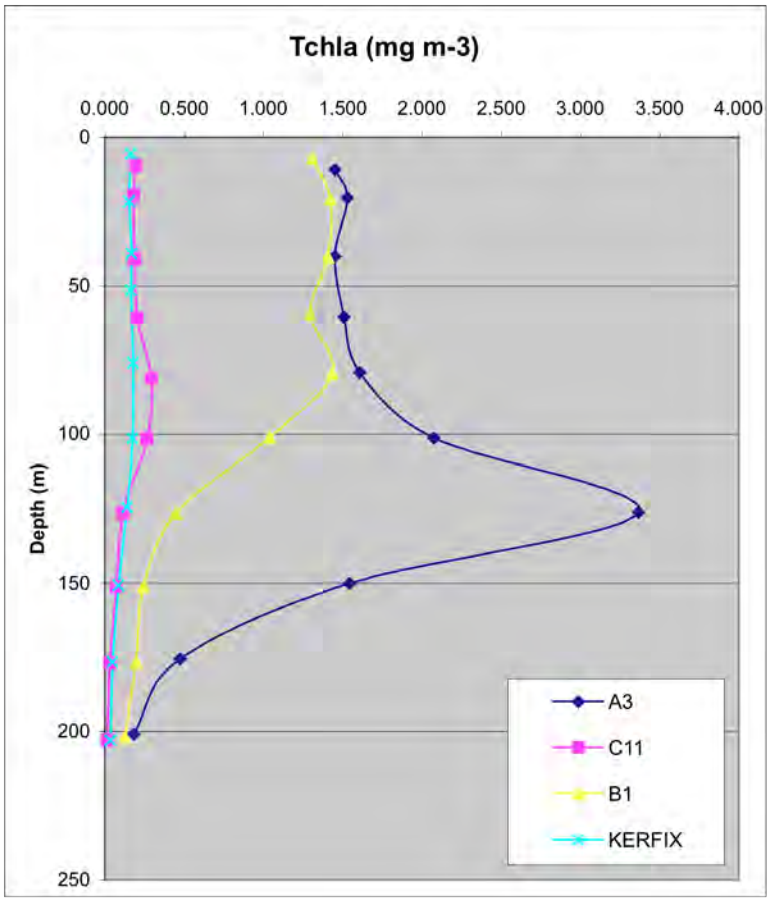

Figure 4.5: Vertical distribution of chlorophyll, as total chlorophyll-*a* (mg m^{-3}), along stations A03, C11, B1 and KERFIX. From Uitz *et al.* [2009]

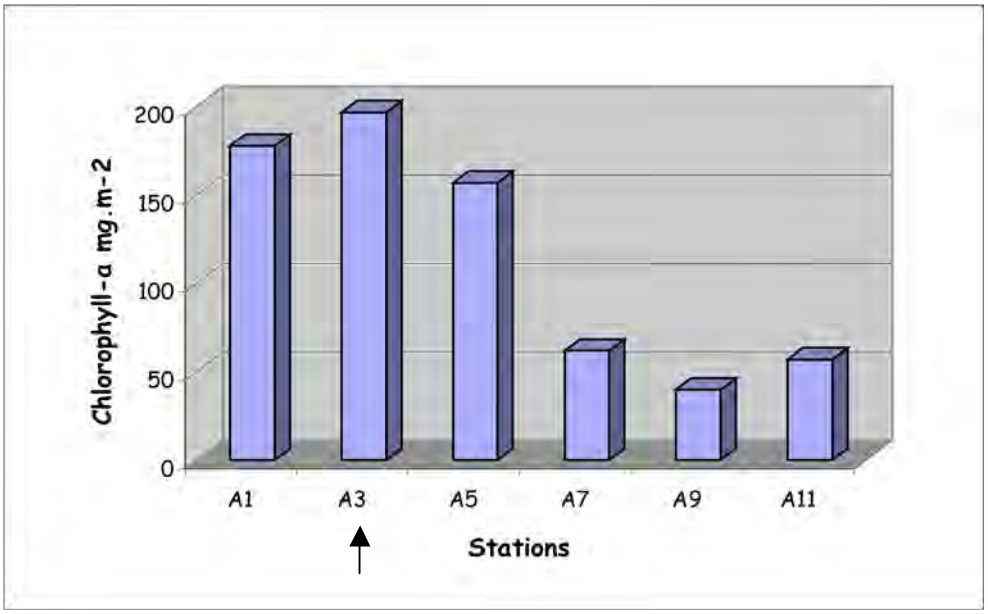

Figure 4.6: Integrated Chlorophyll (0-125m) in mg m^{-2} along transect A. On-Plateau reference site (*i.e.*, A3) is highlighted. Published by Uitz et al. [2009].

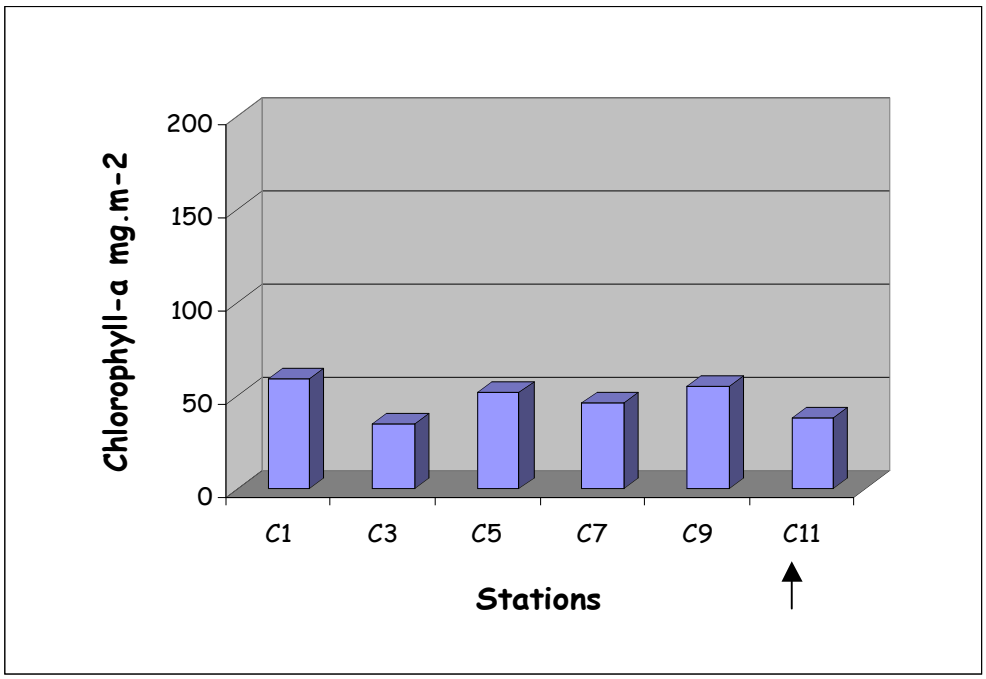

Figure 4.7: Integrated Chlorophyll (0-125m) in mg.m^{-2} along transect C. Off-Plateau reference site (*i.e.*, C11) is highlighted. Published by Uitz et al. [2009].

Four profiles of Primary Production observed in A03 are presented in Figure 4.8a. Values were quite constant during the time frame of the KEOPS study. Primary production was close to 40 mg C m^{-3} d^{-1} in surface and decreased to 5 mg C m^{-3} d^{-1} below 30m. For the HNLC reference station three profiles of Primary Production are presented in Figure 4.8b. Profiles were similar during 10 days with values ranged between 3.5 and 0.5 mg C m^{-3} d^{-1} from surface to 120m.

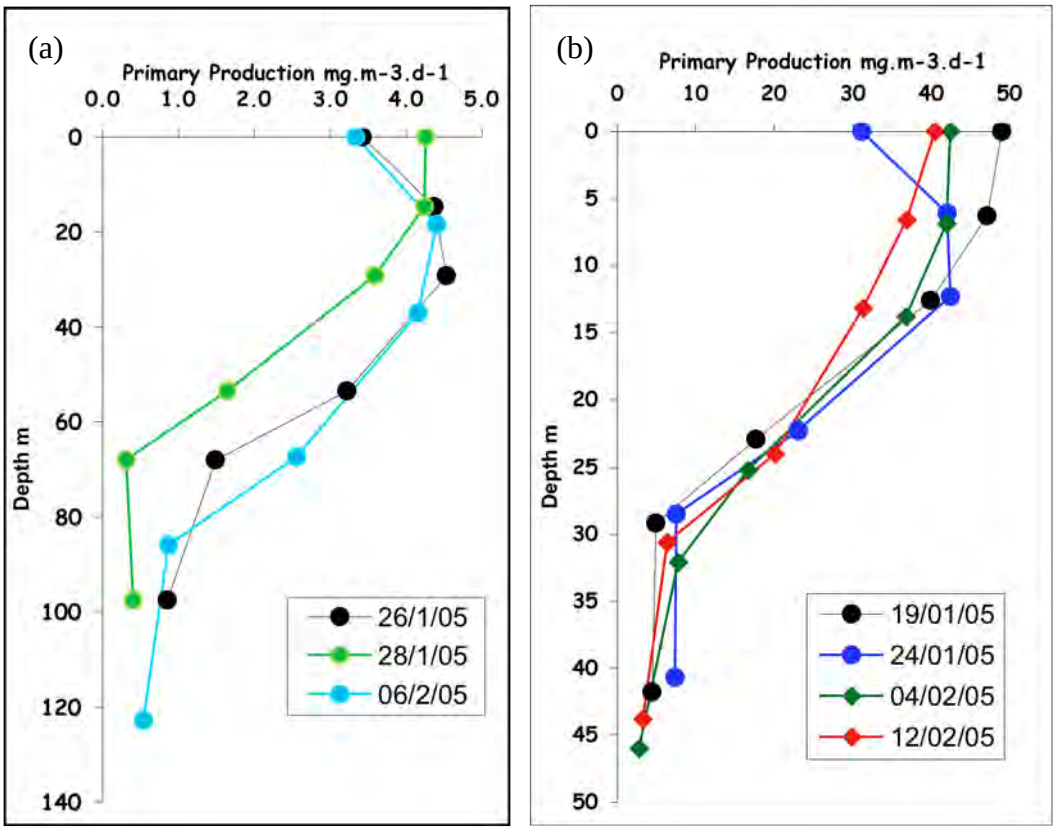

Figure 4.8: Vertical distribution of primary production (mg C m^{-3} d^{-1}) at reference stations for a) off-Plateau and b) on-Plateau along the KEOPS campaign [*Uitz et al.*, 2009].

In both on- and off-Plateau stations, the planktonic ecosystem structure was dominated by large diatoms and large copepods [*Armand et al.*, 2008; *Carlotti et al.*, 2008]. Bacterial activity was elevated over the plateau [*Obernosterer et al.*, 2008] and the utilisation of new nitrogen by phytoplankton also appeared to be greater [*Trull et al.*, 2008b]. At the time of the KEOPS survey, particulate carbon export over the

plateau was approximately twice that of surrounding waters [*Savoye et al.*, 2008; *Trull et al.*, 2008b]. Based on surface dissolved inorganic carbon concentrations a similar enhancement seems to persist over the full season [*Jouandet et al.*, 2008].

4.3 The Kerguelen plateau phytoplankton bloom

To provide regional context for the Kerguelen bloom, an annual mean ocean color composite image (Fig. 4.9) and a series of SCHL images during the bloom period (Fig. 4.10) are here presented.

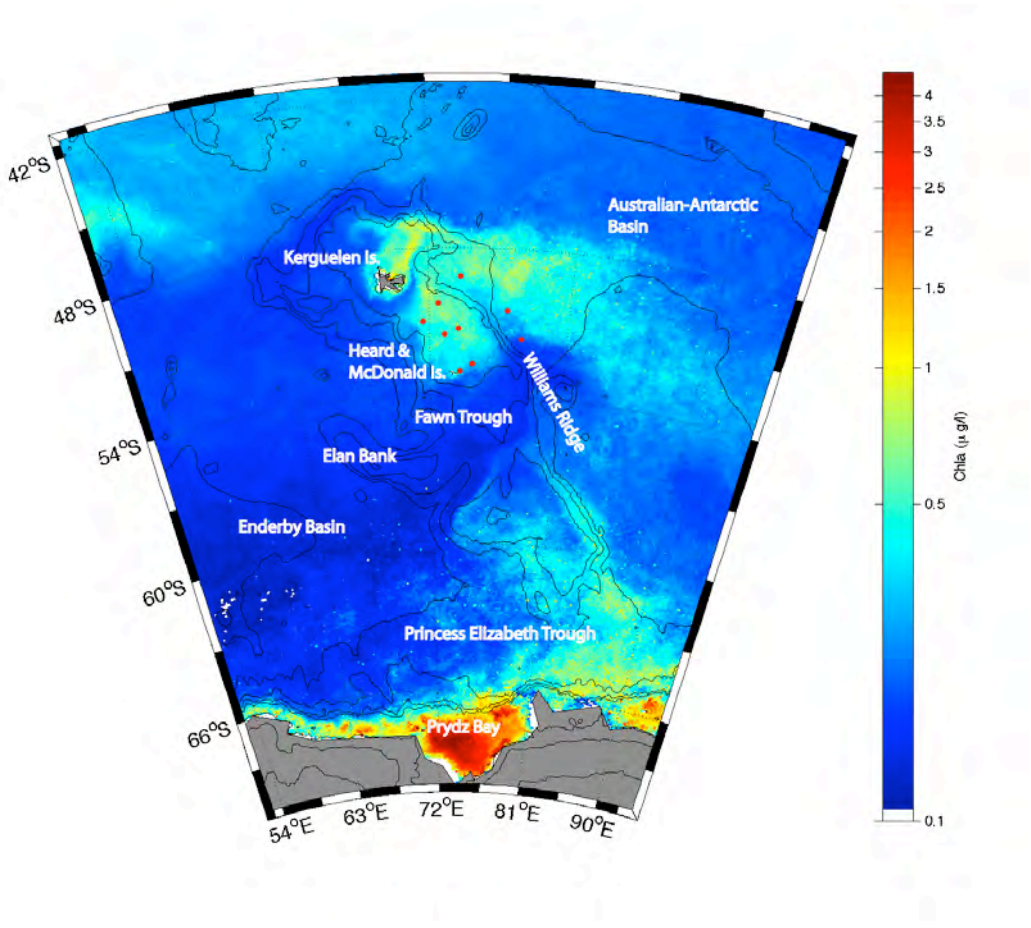

Figure 4.9: Chlorophyll-*a* climatology (1997-2007) from the MODIS-Aqua sensor showing major topography and KEOPS sampling sites [*Mongin et al.*, 2008].

To estimate the spatial distribution of surface chlorophyll-*a* concentrations (SCHL, in mg m^{-3}), 8-day composite images at 4-km resolution from the Moderate Resolution Imaging Spectroradiometer (MODIS/Aqua) were used. Because of high cloud cover, only 18 such images could be exploited for the 2004/2005 season (for which cloud coverage was equal or smaller than 30%). The SCHL distribution over this region can be separated into 4 regimes:

i) North of the SAF (subantarctic front), in the subtropical waters (40°S- 45°S) the SCHL is usually low (max of 1.5 mg Chla m-3) and develops late in the season (January).

ii) In the southeast, an area of elevated SCHL forms near the Banzare bank probably associated with meandering of the Southern Antarctic Circumpolar Current (ACC) Front.

iii) In an east-west band just to the north of Kerguelen Island, there is an area of high SCHL associated with mesoscale eddies within the SAF [*Moore & Abbott*, 2000]. This activity often merges with the coastal plume of SCHL around Kerguelen Island and sometimes extends southeast to merge with the high SCHL over and to the east of the plateau.

iv) The last pattern is the bloom studied during the KEOPS project, over shallow waters (1000 m) between Kerguelen and Heard islands. This bloom starts sooner (November) than in waters to the north (January, for 40°-45°S). It has a round shape and seems to extend from a central point within the plateau.

The seasonality and strength of these four SCHL features are different, and the possible triggering factors of these blooms may also be different. Among them, the KEOPS bloom appears unique by its shape (round) and duration (nearly 3 months).

Possible links between the bathymetry and the SCHL distributions already have been studied in the Southern Ocean [*Moore & Abbott*, 2000; *Sokolov & Rintoul*, 2007b; *Tyrrell et al.*, 2005] including the Kerguelen zone [*Pollard et al.*, 2002]. In this study, those links are explored in the context of the KEOPS project by examining high-resolution images and developing a comprehensive description of the distribution of SCHL on and around the central plateau.

Focusing in on the Kerguelen plateau bloom studied by the KEOPS program, Fig. 4.10 presents eight images of the SCHL in the Kerguelen region (48°S-55°S 69°E-78°E), from November through early February. The bloom starts to develop in November over the plateau in the 500- 1000 m depth zone. By the end of November, the bloom occupied most of the area between the two islands. It then spread outside the plateau to the east, apparently under the influence of the meandering flow within the SAF [*Mongin et al.*, 2009]. By December, the bloom had started to fade but the SCHL tongue was still present. In late January, the bloom shrank back to occupy only the part of the plateau between the two islands.

The SCHL does extend off the plateau to some degree, especially in its northwest-southeast direction and this appears to reflect both advection from the plateau and southward meandering of the SAF [*Maraldi et al.*, 2009]. There was always a thin band of low SCHL in the Polar Front trough just south of Kerguelen Island (40°S 70°E) that divides the main bloom from the Kerguelen coastal waters. This is an important feature for the evaluation of hypotheses about the processes that fuel the plateau bloom, in that it suggests that inputs from Kerguelen Island are probably not important in the delivery of iron or other materials [*Blain et al.*, 2008b]. From Figures 4.9 and 4.10, it is clear that the bloom shape is strongly determined by the southeastern trench. This area has elevated SCHL in comparison to the shallower plateau and the southeastern ridge to its east, in both spring and autumn. The elevated SCHL is usually located in relatively deep waters (300-500m) rather than the shallowest waters (0-200m), possibly as a result of higher currents within these troughs and associated increased delivery of iron from deep to shallow waters..

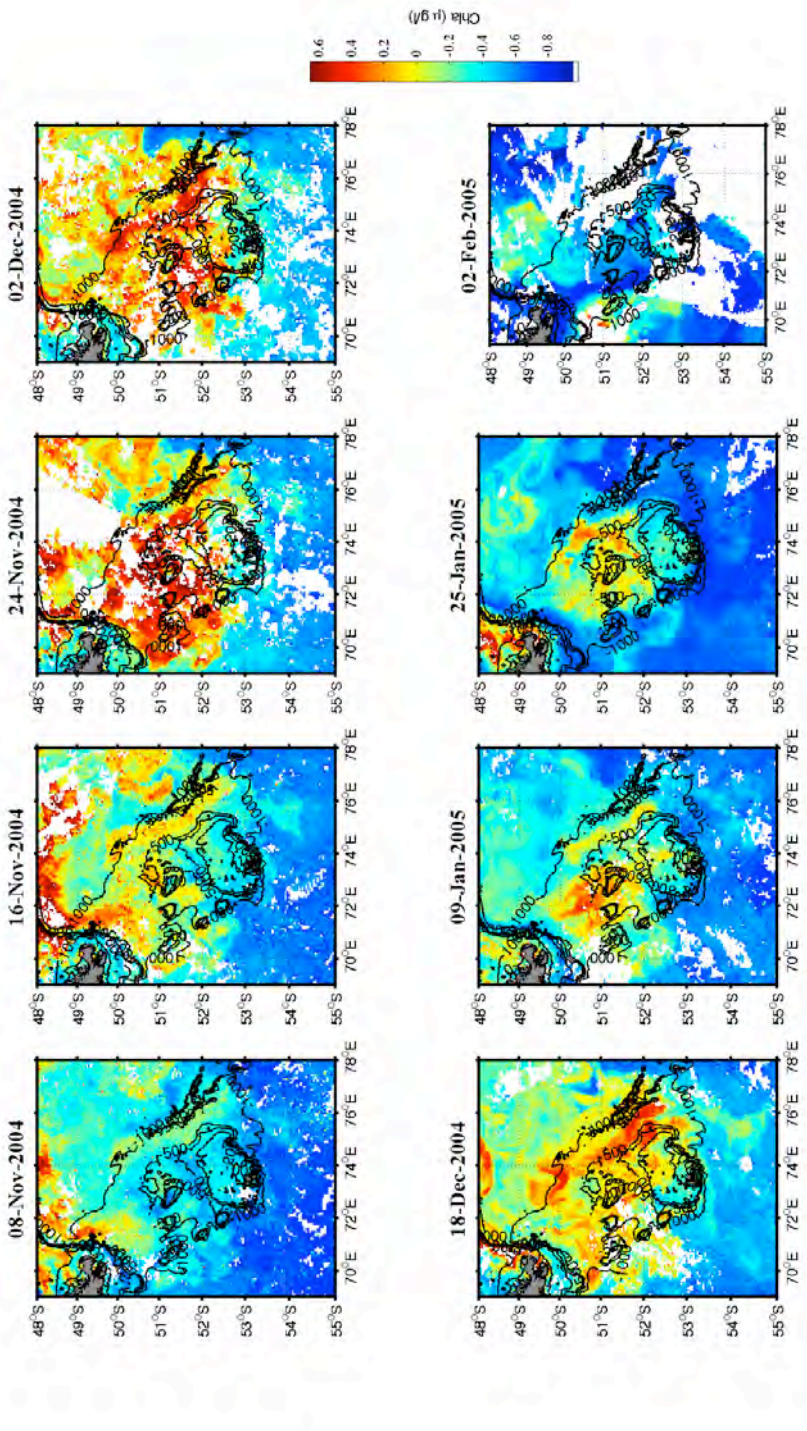

Figure 4.10: MODIS/Aqua SCHL images during the bloom period (chosen upon clouds coverage conditions). Overlay is the bathymetry field. From Mongin, Molina & Trull [2008].

Further investigation of daily, 4 km, level 2 MODIS products was performed on data provided by the Remote Sensing Facility at the Commonwealth Scientific and Industrial Research Organisation (CSIRO) Marine Labs in Hobart, Tasmania. When assembled together (Fig. 4.11), the MODIS-derived SCHL time evolution at the individual KEOPS station location show a typical polar seasonality with a single peak in early summer rather than the bimodal early spring and early autumn peaks typical of the subantarctic waters [*Sokolov*, 2008; *Trull et al.*, 2001a]. These two regimes are thus the central focus of the following sections.

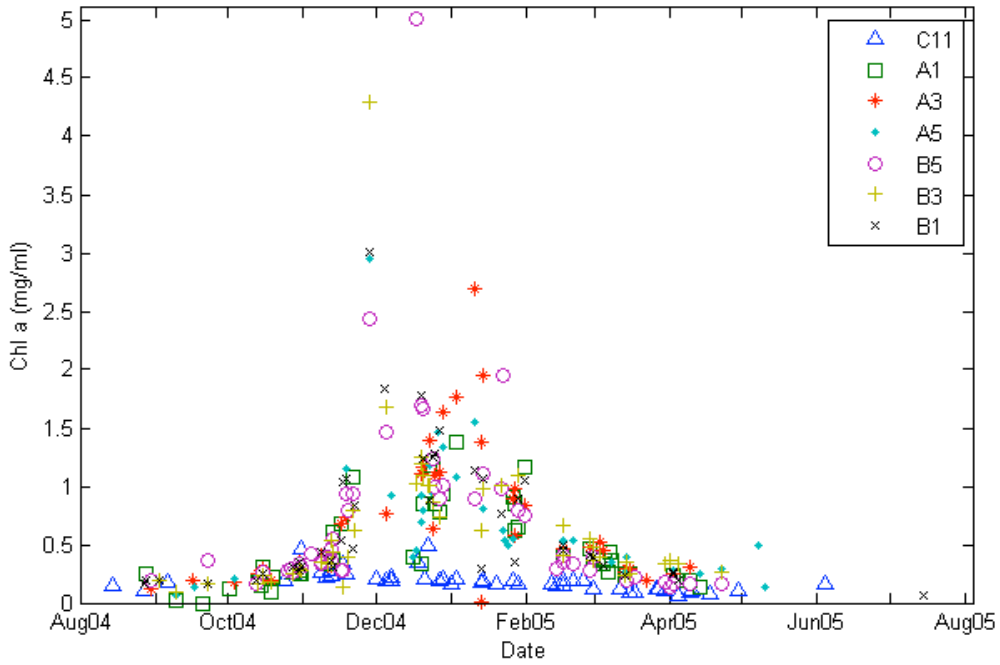

Figure 4.11: SCHL time series at the KEOPS cruise stations using high resolution MODIS/Aqua image.

4.4 Biogeochemical simulations and results

Our purpose here is to examine, using a 1-D biological model, the biogeochemical dynamics that occurred both inside and outside of the naturally-fertilized Kerguelen Plateau bloom in the Southern Ocean. We focus, in particular, on three main issues governing the phytoplankton biomass: variations in mixed layer

depth (*i.e.*, mixed layer light field), the role of iron, and the effect of grazing. We do not explicitly consider the possible influence of microbial nutrient recycling, but we do comment on whether this omission in the model could explain aspects of the difference between our simulations and the observations.

a. The NPZD model

The biological model is the nitrogen-based model described in Chapter 2. The model includes four components, namely nutrients (*N*), phytoplankton (*P*), zooplankton (*Z*) and a detritus pool (*D*). The variations of nitrogen concentrations in each element are expressed in a system of four differential equations:

$$\frac{dN}{dt} = rem\ D + \varepsilon_Z\ Z\ - \mu\,(MLD, t, N)\ \ P - \frac{(N_0 - N)w^+(t)}{MLD} \tag{4.1}$$

$$\frac{dP}{dt} = \mu\,(MLD, t, N)\ P - G(P)\ Z - \varepsilon_P\ P - \frac{w^+(t)P}{MLD} \tag{4.2}$$

$$\frac{dZ}{dt} = \gamma_z\, G(P)\ Z - zmort\ Z^2 - \varepsilon_Z\ Z - \frac{w^+(t)Z}{MLD} \tag{4.3}$$

$$\frac{dD}{dt} = (1 - \gamma_z)\ G(P)\ Z + \varepsilon_P\ P + zmort\ Z^2 - rem\ D - \left(\frac{w_S + w^+(t)D}{MLD}\right) \tag{4.4}$$

The different terms of these equations express phytoplankton growth rate, grazing of phytoplankton by zooplankton (with assimilation efficiency), mortality of phytoplankton and zooplankton, excretion of zooplankton and remineralisation of detritus to nutrients (see Table 4.2 for further details and parameter values).

Table 4.2 Parameters of the ecosystem model.

Parameter	***Symbol***	***Values***	***Units***
	Phytoplankton (P) Coefficients		
Initial slope of P-I curve	α	0.025	$d^{-1}/(W\ m^{-2})$
Photosynthetically active radiation fraction	PAR	0.43	*non-dimensional*
Attenuation coefficient of seawater	k_w	0.04	m^{-1}
Light attenuation by phytoplankton	k_P	0.03	m^{-1} (mmol N m^{-3})$^{-1}$
Maximum growth rate	$\mu_{max} = a \cdot b^{cT}$		
	a	0.6	(d^{-1})
	b	1.066	*non-dimensional*
	c	1.0	(°C)$^{-1}$
Half saturation constant for N uptake	K_N	0.5	(mmol N m^{-3})
Phytoplankton mortality	ε_P	0.03	(d^{-1})
	Zooplankton (Z) Coefficients		
Zooplankton assimilation efficiency	γ_z	0.75	*non-dimensional*
Maximum grazing rate	g	2.0	(d^{-1})
Prey capture rate	pc	1.5	(mmol N m^{-3})$^{-2}$ d^{-1}
Quadratic mortality rate	*zmort*	0.20	(mmol N m^{-3})$^{-1}$ d^{-1}
Zooplankton excretion rate	ε_Z	0.01	(d^{-1})
	Detrital (D) Coefficients		
Detrital remineralisation rate	*rem*	0.050	(d^{-1})
Detrital sinking rate	w_S	3.0	m d^{-1}
	Nutrient (N) Coefficients		
NO_3 concentration below mixed layer	N_0	25	(mmol N m^{-3})
	Mixed layer Coefficients		
Rate of mixed-layer depth increase	w^+		m d^{-1}

Photosynthesis and grazing expressions

Photosynthesis growth rate $$\mu(z,t,N) = \min\left\{\mu(z,t), \mu_{\max}\frac{N}{(K+N)}\right\} \quad (4.5)$$

Growth rate without nutrient limitation $$\mu(z,t) = \frac{\mu_{\max}\alpha I}{\sqrt{(\mu_{\max}^2 + \alpha^2 I^2)}} \quad (4.6)$$

Maximum growth rate $$\mu_{\max}(T) = ab^{cT} \quad (4.7)$$

Solar radiation $$I(z,t) = I_0(t)_{PAR}\exp\left(-(k_w + k_p P)z\right) \quad (4.8)$$

Zooplankton grazing expression $$G(P) = \frac{g\ pc\ P^2}{g + pc\ P^2} \quad (4.9)$$

where: *min*{x,y} is the function "minimum between x and y",
z is depth, (in m)
t is time,
T is temperature (°C)
and θ is the angle of incidence at noon (in radian)

b. Model numerics

The full set of differential equations describing the ecosystem model was solved using a fourth-order Runge-Kutta algorithm. The simulations were run for three year, with the second year of data being used for the analysis. Typically by the second year, the model achieved a steady state annual cycle which was not sensitive to the initial conditions.

The base-line simulation used the initialisation described below and the values of the biological parameters as listed in Table 4.2. For the conversion from solar radiation to PAR, a factor of 43% was taken according to Jerlov [1976], and as the Southern Ocean belongs to oceanic type I [*Hense et al.*, 2000; *Wang et al.*, 2003], a k_w = 0.04 m^{-1} was used as the attenuation coefficient of sea water. The self-shading parameter k_P= 0.03 m^2 mmol N^{-1} and the initial slope α = 0.025 (W m^{-2})$^{-1}$ day^{-1} of the P-I curve were taken from OG99. The model was initialised with winter values in all

compartments. For phytoplankton, a value of 0.1 mmol N m^{-3} was taken, and for zooplankton 0.01 mmol N m^{-3}. Following the WOCE data set, initial nutrient concentration was 25 mmol N m^{-3} for nitrate. Detritus was initialised with a small value (0.01 mmol N m^{-3}). The model was forced by annual cycles of the mixed layer depth, solar radiation and sea surface temperature (SST) (Fig. 2.9). For the purposes of comparing the results to satellite biomass estimates, a fixed chlorophyll-to-nitrogen ratio of 1.59 g mol^{-1} was used.

c. Reference simulation

An initial modelling experiment used ecosystem model parameters taken from the literature, in particular, from Oschlies & Garçon [1999] and Schartau & Oschlies [2003a]. These were essentially the values listed in Table 4.2. The main results of this first simulation (Fig. 4.12) showed that this model is able to reproduce the typical HNLC cycle in Subantarctic surface waters. The simulated annual cycle of *P*, *Z* and *N* were in good agreement with observations during the Southern Ocean (HNLC) spring bloom [*Carlotti et al.*, 2008; *Lefèvre et al.*, 2008; *Mongin et al.*, 2008]. The absence of a strong decrease in nitrate concentration in summer is a prominent feature of the ecosystem near the Antarctic Polar Front and has been repeatedly observed [*Blain et al.*, 2001; *Bowie et al.*, 2009; *Loscher et al.*, 1997] and is also a distinctive feature of model studies in the Southern Ocean [*Lancelot et al.*, 2000; *Pondaven et al.*, 2000; *Wang et al.*, 2003]. In the model as in the observations, the off-Plateau bloom starts in late October and reaches its maximum by mid-November (0.35 mmol N m^{-3}). From February onwards, the decline of the solar radiation and further deepening of the mixed layer leads to a decrease of phytoplankton biomass. By April, phytoplankton concentration has gone below 0.2 mmol N m^{-3} and zooplankton has decreased to concentrations lower than 0.3 mmol N m^{-3}. During winter, nutrients are replenished due to further entrainment and cross-thermocline mixing. Maximum concentrations of 25 mmol N m^{-3} for nitrate occur just before the phytoplankton starts to develop.

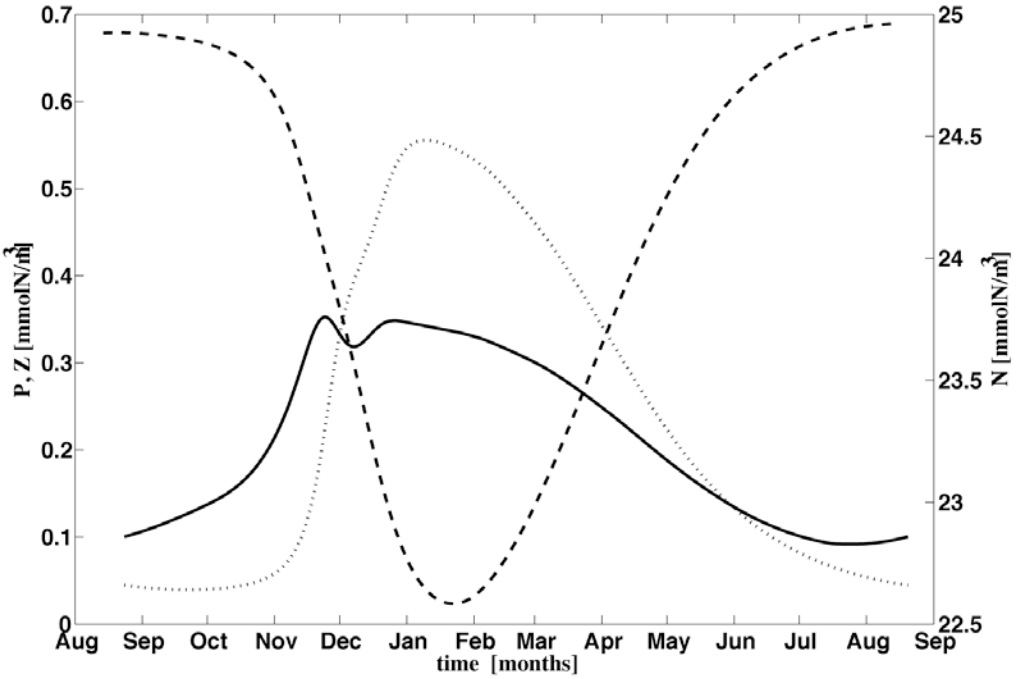

Figure 4.12: Simulated concentration in the reference run of the ecosystem model for the mixed-layer nitrate concentration (dashed line), phytoplankton concentration (solid line) and zooplankton concentration (dotted line).

When compared to MODIS/Aqua SCHL data, the model simulates reasonably well the seasonal cycle of mixed-layer chlorophyll at the off-Plateau reference station. However at the on-Plateau reference site, in the fertilization zone, the surface chlorophyll *a* distribution as simulated by the model does not reproduce the seasonal variability established by remote sensing data analysis (Fig. 4.13). The model fails to simulate the SCHL maximum over the plateau but it also fails in capturing its early development. Comparing the MODIS-Aqua SCHL time series on- and off-Plateau (Fig. 4.13) reveals that this early start is a real feature of the central plateau bloom. A main feature of the model is that the reference simulation reproduces the HNLC cycle in Subantarctic surface waters that are proven to be iron limited [*Blain et al.*, 2007], therefore it is assumed that the set of parameters used in this simulation are representative of iron limitation conditions.

In the sections that follow, we first describe the fluxes that characterise the reference simulation, and then consider how varying mixed layer dynamics, zooplankton mortality and iron supply could improve the match between the model

and observations over the plateau. We focus on these three effects because our exploration of the model sensitivity (chapter 3) identified them as key features. Importantly, the mismatches in SCHL maximum and seasonality are not easy to explain as a result of the simplicity of our model. For example, inclusion of nutrient recycling via a microbial loop would not be able to simulate either an earlier bloom start or a higher magnitude peak, and the data do not require a longer bloom duration than what we are able to achieve with the simple model.

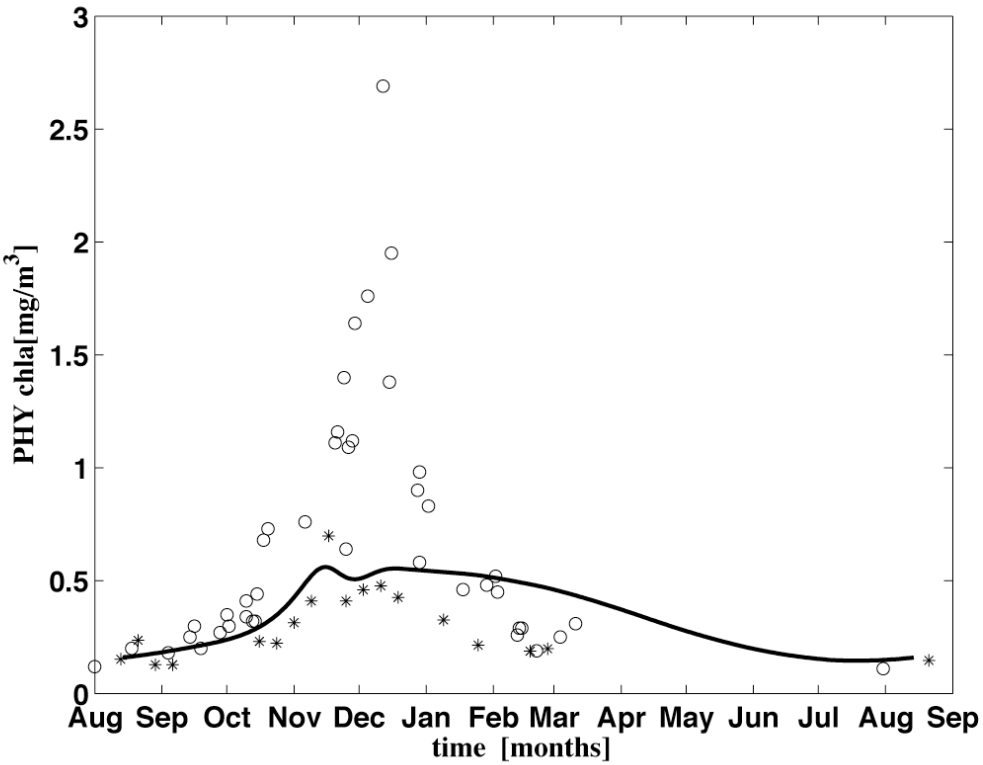

Figure 4.13: Comparisons of the modeled seasonal cycle (solid line) of SCHL (mg Chl *a* m^{-3}) and MODIS/Aqua SCHL data for the on-Plateau and off-Plateau sites, illustrated in circles and asterisks respectively.

Time series of the nitrogen fluxes between the different compartments (Fig. 4.14) indicate that phytoplankton growth is predominantly balanced by zooplankton grazing while phytoplankton mortality appears to play a minor role. Similar to that, zooplankton growth is balanced by mortality (including feeding pressure by higher predators) while excretion in negligible (Fig. 4.15). In addition to the grazing control by zooplankton on phytoplankton biomass accumulation, the low supply of iron to the

Southern Ocean HNLC waters may limit phytoplankton ability to take up excess nitrate [*Bowie et al.*, 2001; *Dugdale & Wilkerson*, 1991; *Trull et al.*, 2008b].

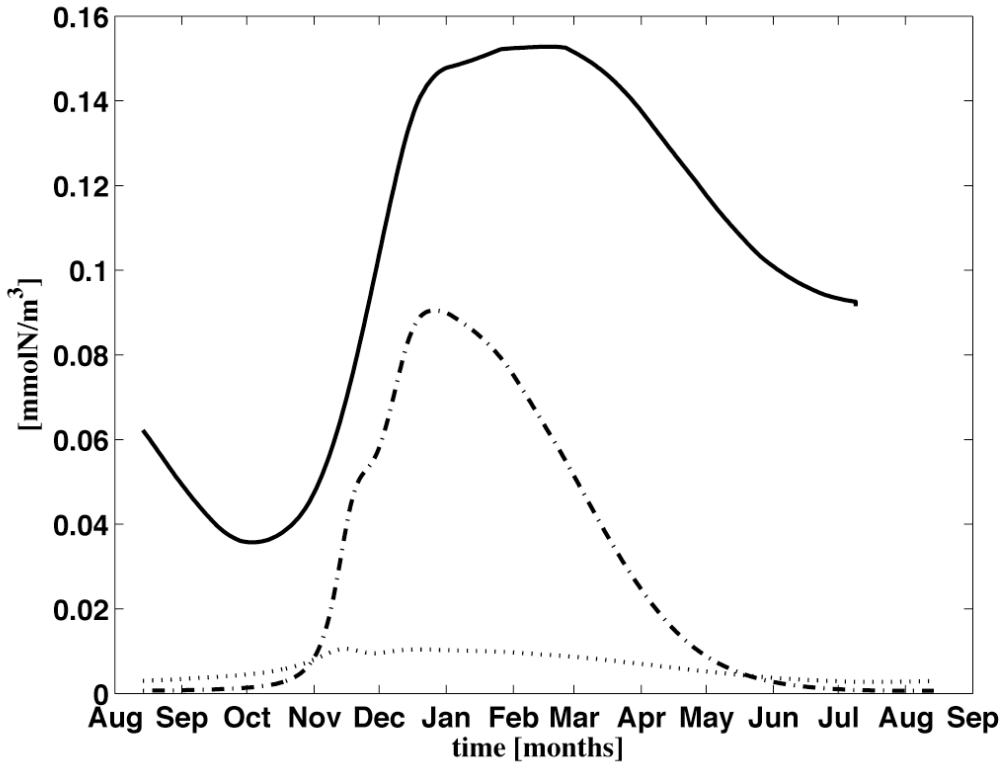

Figure 4.14: Nitrogen fluxes for the phytoplankton compartment. Displayed are phytoplankton growth (solid line), zooplankton grazing (dashed line), and mortality (dotted line).

Thus, the main results of this first simulation give thoroughly reasonable results for outside the plateau (*i.e.*, off-Plateau site). However, the small seasonal bloom in deeper waters outside the plateau differs significantly from the one observed at the reference bloom station over the plateau (*i.e.*, on-Plateau site). This difference that may reflect greater iron availability at on-Plateau than off-Plateau, or possibly other factors such as differences in grazing pressure or the seasonality of stratification, are discussed in the next sections.

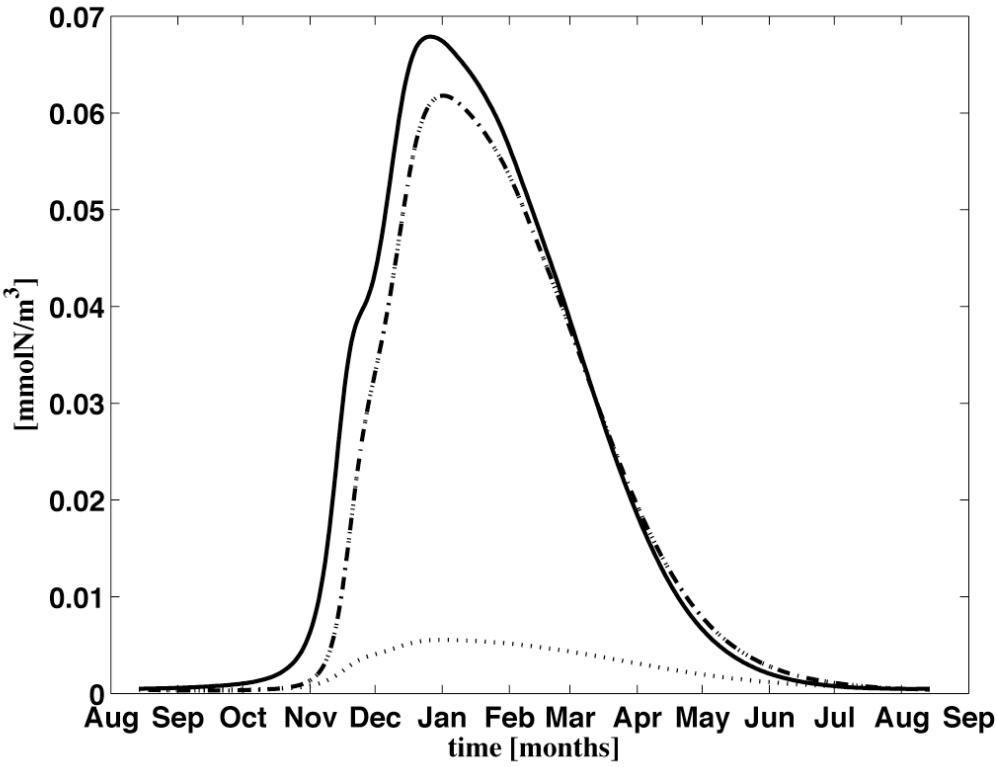

Figure 4.15: Nitrogen fluxes for the zooplankton compartment. Displayed are zooplankton growth (solid line), zooplankton mortality (dashed line), and excretion (dotted line).

Because the principal aim of the study was to investigate the controls affecting the magnitude of the elevated phytoplankton biomass found on and around the naturally iron-fertilized Kerguelen Plateau in the Southern Ocean, the diagnosed surface chlorophyll *a* (SCHL) was an obvious choice to represent model outputs.

c. The influence of mixed layer dynamics

To study the impact of mixed layer dynamics on the development of a phytoplankton bloom, two experiments were performed with the mixed layer depth constantly increased by 40 m and decreased by 40 m, respectively (Figs. 4.16). In both experiments, phyto- and zooplankton show small changes in biomass in wintertime and during the bloom. Apart from that, the effect on the biomasses of

phyto- and zooplankton was rather negligible. An interesting observation from these results was that a mixed layer constantly increased by 40 m improves the model performances in simulating the SCHL dynamics in *HNLC* waters. Nevertheless, the onset of the phytoplankton bloom was not affected and therefore, another experiment was designed to explore the effects of a temporal shift in the mixed layer seasonal stratification.

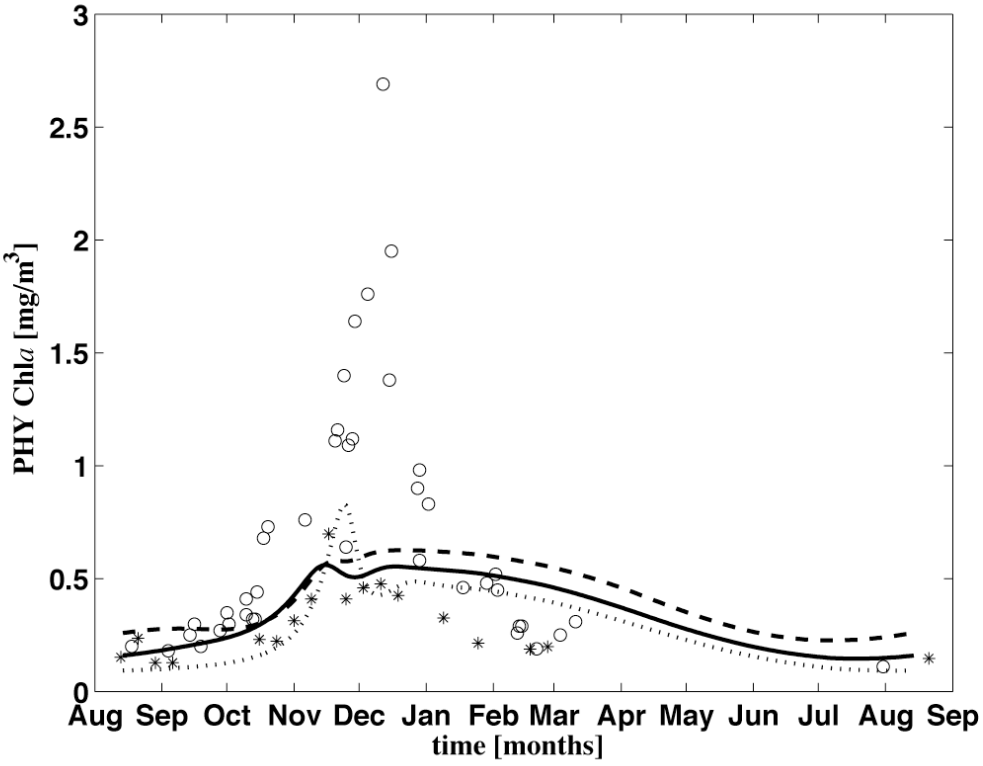

Figure 4.16: Simulated concentrations of phytoplankton (mg Chl*a* m^{-3}) in the reference simulation (solid line) and experiments with changing the offset of the *MLD* of +40 m (dotted line) and -40 m (dashed line). Satellite-derived estimates of SCHL at the on- and off-Plateau sites are also illustrated, with asterisks and circles respectively.

In this second *MLD* experiment, simulations were carried out with the mixed layer seasonal dynamics shifted 30 days forward and 30 days backwards, while the mixed layer depths remained unchanged. Figure 4.17 illustrates the model results for nitrate, phytoplankton and zooplankton, along with the *MLD* seasonality used in the experiment simulations.

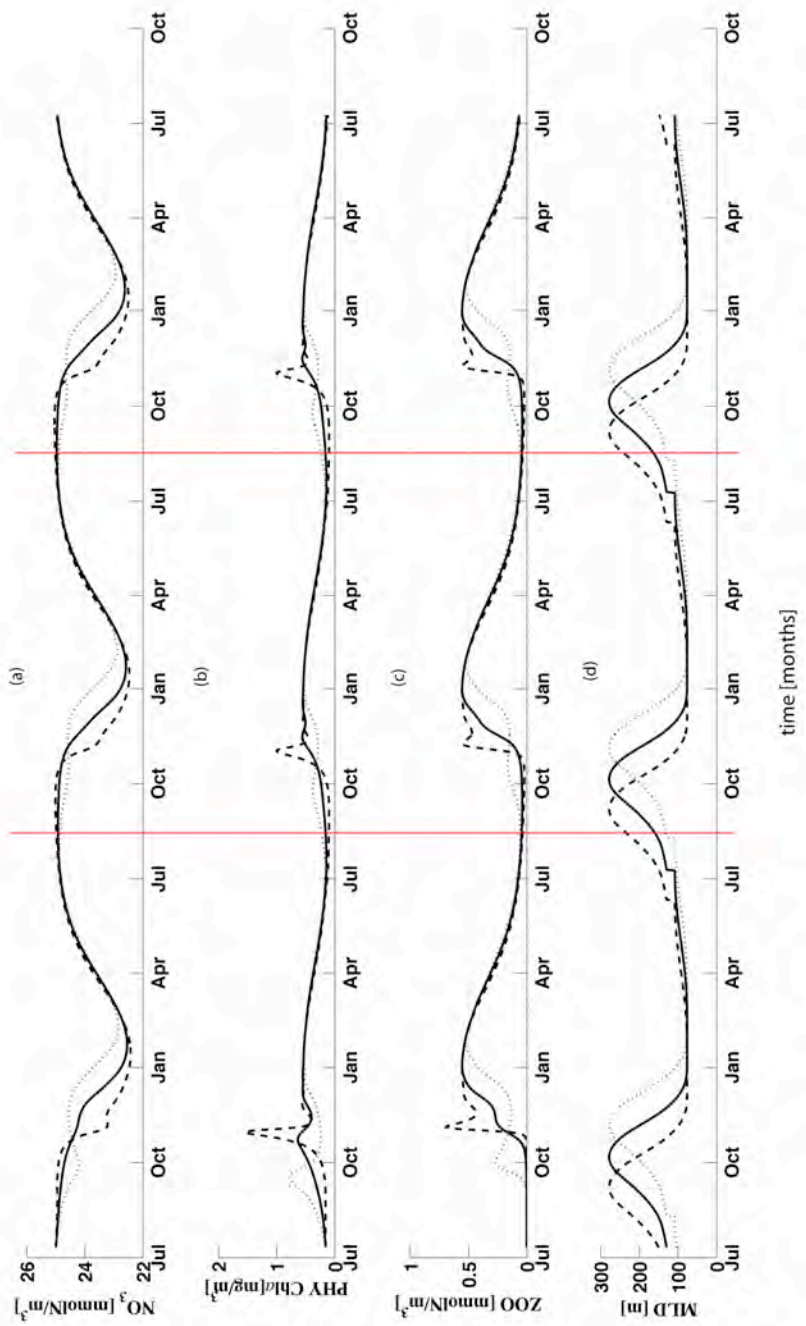

Figure 4.17: Simulated concentrations of (a) nitrate, (b) phytoplankton and (c) zooplankton in the reference simulation (solid line) and experiments with 30 days backward (dashed line) and 30 days forward (dotted line) shifted mixed layer dynamics. Panel (d) illustrate the resulting *MLD* cycle used in the experiments. Redlines denote the second year of simulation, which was used for further analysis.

A temporal shifting in mixed layer dynamics resulted in no significant changes in any state variable during winter. However, an earlier shallowing of the mixed layer yields a higher maximum phytoplankton concentration in early November and slightly changes the onset of the bloom (Fig. 4.18). This can be attributed to a better coupling between solar radiation and mixed layer seasonal dynamics (see Fig. 2.8).

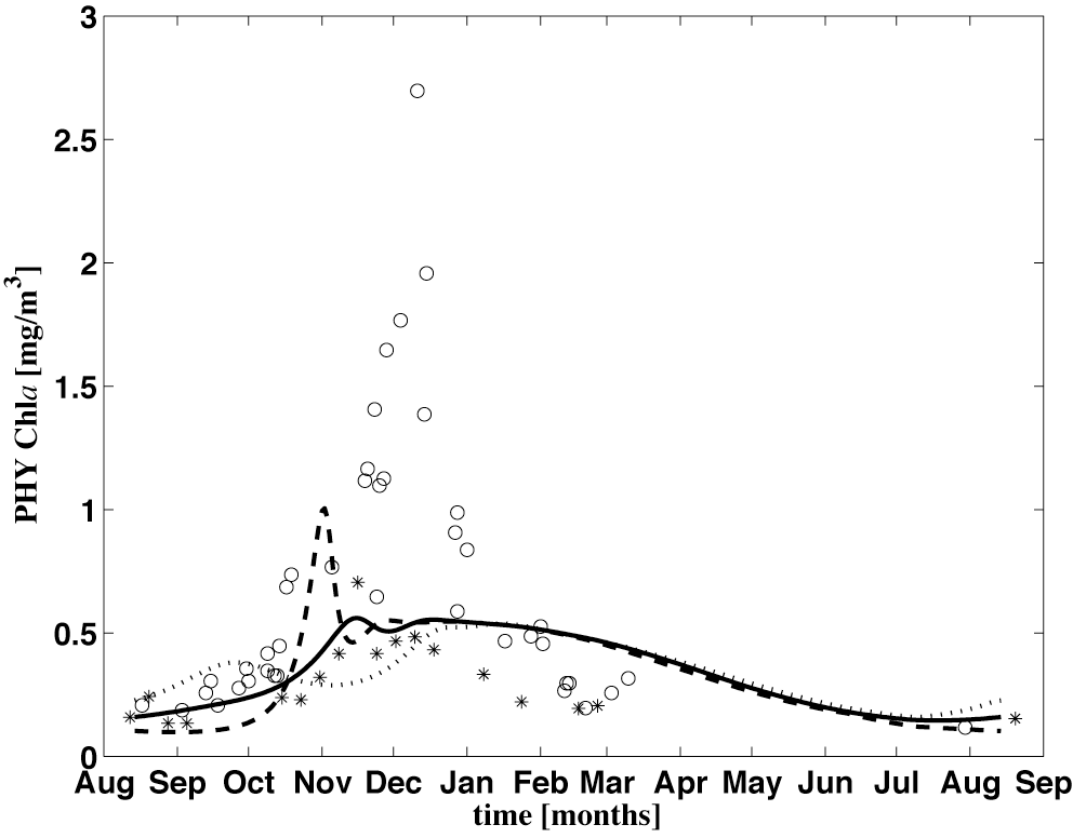

Figure 4.18: Simulated concentrations of phytoplankton (mg Chl*a* m^{-3}) in the reference simulation (solid line) and experiments with 30 days backward (dashed line) mixed layer seasonality and 30 days forward (dotted line) shifted mixed layer dynamics. Satellite-derived estimates of SCHL at the on- and off-Plateau sites are illustrated with asterisks and circles, respectively.

A later stratification produces a lower phytoplankton maximum and shows a bi-modal ‘unsuccessful’ onset of the bloom (Figs. 4.17 - 4.18), which can be explained by the limited response of phytoplankton to the seasonal rise of solar radiation along with a deep mixed layer. From January onwards, the decline of solar radiation leads to

a decrease of phytoplankton biomass in both of the experiments as in the reference simulation.

Figure 4.18 illustrates that when compared to observations the premature spring bloom caused by the simulated earlier mixed-layer stratification, only accounts for about 20% of the observed SCHL difference between the HNLC off-Plateau and the iron-rich on-Plateau waters. The simulated algal bloom reaches a maximum of about 1 mg Chl*a* m^{-3} in early November.

e. Experiments with zooplankton mortality

The previously reported sensitivity analysis (see section 3) along with figures 4.12 and 4.14 showed that the most important biological control on phytoplankton seasonal dynamics is herbivore grazing. There are two factors that determine the zooplankton grazing pressure, the zooplankton grazing rate and the zooplankton biomass.

The first of these two factors is controlled by two parameters *pc* and *g* and the sensitivity analysis showed that *pc* is the most important (Table 3.1). The sensitivity analysis, however, also demonstrated that the presence of zooplankton with a low prey capture rate is not a sufficient condition for the development of a bloom, and the reason for this bears on the second of the factors discussed above, the zooplankton biomass.

Figure 4.15 shows that zooplankton biomass is predominantly balanced by zooplankton mortality. The zooplankton mortality term, which is often called the 'closure term' [*Edwards & Yool*, 2000; *Steele & Henderson*, 1992], because it closes the model at the top trophic level, primarily represents consumption of the zooplankton by higher predators. As already mentioned, a quadratic mortality term is used in this study, which assumes that higher predators have a biomass proportional to that of the zooplankton [*Edwards & Brindley*, 1999].

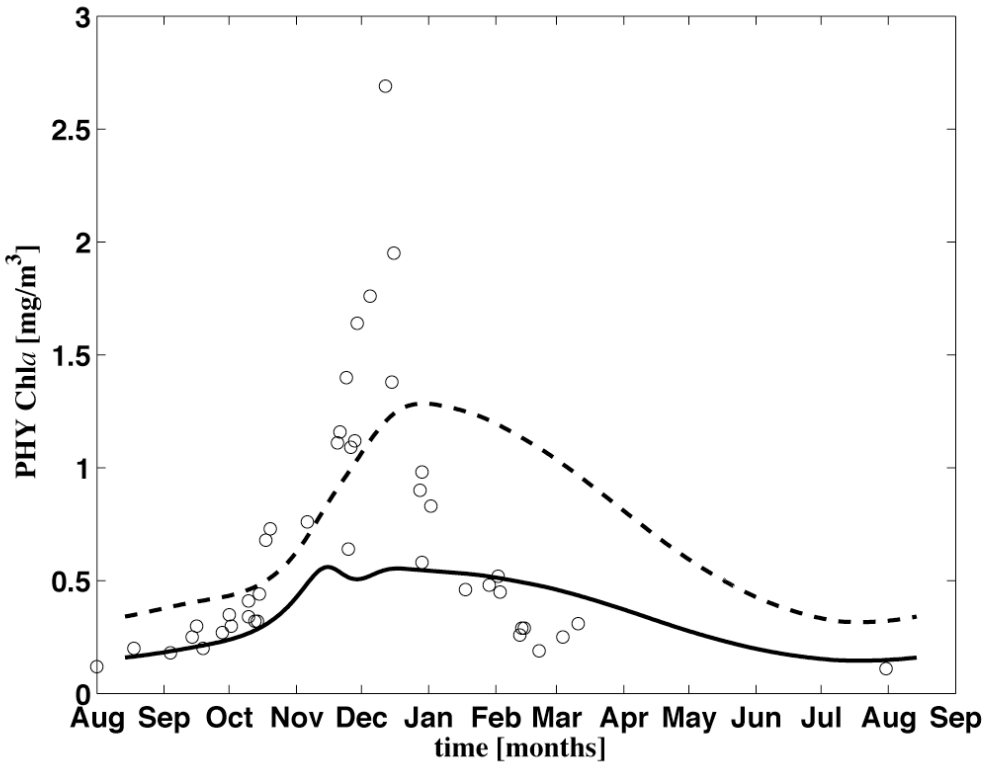

Figure 4.19: Simulated concentrations of SCHL (mg Chl*a* m^{-3}) in the HNLC-reference simulation (solid line) along with SCHL concentrations simulated with the zooplankton mortality parameter set to a value of 1.5 (mmol N $m^{-3})^{-1}$ day^{-1} (dashed line). MODIS-Aqua SCHL observations for the on-Plateau site are illustrated with circles.

A set of simulations was carried out to determine the parameter value of zooplankton mortality that makes the model sensitive to changes in the phytoplankton photosynthetic performance. By setting the zooplankton mortality parameter to 1.5 (mmol N $m^{-3})^{-1}$ day^{-1}, the model improves its capacity to simulate the maximum observed SCHL (Fig. 4.19), and more importantly for this study, it results in a relaxation of grazing pressure that leads to a higher sensitivity of the model to changes in the photosynthetic parameterisation.

d. The role of iron

The photosynthetic performance of phytoplankton in our model, in addition to nitrogen-based regulation, is described by two light related parameters: α describes

light limited photosynthesis, and μ_{max} gives a measure of the light-saturated phytoplankton growth rate. These two parameters are used in equation 2.11 that controls the productivity of the phytoplankton compartment.

As already mentioned, field and laboratory experiments have shown that iron addition enhances phytoplankton growth, or vice versa, that iron deficiency slows primary production [*Martin & Fitzwater*, 1988; *van Leeuwe & Stefels*, 2007]. In the Southern Ocean, Boyd *et al.* [2000] reported that the phytoplankton growth rates in iron-enriched waters were ~ 2-fold higher than rates in the surrounding HNLC waters. In addition to that, Lindley *et al.* [1995] as well as Lindley & Barber [1998] recorded higher (doubled) α values in iron-enriched experiments. During the KEOPS campaign similar differences were find between the on-Plateau (iron fertilized zone) and the off-Plateau (iron limited) surface waters [B. Griffiths, personal communication, February 2007].

The effect of iron fertilization was tested by a couple of model experiments with enhanced maximum growth rates and α (initial slope of P-I curve) values. As a consequence of doubling α and holding I_k (a measure of the irradiance at light saturated growth; see Fig. 2.6) constant, μ_{max} (the potential maximum specific phytoplankton growth rate) was also doubled, since μ_{max} equates to $\alpha \times I_k$ [*Chai et al.*, 2007; *Kirk*, 1994]. To simulate the enhanced photosynthetic performance with additional iron in the model, α was doubled (0.025 to 0.05 day^{-1} $(W\ m^{-2})^{-1}$) and μ_{max} was also enhanced by doubling the maximum growth rate parameter (Eq. 2.14) from 0.6 to 1.2 day^{-1}. Figure 4.20 shows two important features of the model. Firstly it shows how the reference simulation, with low zooplankton mortality and therefore strong grazer-control, is basically insensitive to changes in the photosynthetic efficiency. Secondly it shows the important effects of those same changes in the photosynthetic parameterisation in the presence of higher zooplankton mortality (i.e. lower grazing pressure).

By doubling both photosynthetic parameters (*i.e.*, α and μ_{max}) the modelled phytoplankton biomass increased by a factor of ~ 5, reaching a maximum on January with a surface value of 2.8 mg Chl*a* m^{-3}, which compares well with the observed satellite-derived SCHL (Fig. 4.20).

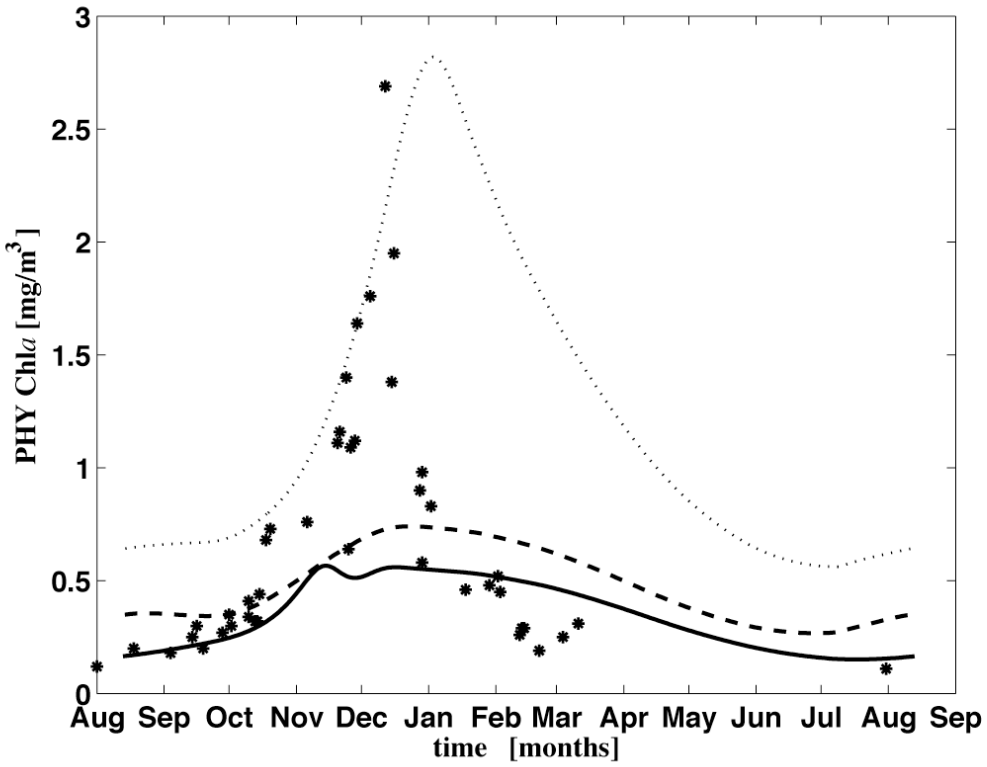

Figure 4.20: Modeled SCHL concentrations (mg Chl*a* m^{-3}) in the HNLC simulation (solid line) along with experiments with the two light related parameters (α and μmax) doubled. Results with zooplankton mortality unchanged and set to 1.5 (mmol N $m^{-3})^{-1}$ day^{-1} are illustrated with dashed and dotted lines, respectively. MODIS-Aqua SCHL observations for the on-Plateau site are also illustrated (asterisks).

Given that using higher photosynthetic parameters (*i.e.*, μ_{max} and α) is equivalent to removing or greatly reducing all physiological limitations due to micronutrients such as iron [*Boyd*, 2002; *Timmermans et al.*, 2004], a new set of experiments was designed to better simulate the effects of natural iron fertilization in the central Kerguelen plateau area. Values of the initial slope of P-I curve (α) along with the maximum growth rate parameter (Eq. 2.14) were set to increase during a theoretical iron enrichment period [see *Mongin et al.*, 2008]. Consequently, temporal changes for α and the μ_{max} parameter were introduced in the model simulations (Fig. 4.21).

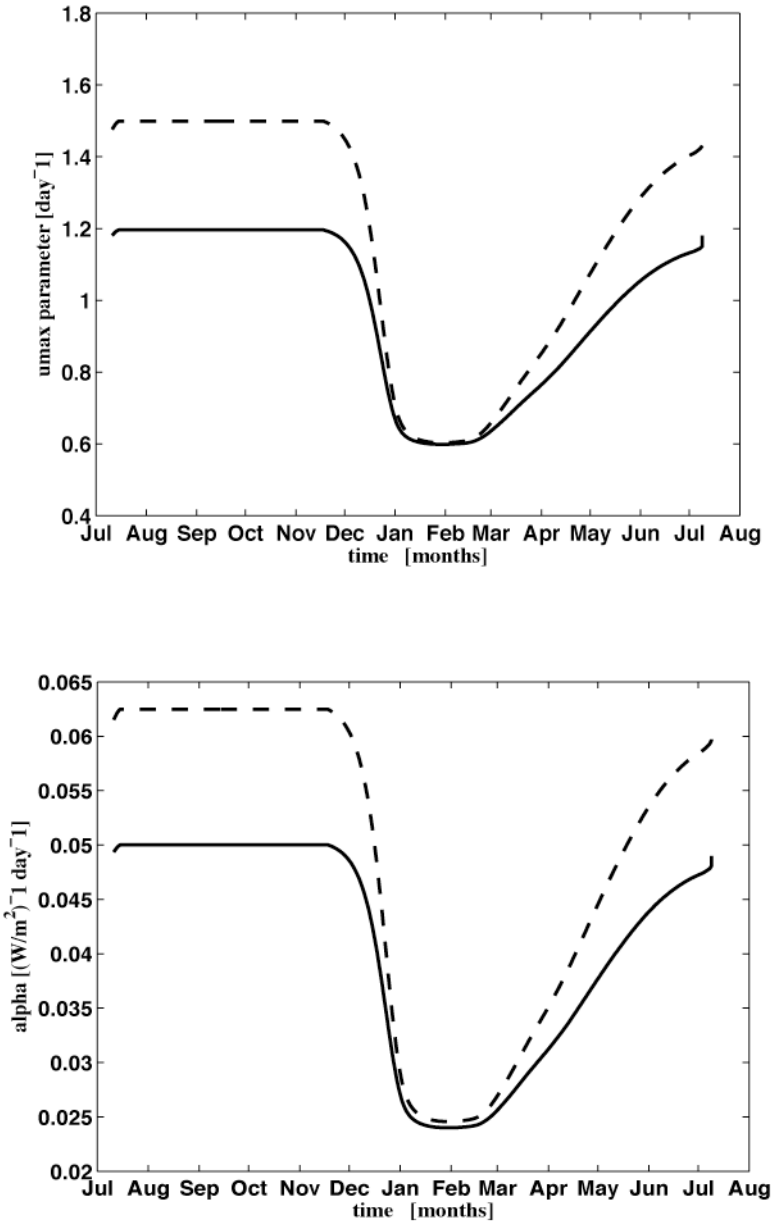

Figure 4.21: (top panel) temporal changes of μ_{max} (photosynthetic capacity); (bottom panel) temporal variations of α (initial slope of P-I curve). α and μ_{max} are set to increase by two (solid line) and 2.5 (dashed line) times.

This was done considering the observed results after the iron infusions at SOIREE and IronExII [*Hall & Safi*, 2001; *Hannon et al.*, 2001; *Landry et al.*, 2000], where α and μ_{max} were reported to increase by two and three times respectively. Denman & Peña [1999] used an *NPZD* model and the same approach to simulate the effects of iron limitation in the northeast subarctic Pacific Ocean. Fujii *et al.* [2005] used another one-dimensional ecosystem model and the same method of iron treatment to

investigate similarity and difference of iron fertilization experiments in several HNLC regions. The simulations were ultimately carried out with α and the μ_{max} parameters set to increase by two and 2.5 times to keep both parameter values within the range of values from a sample of the modelling literature [*Bowie et al.*, 1985; *Chavez et al.*, 1991; *Geider et al.*, 1998; *Hense et al.*, 2000].

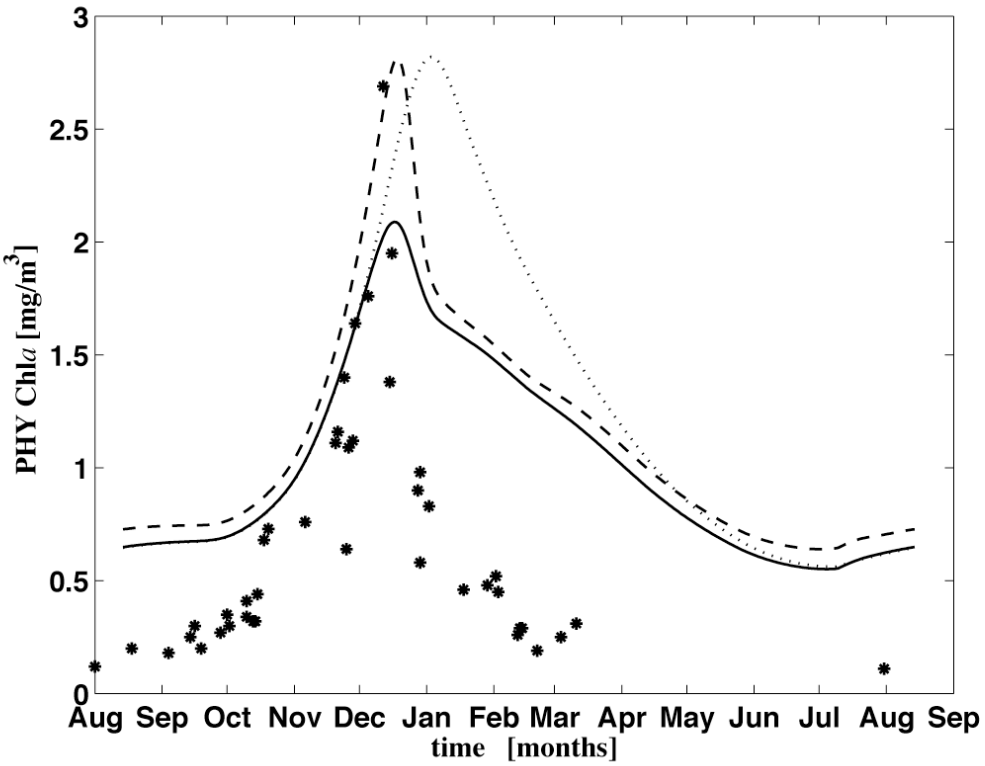

Figure 4.22: Model results of SCHL [mg Chl*a* m^{-3}] simulated with photosynthetic parameters α and μ_{max} increased 2 times without temporal changes (dotted line), and set to increase 2 (solid line) and 2.5 (dashed line) times as describe in Fig. 4.22. Satellite-derived SCHL observations for the on-Plateau site are shown with asterisks.

Figure 4.22 illustrates SCHL concentrations simulated without temporal changes in the photosynthetic parameter values (*i.e.*, from the experiment with α and μ_{max} doubled for the entire duration of the simulation; see Fig. 4.20), together with SCHL from simulations that include the prescribed temporal changes (Fig. 4.21) in the key photosynthetic parameters, α and μmax. The model results showed that by including temporal variations in the phytoplankton photosynthetic performance, which are

intended to simulate the iron effects, the modeled algal bloom changed its duration and timing. When temporarily increasing α and μ_{max} by 2.5 times their original values, the model reproduces the observed SCHL maxima of ~2.8 mg Chl*a* m^{-3} by mid December. However, when α and μ_{max} are only increased by 2 times, the simulated SCHL reaches a mid December maximum of about 2.0 mg Chl*a* m^{-3}.

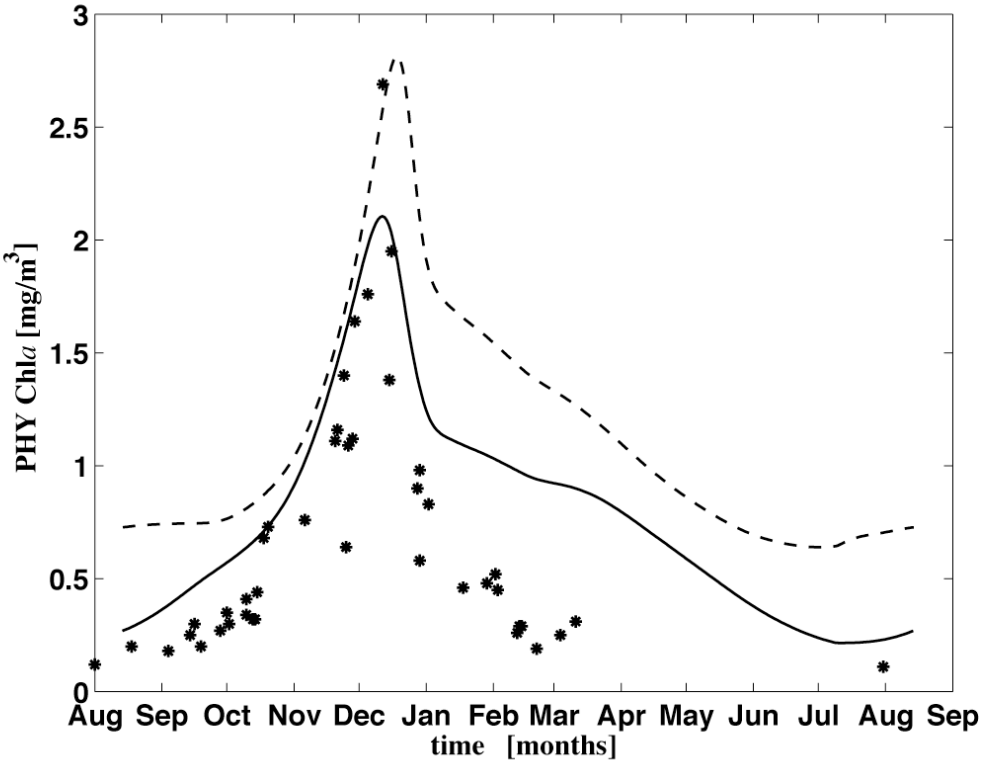

Figure 4.23: Model results of SCHL [mg Chl*a* m^{-3}] simulated with temporal variations in the photosynthetic parameters (*i.e.*, α and μ_{max}) and increased zooplankton mortality are illustrated with a dashed line. The solid line illustrates simulated SCHL considering a higher phytoplankton mortality (ε_P of 0.05 d^{-1}). The satellite-derived SCHL observations for the on-Plateau site are shown with asterisks.

An additional refinement considering the possibility of greater phytoplankton mortality is explored in Figure 4.23. By increasing the phytoplankton specific mortality term (ε_P), from 0.03 to 0.05 d^{-1}, in simulations that include the 'iron-induced' temporal variations in the phytoplankton photosynthetic performance, the

model improves its capacity to simulate the SCHL seasonal cycle. When including greater phytoplankton mortality, the model simulates the observed SCHL winter concentrations at the on-Plateau site, together with a spring SCHL bloom that peaks at about 2 mg Chl*a* m^{-3} in early December.

4.5 Discussion

The reference simulation demonstrated that the one-dimensional biogeochemical model, which was originally calibrated against observations at three time-series and process-study sites, provides a fair simulation of the annual cycle of plankton growth and decay in the HNLC waters outside the Kerguelen plateau (Fig. 4.12 - 4.13). Maximum phyto- and zooplankton concentrations as well as the annual cycle of nitrate depletion and replenishment are realistically reproduced (Fig. 4.12). However, when compared to SCHL observations over the Kerguelen plateau, the model totally fails to simulate the broad characteristics of the central plateau bloom (Fig. 4.13).

Model experiments including changes in magnitude and seasonality for the mixed layer dynamics show surprisingly low sensitivity of the surface chlorophyll concentrations. Experiments with different annual cycles of mixed layer depth indicate that the effect on the biomasses of phyto- and zooplankton is relatively unimportant (Figs 4.16 - 4.18). Even if the mixed layer never gets shallower than 100 m, plankton concentrations are only slightly reduced (Fig. 4.16).

When experimenting with an early water-column stratification, the modelled maximum chlorophyll concentration increased by only ~ 0.4 mg Chl*a* m^{-3} (Fig. 4.18). These results could be explained in part by strong biological controls (*e.g.*, grazing, growth rates), and in part by the seasonal light supply. There are ways in which these mixed layer experiments could be extended, for example combining earlier and shallower water-column stratification (assuming correspondence with the on-Plateau mixed layer regime), and relaxing the key biological controls. However, without a seasonal cycle of observations this is not likely to be rewarding, especially given the considerable structure within the bloom, which probably includes variable seasonal cycles at individual locations [*Maraldi et al.*, 2009; *Mongin et al.*, 2009].

From the sensitivity analysis and from the reference simulation, another factor emerged as a possible cause of the model and data difference at the iron-enriched zone over the Kerguelen plateau. Experiments with zooplankton mortality, *zmort*, which is the main control of zooplankton biomass (Fig. 4.15), feature a high sensitivity for a moderate range of values. While the reference simulation with *zmort* = 0.2 (mmol N^{-3})$^{-2}$ day^{-1} reveals a strong top-down control of the phytoplanktonic biomass, experiments with a higher *zmort* of 1.5 (mmol N^{-3})$^{-2}$ day^{-1} result in a relaxation of grazing pressure on the phytoplankton. Consequently, zooplankton mortality by itself does not only reduce the model-data misfit by ~ 30 % at the iron-rich reference location (Fig. 4.19), but also enhances the model's sensitivity to variations in the photosynthetic efficiency (Fig. 4.20).

The possible effects of the natural iron fertilization were investigated in a couple of experiments with enhanced photosynthetic performance. It turns out that by doubling α and μ_{max} for the entire period of the simulation, the modelled phytoplankton component reproduces surface chlorophyll values at the on-Plateau site (Fig. 4.20).

While this is true in terms of the magnitude of SCHL, the seasonal timing, duration and decay of the phytoplankton bloom were not perfect, reaching the maximal biomass approximately three weeks later and ending three months too late in comparison to the SCHL observations over the plateau. Nonetheless, accepting these differences as second-order effects, the simulation shown that approximately 70 % of the model-data difference at the on-Plateau site can be attributed to the enhanced photosynthetic parameters. Results from Chai *et al*. [2007] and Fujii *et al.* [2005] have also verified that doubling these photosynthetic parameters accounted for most of the phytoplankton response to iron enrichments in several HNLC regions.

When applying a theoretical seasonal cycle of the photosynthetic parameters α and μ_{max} (Fig. 4.21) to mimic biological iron depletion, the model captures most of the observed biogeochemical response to the natural iron-enrichment at the on-Plateau site. The modelled magnitude and timing of maximal algal biomass compares remarkably well with the satellite-derived observations (Fig. 4.22), and are similar to the model results reported by Mongin *et al.* [2008] at the same site.

However, the simulated winter values of SCHL are significantly higher than the observations (Fig. 4.22). This discrepancy between the observation and simulation is probably due to the interaction of environmental controls, that is, the limitation of processes by more than one factor such as iron and irradiance [*Boyd et al.*, 1999; 2001; *Greene et al.*, 1991]. Raven [1990] proposed an antagonistic relationship between light climate and iron supply, such that at low irradiance the algal cellular requirements for iron could increase by up to 50-fold. Sunda & Hunstman [1997] suggested that iron-light co-limitation might be particularly relevant to the deep mixed layers of the Southern Ocean. Thus its highly probable that using a higher maximum specific growth rate (to simulate the enhanced photosynthetic performances with additional iron in the model) is equivalent to reducing the effect of light limitation.

The model results with temporal changes in the photosynthetic parameterisation reproduce the observations well in terms of the bloom duration and decay, improving the model's performances when compared with simulations without temporal changes in α and μ_{max} (Fig. 4.22). Further improvement can be achieved by considering the possibility of greater phytoplankton mortality (Fig. 4.23).

The algal bloom starts in early October, reaches its maxima in early December and then rapidly decreases to SCHL values below 1.5 mg Chl*a* m^{-3} by the end of December. However, after December, the modelled SCHL appears to take several months before reaching the minimal seasonal value. In contrast, satellite observations indicate that by the end of February the phytoplankton bloom has come to an end attaining values below 0.2 mg Chl*a* m^{-3}.

This discrepancy between model and observation could be due in part to the seasonality of α and μ_{max}, and in part to factors simultaneously limiting phytoplankton processes in the Southern Ocean, such as iron/silicic acid [*Hutchins et al.*, 2001; *Leblanc et al.*, 2005; *Smetacek*, 1998]. A seasonal progression of factors controlling phytoplankton bloom dynamics in the Southern Ocean proposed by Boyd [2002] suggests that silicic acid might be limiting between January and March, which is in fact plausible since reported silicic acid concentrations during KEOPS were very low at the on-Plateau site (Fig. 4.3). The processes controlling the residence time and the bioavailability of iron might also be affecting the biological community response to changes in iron concentrations [*Bowie et al.*, 2009]. Rapid export of biomass by

processes such as aggregation could as well play a role [*Ebersbach & Trull*, 2008; *Waite et al.*, 2005].

There are also a number of aspects of the remote sensing observations that might accentuate the model-data differences. The SCHL field is far from homogenous over the plateau (Fig. 4.10), and shows higher values over regions that are suggested to receive higher iron inputs due to strong currents [*Blain et al.*, 2008b; *Maraldi et al.*, 2009; *Mongin et al.*, 2008]. Therefore, spatio-temporal variability in the iron infusion process may affect the phytoplankton response, and more importantly, it may introduce inaccuracy on the remote sensing interpretation. In addition, satellite-derived observations are often too compromised by cloud cover to capture the time-dependent internal structure within the bloom. It is also important to point out that since ocean color observations provide information only on the first 5 m of the water column, the satellite SCHL estimates fail to capture deep chlorophyll maximum (DCM) features and therefore satellite data might be underestimating SCHL concentrations.

The simulations and their evaluation have so far focused on the ability of the model to reproduce the phytoplankton biomass bloom, although the model also simulates other compartments, such as NO_3 and zooplankton (Fig. 4.24).

As shown in Fig. 4.24, achieving high algal biomass occurs with relatively small differences in zooplankton (in comparison to the HNLC simulations) but consumes large amounts of nitrate. However, during KEOPS, the observed concentrations of nitrate at the core of the bloom never went below 20 μM [*Mosseri et al.*, 2008] in surface waters (see Fig. 4.3).

This mismatch between model and observations can be explained by several factors. Firstly, the role of the large stock of ammonium, supporting diatom growth, that was observed during the KEOPS campaign [*Blain et al.*, 2008a; *Mosseri et al.*, 2008] is not taken into account by the model used in this study. It therefore can be expected that the simulated amount of nitrate (as the only source of nitrogen) consumed by the phytoplankton component results in a reduction in the concentration of nitrate in surface waters.

Secondly, the supply of nitrate to the bloom by exchange with the relatively nitrate-rich surrounding surface waters (*i.e.*, horizontal supply) that has been

estimated to be between 10 and 20% of the removed nitrate [*Jouandet et al.*, 2008], is not included in the *NPZD* simulations, underestimating the simulated nitrate concentrations in surface waters.

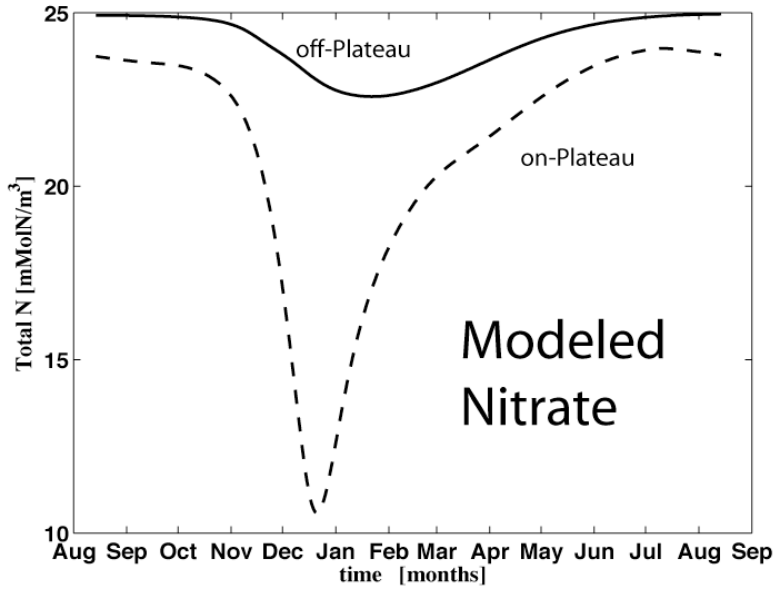
off-Plateau
on-Plateau
Modeled
Nitrate
Total N [mMolN/m3]
25
20
15
10
Aug Sep Oct Nov Dec Jan Feb Mar Apr May Jun Jul Aug Sep
time [months]

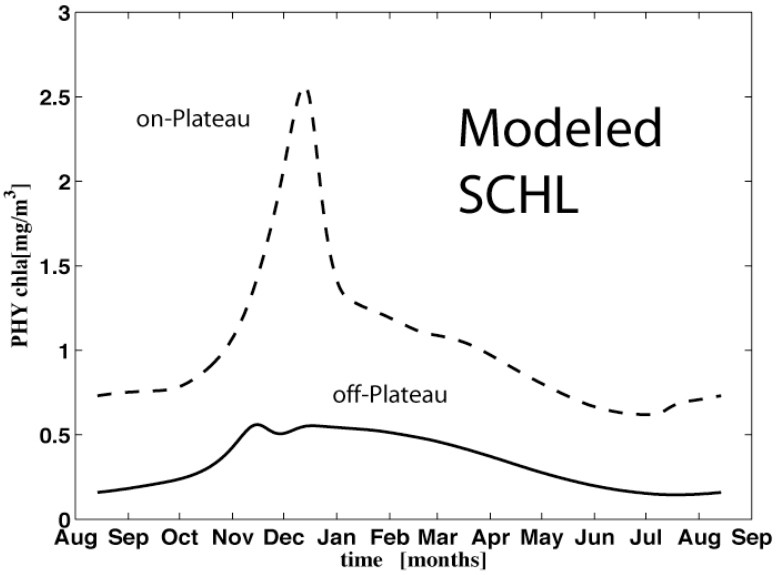
on-Plateau
Modeled
SCHL
off-Plateau
PHY chla[mg/m3]
3
2.5
2
1.5
1
0.5
0
Aug Sep Oct Nov Dec Jan Feb Mar Apr May Jun Jul Aug Sep
time [months]

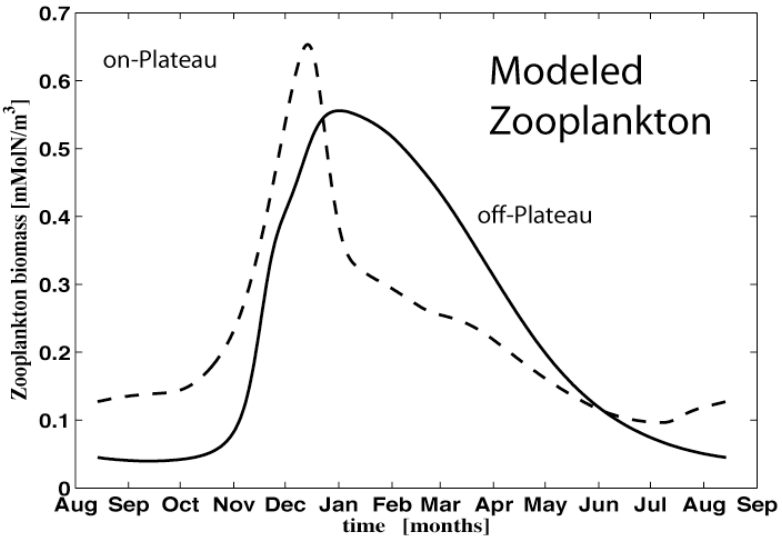
on-Plateau
Modeled
Zooplankton
off-Plateau
Zooplankton biomass [mMolN/m3]
0.7
0.6
0.5
0.4
0.3
0.2
0.1
0
Aug Sep Oct Nov Dec Jan Feb Mar Apr May Jun Jul Aug Sep
time [months]

Figure 4.24: Comparison between the modeled on- and off-Plateau results. Simulated mixed layer response of (a) phytoplankton, (b) zooplankton and (c) nitrate for the 'iron rich' and HNLC conditions are represented by the dashed and solid lines, respectively.

Explanations for the slight differences between the simulated on- and off-plateau zooplankton seasonal cycles (Fig. 4.24) are restrained by the lack of observations at different times in the season and for both contrasting sites (HNLC and iron-rich conditions).

In the *NPZD*-model used in this study the zooplankton compartment represents the herbivores biomass, and predators are only indirectly represented by the quadratic term of the zooplankton mortality. The waters of the Kerguelen Islands are considered the most fish productive areas of the Indian sector of the Southern Ocean [*Andriashev*, 1966; *Duhamel*, 1987], where the importance of zooplankton as food for the local icthyofauna has been extensively documented [*Duhamel & Hureau*, 1985; *Duhamel et al.*, 2000; *Mayzaud et al.*, 2002; *Semelkina*, 1987; *Williams & Duhamel*, 1994].

The KEOPS study clearly showed that the iron-fuelled net production of carbon over a relatively long time period (3 months) sustained a high mesozooplankton biomass [*Carlotti et al.*, 2008] and resulted in substantial export of particulate organic matter out of the mixed layer [*Ebersbach & Trull*, 2008; *Savoye et al.*, 2008]. The reported zooplankton stocks showed unambiguous differences between the off- and on-Plateau sites [*Carlotti et al.*, 2008], indicating that zooplankton growth was stimulated in the iron-rich region.

The community structure of mesozooplankton with diverse trophic groups of herbivorous and carnivorous, including crustaceans and gelatinous zooplankton, indicated a developed multi-trophic level food web within the mesozooplankton [*Carlotti et al.*, 2008] and the macrozooplankton [*Stemmann et al.*, 2008].

Considering such meso- and macrozooplankton stocks, the high quadratic mortality term imposed on the herbivore standing stock may not be in conflict with observations. Furthermore, the importance of these zooplankton stocks in the functioning of the naturally fertilized ecosystem of the Kerguelen plateau remains unclear, and our model results strongly support the views that the interplay of multiple

factors is essential to explain the results from natural or artificial iron fertilizations [*Chai et al.*, 1996; *Cullen*, 1995; *Price et al.*, 1994].

Despite the model limitations, it is hoped that the work in this chapter may provide a background to any more serious attempt to model the trophic interactions between phyto- and zooplankton, and the changes related to the environmental conditions (*e.g.*, iron availability).

4.6 Conclusions

We conclude that the 'original' model configuration, which disregards possible iron fertilization, is not able to reproduce general features of the plankton distribution over the Kerguelen plateau in the Southern Ocean. As the model gives reasonable representation of the surroundings waters dynamics, namely the occurrence of the HNLC area in the ACC, this does imply that such dynamics (or model parameterisation) alone cannot be responsible for the observed phytoplankton maximum on the plateau.

The reference simulation reveals that the four-compartment ecosystem model has a strong top-down control, such as grazing by zooplankton that is a key determinant for phytoplankton processes.

Experiments with a theoretical seasonal cycle of the photosynthetic parameters, α and μ_{max}, shown that such model modifications are enough to assess the iron influence on the plankton system, provided high trophic levels are more developed and reduce grazing.

Simply increasing α and μ_{max} by a factor of 2.5 simulated the phytoplankton bloom over the Kerguelen plateau well, especially in terms of its seasonal amplitude.

4.7 References

Andriashev, A. P. (1966), A general review of the Antarctic fish fauna, *Biological reports of the Soviet Antarctic Expedition, 1955-1958:(Rezul taty biologicheskikh issledovani Sovetsko antarkticheskoi ekspeditsii, 1955-1958)*, 343.

Armand, L. K., V. Cornet-Barthaux, J. Mosseri, et al. (2008), Late summer diatom biomass and community structure on and around the naturally iron-fertilised Kerguelen Plateau in the Southern Ocean, *Deep-Sea Research Part II: Topical Studies in Oceanography*, *55*(5-7), 653-676.

Bakker, D. C. E., Y. Bozec, P. D. Nightingale, et al. (2005), Iron and mixing affect biological carbon uptake in SOIREE and EisenEx, two Southern Ocean iron fertilisation experiments, *Deep-Sea Research Part I: Oceanographic Research Papers*, *52*(6), 1001-1019.

Blain, S., P. Treguer, S. Belviso, et al. (2001), A biogeochemical study of the island mass effect in the context of the Iron Hypothesis: Kerguelen Islands, Southern Ocean, *Deep-Sea Research I*, *48*, 163-187.

Blain, S., P. N. Sedwick, F. B. Griffiths, et al. (2002), Quantification of algal iron requirements in the Subantarctic Southern Ocean (Indian Sector), *Deep-Sea Research II*, *49*, 3255-3273.

Blain, S., B. Quéguiner, L. Armand, et al. (2007), Impacts of natural iron fertilisation on the Southern Ocean, *Nature*, *446*, 1070-1074, doi:1010.1038/nature05700.

Blain, S., B. Queguiner, and T. W. Trull (2008a), The natural iron fertilization experiment KEOPS (Kerguelen Ocean and Plateau compared Study): an overview, *Deep Sea Research II*, *55*(5-7), 559-565.

Blain, S., G. Sarthou, and Laan.P. (2008b), Distribution of dissolved iron during the natural iron fertilisation experiment KEOPS (Kerguelen Island, Southern Ocean) . *Deep Sea Research II*, *55*(5-7), 594-605.

Bowie, A. R., M. T. Maldonado, R. D. Frew, et al. (2001), The fate of added iron during a mesoscale fertilisation experiment in the polar Southern Ocean, *Deep Sea Research (Part II, Topical Studies in Oceanography)*, *48*, 2703-2743.

Bowie, A. R., D. Lannuzel, T. A. Remenyi, et al. (2009), Biogeochemical iron budgets of the Southern Ocean south of Australia: Decoupling of iron and nutrient cycles in the subantarctic zone by the summertime supply, *Global Biogeochem. Cycles*, *23*.

Bowie, G. L., W. B. Mills, D. B. Porcella, et al. (1985), Rates, constants, and kinetics formulations in surface water quality modeling, *Env. Res. Lab., USEPA, EPA/600/3-85/040. Athens, GA*.

Boyd, P., J. LaRoche, M. Gall, et al. (1999), Role of iron, light, and silicate in controlling algal biomass in subantarctic waters SE of New Zealand, *Journal of Geophysical Research*, *104*(C6), 13395-13408.

Boyd, P., A. Watson, C. S. Law, et al. (2000), A mesoscale phytoplankton bloom in the polar Southern Ocean stimulated by iron fertilization, *Nature*, *407*, 695-702.

Boyd, P. W., A. C. Crossley, G. R. DiTullio, et al. (2001), Control of phytoplankton growth by iron supply and irradiance in the subantarctic Southern Ocean: Experimental results from the SAZ Project, *Journal of Geophysical Research*, *106*(C12), 31573-31584.

Boyd, P. W. (2002), Environmental factors controlling phytoplankton processes in the Southern Ocean, *Journal of Phycology*, *38*(5), 844-861.

Boyd, P. W., T. Jickells, C. S. Law, et al. (2007), Mesoscale Iron Enrichment Experiments 1993-2005: Synthesis and Future Directions, *Science*, *315*(5812), 612-617, DOI: 610.1126/science.1131669.

Brzezinski, M. A., D. M. Nelson, V. M. Franck, et al. (2001), Silicon dynamics within an intense open-ocean diatom bloom in the Pacific sector of the Southern Ocean, *Deep-Sea Research Part II: Topical Studies in Oceanography*, *48*(19-20), 3997-4018.

Carlotti, F., D. Thibault-Botha, A. Nowaczyk, et al. (2008), Zooplankton community structure, biomass and role in carbon fluxes during the second half of a phytoplankton bloom in the Eastern sector of the Kerguelen shelf (January - February 2005), *Deep Sea Research II*, *55*(5-7), 720-733.

Chai, F., S. T. Lindley, and R. T. Barber (1996), Origin and maintenance of a high nitrate condition in the equatorial Pacific, *Deep Sea Research Part II: Topical Studies in Oceanography*, *43*(4-6), 1031-1064.

Chai, F., M. S. Jiang, Y. Chao, et al. (2007), Modeling responses of diatom productivity and biogenic silica export to iron enrichment in the equatorial Pacific Ocean, *Global Biogeochemical Cycles*, *21*(3).

Chavez, F. P., K. R. Buck, K. H. Coale, et al. (1991), Growth Rates, Grazing, Sinking, and Iron Limitation of Equatorial Pacific Phytoplankton, *Limnology and Oceanography*, *36*(8), 1816-1833.

Coale, K. H., K. S. Johnson, F. P. Chavez, et al. (2004), Southern Ocean iron enrichment experiment: carbon cycling in high and low-Si waters, *Science*, *304*, 408-414.

Comiso, J. C., C. R. McClain, C. W. Sullivan, et al. (1993), Coastal zone color scanner pigment concentrations in the Southern Ocean and relationships to geophysical surface features, *Journal of Geophysical Research*, *98*, 2419-2451.

Cullen, J. J. (1991), Hypotheses to Explain High-Nutrient Conditions in the Open Sea, *Limnology and Oceanography*, *36*(8), 1578-1599.

Cullen, J. J. (1995), Status of the iron hypothesis after the Open-Ocean Enrichment Experiment, *Limnology and Oceanography*, *40*(7), 1336-1343.

Denman, K. L., and M. A. Peña (1999), A coupled 1-D biological/physical model of the northeast subarctic Pacific Ocean with iron limitation, *Deep-Sea Research Part II: Topical Studies in Oceanography*, *46*(11-12), 2877-2908.

Dugdale, R. C., and F. P. Wilkerson (1991), Low Specific Nitrate Uptake Rate: A Common Feature of High-Nutrient, Low-Chlorophyll Marine Ecosystems, *Limnology and Oceanography*, *36*(8), 1678-1688.

Duhamel, G., and J. C. Hureau (1985), The role of zooplankton in the diets of certain Sub-Antarctic marine fish.

Duhamel, G., P. Koubbi, and C. Ravier (2000), Day and night mesopelagic fish assemblages off the Kerguelen Islands (Southern Ocean), *Polar Biology*, *23*(2), 106-112.

Duhamel, G. U. Y. (1987), Distribution and abundance of fish on the Kerguelen Islands shelf, Dept. of Vertebrate Zoology, Swedish Museum of Natural History.

Ebersbach, F., and T. W. Trull (2008), Sinking particle properties from polyacrylamide gels during the KErguelen Ocean and Plateau compared Study (KEOPS): Zooplankton control of carbon export in an area of persistent

natural iron inputs in the Southern Ocean, *Limnology and Oceanography*, *53*, 212-224.

Edwards, A. M., and J. Brindley (1999), Zooplankton mortality and the dynamical behaviour of plankton population models, *Bulletin of Mathematical Biology*, *61*(2), 303-339.

Edwards, A. M., and A. Yool (2000), The role of higher predation in plankton population models, *Journal of Plankton Research*, *22*(6), 1085-1112.

Ellwood, M. J., P. W. Boyd, and P. Sutton (2008), Winter-time dissolved iron and nutrient distributions in the Subantarctic Zone from 40-52S; 155-160E, *Geophysical Research Letters*, *35*(11).

Fennel, K., M. R. Abbott, Y. H. Spitz, et al. (2003), Modeling controls of phytoplankton production in the southwest Pacific sector of the Southern Ocean, *Deep-Sea Research Part II: Topical Studies in Oceanography*, *50*(3-4), 769-798.

Figueiras, F. G., B. Arbones, and M. Estrada (1999), Implications of bio-optical modeling of phytoplankton photosynthesis in Antarctic waters: Further evidence of no light limitation in the Bransfield Strait, *Limnology and Oceanography*, *44*(7), 1599-1608.

Franck, V. M., M. A. Brzezinski, K. H. Coale, et al. (2000), Iron and silicic acid concentrations regulate Si uptake north and south of the Polar Frontal Zone in the Pacific Sector of the Southern Ocean, *Deep Sea Research Part II: Topical Studies in Oceanography*, *47*(15-16), 3315-3338.

Frey, F. A., M. F. Coffin, P. J. Wallace, et al. (2000), Origin and evolution of a submarine large igneous province: The Kerguelen Plateau and Broken Ridge, southern Indian Ocean, *Earth & Planetary Science Letters*, *176*(1), 73-89.

Frost, B. (1991), The role of grazing in nutrient-rich areas of the open sea, *Limnology and Oceanography*, *36*, 1834-1850.

Fujii, M., N. Yoshie, Y. Yamanaka, et al. (2005), Simulated biogeochemical responses to iron enrichments in three high nutrient, low chlorophyll (HNLC) regions, *Progress in Oceanography*, *64*(2-4), 307-324.

Geider, R. J., H. L. McIntyre, and T. M. Kana (1998), A dynamic regulatory model of phytoplankton acclimation to light, nutrients and temperature, *Limnology and Oceanography*, *43*, 679-694.

Greene, R. M., R. J. Geider, and P. G. Falkowski (1991), Effect of Iron Limitation on Photosynthesis in a Marine Diatom, *Limnology and Oceanography*, *36*(8), 1772-1782.

Hall, J., K. Safi, and A. Cumming (2004), Role of microzooplankton grazers in the subtropical and subantarctic waters to the east of New Zealand, *New Zealand Journal of Marine and Freshwater Research*, *38*(1), 91-101.

Hall, J. A., and K. Safi (2001), The impact of in situ Fe fertilisation on the microbial food web in the Southern Ocean, *Deep-Sea Research Part II*, *48*(11-12), 2591-2613.

Hannon, E., P. W. Boyd, M. Silvoso, et al. (2001), Modeling the bloom evolution and carbon flows during SOIREE: Implications for future in situ iron-enrichments in the Southern Ocean, *Deep-Sea Research Part II: Topical Studies in Oceanography*, *48*(11-12), 2745-2773.

Hense, I., U. V. Bathmann, and R. Timmermann (2000), Plankton dynamics in frontal systems of the Southern Ocean, *Journal of Marine Systems*, *27*(1-3), 235-252.

Hutchins, D. A., P. N. Sedwick, G. R. DiTullio, et al. (2001), Control of phytoplankton growth by iron and silicic acid availability in the subantarctic

Southern Ocean: Experimental results from the SAZ Project, *J. Geophys. Res*, *106*, 31,559ñ531,572.

Jerlov, N. G. (1976), *Marine optics*, xiii, 231 pp., Elsevier Scientific Pub. Co., Amsterdam ; New York.

Jouandet, M. P., S. Blain, N. Metzl, et al. (2008), A seasonal carbon budget for a naturally iron fertilized bloom over the Kerguelen plateau in the Southern Ocean., *Deep Sea Research II*, *55*(5-7), 856-867.

Kirk, J. T. O. (1994), *Light and photosynthesis in aquatic ecosystems*, xvi, 509 pp., Cambridge University Press, Cambridge England.

Lancelot, C., E. Hannon, S. Becquevort, et al. (2000), Modeling phytoplankton blooms and carbon export production in the Southern Ocean: dominant controls by light and iron in the Atlantic sector in Austral spring 1992, *Deep Sea Research-Part I-Oceanographic Research Papers*, *47*(9), 1621-1662.

Landry, M. R., M. E. Ondrusek, S. J. Tanner, et al. (2000), Biological response to iron fertilization in the eastern equatorial Pacific (IronEx II). I. Microplankton community abundances and biomass, *Marine Ecology Progress Series*, *201*, 27-42.

Le Quéré, C., C. Rödenbeck, E. T. Buitenhuis, et al. (2007), Saturation of the Southern ocean CO2 sink due to recent climate change, *Science*, *316*, DOI:10.1126/science.1136188, 1131735-1131738.

Leblanc, K., C. E. Hare, P. W. Boyd, et al. (2005), Fe and Zn effects on the Si cycle and diatom community structure in two contrasting high and low-silicate HNLC areas, *Deep Sea Research Part I: Oceanographic Research Papers*, *52*(10), 1842-1864.

Lefèvre, D., C. Guigue, and I. Obernosterer (2008), The metabolic balance at two contrasting sites in the Southern Ocean: The iron-fertilized Kerguelen area and HNLC waters, *Deep-Sea Research Part II: Topical Studies in Oceanography*, *55*(5-7), 766-776.

Lindley, S. T., R. R. Bidigare, and R. T. Barber (1995), Phytoplankton photosynthesis parameters along 140 W in the equatorial Pacific, *Deep Sea Research Part II: Topical Studies in Oceanography*, *42*(2-3), 441-463.

Lindley, S. T., and R. T. Barber (1998), Phytoplankton response to natural and experimental iron addition, *Deep-Sea Research Part II*, *45*(6), 1135-1150.

Loscher, B. M., H. J. W. De Baar, J. T. M. De Jong, et al. (1997), The distribution of Fe in the Antarctic circumpolar current, *Deep Sea Research Part II: Topical Studies in Oceanography*, *44*(1-2), 143-187.

Lourey, M. J., and T. W. Trull (2001), Seasonal nutrient depletion and carbon export in the Subantarctic and Polar Frontal Zones of the Southern Ocean south of Australia, *Journal of Geophysical Research. C. Oceans*, *106*(C12), 31463-31488.

Maraldi, C., M. Mongin, R. Coleman, et al. (2009), The influence of lateral mixing on a phytoplankton bloom: Distribution in the Kerguelen Plateau region, *Deep Sea Research Part I: Oceanographic Research Papers*, *56*(6), 963-973.

Martin, J. H., and S. E. Fitzwater (1988), Iron deficiency limits phytoplankton growth in the north-east pacific subarctic, *Nature*, *331*(6154), 341-343.

Martin, J. H. (1990a), Glacial-interglacial CO_2 change: The iron hypothesis, *Paleoceanography*, *5*, 1-13.

Martin, J. H., R. M. Gordon, and S. E. Fitzwater (1990b), Iron in Antarctic waters, *Nature*, *345*, 156-158.

Mayzaud, P., V. Tirelli, A. Errhif, et al. (2002), Carbon intake by zooplankton: Importance and role of zooplankton grazing in the Indian sector of the Southern Ocean, *Deep Sea Research II*, *49*(16), 3169-3188.

Metzl, N., B. Tilbrook, and A. Poisson (1999), The annual fCO_2 cycle and the air-sea CO_2 flux in the sub-Antarctic ocean, *Tellus*, *51B*, 849-861.

Mitchell, B. G., E. A. Brody, O. Holm-Hansen, et al. (1991), Light Limitation of Phytoplankton Biomass and Macronutrient Utilization in the Southern Ocean, *Limnology and Oceanography*, *36*(8), 1662-1677.

Mongin, M., E. Molina, and T. W. Trull (2008), Seasonality and scale of the Kerguelen plateau phytoplankton bloom: A remote sensing and modeling analysis of the influence of natural iron fertilization in the Southern Ocean, *Deep Sea Research Part II: Topical Studies in Oceanography*, *55*(5-7), 880-892.

Mongin, M. M., E. R. Abraham, and T. W. Trull (2009), Winter advection of iron can explain the summer phytoplankton bloom that extends 1000 km downstream of the Kerguelen Plateau in the Southern Ocean, *Journal of Marine Research*, *67*(2), 225-237.

Moore, J. K., and M. R. Abbott (2000), Phytoplankton chlorophyll distributions and primary production in the Southern Ocean, *Journal of Geophysical Research*, *105*(C12), 28,709 –728,722.

Moore, J. K., and M. R. Abbott (2002), Surface chlorophyll concentrations in relation to the Antarctic Polar Front: seasonal and spatial patterns from satellite observations, *Journal of Marine Systems*, *37*, 69-86.

Morel, F. M. M., J. G. Reuter, and N. M. Price (1991), Iron nutrition of phytoplankton and its possible importance in the ecology of ocean regions with high nutrient and low biomass, *Oceanography*, *4*, 56-61.

Mosseri, J., B. Quéguiner, L. Armand, et al. (2008), Impact of iron on silicon utilization by diatoms in the Southern Ocean: a case study of the Si/N cycle decoupling in a naturally iron-enriched area, *Deep Sea Research II*, *55*(5-7), 801-819.

Obernosterer, I., U. Christaki, D. Lef√®vre, et al. (2008), Rapid bacterial mineralization of organic carbon produced during a phytoplankton bloom induced by natural iron fertilization in the Southern Ocean, *Deep-Sea Research Part II: Topical Studies in Oceanography*, *55*(5-7), 777-789.

Oschlies, A., and V. Garçon (1999), An eddy-permitting coupled physical-biological model of the North Atlantic. 1. Sensitivity to advection numerics and mixed layer physics, *Global Biogeochemical Cycles*, *13*(1), 135-160.

Park, Y.-H., J.-L. Fuda, I. Durand, et al. (2008a), Internal tides and vertical mixing over the Kerguelen Plateau, *Deep Sea Research II*, *55*(5-7), 582-593.

Park, Y.-H., F. Roquet, J.-L. Fuda, et al. (2008b), Large-scale circulation over and around the Northern Kerguelen Plateau, *Deep Sea Research II*, *55*(5-7), 566-581.

Pitchford, J. W., and J. Brindley (1999), Iron limitation, grazing pressure and oceanic high nutrient-low chlorophyll (HNLC) regions, *Journal of Plankton Research*, *21*(3), 525-547.

Pollard, R. T., M. I. Lucas, and J. F. Read (2002), Physical controls on biogeochemical zonation in the Southern Ocean, *Deep Sea Research II*, *49*(16), 3289-3305.

Pondaven, P., D. Ruiz-Pino, C. Fravalo, et al. (2000), Interannual variability of Si and N cycles at the time-series station KERFIX between 1990 and 1995 - A 1-D modelling study, *Deep-Sea Research I*, *47*(2), 223-257.

Price, N. M., B. A. Ahner, and F. M. M. Morel (1994), The equatorial Pacific Ocean: Grazer-controlled phytoplankton populations in an iron-limited ecosystem, *Limnology and Oceanography*, *39*(3), 520-534.

Raven, J. A. (1990), Predictions of Mn and Fe use efficiencies of phototrophic growth as a function of light availability for growth and C assimilation pathway, *New Phytology*, *116*, 1-17.

Rintoul, S. R., and T. W. Trull (2001), Seasonal evolution of the mixed layer in the Subantarctic Zone south of Australia, *Journal of Geophysical Research. C. Oceans*, *106*(C12), 31447-31462.

Roquet, F., Y. H. Park, C. Guinet, et al. (2009), Observations of the Fawn Trough Current over the Kerguelen Plateau from instrumented elephant seals, *Journal of Marine Systems*, *78*(3), 377-393.

Savoye, N., T. W. Trull, S. H. M. Jacquet, et al. (2008), ^{234}Th-based export fluxes during a natural iron fertilization experiment in the Southern Ocean (KEOPS), *Deep Sea Research II*, *55*(5-7), 841-855.

Schartau, M., and A. Oschlies (2003a), Simultaneous data-based optimization of a 1D-ecosystem model at three locations in the North Atlantic: Part I-Method and parameter estimates, *Journal of Marine Research*, *61*(6), 765-793.

Semelkina, A. N. (1987), Development of the zooplankton in the Kerguelen Islands region in the years 1987-1988, *Rapports des campagnes ‡ la mer: Campagnes SKALP*, 93ñ01.

Smetacek, V. (1998), Diatoms and the silicate factor, *Nature*, *391*, 224-225.

Sokolov, S., and S. R. Rintoul (2007b), On the relationship between fronts of the Antarctic Circumpolar Current and surface chlorophyll concentrations in the Southern Ocean, *J. Geophys. Res. – Oceans*, *112*(C07030), doi: 10.1029/2006JC004072.

Sokolov, S. (2008), Chlorophyll blooms in the Antarctic Zone south of Australia and New Zealand in reference to the Antarctic Circumpolar Current fronts and sea ice forcing, *Journal of Geophysical Research. C. Oceans*, *113*(3).

Steele, J. H., and E. W. Henderson (1992), The role of predation in plankton models, *Journal of Plankton Research*, *14*(1), 157-172.

Stemmann, L., M. Youngbluth, K. Robert, et al. (2008), Global zoogeography of fragile macrozooplankton in the upper 100-1000 m inferred from the underwater video profiler, *ICES Journal of Marine Science*.

Strass, V., B. Cisewski, S. Gonzales, et al. (2005), The physical setting of the European Iron Fertilization Experiment EIFEX in the Southern Ocean, *Rep. Polar Mar. Res*, *500*, 15ñ49.

Sullivan, C. W., K. R. Arrigo, C. R. McClain, et al. (1993), Distributions of phytoplankton blooms in the Southern Ocean, *Science*, *262*(5141), 1832-1837.

Sunda, W. G., and S. A. Huntsman (1997), Interrelated influence of iron, light and cell size on marine phytoplankton growth, *Nature*, *390*, 389-392.

Takahashi, T., S. C. Sutherland, C. Sweeney, et al. (2002), Global sea-air CO2 flux based on climatological surface ocean pCO2, and seasonal biological and temperature effects, *Deep Sea Research (Part II, Topical Studies in Oceanography)*, *49*(9-10), 1601-1622.

Timmermans, K. R., W. Stolte, and H. J. W. de Baar (2004), Iron-mediated effects on nitrate reductase in marine phytoplankton, *Marine Biology*, *121*(2), 389-396, 310.1007/BF00346749.

Trull, T. W., S. R. Rintoul, M. Hadfield, et al. (2001a), Circulation and seasonal evolution of Polar waters south of Australia: Implications for iron fertilisation of the Southern Ocean, *Deep Sea Research (Part II, Topical Studies in Oceanography)*, *48*(11/12), 2439-2466.

Trull, T. W., D. Davies, and K. Casciotti (2008a), Insights into nutrient assimilation and export in naturally iron-fertilized waters of the Southern Ocean from nitrogen, carbon and oxygen isotopes, *Deep Sea Research Part II: Topical Studies in Oceanography*, *55*(5-7), 820-840.

Trull, T. W., D. Davies, and K. Casciotti (2008b), Insights into nutrient assimilation and export in naturally iron-fertilized waters of the Southern Ocean from nitrogen, carbon, and oxygen isotopes., *Deep Sea Research II*, *55*(5-7), 820-840, doi:810.1016/j.dsr1012.2007.1012.1035.

Tsuda, A., S. Takeda, H. Saito, et al. (2007), Evidence for the grazing hypothesis: Grazing reduces phytoplankton responses of the HNLC ecosystem to iron enrichment in the western subarctic pacific (SEEDS II), *Journal of Oceanography*, *63*(6), 983-994.

Tyrrell, T., A. Merico, J. J. Waniek, et al. (2005), Effect of seafloor depth on phytoplankton blooms in high-nitrate, low-chlorophyll (HNLC) regions, *J. Geophys. Res.*, *110*.

Uitz, J., H. Claustre, F. B. Griffiths, et al. (2009), A phytoplankton class-specific primary production model applied to the Kerguelen Islands region (Southern Ocean), *Deep-Sea Research Part I: Oceanographic Research Papers*, *56*, 541-560.

van Leeuwe, M. A., and J. Stefels (2007), Photosynthetic responses in Phaeocystis antarctica towards varying light and iron conditions, *Biogeochemistry*, *83*(1), 61-70.

Waite, A. M., O. Gustafsson, O. Lindahl, et al. (2005), Linking ecosystem dynamics and biogeochemistry: Sinking fractionation of organic carbon in a Swedish fjord, *Limnology and Oceanography*, *50*(2), 658-671.

Wang, X., R. J. Matear, and T. W. Trull (2003), Nutrient utilization ratios in the Polar Frontal Zone in the Australian sector of the Southern Ocean: a model, *Global Biogeochemical Cycles*, *17*(1), 1009, doi:1010.1029/2002GB001938.

Williams, R., and G. Duhamel (1994), Studies of fish of the Indian Ocean sector of the Southern Ocean during the BIOMASS Programme, *Southern Ocean ecology-the BIOMASS perspective*, 211-229.

CHAPTER FIVE

Seasonality of the ecosystem response to iron stimulation in the Southern Ocean

5.1 Abstract

Mesoscale iron enrichment experiments and studies of natural iron inputs, in high nitrate low chlorophyll (HNLC) ocean waters have demonstrated that iron limitation is widespread and affects air-sea fluxes of atmospheric carbon dioxide and thus global climate. Of the HNLC regions, the Southern Ocean plays the greatest role in the global carbon cycle, and the dominant controls on net algal production remain controversial. Although broad ecosystem responses among mesoscale iron enrichment experiments are similar in different oceanic regions, the biomass generated and carbon dioxide drawdown at the surface differ substantially. Here a biogeochemical model is used to investigate the effect of iron on phytoplankton growth in response to different iron-enrichment simulations in the Australasian-Pacific sector of the Southern Ocean. While the ecosystem model represents a simple approximation of the complex lower trophic ecosystems of this region, simulated chlorophyll concentrations reproduce the main characteristics of the first Southern Ocean Iron Release Experiment (SOIREE), and surrounding HNLC environment. Further runs with the same iron addition treatment differed dramatically according to location and time of the year of the simulated iron infusions. The magnitude of the iron-induced biogeochemical responses in the surface water, such as maximum chlorophyll concentration, is strongly controlled by both light and grazing pressure, and shows highest values during the early spring infusions. In contrast, the highest POC export estimates are observed during the summer infusions. These findings suggest that not only light limitation but also the overwintering biomass of phytoplankton and its principle grazers are crucial factors in the response of phytoplankton community to iron enrichment.

5.2 Introduction

In high-nutrient, low-chlorophyll (HNLC) regions, iron limitation and its effect on phytoplankton growth and carbon export are well recognized [*Cullen*, 1991; *Martin & Fitzwater*, 1988; *Martin*, 1990a]. Several mesoscale iron fertilization experiments [*Boyd et al.*, 2007] and natural iron enrichments associated with island formations [*Blain et al.*, 2007; *Pollard et al.*, 2007] confirmed low dissolved iron concentrations (sub-nanomolar) are the main factor in limiting phytoplankton processes in these regions.

These mesoscale experiments generally match the results of deckboard, bottle incubations experiments that also show intensified diatom growth with increased iron availability [*Boyd et al.*, 1996; *Timmermans et al.*, 2001]. However, the observed responses of the phytoplankton communities were dramatically different among these iron enrichment experiments in the HNLC regions [*Boyd et al.*, 2007; *de Baar et al.*, 2005; *Fujii et al.*, 2005].

For instance, the iron induced maximum surface chlorophyll and decrease of surface carbon dioxide partial pressure (pCO_2) were as large as 19 mg m^{-3} and 94 μatm at SEEDS (the subartic Pacific Iron Experiment for Ecosystem Dynamics Study) in the subarctic western North Pacific [*Tsuda et al.*, 2007], but as small as 2 mg m^{-3} and 20 to 30 μatm at SOIREE (Southern Ocean Iron Release Experiment) [*Boyd et al.*, 2000] and EisenEx (the Carbondioxide Uptake Southern Ocean/Eisen Experiment) [*Bakker et al.*, 2005].

Through the comparison of eight iron experiments, de Baar *et al.* [2005] showed that the iron-induced maximum chlorophyll, the maximum DIC removal, and the overall DIC/Fe efficiency all scale inversely with the mixed layer depth (*MLD*), a proxy for the average light level for phytoplankton growth in the surface layer. Lateral mixing, sea-surface irradiance, temperature, and grazing play additional roles.

Unlike bottle incubations, replication of the complex and logistically demanding in situ Fe enrichment experiments at the same location is a challenging task. Applying a marine ecosystem model to the SOIREE site is thus a useful means to study the ecosystem response to iron addition, in timescales ranging from seasonal to

interannual, as well as to evaluate the robustness of the simulated fields to ecosystem model parameterization and surface forcing.

The HNLC waters of the Southern Ocean merit particular attention not only because of the extensive uptake of CO_2 and intensive exchange with the atmosphere [*Metzl et al.*, 1999; *Takahashi et al.*, 2002], but also because it is a region of intermediate and deep water formation [*Sloyan & Rintoul*, 2001] that replenishes the nutrient supply to global ocean surface waters [*Sarmiento et al.*, 2004].

Multiple factors impact the seasonal cycle of phytoplankton growth in vast regions of the Southern Ocean [*Boyd et al.*, 1999; *Fennel et al.*, 2003; *Hutchins et al.*; *Mayzaud et al.*, 2002; *Mitchell et al.*, 1991], with light limitation dominating during early spring followed by iron limitation after the onset of water column stratification. During the austral summer diatom growth may become silicon limited, particularly in subantarctic waters [*Franck et al.*, 2000; *Mosseri et al.*, 2008]. The deep mixed layers of the Southern Ocean also result in co-limitation by iron and light, such that under lower light levels, the phytoplankton cellular requirement for iron increases [*Boyd*, 2002; *Sunda & Huntsman*, 1997].

SOIREE was conducted over 13 days in austral summer of 1999 in polar waters south of Australia (61°S, 140°E; see Fig. 5.1), and involved fertilizing surface waters on days 1, 3, 5 and 7 [*Boyd et al.*, 2000]. Trull *et al.* [2001a] reported on the seasonal evolution of the water column properties at the SOIREE site, where high nutrient concentrations throughout the year and moderate mixed-layer depths (as shown in Fig. 5.2) are observed.

A strong seasonal thermocline, mainly driven by warming during summer, was observed along with a summer nitrate reduction of ~ 15% of its winter value within the mixed layer. Cooling and convective mixed layer deepening started in late summer, and silicic acid and nitrate (and phosphate) concentrations remained high in the mixed layer despite considerable seasonal depletion. Surface iron concentrations at the SOIREE site were very low (< 0.1 nM) [*Bowie et al.*, 2001], and sub-optimal values of photosynthetic competence confirmed that the phytoplankton community was iron-stressed [*Boyd et al.*, 2000]. Furthermore, the region shows very low chlorophyll *a* concentrations (< 0.6 mg m^{-3}) throughout the year [*Sokolov*, 2008].

The addition of iron over an area of about 55 km^2 increased concentrations of dissolved iron to ~3 nM, and subsequently enhanced phytoplankton stocks and production [*Bowie et al.*, 2001]. A fivefold increase in chlorophyll *a* concentrations, reaching up to ~ 1.5 mg m^{-3}, was observed by the end of the site occupation. This iron-induced bloom was dominated by diatoms [*Gall et al.*, 2001] and resulted in a significant reduction of both dissolved nutrient concentrations and pCO_2 [*Bakker et al.*, 2001].

Although the SOIREE results confirmed that iron supply controls phytoplankton growth and community composition at this site in summer, a subsequent iron-mediated enhancement of downward particulate organic carbon (POC) export was not observed [*Nodder et al.*, 2001; *Trull & Armand*, 2001b]. The fate of the accumulated algal carbon remains unknown, and is suggested to depend on the interplay between the export mechanisms, remineralisation and water mass subduction [*Boyd et al.*, 2000]. Aumont & Bopp [2006] succeed in simulating the main features of SOIREE with a more complex iron-containing 3d ecosystem model (i.e. PISCES), but did not expand their simulations into other regions of the Southern Ocean.

The purpose of the present study is to examine, using numerical simulations with implicit iron limitation, the regional ecosystem dynamics of the Australasian-Pacific sector of the Southern Ocean (Fig. 5.1) in response to iron-induced changes in algal physiology at both different locations and times of the year. The simulations focus on the interactions between phytoplankton, light, iron limitation and grazing.

We apply the biogeochemical model to 25 iron-infusion experimental sites (Fig. 5.1) along 140°E, with 26 iron-fertilization events simulated at each site (*i.e.*, once per fortnight). Comparison of model results among these sites enables us to identify how differences in both physical environment and plankton physiology affect biogeochemical response to iron-induced changes in alpha and μmax. The relative simplicity (*i.e.*, four components *NPZD*) of the ecosystem model provides an ideal configuration to perform simulations with different physical environmental conditions.

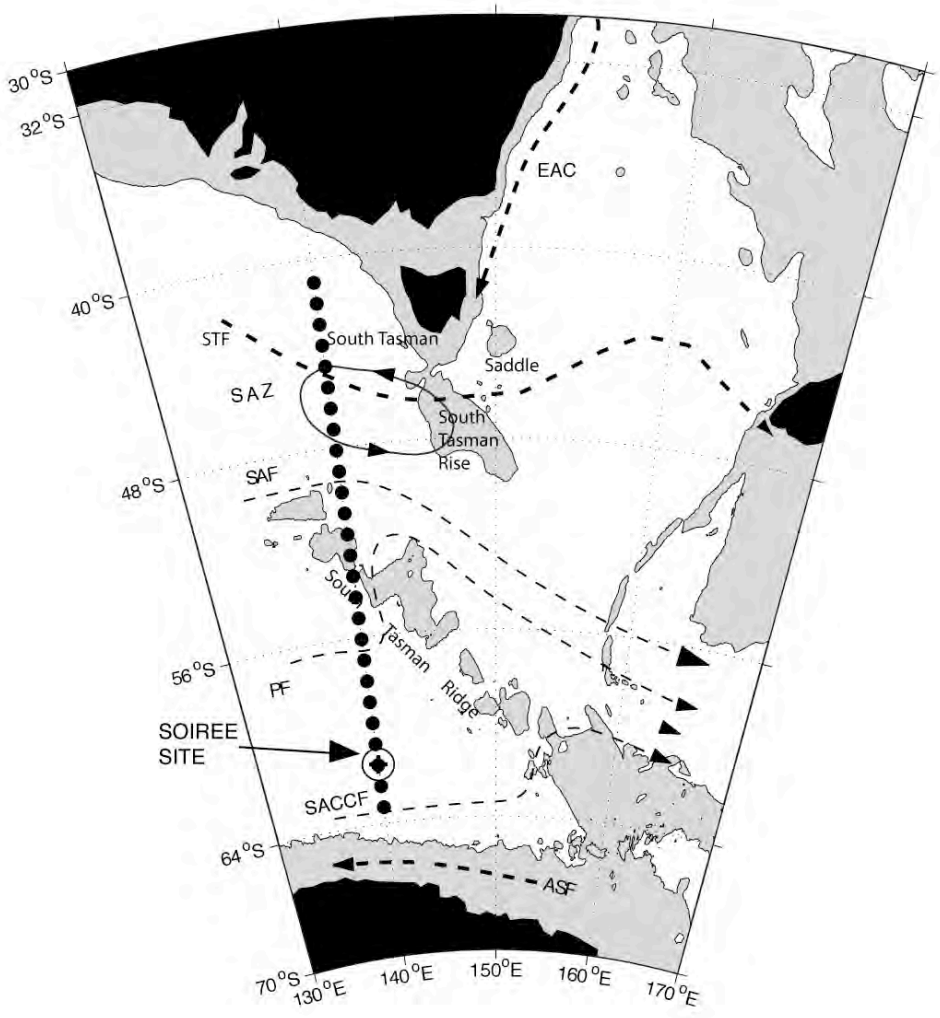

Figure 5.1: Map showing the experimental sites (black dots), the SOIRRE study site, and a summary of the main features for the regional circulation south of Australia. EAC, extension of East Australian Current; STF, Subtropical Front; SAF, Subantarctic Front; PF, Polar Front; SACCF, southern ACC front; ASF, Antarctic Slope Front. Bathymetry higher than 2000 m appears as shaded contours. Modified from [*Herraiz-Borreguero & Rich Rintoul*, 2011].

In the following section 5.4, the lower trophic ecosystem model and the experimental design with changes in the photosynthetic performance and physical forcing are described. The results based on variations of SOIREE and further simulations that implemented different meteorological forcing (*i.e.*, mixed layer depth, sea-surface irradiance and temperature) for the corresponding different locations are discussed in Section 5.4, along with their implications for purposeful mesoscale iron fertilization. A summary is provided in Section 5.5.

5.3 Model description and experimental design

An *NPZD* model [*Oschlies & Garçon*, 1999], which has been recently applied to explore the influence of natural iron fertilization around the Kerguelen-Heard Island region (see Chapter 4), was used to express the basic pelagic ecological processes in the Australian sector of the Southern Ocean. In the model, the four components (dissolved inorganic nitrogen concentration (*N*); phytoplankton biomass (*P*); zooplankton biomass (*Z*); and detritus (*D*)) are expressed in terms of nitrogen concentration.

The processes incorporated in the governing equations (Table 5.1) include autotrophic growth of phytoplankton controlled by light and a single macro-nutrient (nitrate). Uptake of nitrogen by phytoplankton during the growth process is represented via Michaelis-Menten formulation, and grazing by zooplankton upon phytoplankton with a Holling type III formulation. The model also allows for inefficient grazing by zooplankton upon phytoplankton through a “feeding efficiency” constant. Natural loss processes (*i.e.*, mortality) are linear in *P* for phytoplankton and quadratic in *Z* for zooplankton, and remineralisation of detritus is also linear in *D*. Values for the parameters of the *NPZD* model are listed in Table 5.2.

The differential equations describing the ecosystem model are solved using a fourth-order Runge-Kutta algorithm. A 2-year spinup cycle is performed to ensure that the model achieved a steady state independent of the initial condition. The model is forced by annual cycles of the mixed layer depth, solar radiation and sea surface temperature (SST). All biological source and sink terms (*e.g.*, phytoplankton growth, zooplankton grazing) are computed at every time step. Winter initial conditions for

nitrate are derived from oceanographic data from the Australian Southern Ocean WOCE Hydrographic Program, along the approximately 140°E SR3 meridian [*Rintoul & Trull*, 2001]. Initial conditions for phytoplankton, zooplankton, and detritus are set to small values (0.01 mmol N m^{-3}).

To simulate the effects of iron enrichment, the values of μmax [day^{-1}] and α [W^{-1} m^2 day^{-1}] for phytoplankton were set to step increase from day 1 (the date on which the iron is infused into the surface waters), kept at the maximum (two and a half times higher than the initial values; see Table 5.2) until day 14, and then set to decrease to the initial values. Similar procedures have also been used in previous modelling studies to investigate the effect and impact of iron fertilization on phytoplankton growth dynamics [*Chai et al.*, 2007; *Denman & Peña*, 1999; *Denman et al.*, 2006; *Fujii et al.*, 2005].

To investigate the effects on the phytoplankton community in response to different location and time of the year, several sets of runs were conducted with selected different physical forcing conditions in reference to the corresponding experiment sites. The first set of experiments investigated the SOIREE site and the effects of iron-enrichment at different times of the year, where 26 iron infusions (each one lasting for 14 days) were simulated. The second set of experiments is a spatial extrapolation of the first experiment, focusing on the effect of the same 26 iron infusions at 25 different latitudes along the 140°E meridian (Fig. 5.1) south of Australia.

Surface forcing values including short-wave solar radiation and sea surface temperature (SST) were obtained from the International Comprehensive Ocean-Atmosphere Date Set (ICOADS) [*Worley et al.*, 2005], and *MLD* data was obtained from Sallée *et al.* [2010]. The model was run at each site without fertilization to define the “out of patch” HNLC waters. For the fertilized patch cases, the model was run at 25 different latitudes, from -63.5°S to -39.5°S, along with the simulated 26 iron infusions at different times of the year at each site.

Table 5.1: Biological source and sink terms for the *NPZD* model, and growth functions for phytoplankton and zooplankton (see Table 5.2 for parameters definitions and values).

***NPZD* Lower Trophic Ecosystem Model**

Nitrate: $\frac{dN}{dt} = rem\ D + \varepsilon_Z\ Z\ - \mu\ (MLD, t, N)\ \ P - \frac{(N_0 - N)w^+(t)}{MLD}$

Phytoplankton: $\frac{dP}{dt} = \mu\ (MLD, t, N)\ P - G(P)\ Z - \varepsilon_P\ P - \frac{w^+(t)P}{MLD}$

Zooplankton: $\frac{dZ}{dt} = \gamma_z\ G(P)\ Z - zmort\ Z^2 - \varepsilon_Z\ Z - \frac{w^+(t)Z}{MLD}$

Detritus: $\frac{dD}{dt} = (1 - \gamma_z)\ G(P)\ Z + \varepsilon_P\ P + zmort\ Z^2 - rem\ D - (\frac{w_S + w^+(t)D}{MLD})$

Phytoplankton growth: $\mu = \min\{\mu_I\ (t, MLD, P), \mu_N\ (N)\}$

Light-limited phytoplankton growth:

$$\mu_I(t, MLD, P) = \frac{1}{MLD}\int_0^{MLD} F(I_0(t)e^{-(kw+kcP)z})dz$$

Photosynthesis-irradiance curve: $F(I) = \frac{\mu_{\max}\alpha I}{\sqrt{(\mu_{\max}^2 + \alpha^2 I^2)}}$

Zooplankton growth rate: $G(P) = \frac{g\ pc\ P^2}{g + pc\ P^2}$

Nitrate limitation: $\mu_N(N) = \mu_{\max}(\frac{N}{K_N + N})$

Table 5.2: Parameter names, symbols, values, and units for the *NPZD* model.

Parameter Name	***Symbol***	***Values***	***Units***
	Phytoplankton (P) Coefficients		
Initial slope of P-I curve	α	0.025	$d^{-1}/(W\ m^{-2})$
Photosynthetically active radiation fraction	PAR	0.43	*non dimensional*
Attenuation coefficient of seawater	k_w	0.04	m^{-1}
Light attenuation by phytoplankton	k_P	0.03	m^{-1} (mmol N $m^{-3})^{-1}$
Maximum growth rate parameters	a	0.6	(d^{-1})
	b	1.066	
	c	1.0	$(°C)^{-1}$
Half saturation constant for N uptake	K_N	0.5	(mmol N m^{-3})
Phytoplankton mortality	ε_P	0.03	(d^{-1})
	Zooplankton (Z) Coefficients		
Zooplankton assimilation efficiency	γ_z	0.75	*non dimensional*
Maximum grazing rate	g	2.0	(d^{-1})
Prey capture rate	pc	1.5	(mmol N $m^{-3})^{-2}$ d^1
Quadratic mortality rate	$zmort$	0.20	(mmol N $m^{-3})^{-1}$ d^{-1}
Zooplankton excretion rate	ε_Z	0.03	(d^{-1})
	Detrital (D) Coefficients		
Detrital remineralization rate	rem	0.050	(d^{-1})
Detrital sinking rate	w_S	3.0	m d^{-1}
	Nutrient (N) Coefficients		
NO_3 concentration below mixed layer	N_0	25	(mmol N m^{-3})
	Mixed layer Coefficients		
Rate of mixed-layer depth increase	w^+		m d^{-1}

5.4 Results and discussion

The results from the *NPZD* model are extracted from the third year of a simulation in the form of daily means. The model fields thus include a 2-year spinup (not shown), which allows for the biological seasonal cycles to fully establish. Simulated chlorophyll concentrations are obtained by multiplying simulated phytoplankton nitrogen concentrations by a Chl*a*:N ratio of 1.59 gChl*a* molN^{-1} (derived from a C:N Redfield ratio of 106:16 molC molN^{-1} and a C:Chl*a* ratio of 50:1 gC gChl*a*$^{-1}$ from Fasham *et al.* [1990]).

5.4.1 SOIREE Biogeochemical Simulation

The model performance was evaluated using the SOIREE results, which served as a reference state. The model results in the "out of patch" reproduce the observations reasonably well, *i.e.* surface chlorophyll (SCHL) observations at the start of the SOIREE experiment range from 0.3 [mg m^{-3}] to 0.6 [mg m^{-3}] in a seasonal mixed layer of about 65 m [*Trull et al.*, 2001a] (Fig. 5.2). Simulated nitrate concentrations prior to the bloom were around 25 mmol N m^{-3} (Fig. 5.4) and compare well with the pre-infusion 25.6 mmol N m^{-3} observed at SOIREE site [*Frew et al.*, 2001]. Due to the seasonal algal growth in this region [*Bishop & Rossow*, 1991], these late summer concentrations are smaller than the wintertime levels reported by [*Rintoul & Bullister*, 1999].

However, the largest "out of patch" chlorophyll concentrations in the model (~0.7 mg m^{-3}) occur during early spring (*i.e.*, September-October) (Fig. 5.2), which can be mainly explained by the interaction of the overwintering zooplankton population and the light environment in the surface layer.

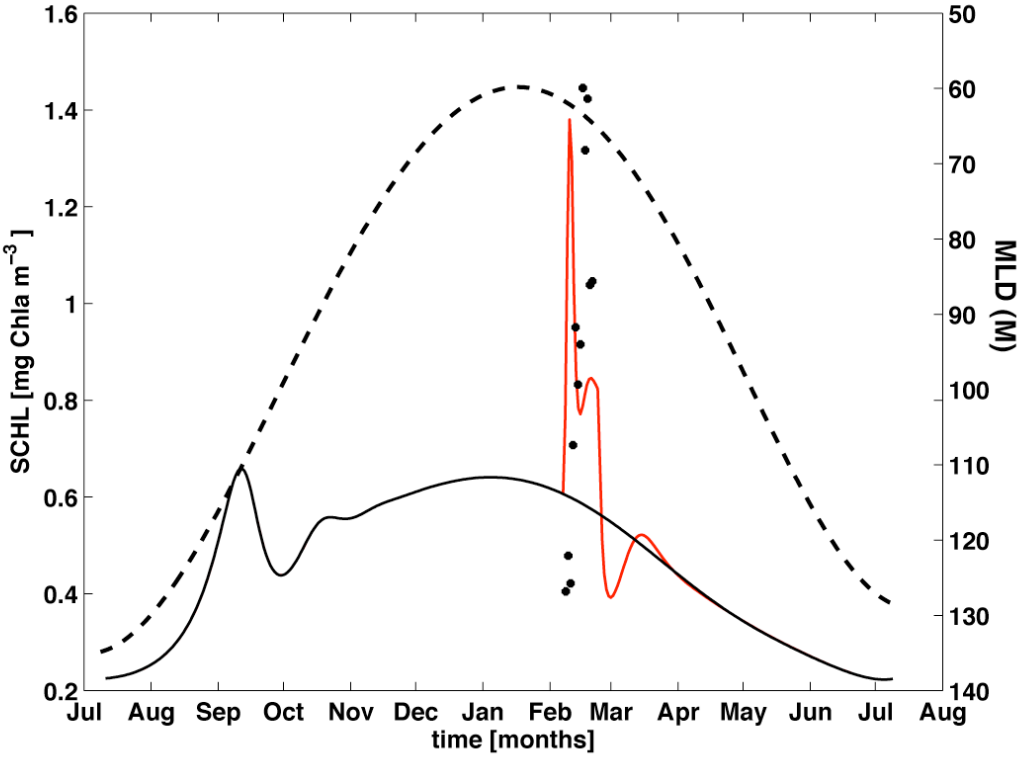

Figure 5.2: Simulated "out of patch" (black solid line) and "fertilised patch" (red line) SCHL concentrations (in mg Chl*a* mg^{-3}) at the SOIREE site. *MLD* seasonality and SOIREE SCHL observations are illustrated by dashed line and black dots, respectively.

Simulated phytoplankton in the patch promptly diverges in response to the initial increase in light levels, but are rapidly grazed upon, highlighting the role of grazers to explain the absence of significant blooms in oceanic HNLC regions [*Banse*, 1996; *Morel et al.*, 1991; *Pitchford & Brindley*, 1999] (Fig. 5.3). The exploration of the model sensitivity (chapter 3) identified the strong top-down control (i.e. grazing) as a key feature of the model. Importantly, the double peak in SCHL (Fig. 5.2) can be explained by the tightly coupled phytoplankton/zooplankton response that is mainly balanced by the zooplankton mortality term.

When compared to the "fertilized patch", the model results replicate the observations after the iron infusion, *i.e.* a rapid increase in SCHL reaching a maximum of about 1.4 [mg m^{-3}] (Fig. 5.2). However, due to strong grazing pressure (Fig. 5.3), the simulated chlorophyll-*a* levels are rapidly constrained and drop to about half of their maxima by day 7 of treatment and kept at these levels until the end of the

simulated iron-enrichment event (*i.e.*, day 14). The algal bloom then terminates with the end of the simulated iron-infusion, driving the phytoplankton stock below the 'out of patch' concentrations, before returning to these base levels.

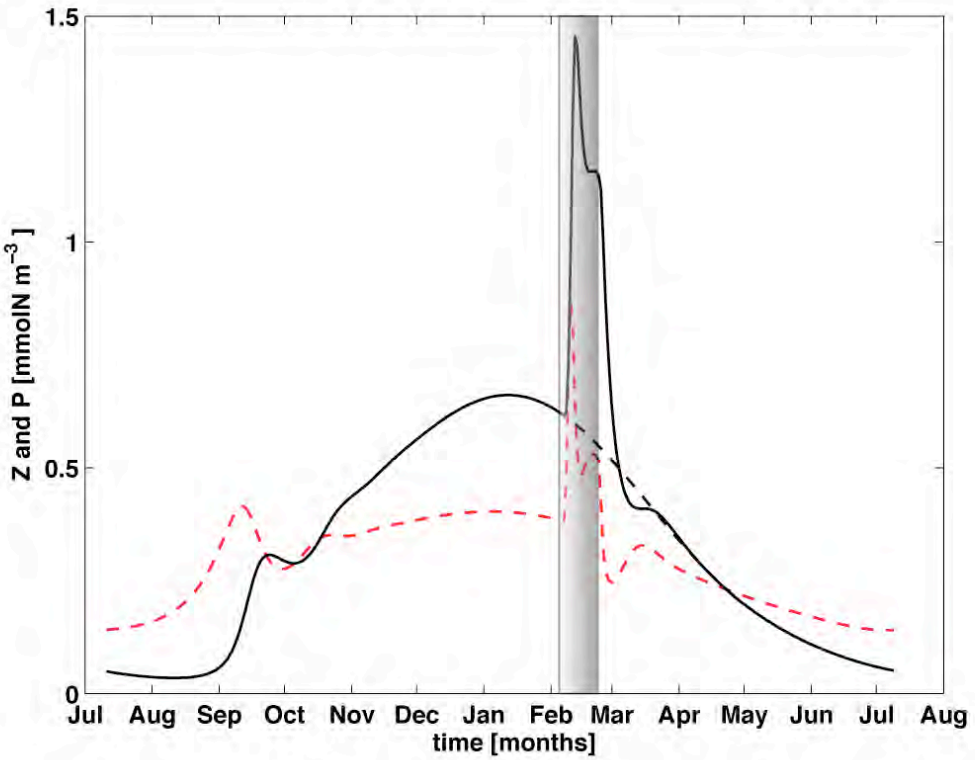

Figure 5.3: Simulated seasonal evolution of zooplankton (black solid line) and phytoplankton (in mmol N mg^{-3}) (red dashed line) at the SOIREE site. A dashed black line shows the zooplankton biomass' out of patch". Shared area illustrates the iron-infusion period.

In contrast to model results, the observed SOIREE bloom lasted for more than 40 days after the initial fertilization. This delay in the timing of the decline of the SOIREE bloom is thought to be driven by the persistence of elevated iron levels (*e.g.*, maintained by high concentrations of iron-binding ligands) at the end of the observation period [*Bowie et al.*, 2001; *Boyd et al.*, 2000; *Croot et al.*, 2001]. The stirring, growth and diffusion of the fertilized patch, which enhances the macronutrient inventory of the bloom through entrainment and prevents the onset of silicic acid limitation, also plays a key role on the SOIREE bloom longevity [*Abraham et al.*, 2000].

The simulated seasonal evolution of nitrate, which is illustrated in Figure 5.4, shown that the biological draw-down was 4.5 mmol N m^{-3} (assuming the reduction of nitrate concentrations was due to algal uptake). These model results are comparable with the macronutrient consumption (3.2 mmol N mg^{-3}) derived from nutrient concentrations 'inside the patch' and 'outside the patch" [*Bakker et al.*, 2001; *Frew et al.*, 2001].

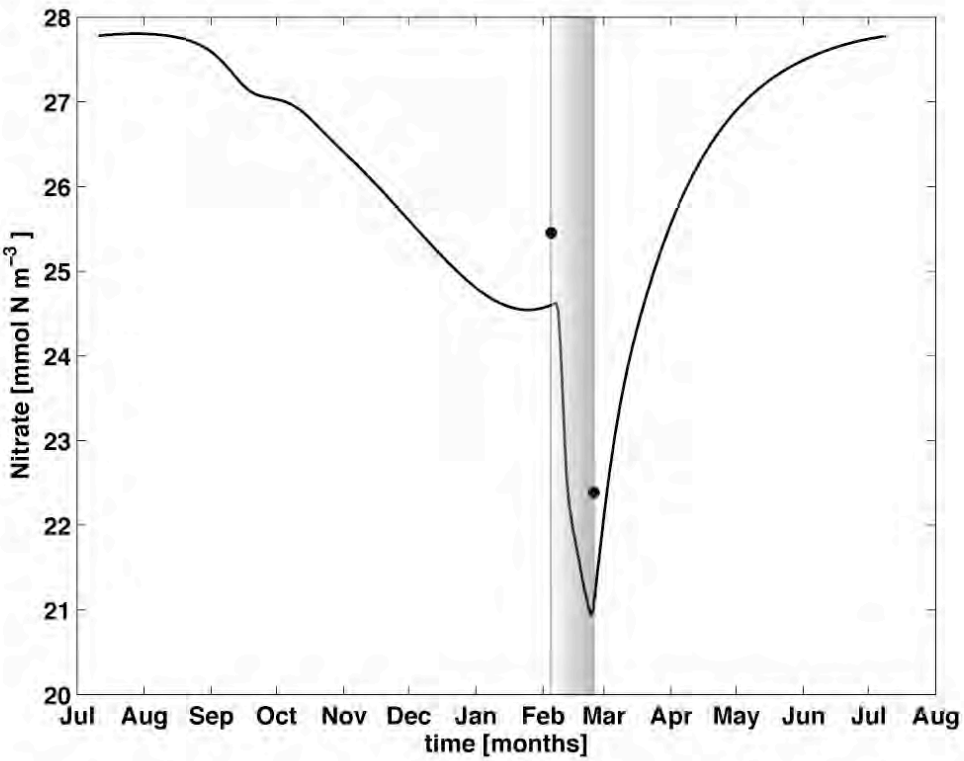

Figure 5.4: Simulated NO_3 concentrations in the mixed layer at the SOIREE site. Shared area shows the iron-infusion period. Black dotes indicate the NO_3 observations from SOIREE at the time of the first and last infusions. Published by Frew *et al.*, [2001].

5.4.2 Biogeochemical response to further Fe infusions at the SOIREE site

Since the model is able to simulate the ecosystem dynamics at the HNLC "out of patch" waters and the "fertilized patch", undertaking biogeochemical simulations in

response to similar iron enrichments occurring at different times of the year is useful to examine the projected outcomes for any future iron enrichment experiments.

The modelled, daily-averaged results of the phytoplankton component in response to 26 identical iron-induced treatments (*i.e.,* a fortnight resolution) evenly distributed across the year at the SOIREE site are shown in Figure 5.5. Simulating iron-induced changes in the algal physiology of the surface waters at the SOIREE site increased phytoplankton growth in most treatments, though the response differed between the seasons. Arrigo & Tagliabue [2005] found that the intensity of an Fe-stimulated phytoplankton bloom in the Southern Ocean depends highly on the timing of fertilisation. On average, our model results show that the SCHL concentrations in response to iron infusions during spring exceed the simulated values during summer infusions by a factor of 1.4. Reports form Arrigo & Tagliabue [2005] indicated that the optimal timing of fertilisation in terms of algal biomass and macronutrients draw-down was late December. However, their work was performed in the Ross Sea, the most productive of the Southern Ocean, which is a region that experience seasonal sea ice cover, and therefore early in the season surface waters are not iron limited due to iron release during sea ice melting.

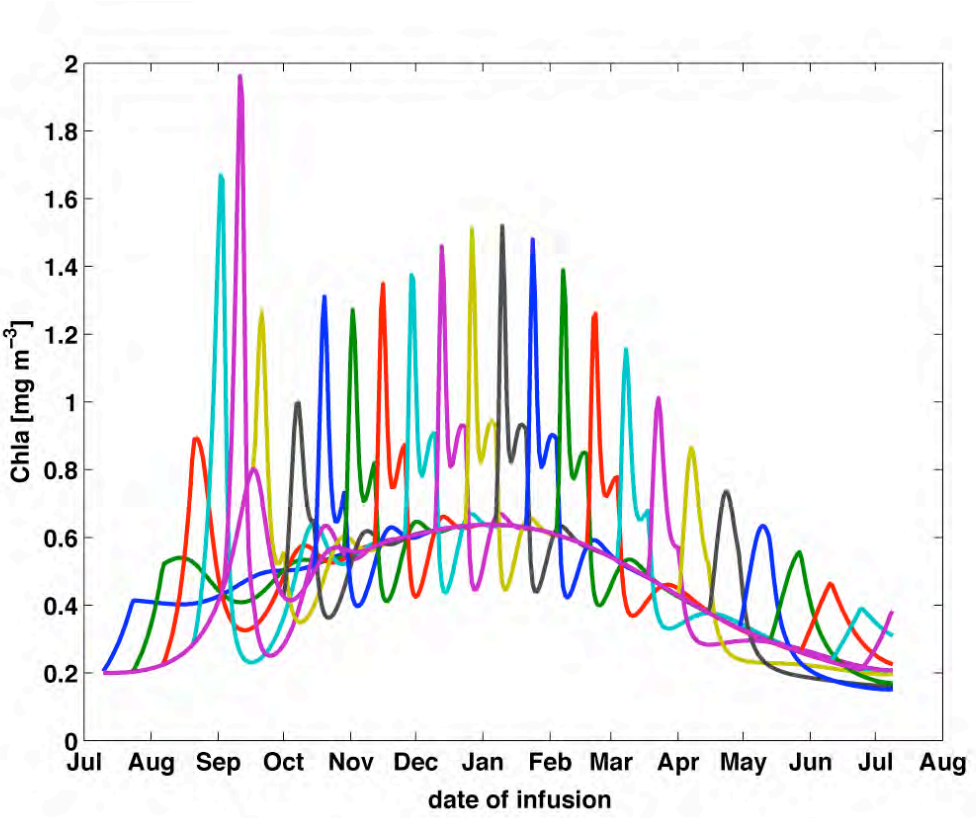

Figure 5.5: Simulated chlorophyll-*a* concentrations in response to 26 different iron-infusions events evenly distributed (*i.e.*, 2 weeks resolution) across the year at the SOIREE site.

As expected, the largest chlorophyll concentrations (~2 mg m^{-3}) in the model occur during the spring infusions (*i.e.*, September-October) and are mainly explained by the zooplankton and phytoplankton temporal history. Since winter production in the Southern Ocean is severely limited by low light conditions, overwintering phytoplankton stock leads to almost "extinction" of the zooplankton component in both model and observations [*Hosie et al.*, 2003]. Then in early spring, when growth conditions are no longer light-limited, phytoplankton biomass increased rapidly escaping from zooplankton grazing pressure. This may also be caused by the simulated iron addition relieving light limitation through improved phytoplankton photosynthetic performance [*Boyd & Abraham*, 2001; *Takeda*, 1998]. It takes about 2 days for the simulated zooplankton to respond to the increased phytoplankton biomass during early spring infusions. These components decreased linearly thereafter to near "out of patch" levels (Fig. 5.5), suggestive of strong grazing control under sub-optimal light levels.

During summer (*i.e.*, January) and fall (*i.e.*, April), the model still responds to the simulated iron-infusions, but the changes in the "fertilized patch" chlorophyll concentrations are controlled by a well-developed zooplankton stock (Fig. 5.6). Despite grazers rapidly controlling the algal bloom in both summer and fall infusions, light availability prevents a complete decline of the phytoplankton bloom during summer infusions (although chlorophyll-*a* levels drop to about half of their peak values), and allows algal biomass to return to 'out of patch' levels at the end of each infusion (Fig. 5.5). These results corroborate that light limitation is unlikely to be a major control on the initial response to iron fertilization in austral summer [*Boyd*, 2002; *Trull et al.*, 2001a].

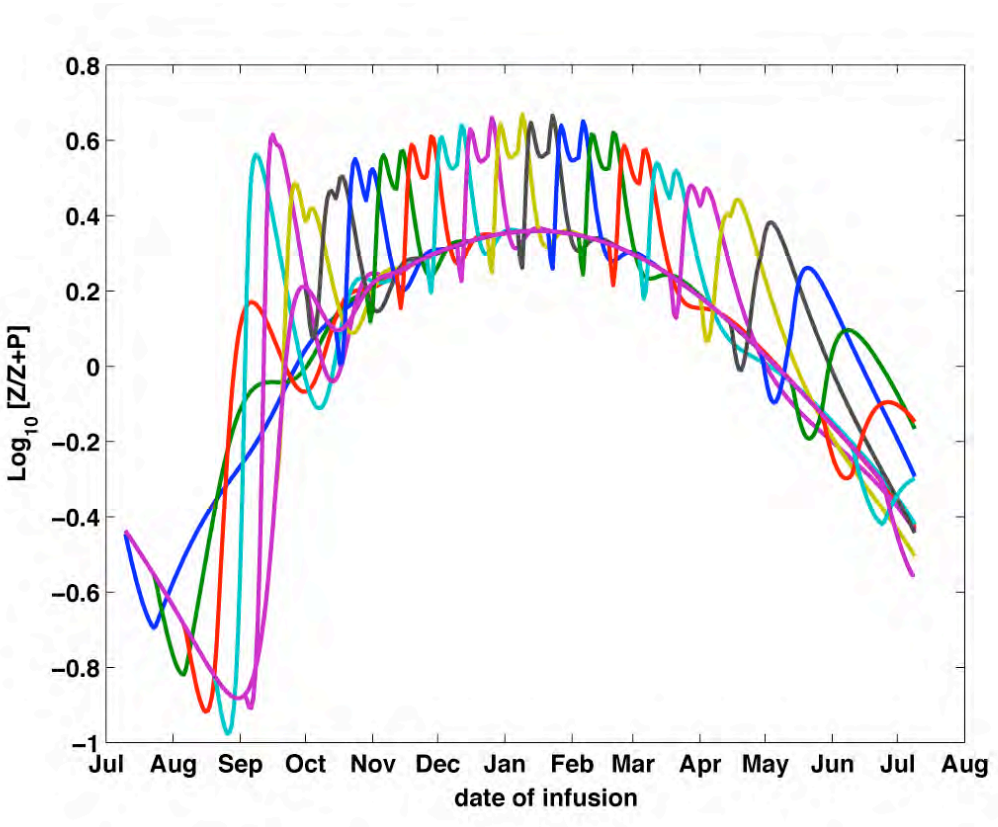

Figure 5.6: Seasonality of the simulated zooplankton (*Z*) and phytoplankton (*P*) relationship, represented as the $\log_{10}$ of Z/Z+P for each one of the 26 iron-induced simulations.

The simulated course of the surface detritus component contrasts with the corresponding simulated chlorophyll values. Figure 5.7 showed that while the modelled maxima chlorophyll concentration per simulated infusion occurs at the time of the early-September's infusion, the modelled detritus stock reaches its highest value in response to the January's infusion.

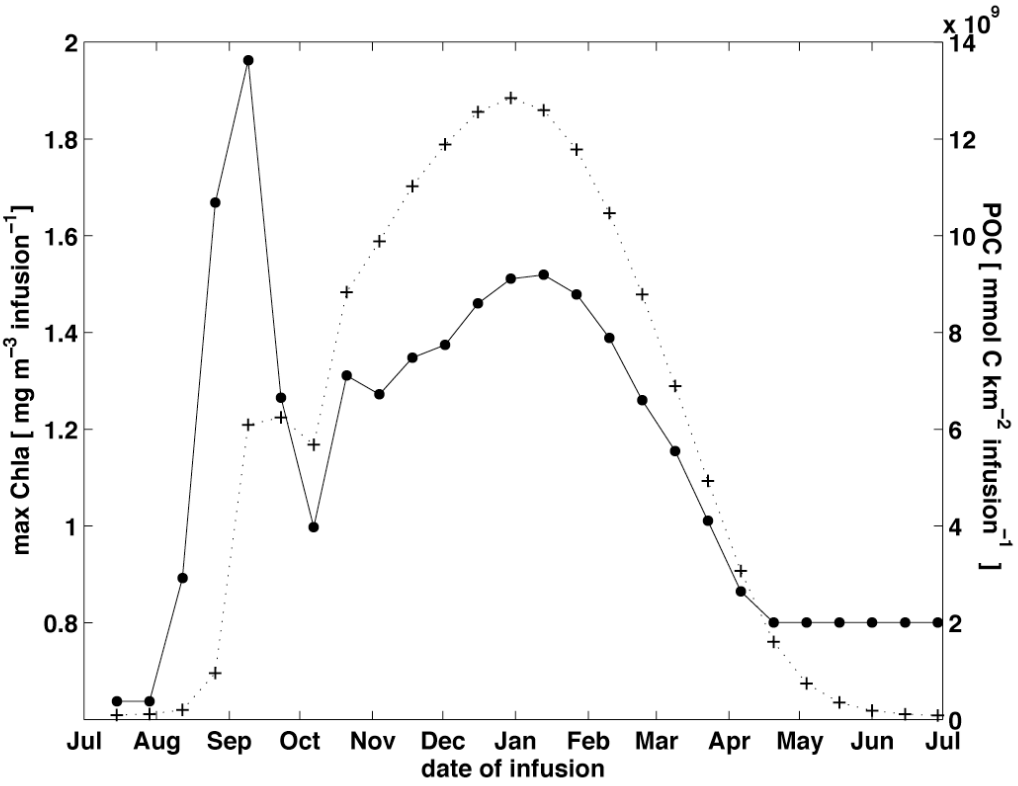

Figure 5.7: Results obtained from the simulations for the "fertilized patch" at the SOIREE site in response to 26 simulated iron additions. Maximum chlorophyll-*a* concentrations and estimates of particulate organic carbon (POC; estimated from the detritus component) are illustrated with dots and plus signs, respectively.

To quantify the amount of fixed carbon in the detritus compartment that is fuelled by the simulated iron fertilizations (see Fig. 5.7), detritus model results for the "out of patch" are subtracted from the "fertilized patch" model outputs, and converted to mmol C km^{-2} using a constant C:N Redfield ratio of 106:16 mol C mol N^{-1}. The application of Redfield nutrient stoichiometry could lead to either overestimations or underestimations in the predictions of primary productivity, depending mainly on macronutrient utilization patterns and on phytoplankton taxonomic composition (not included in this model) [*Dunbar & Leventer*, 1992; *Sedwick et al.*, 2000]. For instance Tagliabue & Arrigo [2005] reported that when Redfield C/N/P stoichiometry was applied, net primary production (NPP) was overestimated in areas normally dominated by diatoms.

In summer, when light limitation is relieved and the mixed layers are shallower, natural biomass levels are high and the induced blooms are more effectively grazed, resulting in higher particulate organic carbon (POC) production which accumulates in the detritus model compartment.

Overall, the ecosystem model predicts the magnitude and timing of nitrate, chlorophyll, zooplankton and detritus pools in response to iron-infusions simulated at 26 dates in the year at the SOIREE site.

Modelling experiments in different seasons have shown that while blooms induced at the time of peak "out of patch" algal-biomass (*i.e.*, spring) resulted in higher surface chlorophyll levels, blooms induced in summer resulted in higher POC accumulation in the mixed layer. This excess of POC that is accumulated in the surface layer, despite remineralisation, represents a fixed carbon pool that could potentially be exported from the mixed layer to the ocean interior. In order to assess what fraction of the fixed carbon pool is to be exported out of the surface layer, further modelling studies focusing on the development of more complex nutrient recycle and sinking rate functions must be carry out. The examination of the influence of iron on nitrogen and carbon metabolism by the microbial food-web (e.g. from isotopic composition), observations of sinking-particles velocities and composition (e.g. from sediment traps), along with export estimates (e.g. from ^{234}Th inventories) are some of the key aspects that could be incorporated in model development and parameterisation.

5.4.3 Extrapolation to Southern Ocean waters

Although the SOIREE site is broadly representative of a vast region of circumpolar HNLC waters [*Boyd et al.*, 2000], the distributions of primary production, macronutrients and iron are not uniform in the Southern Ocean. The fronts of the Antarctic Circumpolar Current (ACC) delimit zones with similar physical, chemical and biological properties and similar seasonal evolution [*Orsi et al.*, 1995; *Sokolov & Rintoul*, 2007b] (Fig. 5.1).

Following Trull *et al.* [2001a], the main oceanographic fronts and surface waters south of Australia are, from north to south, the Subtropical Front (STF), the Subantarctic Zone (SAZ), the Subantarctic Front (SAF), the Polar Frontal Zone (PFZ), the Polar Front (PF), the Antarctic Zone (AZ), and the Southern Antarctic Circumpolar Current Front (SACCF).

For instance, the SAZ is characterized by deep winter mixed layers and low silicate concentrations. South of the PF, the seasonal changes in *MLD* are smaller than found in SAZ, and surface waters are rich in macronutrients year-round [*Sokolov & Rintoul*, 2007b]. In summer, the *MLD* is the shallowest and changes gradually across the Southern Ocean, with the deepest *MLD* observed close to the SAF [*Sokolov*, 2008]. Macronutrient concentrations (silicate, phosphate and nitrate) increase with latitude throughout these fronts, and by the end of the growing season, silicate becomes depleted north of the PF. Seasonal depletion of nitrate and phosphate are larger in the SAZ relative to that in the PFZ [*Lourey & Trull* 2001; *Wang et al.*, 2003]. Sedwick *et al.* [2008] and Bowie *et al.* [2009] have recently reported on the distribution of dissolved iron (dFe) in Southern Ocean surface waters, and have found a general north-to-south decrease in dFe concentrations in the Australian sector.

Model results from the simulated iron-fertilization experiments that were nominally carried out across each of the Southern Ocean fronts at 140°E, are displayed in Figs. 5.8 and 5.9. These results confirm that south of the PF the highest chlorophyll values are observed when the simulated iron-fertilizations occur in spring (*i.e.*, September). Since in the model the iron infusions are simulated with changes in the phytoplankton photophysiology, increasing the phytoplankton growth rates would have a bigger effect under light limiting conditions (early in the season), whereas increasing iron stocks would impact primary productivity under either light limiting or light saturated conditions.

Figure 5.8 shows that in both the PFZ and the SAZ, the simulated maximal SCHL levels occur during the mid-summer infusions (*i.e.*, December-January). However, the model appears to be less sensitive to the iron-induced changes occurring in the PFZ. This may be explained by the lower light levels for phytoplankton growth in the surface layers, which are affected by the deepening of the mixed layer in the PFZ [*Rintoul et al.*, 1997; *Sokolov & Rintoul*, 2007b].

North of the STF, the higher SCHL levels are produced in response to simulated iron-infusions occurring early in the growing season (*i.e.*, October-December). The absence of a strong algal response to early spring infusions north of the PF is an interesting feature of the model results.

The onset of stratification in the PFZ and SAF, which is thought to occur in November [*Parslow et al.*, 2001], prevents the formation of a surface bloom prior to a significant mixed layer shoaling in December. In addition, north of the SAF higher light levels during winter may also play a part by sustaining an overwintering zooplankton stock that could efficiently graze on iron-fuelled blooms.

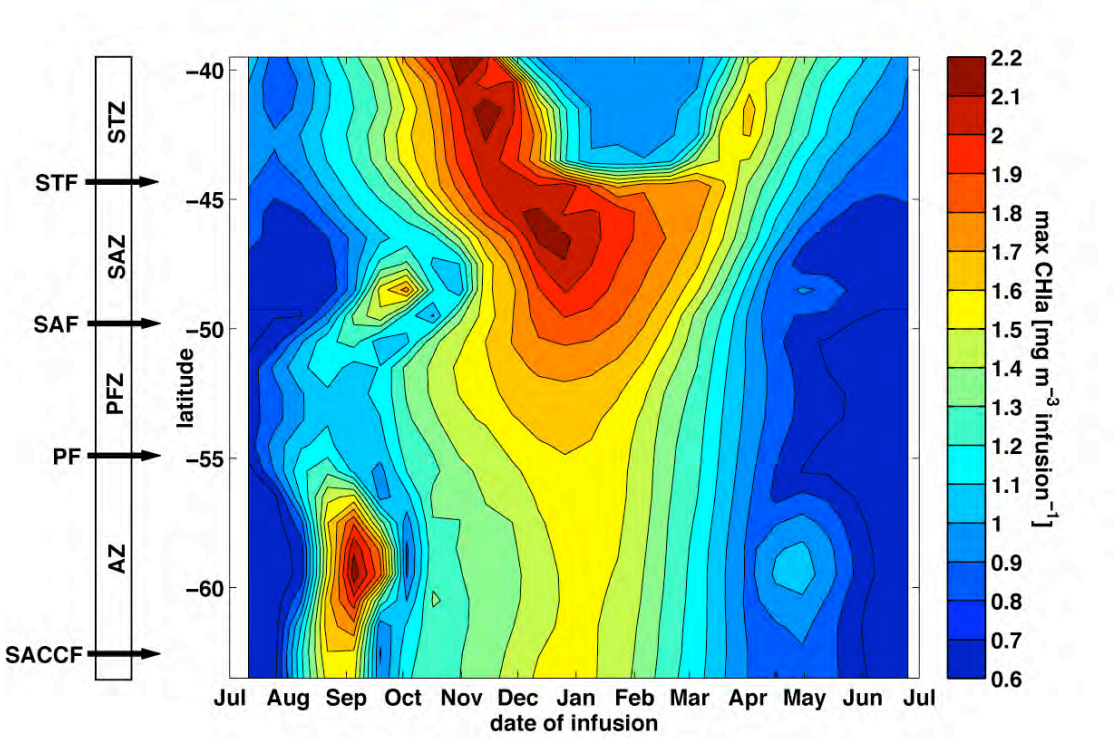

Figure 5.8: Contoured seasonality in simulated maximum chlorophyll-*a* concentrations (mg Chl*a* m^{-3} $infusion^{-1}$) in response to iron infusions along the 140°E meridian south of Australia. Approximate locations of fronts are shown (STF= Sub-Tropical Front, SAF=Sub-Antarctic Front, PF=Polar Front, SACCF=Southern ACC Front), separating distinct water masses (STZ=Sub-Tropical Zone, SAZ=Sub-Antarctic Zone, PFZ=Polar Frontal Zone, AZ=Antarctic Zone).

North of the SAF, late summer and mid-summer mixed layer nitrate depletion in the SAZ and STZ respectively affect the magnitude of the iron-induced blooms. In the STZ, blooms induced at the usual (*i.e.*, 'out-of patch') time of peak biomass (*i.e.*,

December-February) take place in a nitrate depleted mixed layer, resulting in a modest model-response to iron fertilization (Fig. 5.8). By March the convective mixed layer deepening supplies the surface layer with nitrate, which accounts for the phytoplankton response to simulated iron infusions at the end of the growing season.

In the SAZ, while the nitrate concentrations never reach potentially limiting levels [*Trull et al.*, 2001a], the phytoplankton response to simulated iron-infusions in mid-summer draws down the nitrate levels to exhaustion, preventing a higher response of algal biomass.

The implicit iron addition in the model acts to stimulate algal performance through improved phytoplankton physiology, regardless of the sources of iron to surface open Southern Ocean waters. Thus, whether the iron input comes from natural sources (e.g. upwelling, dust delivery, entrainment from shelf sediments, lateral advection; [*Bowie et al.*, 2009]) or artificial fertilization, does not alter the applicability of the model predictions, except to the extent that the mode of iron delivery may also affect mixed layer depth, temperature, light, or nutrient supply. Interestingly, the maximum of dust delivery to northern Southern Ocean waters occurs during the summer (December-February) season [*Gabric et al.*, 2010].

When it comes to the spatiotemporal response of the POC accumulation (*i.e.*, the detrital pool) to the simulated iron infusions (Fig. 5.9), the model results are tightly coupled with the simulated SCHL pattern, except for the AZ (*e.g.*, SOIREE site), most notably during spring.

These results highlight the importance of overwintering planktonic biomass in controlling the ecosystem response to spring iron fertilization events, particularly in the AZ. They also show that high SCHL levels are not an unequivocal indicator of high POC production in Southern Ocean waters.

Figure. 5.9 could also be interpreted as informing about the optimal time and location for iron fertilization events to be more effective in terms of potential carbon sequestration. Whether this translates into increased carbon export is a key question that has yet to be resolved [*Boyd et al.*, 2007], and is beyond the scope of this study.

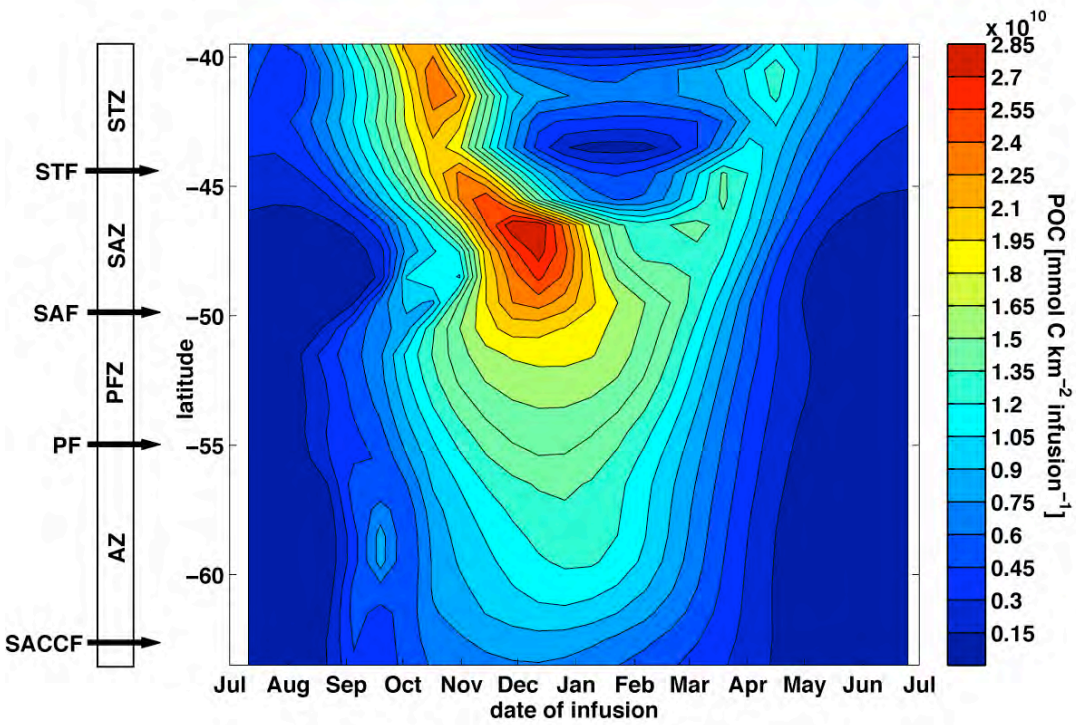

Figure 5.9: Contoured seasonality in estimates of particulate organic carbon (POC) (mmol C km^{-2} $infusion^{-1}$) in response to iron infusions along the 140°E meridian south of Australia. Approximate locations of fronts are shown (STF= Sub-Tropical Front, SAF=Sub-Antarctic Front, PF=Polar Front, SACCF=Southern ACC Front), separating distinct water masses (STZ=Sub-Tropical Zone, SAZ=Sub-Antarctic Zone, PFZ=Polar Frontal Zone, AZ=Antarctic Zone).

5.5 Conclusions

These modelling experiments provide information about the ecosystem response to simulated iron fertilisation in regions with different seasonal cycles and nutrient dynamics within the Australasian-Pacific sector of the Southern Ocean. Despite its simplicity, the model represents reasonably well the full seasonal cycle in chlorophyll concentrations over the study area when compared with SCHL concentrations derived from satellite ocean color measurements [*Sokolov*, 2008].

With the same set of model parameters previously used to simulate a natural iron-fertilization in the SAZ (see Chapter 4), the model was able to reproduce the iron-fuelled bloom observed during the SOIREE artificial fertilization [*Boyd et al.*, 2000].

Model results suggest that mid summer infusions (*i.e.*, December) in the SAZ appear to be the more favourable in accumulating POC production in the mixed layer.

The representation of the main ‘out-of-patch’ and ‘fertilized-patch’ characteristics of surface waters south of Australia establishes a basis for future modelling efforts to address additional aspects of the ecosystem response, such as, silicate limitation, ammonium recycling, and iron cycling. Such developments are important to increase our knowledge of the effects of large-scale iron fertilization on ocean ecosystem dynamics, air-sea gas fluxes, biogeochemical processes, and carbon sequestration.

5.6 References

Abraham, E. R., C. S. Law, P. W. Boyd, et al. (2000), Importance of stirring in the development of an iron-fertilized phytoplankton bloom, *Nature*, *407*, 727-730.

Arrigo, K. R., and A. Tagliabue (2005), Iron in the Ross Sea: 2. Impact of discrete iron addition strategies, *J. Geophys. Res*, *110*(C03010), C03010.

Aumont, O., and L. Bopp (2006), Globalizing results from ocean in situ iron fertilization studies, *Global Biogeochemical Cycles*, *20*(2), 10.1029.

Bakker, D. C. E., A. J. Watson, and C. S. Law (2001), Southern Ocean iron enrichment promotes inorganic carbon drawdown, *Deep-Sea Research II*.

Bakker, D. C. E., Y. Bozec, P. D. Nightingale, et al. (2005), Iron and mixing affect biological carbon uptake in SOIREE and EisenEx, two Southern Ocean iron fertilisation experiments, *Deep-Sea Research Part I: Oceanographic Research Papers*, *52*(6), 1001-1019.

Banse, K. (1996), Low seasonality of low concentrations of surface chlorophyll in the Subantarctic water ring: underwater irradiance, iron, or grazing?, *Progress in Oceanography*, *37*, 241-291.

Bishop, J. K. B., and W. B. Rossow (1991), Spatial and temporal variability of global surface solar irradiance, *Journal of Geophysical Research*, *96*, 16839-16858.

Blain, S., B. Quéguiner, L. Armand, et al. (2007), Impacts of natural iron fertilisation on the Southern Ocean, *Nature*, *446*, 1070-1074, doi:1010.1038/nature05700.

Bowie, A. R., M. T. Maldonado, R. D. Frew, et al. (2001), The fate of added iron during a mesoscale fertilisation experiment in the polar Southern Ocean, *Deep Sea Research (Part II, Topical Studies in Oceanography)*, *48*, 2703-2743.

Bowie, A. R., D. Lannuzel, T. A. Remenyi, et al. (2009), Biogeochemical iron budgets of the Southern Ocean south of Australia: Decoupling of iron and nutrient cycles in the subantarctic zone by the summertime supply, *Global Biogeochem. Cycles*, *23*.

Boyd, P., J. LaRoche, M. Gall, et al. (1999), Role of iron, light, and silicate in controlling algal biomass in subantarctic waters SE of New Zealand, *Journal of Geophysical Research*, *104*(C6), 13395-13408.

Boyd, P., A. Watson, C. S. Law, et al. (2000), A mesoscale phytoplankton bloom in the polar Southern Ocean stimulated by iron fertilization, *Nature*, *407*, 695-702.

Boyd, P., and E. Abraham (2001), Iron-mediated changes in phytoplankton photosynthetic competence during SOIREE, *Deep Sea Research (Part II, Topical Studies in Oceanography)*, *48*, 2529-2550.

Boyd, P. W., D. L. Muggli, D. E. Varela, et al. (1996), In vitro iron enrichment experiments in the NE subarctic pacific, *Marine Ecology Progress Series*, *136*(1-3), 179-193.

Boyd, P. W. (2002), Environmental factors controlling phytoplankton processes in the Southern Ocean, *Journal of Phycology*, *38*(5), 844-861.

Boyd, P. W., T. Jickells, C. S. Law, et al. (2007), Mesoscale Iron Enrichment Experiments 1993-2005: Synthesis and Future Directions, *Science*, *315*(5812), 612-617, DOI: 610.1126/science.1131669.

Chai, F., M. S. Jiang, Y. Chao, et al. (2007), Modeling responses of diatom productivity and biogenic silica export to iron enrichment in the equatorial Pacific Ocean, *Global Biogeochemical Cycles, 21*(3).

Croot, P. L., A. R. Bowie, R. D. Frew, et al. (2001), Retention of dissolved iron and FeII in an iron induced Soutern Ocean phytoplankton bloom, *Geophysical Research Letters, 28*(18), 3425-3428.

Cullen, J. J. (1991), Hypotheses to Explain High-Nutrient Conditions in the Open Sea, *Limnology and Oceanography, 36*(8), 1578-1599.

de Baar, H. J. W., P. W. Boyd, K. H. Coale, et al. (2005), Synthesis of iron fertilization experiments: from the iron age to the age of enlightenment, *Journal of Geophysical Research. C. Oceans, 110*, doi:10.1029/2004GC002601.

Denman, K. L., and M. A. Peña (1999), A coupled 1-D biological/physical model of the northeast subarctic Pacific Ocean with iron limitation, *Deep-Sea Research Part II: Topical Studies in Oceanography, 46*(11-12), 2877-2908.

Denman, K. L., C. Voelker, M. Angelica Peña, et al. (2006), Modelling the ecosystem response to iron fertilization in the subarctic NE Pacific: The influence of grazing, and Si and N cycling on CO2 drawdown, *Deep Sea Research (Part II, Topical Studies in Oceanography), 53*(20-22), 2327-2352.

Dunbar, R. B., and A. Leventer (1992), Seasonal variation in carbon isotopic composition of antarctic sea ice and open-water plankton communities, *Antarctic Journal of the United States, 27*, 79-81.

Fasham, M. J. R., H. W. Ducklow, and S. M. McKelvie (1990), A nitrogen-based model of plankton dynamics in the oceanic mixed layer, *Journal of Marine Research, 48*(3), 591-639.

Fennel, K., M. R. Abbott, Y. H. Spitz, et al. (2003), Modeling controls of phytoplankton production in the southwest Pacific sector of the Southern Ocean, *Deep-Sea Research Part II: Topical Studies in Oceanography, 50*(3-4), 769-798.

Franck, V. M., M. A. Brzezinski, K. H. Coale, et al. (2000), Iron and silicic acid concentrations regulate Si uptake north and south of the Polar Frontal Zone in the Pacific Sector of the Southern Ocean, *Deep Sea Research Part II: Topical Studies in Oceanography, 47*(15-16), 3315-3338.

Frew, R., A. Bowie, P. Croot, et al. (2001), Macronutrient and trace-metal geochemistry of an in situ iron-induced Southern Ocean bloom, *Deep-sea research. Part 2. Topical studies in oceanography, 48*(11-12), 2467-2481.

Fujii, M., N. Yoshie, Y. Yamanaka, et al. (2005), Simulated biogeochemical responses to iron enrichments in three high nutrient, low chlorophyll (HNLC) regions, *Progress in Oceanography, 64*(2-4), 307-324.

Gabric, A. J., R. A. Cropp, G. H. McTainsh, et al. (2010), Australian dust storms in 2002-2003 and their impact on Southern Ocean biogeochemistry, *Global Biogeochemical Cycles, 24*(2).

Gall, M. P., P. W. Boyd, J. Hall, et al. (2001), Phytoplankton processes. Part 1: Community structure during the Southern Ocean Iron RElease Experiment (SOIREE), *Deep-Sea Research Part II: Topical Studies in Oceanography, 48*(11-12), 2551-2570.

Herraiz-Borreguero, L., and S. Rich Rintoul (2011), Regional circulation and its impact on upper ocean variability south of Tasmania, *Deep-sea research. Part 2. Topical studies in oceanography, 58*(21-22), 2071-2081.

Hosie, G. W., M. Fukuchi, and S. Kawaguchi (2003), Development of the Southern Ocean Continuous Plankton Recorder survey, *Progress in Oceanography*, *57*(2-4), 263-283.

Hutchins, D. A., P. N. Sedwick, G. R. DiTullio, et al. Control of phytoplankton growth by iron and silicic acid availability in the Subantarctic Southern Ocean: experimental results from the SAZ project, *Journal of Geophysical Research, submitted*.

Lourey, M. J., and T. W. Trull (2001), Seasonal nutrient depletion and carbon export in the Subantarctic and Polar Frontal Zones of the Southern Ocean south of Australia, *Journal of Geophysical Research. C. Oceans*, *106*(C12), 31463-31488.

Martin, J. H., and S. E. Fitzwater (1988), Iron deficiency limits phytoplankton growth in the north-east pacific subarctic, *Nature*, *331*(6154), 341-343.

Martin, J. H. (1990a), Glacial-interglacial CO_2 change: The iron hypothesis, *Paleoceanography*, *5*, 1-13.

Mayzaud, P., V. Tirelli, A. Errhif, et al. (2002), Carbon intake by zooplankton: Importance and role of zooplankton grazing in the Indian sector of the Southern Ocean, *Deep Sea Research II*, *49*(16), 3169-3188.

Metzl, N., B. Tilbrook, and A. Poisson (1999), The annual fCO_2 cycle and the air-sea CO_2 flux in the sub-Antarctic ocean, *Tellus*, *51B*, 849-861.

Mitchell, B. G., E. A. Brody, O. Holm-Hansen, et al. (1991), Light Limitation of Phytoplankton Biomass and Macronutrient Utilization in the Southern Ocean, *Limnology and Oceanography*, *36*(8), 1662-1677.

Morel, F. M. M., J. G. Reuter, and N. M. Price (1991), Iron nutrition of phytoplankton and its possible importance in the ecology of ocean regions with high nutrient and low biomass, *Oceanography*, *4*, 56-61.

Mosseri, J., B. Quéguiner, L. Armand, et al. (2008), Impact of iron on silicon utilization by diatoms in the Southern Ocean: a case study of the Si/N cycle decoupling in a naturally iron-enriched area, *Deep Sea Research II*, *55*(5-7), 801-819.

Nodder, S. D., M. A. Charette, A. M. Waite, et al. (2001), Particle transformations and export flux during an *in situ* iron-stimulated bloom in the Southern Ocean, *Geophysical Research Letters*, *28*(12), 2409-2412.

Orsi, A. H., T. I. Whitworth, and W. D. J. Nowlin (1995), On the meridional extent and fronts of the Antarctic Circumpolar Current, *Deep-Sea Research*, *42*(5), 641-673.

Oschlies, A., and V. Garçon (1999), An eddy-permitting coupled physical-biological model of the North Atlantic. 1. Sensitivity to advection numerics and mixed layer physics, *Global Biogeochemical Cycles*, *13*(1), 135-160.

Parslow, J., P. Boyd, S. R. Rintoul, et al. (2001), A persistent sub-surface chlorophyll maximum in the Polar Frontal Zone south of Australia: seasonal progression and implications for phytoplankton-light-nutrient interactions, *Journal of Geophysical Research. C. Oceans*, *106*, 31543-31557.

Pitchford, J. W., and J. Brindley (1999), Iron limitation, grazing pressure and oceanic high nutrient-low chlorophyll (HNLC) regions, *Journal of Plankton Research*, *21*(3), 525-547.

Pollard, R., R. Sanders, M. Lucas, et al. (2007), The Crozet Natural Iron Bloom and Export Experiment (CROZEX), *Deep-Sea Research II, Volume 54, Issue 18-20, p. , 54*(18-20), 1905-1914.

Rintoul, S. R., J. R. Donguy, and D. H. Roemmich (1997), Seasonal evolution of upper ocean thermal structure between Tasmania and Antarctica, *Deep Sea Research (Part I, Oceanographic Research Papers)*, *44*(7), 1185-1202.

Rintoul, S. R., and J. L. Bullister (1999), A late winter hydrographic section from Tasmania to Antarctica, *Deep-Sea Research*, *46*, 1417-1454.

Rintoul, S. R., and T. W. Trull (2001), Seasonal evolution of the mixed layer in the Subantarctic Zone south of Australia, *Journal of Geophysical Research. C. Oceans*, *106*(C12), 31447-31462.

Sallée, J. B., K. Speer, S. R. Rintoul, et al. (2010), Southern Ocean thermocline ventilation, *Journ. of Phys. Ocean.*, *40*(3), 509-529.

Sarmiento, J. L., N. Gruber, M. A. Brzezinski, et al. (2004), High-latitude controls of thermocline nutrients and low latitude biological productivity, *Nature*, *427*, 56-60.

Sedwick, P. N., G. R. DiTullio, and D. J. Mackey (2000), Iron and manganese in the Ross Sea, Antarctica: Seasonal iron limitation in Antarctic shelf waters, *Journal of Geophysical Research-Oceans*, *105*(C5), 11321-11336.

Sedwick, P. N., A. R. Bowie, and T. W. Trull (2008), Dissolved iron in the Australian sector of the Southern Ocean (CLIVAR SR3 section): Meridional and seasonal trends, *Deep Sea Research (Part I, Oceanographic Research Papers)*, *55*((8)), 911-925, doi:910.1016/j.dsr.2008.1003.1011.

Sloyan, B. M., and S. R. Rintoul (2001), Circulation, renewal, and modification of Antarctic mode and intermediate water, *Journal of Physical Oceanography*, *31*(4), 1005-1030.

Sokolov, S., and S. R. Rintoul (2007b), On the relationship between fronts of the Antarctic Circumpolar Current and surface chlorophyll concentrations in the Southern Ocean, *J. Geophys. Res. – Oceans*, *112*(C07030), doi: 10.1029/2006JC004072.

Sokolov, S. (2008), Chlorophyll blooms in the Antarctic Zone south of Australia and New Zealand in reference to the Antarctic Circumpolar Current fronts and sea ice forcing, *Journal of Geophysical Research. C. Oceans*, *113*(3).

Sunda, W. G., and S. A. Huntsman (1997), Interrelated influence of iron, light and cell size on marine phytoplankton growth, *Nature*, *390*, 389-392.

Tagliabue, A., and K. R. Arrigo (2005), Iron in the Ross Sea: 1. Impact on CO2 fluxes via variation in phytoplankton functional group and non-Redfield stoichiometry, *J Geophys Res*, *110*, C03009.

Takahashi, T., S. C. Sutherland, C. Sweeney, et al. (2002), Global sea-air CO2 flux based on climatological surface ocean pCO2, and seasonal biological and temperature effects, *Deep Sea Research (Part II, Topical Studies in Oceanography)*, *49*(9-10), 1601-1622.

Takeda, S. (1998), Influence of iron availability on nutrient consumption ratio of diatoms in oceanic waters, *Nature*, *393*, 774-777.

Timmermans, K. R., L. J. A. Gerringa, H. J. W. De Baar, et al. (2001), Growth rates of large and small Southern Ocean diatoms in relation to availability of iron in natural seawater, *Limnology and Oceanography*, *46*(2), 260-266.

Trull, T. W., S. R. Rintoul, M. Hadfield, et al. (2001a), Circulation and seasonal evolution of Polar waters south of Australia: Implications for iron fertilisation of the Southern Ocean, *Deep Sea Research (Part II, Topical Studies in Oceanography)*, *48*(11/12), 2439-2466.

Trull, T. W., and L. Armand (2001b), Insights into Southern Ocean carbon export from the $d^{13}C$ of particles and dissolved inorganic carbon during the SOIREE

iron fertilisation experiment, *Deep Sea Research (Part II, Topical Studies in Oceanography)*, *48*(11/12), 2655-2680.

Tsuda, A., S. Takeda, H. Saito, et al. (2007), Evidence for the grazing hypothesis: Grazing reduces phytoplankton responses of the HNLC ecosystem to iron enrichment in the western subarctic pacific (SEEDS II), *Journal of Oceanography*, *63*(6), 983-994.

Wang, X., R. J. Matear, and T. W. Trull (2003), Nutrient utilization ratios in the Polar Frontal Zone in the Australian sector of the Southern Ocean: a model, *Global Biogeochemical Cycles*, *17*(1), 1009, doi:1010.1029/2002GB001938.

Worley, S. J., S. D. Woodruff, R. W. Reynolds, et al. (2005), ICOADS release 2.1 data and products, *International Journal of Climatology*, *25*(7), 823-842.

CHAPTER SIX

General Conclusions

6.1 Summary and Main Findings

The potential role of iron as a growth-limiting nutrient for phytoplankton in the ocean has been a topic of interest for over half a century [*Hart*, 1942]. Popularised in the 1980s, this theory has recently been proven during large-scale natural and artificial iron fertilisation experiments [*Blain et al.*, 2007; *Boyd et al.*, 2007; *de Baar et al.*, 1995; *Pollard et al.*, 2009]. However, our understanding of the influence of iron availability on the ecosystem dynamics and the associated control of carbon transfer to the deep ocean is poorly constrained by observations. Most of what is known about these interactions, for the present and under future climate change scenarios, comes from numerical models. This thesis has modified and applied a simple biogeochemical plankton model for the investigation of possible lower trophic level ecosystem responses to simulated iron inputs.

In Chapter 2 the four-compartment model was adapted from the previous endeavours of Oschlies & Garçon [1999] to address the seasonal cycle of macro-nutrients and phytoplankton productivity in HNLC waters surrounding the Kerguelen plateau, in the Indian sector of the Southern Ocean. The model was forced with surface light values, sea surface temperatures, and model-derived mixed layer depths. The NPZD model reproduced successfully seasonal variations of nitrate concentrations, phytoplankton and zooplankton biomasses.

Chapter 3 investigated the main biological and physical factors controlling the timing and magnitude of the usual seasonal phytoplankton maximum observed in the HNLC waters off the Kerguelen plateau. Based on the hypotheses raised early in the Chapter, a series of model sensitivity studies were conducted in order to determine which parameters or forcing functions could account for the difference between the ‘off-Plateau’ (HNLC) and the ‘on-Plateau’ (iron-rich waters) spring blooms. The sensitivity experiments showed that no single parameter could be considered a sufficient explanation. However, by varying one parameter at the time, the experiments revealed a strong top-down control in the model. Only tests with zooplankton mortality and grazing terms resulted in significant changes in surface chlorophyll concentrations. The sensitivity study therefore suggested that only a

combination of model parameters would explain the main differences in regulating primary productivity between the HNLC and the iron-rich waters.

Observations suggest that the critical difference between the two contrasted environments (*i.e.*, (i) the natural iron-fertilized waters of the Kerguelen plateau and (ii) the nearby HNLC offshore waters) studied during KEOPS, is the presence or absence of a spring phytoplankton bloom. Chapter 4 sought to capture this persistent difference by means of numerical simulations. Since iron supply has a demonstrated role in photosynthesis, the two photosynthetic parameters in the model (α and μ_{max}) were modified according to results from bottle experiments. Increasing these parameter values provided a means to simulate high iron availability, and therefore a seasonal variation of such iron availability was also included in the Kerguelen plateau simulations. In addition, in order to increase the model sensitivity to changes in the photosynthetic performance, a relaxation of grazing pressure was found to be necessary. Work investigating parameter ranges suggested this could be achieved by reducing the grazing performance or the herbivore biomass. While zooplankton observations over the fertilised area argue against reducing the herbivore's grazing performance, the iron-stimulated multi-trophic level food web within the zooplankton community supports the idea of increasing the herbivores mortality (by predators) in the on-Plateau simulations. Thus by increasing the zooplankton mortality and setting fixed seasonal variations of the photosynthetic parameters, the numerical model was shown to produce results that are consistent with observations, and with other biogeochemical models [*Aumont & Bopp*, 2006; *Mongin et al.*, 2008].

In Chapter 5 the same modelling framework was used to simulate the observed outcomes of the first Southern Ocean mesoscale iron enrichment experiment, (SOIREE). The model has shown that by raising the parameters α and μ_{max} by a factor of 2.5 during the SOIREE-site occupation period (*i.e.*, 13 days), surface chlorophyll and nitrate concentrations in iron-fertilised waters can be modelled with a high degree of realism (in comparison with observations). This approach was then expanded to investigate possible differences in response to iron fertilisation, as a function of both the seasonal timing of fertilisation, and the latitudinal location of fertilisations (using seasonal cycles of water column properties for the Australian sector of the Southern Ocean from -63.5° to -39.5° S). Further iron-addition simulations at the SOIREE site showed that the largest chlorophyll response occurred at the time of the spring

infusions. This characteristic also occurred across the range of investigated latitudes in that the highest chlorophyll concentrations were simulated at the time of the usual seasonal phytoplankton maximum. Northerly regions had two distinct time periods in which phytoplankton response were strong. The iron fertilization therefore tends to amplify the seasonal cycle. On the other hand, when tracing the fate of these induced blooms in terms of the POC response, the results revealed a decoupling of chlorophyll levels and POC in the Antarctic Zone. The greatest phytoplankton response in the Antarctic Zone (occurring in spring) does not result in the equivalent maximum POC accumulation (occurring in summer). This response derived from seasonality of light availability, and in the abundance of grazing zooplankton, in the model.

This research contributes to the understanding of how the interactions between surface iron inputs and other forcing mechanisms such as stratification and light availability can affect marine plankton ecosystems. It also highlights the importance of internal ecosystem dynamics in regulating the timing and magnitude of responses to external forcing. These insights assist in assessing global ocean carbon budgets and modelling scenarios of global climate and environmental change.

The main conclusions from this study are as follows:

1. Zooplankton plays a key role in the success of the biogeochemical model, while detritus is mostly redundant.
2. Model solutions for polar waters are sensitive to phytoplankton photosynthesis (α, k_w and a) and zooplankton grazing parameters (pc, g, and $zmort$).
3. The model has the ability to distinguish between HNLC waters and iron-enriched waters.
4. Increasing the photosynthetic parameters by a factor of 2.5 is sufficient to assess the phytoplankton response to elevated iron inputs, provided low grazing pressures.
5. High surface chlorophyll concentrations are not an unequivocal indicator of high POC production in Southern Ocean waters.

6. The model results inform the projected outcomes of any future iron enrichment experiments, and suggest the best time and location for fertilisation of Southern Ocean surface waters.

6.2 Perspectives

There are a number of directions in which the work in this thesis could be extended. A particular limitation of the work common to all of the research chapters has been the fact that the ecosystem model omits the iron and silicon cycles. This did not permit any heterogeneity in the phytoplankton response (*e.g.*, diatoms vs. other phytoplankton), despite this being a known phenomenon in relation to iron supply. There are alternative ecosystem models that could be used in parallel to assess the significance of community structure and parameterisation for model predictions [*Tagliabue et al.*, 2009]. More complex iron-containing models have been applied both globally and in the Southern Ocean [*Arrigo & Tagliabue*, 2005; *Aumont & Bopp*, 2006; *Tagliabue & Arrigo*, 2005], however for the first time a biogeochemical model has been used to estimate the effect of simulated iron-additions on POC production across the Australian sector of the Southern Ocean.

Focusing on individual chapters, several lines of further research suggest themselves. As noted in Chapter 3, one of the main characteristics of the model was the strong grazing pressure. While we identify the role of the different zooplankton terms in the model results, a more thorough exploration of different grazing functional forms [*Franks et al.*, 1986] or even different 'closure terms' [*Edwards & Yool*, 2000] could provide interesting insights into the research question examined.

A weakness of Chapter 4's numerical simulation of the Kerguelen plateau bloom was its reliance on a relatively crude numerical approach to explore the parameter space. While the model's complexity favoured this, as well as the model results, the investigation of more powerful numerical approaches [*e.g., Matear*, 1995] would ideally precede any future studies of model performance. Our understanding of the plankton dynamics over the Kerguelen plateau could also be improved by adding another zooplankton component (*e.g.*, predators) or by coupling the model to a zooplankton population model. This will allow us to examine the impacts of food

availability on zooplankton populations, and therefore confirm or reject the assumption of a lower herbivore biomass over the plateau.

Aside from considerations of the nature and range of variability of the photosynthetic parameters used in the experiments of Chapter 5, there are several paths for future research. The development in time of the parameter modification, as a rigid step function that multiplies two parameters by the same constant factor, should be re-examined from a more physiological standpoint. For instance, the experiment links the iron fertilisation directly to the growth rate and in reality the link is much more indirect and influenced by the physiological processes of iron uptake, internal storage and others. An alternative could be a linear function (or other decay function) in the increase and decrease of the parameters, or directly resolve the iron cycle with dynamic nutrient to carbon ratios.

In the SOIREE simulation the simulated iron addition ends on the last day of the SOIREE experiment (day 13) and, as mentioned in Chapter 5, the bloom persisted for several weeks as observed by satellite [*Abraham et al.*, 2000]. This interesting feature of the SOIREE experiment that was not further investigated in this study should not be seen as a model failure since the long-lasting bloom was maintained by high iron concentrations, and by the elongation of the fertilised waters which allowed efficient nutrient exchange along its periphery [*Abraham et al.*, 2000]. The ecosystem response to this persistence in the iron levels could be explored in the model by extending the period of the simulated iron fertilisation (*i.e.*, extend the duration of the enhanced photosynthetic performance).

Finally, the consequences and fate of the accumulation of POC in the surface layers (a proxy of potential carbon export) could be addressed in future work. For instance, by considering of the role of the depth of the mixed layer as well as the conversion of detrital concentrations to carbon export. Geoengineers would be interested not only in knowing the best time to fertilise the ocean, but also how long it should be fertilised and the time scale over which the system would need to be monitored to determine particulate organic carbon export.

6.3 Closing remarks

Although iron fertilisation continues to receive attention as a possible method to decrease CO_2 concentrations in the atmosphere [*Buesseler et al.*, 2008; *Trull et al.*, 2008], more research is required to determine the complex and long-term effects on the microbial community. Most studies in which seawater is amended with iron focus on phytoplankton because of their obvious role in carbon sequestration, but relatively little attention has been paid to the response of zooplankton.

Considerable work still remains to be done to establish a single model which will produce annual patterns of biological activity in agreement with data, when given the appropriate physical forcing (with respect to location) or nested into a GCM. It is hoped that the work in this thesis, by suggesting important parameters, functional forms and caveats, can play a small part in the realisation of such models.

6.4 References

Abraham, E. R., C. S. Law, P. W. Boyd, et al. (2000), Importance of stirring in the development of an iron-fertilized phytoplankton bloom, *Nature*, *407*, 727-730.

Arrigo, K. R., and A. Tagliabue (2005), Iron in the Ross Sea: 2. Impact of discrete iron addition strategies, *J. Geophys. Res*, *110*(C03010), C03010.

Aumont, O., and L. Bopp (2006), Globalizing results from ocean in situ iron fertilization studies, *Global Biogeochemical Cycles*, *20*(2), 10.1029.

Blain, S., B. Quéguiner, L. Armand, et al. (2007), Impacts of natural iron fertilisation on the Southern Ocean, *Nature*, *446*, 1070-1074, doi:1010.1038/nature05700.

Boyd, P. W., T. Jickells, C. S. Law, et al. (2007), Mesoscale Iron Enrichment Experiments 1993-2005: Synthesis and Future Directions, *Science*, *315*(5812), 612-617, DOI: 610.1126/science.1131669.

Buesseler, K. O., S. C. Doney, D. M. Karl, et al. (2008), Ocean iron fertilization-moving forward in a sea of uncertainty, *Science*, *319*, 162.

de Baar, H. J. W., J. T. M. de Jong, D. C. E. Bakker, et al. (1995), Importance of iron for phytoplankton blooms and carbon dioxide drawdown in the Southern Ocean, *Nature*, *373*, 412-415.

Edwards, A. M., and A. Yool (2000), The role of higher predation in plankton population models, *Journal of Plankton Research*, *22*(6), 1085-1112.

Franks, P. J. S., J. S. Wroblewski, and G. R. Flierl (1986), Behavior of a simple plankton model with food-level acclimation by herbivores, *Marine Biology*, *91*(1), 121-129.

Hart, T. J. (1942), Phytoplankton periodicity in Antarctic surface water, *Discovery Reports*, *VIII*, 1-268.

Matear, R. J. (1995), Parameter optimization and analysis of ecosystem models using simulated annealing: A case study at Station P, *Journal of Marine Research*, *53*, 571-607.

Mongin, M., E. Molina, and T. W. Trull (2008), Seasonality and scale of the Kerguelen plateau phytoplankton bloom: A remote sensing and modeling analysis of the influence of natural iron fertilization in the Southern Ocean, *Deep Sea Research Part II: Topical Studies in Oceanography*, *55*(5-7), 880-892.

Oschlies, A., and V. Garçon (1999), An eddy-permitting coupled physical-biological model of the North Atlantic. 1. Sensitivity to advection numerics and mixed layer physics, *Global Biogeochemical Cycles*, *13*(1), 135-160.

Pollard, R., I. Salter, R. Sanders, et al. (2009), Southern Ocean deep-water carbon export enhanced by natural iron fertilization, *Nature*, *457*(7229), 577-580.

Tagliabue, A., and K. R. Arrigo (2005), Iron in the Ross Sea: 1. Impact on CO2 fluxes via variation in phytoplankton functional group and non-Redfield stoichiometry, *J Geophys Res*, *110*, C03009.

Tagliabue, A., L. Bopp, O. Aumont, et al. (2009), Influence of light and temperature on the marine iron cycle: From theoretical to global modeling, *Global Biogeochemical Cycles*, *23*(2).

Trull, T. W., A. R. Bowie, J. Jabour, et al. (2008), Position Analysis: Ocean Fertilisation - Science and Policy Issues, 20 pp, Antarctic Climate & Ecosystems Cooperative Research Centre (ACECRC), Hobart, Tasmania.